# Investigating the Role of LRRK2 in the Visual System in a *Drosophila* Model of Parkinson's Disease

**Rebecca Furmston**

**Doctor of Philosophy**

**University of York**

**Biology**

**September 2016**

# Abstract

The kinase domain *LRRK2-G2019S* mutation is the most common cause of familial Parkinson's disease (PD). Some PD patients report visual defects, which may originate through the loss of dopaminergic (DA) signalling in the retina. Since *Drosophila*, like mammals, have retinal DA neurons, the *in vivo* role of *dLRRK*/*LRRK2* was examined genetically and by using potential therapeutic compounds to treat PD.

Here, it was shown that old *dLRRK*$^{-}$ loss-of-function flies have a deficit in signalling in the visual neurons, though photoreception is unaffected. This deficit is rescued with expression of *dLRRK, hLRRK2* or *mLRRK1* in the DA neurons, but also with *dLRRK* expression in the non-dopaminergic lamina neurons, photoreceptors or glial cells, suggesting a role of extra-synaptic cell-cell signalling. Placing the *dLRRK*$^{-}$ mutation in a white-eyed background proved to be lethal.

In the gain-of-function assay, old flies with DA expression of *LRRK2-G2019S* show a second kind of visual defect, reduced photoreception, indicating cell-cell signalling of LRRK2. Feeding these flies with mitochondrial rescue agents or a kinase inhibitor substantially improves the visual response; the vision of control flies is unaffected. Additionally, white-eyed flies with DA expression of *LRRK2-G2019S* do not show the neurodegeneration seen in red-eyed flies.

Since the mammalian kidney secretes LRRK2 in exosomes, our data may be interpreted by an exosome mediated transfer of LRRK2 between neurons, photoreceptor and glia. Lysosomes are linked to the production of the red/brown pigment granules in the fly eye, as well as to exosomes. As fly pigment granules, like melanosomes, are lysosomal-related organelles, our data provide an explanation for the high sensitivity of DA neurons in PD. Finally, our data suggest novel therapies could result from drugs targeting the eye pigments or through using mitochondrial rescue agents.

# Table of Contents

# Table of Tables

# Table of Figures

# Acknowledgments

Firstly, I would like to thank my supervisors Dr Chris Elliott and Professor Oliver Bandmann for their continued support, encouragement and expert guidance throughout my PhD. Secondly, I would like to thank the members of my Thesis Advisory Panel, Dr Sean Sweeney and Dr Betsy Pownall for their constructive advice, ideas and discussions of my work. I would also like to extend my thanks to our collaborators, Professor Alex Wade for his help with the SSVEP analysis, and Dr Heather Mortiboys for all of her assistance with collecting the UCA and UDCA data.

I am very grateful to all of the members of both the Elliott and Sweeney labs who have been there to offer advice, suggestions and amusement on a daily basis. In particular, I would like to mention Dr Ryan West, Nathan Garnham, Amy Cording and Stavroula Petridi, each of which have greatly helped me with experiments and data analysis and have been there to answer my many questions.

I would also like to thank my friends Katie Jackson, Keir Bailey, Emma Lindsay and Rhi McNeill. Katie has been my best friend since I was 5 years old and I can't thank her enough for her continued friendship, support and craziness. Keir, Emma and Rhi have shared the PhD experience with me. They have listened to me moan, helped me when experiments were not going so well, and have been there to have a good old gossip with! We have shared numerous laughs and I will treasure our lunch hours together forever.

On a more personal note, I would like to thank my mum and dad for supporting me in all of my decisions, for believing in me, and for being there for me throughout everything. I would also like to thank my sister Joanna for always being there to talk to, for being a positive role model, and for understanding the difficulties of a PhD! Finally, I would like to thank Nathan again for being my best friend over the past four years. He has been there for me both in and out of the lab and I couldn't have done any of it without him by my side.

# Declaration

I hereby declare that the work presented in this thesis is my own work, except where stated in the text or figures, and I am the sole author. This work has not previously been presented for an award at this, or any other, University. All sources are acknowledged as References. Permissions from journals have been obtained for all figures that have been adapted from published articles.

Some of the data presented in Chapter 4 have been published as part of scientific articles for which I was listed as an author:

Mortiboys H*, Furmston R*, Bronstad G, Aasly J, Elliott C, Bandmann O. UDCA exerts beneficial effect on mitochondrial dysfunction in *LRRK2*$^{G2019S}$ carriers and in vivo. *Neurology* 2015;10(85):846–52

West RJ, Furmston R, Williams CA, Elliott CJ. Neurophysiology of *Drosophila* models of Parkinson's disease. *Parkinsons Dis.* 2015;381281

# 1 Introduction

## 1.1 Parkinson's disease

### 1.1.1 Overview of Parkinson's disease

Parkinson's disease (PD) is the second most common progressive neurodegenerative disorder after Alzheimer's disease. It is thought to affect approximately 1% of the world's population over the age of 65, with the prevalence increasing to 5% in individuals over the age of 85 years (Farrer, 2006). It is predicted that globally there will be more than two billion people aged 60 years or over by 2050, which is more than double the 841 million elderly people recorded in 2013 (UnitedNations, 2013). As ageing is the biggest risk factor for idiopathic PD, the number of PD cases is expected to dramatically increase over the next 30 years. Consequently, PD will become more of an economic drain due to both direct and indirect costs and will continue to be an important health issue.

Neuropathologically, PD is characterised by the loss of 50-70% of the dopaminergic (DA) neurons most significantly, but not exclusively, from the *substantia nigra pars compacta* (SNpc) region of the midbrain. The basal ganglia and related nuclei, which include the SNpc, are a group of sub-cortical cells primarily involved in motor control. The resultant deficiency of dopamine within the basal ganglia is thought to lead to many of the classical motor symptoms that are characteristic of PD. Accompanying the loss of DA neurons are histological abnormalities. These include the presence of proteinaceous inclusions known as Lewy bodies (LB) and Lewy neurites (LN) in the surviving neurons of the SNpc and in other brain regions such as the locus coeruleus and the cholinergic nucleus basalis of Meynert (Lewy, 1912, Lewy, 1923). The primary structural component of LBs is the presynaptic neuronal protein α-synuclein (Spillantini et al., 1998). Light microscopy and immunological methods have identified a number of other proteins including ubiquitin and neurofilaments in LBs and LNs. Although the presence of LBs and the loss of DA neurons are necessary to histologically diagnose PD, they can occur independently of one another and their severity varies between individual patients.

The ageing process itself is the biggest risk factor for PD, however a number of environmental risk factors have also been suggested including exposure to pesticides, prior head injuries, rural living (Noyce et al., 2012) and the use of β-blockers (Kalia and Lang, 2015). PD was initially considered to be a purely sporadic and non-genetic disorder, however in 1996 a linkage analysis study of a large Italian family with an autosomal dominant form of the disease revealed a mutation in the *α-synuclein* gene as the cause of their PD (Polymeropoulos et al., 1996, Polymeropoulos et al., 1997). This suggested that PD could also be inherited with a genetic component underlying the disease. Although the majority of PD cases are sporadic, it is now known that approximately 10% of all patients have a familial form of PD. A number of other chromosomal loci have since been identified to have a putative link to PD. These specific chromosomal regions are termed *PARK* and are numbered in chronological order of when they were identified (Klein and Westenberger, 2012). As well as *α-synuclein* (*PARK1/PARK4*), other genes that have been identified to cause autosomal dominant forms of PD include *leucine-rich repeat kinase 2* (*LRRK2*; *PARK8*) (Funayama et al., 2002, Paisan-Ruiz et al., 2004, Zimprich et al., 2004), *ubiquitin carboxy-terminal hydrolase-like 1* (*UCH-L1*; *PARK5*) (Wintermeyer et al., 2000), *vacuolar protein sorting 35* (*VPS35*; *PARK17*) (Vilarino-Guell et al., 2011), and *eukaryotic translation initiation factor 4 gamma-1* (*EIF4G1*; *PARK18*) (Chartier-Harlin et al., 2011). Genes have also been identified that cause an autosomal recessive form of PD including *parkin* (*PARK2*) (Kitada et al., 1998), *phosphatase and tensin homolog (PTEN)-induced kinase 1* (*PINK1*; *PARK6*) (Valente et al., 2004), *DJ-1* (*PARK7*) (Bonifati et al., 2003), and *ATP13A2* (*PARK9*) (Di Fonzo et al., 2007). Homozygous loss-of-function (LOF) mutations in *glucocerebrosidase* (*GBA*) are known to cause the lysosomal storage disorder Gaucher's disease; heterozygous LOF mutations in this gene have also been linked to PD (Goker-Alpan et al., 2004). Of these genes, *LRRK2* is the most common cause of familial PD and also the focus of this thesis.

## 1.2 LRRK2

### 1.2.1 The structure of LRRK2

The *LRRK2* gene consists of 51 coding exons and encodes a large protein of 2527 amino acids known as LRRK2 or Dardarin (Figure 1.1). The presence of a conserved

Ras of complex proteins (ROC) domain and its C-terminal of ROC (COR) bi-domain suggests that LRRK2 belongs to the large ROCO family of proteins. The ROC domain of LRRK2 shows GTPase activity, as it is able to bind and hydrolyse GTP. In vertebrates, four ROCO proteins have been identified including LRRK2, leucine-rich repeat kinase 1 (LRRK1), death-associated kinases-1, and malignant fibrous histiocytoma amplified sequences with leucine-rich tandem repeats 1 (Gilsbach and Kortholt, 2014). LRRK2 also contains a kinase domain that has specific serine/threonine kinase activity. The mechanism underlying the activity of the LRRK2 kinase domain and its downstream kinase effectors are still largely unknown. As such, it is not yet clear which family of kinases LRRK2 belongs to, although is has been described as belonging to the mixed-lineage kinases, the mitogen-activated protein kinases family, and to the receptor-interacting protein kinases. The presence of both a GTPase and kinase domain led to the suggestion that LRRK2 is a cell-signalling molecule. The relationship between the GTPase and kinase domains has been an area of investigation. Initial biochemical studies suggested a mechanism whereby the GTPase activity of LRRK2 controlled the kinase activity, and the output of LRRK2 was the phosphorylation of substrate proteins (West et al., 2007). However, more recent studies suggest that the relationship between the GTPase and kinase domains is more complex (Taymans and Cookson, 2010). Mapping LRRK2's autophosphorylation sites *in vitro* has revealed a cluster of autophosphorylation sites within its GTPase domain, and indeed the LRRK2 kinase domain can phosphorylate the ROC domain (Greggio et al., 2009, Kamikawaji et al., 2009, Gloeckner et al., 2010). Autophosphorylation at these sites causes structural changes to the GTPase domain into a configuration that promotes kinase activity (Greggio et al., 2009, Kamikawaji et al., 2009, Gloeckner et al., 2010, Xiong et al., 2012a). This suggests that the combination of GTP binding and LRRK2 autophosphorylation in the GTPase domain regulates GTPase-dependent activity, that in turn controls kinase activity (Xiong et al., 2012a). Furthermore, mutation of an autophosphorylation site in the ROC domain to a phosphothreonine-mimicking glutamate reduces GTP binding (Kamikawaji et al., 2009, Berwick and Harvey, 2011). LRRK2 is also composed of various protein-protein interaction domains including N-terminal armadillo and ankyrin repeats, several leucine-rich repeats and a C-terminal WD40 domain. LRRK2 is found in multiple regions of the brain and in a variety of tissue types. Its cellular localisation is still

unclear but biochemical studies, along with internal reflection microscopy, have provided evidence that LRRK2 cycles between a predominant cytosolic monomeric form with low activity, and a membrane-associated multimeric form with much higher activity (Berger et al., 2010, James et al., 2012, Paisan-Ruiz et al., 2013).

**Figure 1.1 Schematic diagram of the human LRRK2 domains and the PD pathogenic mutations**

Human LRRK2 is composed of several independent domains including armadillo repeats (ARM), ankyrin-like repeats (ANK), leucine-rich repeats (LRR), Ras of complex proteins (ROC) GTPase, C-terminal of ROC (COR), kinase and WD40. ANK, LRR and WD40 are protein-

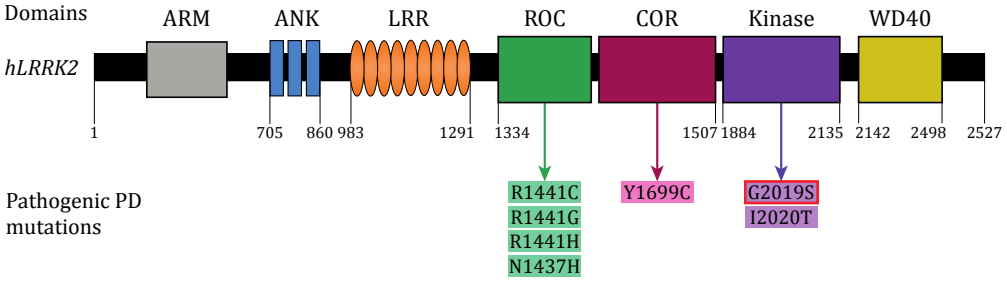


protein interaction domains, whilst the ROC and kinase domains are enzymatic. Multiple mutations in *LRRK2* are found in PD patients. These mutations cluster within the central enzymatic ROC, COR and kinase domains. The most common *LRRK2* mutation is the *G2019S* mutation found within the kinase domain. Adapted with permission from Lee et al. (2012a) and Langston et al. (2016).

### 1.2.2 The function of LRRK2

Despite numerous efforts, the cellular function(s) of LRRK2 still remain unclear. Due to its large size and the presence of both enzymatic and protein-protein interaction domains, LRRK2 has been implicated in a vast array of cellular tasks. It has even been suggested that LRRK2 may serve as a scaffold for the assembly of a multi-protein complex, which acts as a central component of multiple signalling pathways (Ray and Liu, 2012). LRRK2 has been reported to be involved in many of the established signalling cascades such as the mTOR, ERK, WNT, and TLR pathways (Imai et al., 2008, Sancho et al., 2009, Dzamko et al., 2012, Bravo-San Pedro et al., 2013, Paisan-Ruiz et al., 2013). However, it has proven difficult to validate LRRK2s involvement in these pathways because a clear substrate for LRRK2 is still to emerge.

One of the recurring physiological roles that LRRK2 has been implicated in is the regulation of synaptic vesicles. LRRK2 has been found to be associated with membranous structures and vesicles in the mammalian brain and is enriched in the Golgi complex. Matta et al. (2012) used *Drosophila* to demonstrate that LRRK2 plays an essential role in synaptic vesicle endocytosis through phosphorylating endophilin A, an evolutionary conserved protein involved in clathrin-mediated endocytosis. Arranz et al. (2015) showed that LRRK2 phosphorylates the neuronal-specific EndoA1 in mammalian cells, further validating the results seen in *Drosophila.* An interaction between LRRK2 and Rab5b has also been described as regulating synaptic endocytosis (Shin et al., 2008, Yun et al., 2015). Using siRNA knockdown of LRRK2, it was shown that synaptic vesicle endocytosis was markedly reduced but this could be reversed through the introduction of Rab5B (Shin et al., 2008). LRRK2 has also been shown to interact with a number of other synaptic proteins that modulate clathrin-mediated endocytosis of synaptic vesicles including Snapin-1 and NSF (Piccoli et al., 2011, Yun et al., 2013, Piccoli et al., 2014, Arranz et al., 2015). Some studies have suggested that LRRK2 modulates synaptic vesicle exocytosis through interacting with Snapin or through the regulation of presynaptic vesicle release (Piccoli et al., 2011, Yun et al., 2013), however other studies have been unable to validate this link (Shin et al., 2008, Arranz et al., 2015). A number of studies have also been able to provide support for LRRK2 playing a role in vesicular trafficking (Biskup et al., 2006, Higashi et al., 2009, Sanna et al., 2012, MacLeod et al., 2013). When LRRK2 is silenced

in cortical primary neurons, vesicle recycling dynamics are altered and vesicle kinetics are increased, which implicates LRRK2 in the control of vesicle pools within the presynaptic bouton (Migheli et al., 2013, Wallings et al., 2015).

LRRK2 has also been implicated in autophagy pathways. For example, knockout of *LRRK2* in mice leads to the impairment of the autophagy-lysosomal pathway with dramatic increases in apoptotic cell death, oxidative damage and inflammatory response (Tong et al., 2010, Tong et al., 2012). It has been suggested that LRRK2 may be important in multiple systems that are associated with protein disposal. This is because an interaction between LRRK2 and Rab7L1, a genetic risk factor for sporadic PD, has been reported to influence lysosomal protein sorting via the retromer complex that links the endolysosomal protein degradation system with the Golgi apparatus (MacLeod et al., 2013, Paisan-Ruiz et al., 2013).

A role for LRRK2 in neurite outgrowth and branching has also been suggested. This was initially thought to be the consequence of apoptotic processes, however subsequent studies provided evidence to suggest that these morphological changes were actually due to LRRK2 playing a role in the regulation of cytoskeletal dynamics. A delicate interplay between two key components of the cytoskeleton, microtublues and actin, is essential in maintaining the structural polarity of neurons, which is important for their physiological function (Parisiadou and Cai, 2010). There is increasing evidence to suggest that the assembly of abnormal cytoskeletal components is one of the major characteristics of a number of neurodegenerative disorders, including PD. LRRK2 has been reported to interact with tubulin, actin and moesin, all key cytoskeletal proteins (Jaleel et al., 2007, Gandhi et al., 2008, Gillardon, 2009, Meixner et al., 2011). LRRK2's interaction with tubulin is associated with the modulation of microtubule stability and acetylation, which may be mediated via the interaction of LRRK2 and the microtubule-associated protein tau. LRRK2 is capable of phosphorylating tau in the presence of tubulin thereby altering microtubule-tau binding dynamics. LRRK2 may also have a functional role in the rearrangement of the cytoskeleton, which could explain how mutations in this gene alter neurite outgrowth (Parisiadou et al., 2009, Chan et al., 2011).

There is increasing evidence to suggest that LRRK2 has a putative role in the immune system. Although LRRK2 is expressed ubiquitously, high levels of LRRK2 protein and mRNA can be found in peripheral blood mononuclear cells, lymph nodes, spleen and primary microglia (Hakimi et al., 2011, Gillardon et al., 2012). Within the immune system, LRRK2 has been implicated in the activation and maturation of immune cells (Thevenet et al., 2011), controlling the radical burst against pathogens in macrophages (Gardet et al., 2010), and in modulating neuroinflammation through cytokine signalling (Moehle et al., 2012, Gillardon et al., 2013, Wallings et al., 2015). In light of these very specific functions within the immune system, it has been suggested that LRRK2 could have different roles within various cells and tissues (Wallings et al., 2015). Furthermore, the *LRRK2* locus has also been associated with Crohn's disease and susceptibility to leprosy, which provides a genetic link to immune disease (Zhang et al., 2009, Franke et al., 2010, Paisan-Ruiz et al., 2013). However, it is still unclear as to how these data tie into the cellular biology of LRRK2.

### 1.2.3 The role of LRRK2 in PD

The first link between mutations in *LRRK2* and PD was discovered early in the 21st century after Funayama's group reported on a Japanese family with an autosomal dominant form of PD (Funayama et al., 2002). This was linked to a novel genetic risk locus of approximately 166 genes on chromosome 12, which was designated as *PARK8*. Subsequent studies revealed that mutations within the *LRRK2* gene were the genetic cause underlying *PARK8*-associated PD (Paisan-Ruiz et al., 2004, Zimprich et al., 2004). To date, over 100 mutations have been reported in *LRRK2*, however only a handful of these have been proven to cause PD. These mutations include *G2019S*, *I2012T*, *I2020T*, *N1437H*, *R1441C/G/H*, *Y1699C*, and *S1761R* (Paisan-Ruiz et al., 2004, Zimprich et al., 2004, Funayama et al., 2005, Kachergus et al., 2005, Paisan-Ruiz, 2009, Ross et al., 2009, Aasly et al., 2010, Lorenzo-Betancor et al., 2012). The enzymatic core of LRRK2 appears to be of central importance, with all of the established pathogenic mutations clustering within the ROC/COR/kinase domains (See Figure 1.1).

Of the *LRRK2* mutations, the dominant gain-of-function (GOF) *G2019S* mutation found within the kinase domain is the most frequent, being accountable for up to 10%

of sporadic PD cases and up to 42% of familial PD cases (Correia Guedes et al., 2010, Paisan-Ruiz et al., 2013). The *LRRK2-G2019S* mutation has a worldwide distribution but it presents with a higher frequency in North African Arab (42%), Ashkenazi Jewish (28%), and Portuguese (16%) populations (Bras et al., 2005, Lesage et al., 2005, Ozelius et al., 2006, Paisan-Ruiz et al., 2013). The GTPase domain *LRRK2-R1441G* mutation presents with its highest frequency in the Basque population (2.5% of sporadic cases and 46% of familial cases), however it is barely present in other European populations or in North and South America (Gorostidi et al., 2009, Mata et al., 2009, Yescas et al., 2010, Paisan-Ruiz et al., 2013). The second most common *LRRK2* mutation found within Europe is *LRRK2-R1441C,* and this is the main cause of familial PD in Belgian populations (Nuytemans et al., 2008). A small number of families have been reported with the *LRRK2-I2020T* mutation including the Sagamihara kindred, which was the first reported family with LRRK2-linked PD (Funayama et al., 2005). The penetrance of *LRRK2* mutations is age dependent, increasing from 17% at 50 years of age to 85% at 70 years of age (Paisan-Ruiz et al., 2013). Some *LRRK2-G2019S* carriers do not manifest the disease until late into their eighties.

Given the high frequency of *LRRK2-G2019S,* the majority of clinical reports concerning LRRK2-linked PD have focused on this mutation. Most of these reports are in agreement that the phenotypic features of *LRRK2-G2019S* PD closely resemble those seen in idiopathic PD. For example, a large collaborative study has characterised LRRK2-linked PD as a tremor-predominant Parkinsonism with bradykinesia and rigidity that shows a good response to levodopa therapy (Healy et al., 2008). Olfactory dysfunction, a well-characterised, non-motor feature of idiopathic PD, has also been widely studied in *LRRK2-G2019S* patients and most reports are in agreement that these carriers also manifest this symptom (Ponsen et al., 2004, Silveira-Moriyama et al., 2010, Saunders-Pullman et al., 2011, Paisan-Ruiz et al., 2013). Olfactory dysfunction has also been reported in *LRRK2-R1441G* mutation carriers (Ruiz-Martinez et al., 2011). Although there are close similarities between idiopathic PD and LRRK2-linked PD, there are also slight differences between the two forms. Unlike idiopathic PD patients, in general *LRRK2* mutation carriers are rarely reported to show cognitive decline and psychiatric features, however they do show a

high frequency of depression and anxiety (Goldwurm et al., 2006, Alcalay et al., 2010, Shanker et al., 2011, Paisan-Ruiz et al., 2013). A large number of *LRRK2-G2019S* mutation carriers are asymptomatic, thus there is an increasing amount of research that focuses on these carriers in order to try and identify early preclinical biomarkers of PD (Paisan-Ruiz et al., 2013). A high frequency of cognitive impairment, postural instability, action tremor and gait alterations have all been reported in non-manifesting carriers. Olfactory dysfunction has been reported to present at similar levels in healthy mutation carriers and healthy non-carriers, suggesting that this symptom may be independent of *LRRK2* mutations, or occurs at a later stage in the disease process (Paisan-Ruiz et al., 2013, Sierra et al., 2013).

The neuropathology seen in *LRRK2* mutation carriers is thought to be heterogeneous. The loss of DA neurons and the presence of LBs and LNs are the main characteristics, however these are not seen in all cases and even the same mutation within *LRRK2* can lead to diverse neuropathology. LRRK2-linked PD has also been shown to present as tau-, α-synuclein-, or ubiquitin-positive pathologies (Wider et al., 2010, Paisan-Ruiz et al., 2013).

Since mutations in the kinase domain of *LRRK2* were associated with neurotoxicity and PD, the development of LRRK2 kinase inhibitors has been the focus of many drug discovery studies. The first LRRK2 inhibitors that came from library screening efforts were mostly ATP-competitive, meaning that they had selectivity issues and inhibited other kinases in addition to LRRK2 (Kramer et al., 2012). Another common problem seen with the published kinase inhibitors is that they fail to cross the blood-brain barrier (BBB) meaning that their therapeutic application in PD is greatly limited. There are a few kinase inhibitors that show a high selectivity to LRRK2 including LRRK2-IN-1 and BMPPB-32 (Deng et al., 2011, Afsari et al., 2014). The therapeutic potential of LRRK2 kinase inhibitors is still relatively unknown and some may display a loss of potency with the presence of certain *LRRK2* mutations. Furthermore, a pre-clinical safety study of highly potent and selective LRRK2 kinase inhibitors produced by Genentech Inc., recently demonstrated that these small molecules cause adverse side effects on kidney and lung function, thus further clinical trials were stopped (Fuji et al., 2015). Although the majority of investigations have primarily focused on the kinase function of LRRK2, a number of studies suggest that decreased GTPase

activity, due to mutations in either the GTPase domain itself or in the kinase domain of LRRK2, also play a key role in PD pathogenesis (Lewis et al., 2007, Li et al., 2007, West et al., 2007, Berwick and Harvey, 2011, Daniels et al., 2011, Liu et al., 2011a, Xiong et al., 2012a, Xiong et al., 2012b). Due to this, there are increasing efforts to study potential therapeutic strategies that target LRRK2 GTP binding and GTPase activity (Xiong et al., 2012a). See Chapter 3, section 3.4.4 for further discussions on this topic.

### 1.2.4 Current clinical therapies for PD

As yet, there are no cures for PD only symptomatic therapies. Current clinical therapies are unable to prevent the on-going neurodegeneration; rather they alleviate some of the PD symptoms through compensating for the loss of DA neurons (Fox et al., 2011).

Since becoming a licensed drug in the 1960s, L-3,4-dihydroxyphenylalanine (levodopa or L-DOPA) has remained the most potent drug for alleviating symptoms of PD, in particular those related to bradykinesia. Unlike dopamine, the aromatic amino acid levodopa can cross the BBB, so when ingested it can be converted into dopamine via DOPA-decarboxylase to restore striatal dopamine concentrations. When ingested, approximately 70% of levodopa is absorbed from the small intestine and is metabolised in the liver, kidneys and blood (Jankovic, 2002). It is thought that when administered on its own, only 1% of the ingested levodopa dose enters the brain. With the addition of a peripheral DOPA-decarboxylase inhibitor, carbidopa, which prevents the conversion of levodopa to dopamine in peripheral tissues, the proportion of the levodopa dose that enters the brain, can be enhanced to 10% (Cotzias et al., 1969, Jankovic, 2002). Although levodopa is the most effective drug in the symptomatic treatment of PD, prolonged use leads to the development of the wearing-off phenomenon and levodopa-induced dyskinesia (LID) (Cotzias et al., 1969). The risk of developing LID is dependent on a variety of factors including severity of PD, age-of-onset of PD, and the dose and duration of levodopa therapy. Young-onset PD is associated with a higher incidence of LID; 50% of patients aged between 40-59 years develop LID after 5 years of levodopa treatment but only 16% of patients with a disease-onset of over 70 years of age are seen to develop LID

(Kumar et al., 2005, Thanvi et al., 2007). Drugs are available that aim to improve LID without necessitating the reduction of the levodopa dosage. These drugs include amantadine, clozapine, fluoxetine and fipamezole (Jankovic, 2008). The addition of dopamine agonist inhibitors, catechol-o-methyl-transferase inhibitors or MAO-I inhibitors is also used to alleviate levodopa-induced motor abnormalities.

It is thought that levodopa-induced complications are related to the duration of treatment, therefore many parkinsonologists recommend that levodopa therapy should be delayed. In order to achieve this, DA agonists are often used as the initial or early form of DA therapy (Jankovic, 2008). DA agonists directly activate DA receptors, enabling the presynaptic synthesis of dopamine to be bypassed. When taken on their own, DA agonists are only able to provide modest improvements in PD symptoms, however even this slight improvement can be sufficient to delay the use of levodopa by several months or years. This is of particular importance for young-onset PD patients. However, a recent study provided evidence to suggest that the risk and time-of-onset of disabling response fluctuations and dyskinesias is comparable between PD patients given an initial treatment of levodopa or those given an initial treatment of DA agonists (Haaxma et al., 2015); motor function was worse with DA agonist treatment. These results suggest that the initial line of therapy for PD should be levodopa rather than DA agonists.

Neurotrophic factors are small proteins that are known for their role in neuronal development and maintenance (Hefti, 1994, Airaksinen and Saarma, 2002). As these factors exert pro-survival effects on specific populations of cells within the brain and can induce neuronal growth, they have been extensively studied in animal models for their potential therapeutic use in several neurodegenerative disorders (Ramaswamy and Kordower, 2009). Such neurotrophic factors include neurturin, glial cell-line-derived neurotrophic factor (GDNF) and brain-derived neurotrophic factor. Both neurturin and GDNF have been tested in PD clinical trials (Nutt et al., 2003, Gill et al., 2003, Slevin et al., 2007, Marks et al., 2008). The biggest problem with neurotrophic factors is that they are unable to enter into the central nervous system (CNS) meaning that direct application to the patient's brain is necessary. Clinical trials with neurturin and GDNF have thus far been inconsistent due to the lack of an efficient method of administration. Although neurotrophic factors offer a promising therapeutic therapy

for PD, more research and clinical trials will be essential to identify a novel vehicle that can aid in the administration of these factors to desired brain regions (Ramaswamy and Kordower, 2009).

### 1.2.5 Clinical features of PD

#### 1.2.5.1 Motor symptoms

The classical motor symptoms of PD have been recognised since James Parkinson's initial description of PD as a neurological disorder was published in An Essay on the Shaking Palsy in 1817, reprinted in Parkinson (2002). Over 50 years later, the French neurologist Jean Martin Charcot more thoroughly described the clinical spectrum of PD motor symptoms. Charcot also disregarded terms such as shaking palsy and paralysis agitans and gave credit to James Parkinson's earlier work by suggesting that the disease be referred to as Parkinson's disease (Goetz, 2011). Charcot identified non-tremulous forms of PD, consequently suggesting that slowness of movement (bradykinesia) should be distinguished from weakness. The four cardinal motor symptoms of PD can be grouped under the acronym TRAP; Tremor at rest, Rigidity, Akinesia (or bradykinesia) and Postural instability (Jankovic, 2008). The occurrence and severity of these primary motor symptoms is variable amongst patients. Due to this, attempts have been made to classify subtypes of the disease. Although a consensus has not yet been established, two major subtypes have been suggested: tremor-dominant PD and non-tremor-dominant PD (Kalia and Lang, 2015). PD patients may also display a range of secondary motor symptoms, but again these are very variable between patients. An example of a secondary motor symptom is freezing of gait whereby the person will hesitate before stepping forwards or turning. Other examples include difficulty swallowing, speech problems, dystonia, stooped posture and micrographia (Jankovic, 2008).

#### 1.2.5.2 Non-motor symptoms of PD

Although PD is still often considered to be a movement disorder, it is a complex multi-system disorder with patients experiencing a wide range of symptoms with both motor and non-motor features. The non-motor symptoms can include autonomic

dysfunction, cognitive impairment, sleep disorders, neuropsychiatric symptoms, sensory dysfunction, pain and fatigue (Postuma et al., 2012).

Non-motor symptoms of PD can frequently be present in patients before the onset of the main motor symptoms. This prodromal phase of PD can be loosely characterised by rapid eye movement sleep behaviour disorder, constipation, olfactory dysfunction, depression and excessive daytime sleepiness (Braak et al., 2003, Postuma et al., 2012). The pathogenic process that causes PD is thought to be underway during the premotor phase and may not originate within the SNpc. In 2003, Braak described a staging system of PD based upon the examination of α-synuclein deposition patterns within the brain (Braak et al., 2003). Braak's model indicates that α-synuclein deposits initially occur in the dorsal motor nucleus and the anterior olfactory nucleus, this is known as 'Stage 1'. In Stage 2 lesions are seen in pontomedullary regions including the caudal raphe nuclei and the locus coeruleus. It is not until Stage 3 that the SNpc and other regions of the midbrain show α-synuclein deposits. During Stages 4-6, cortical structures become affected. The idea that initial PD pathology may occur outside of the SNpc in non-DA structures of the brain stem suggests a potential for screening non-motor symptoms as a way to detect premotor PD (Postuma et al., 2012). This also provides a potential temporal window in which disease-modifying therapies could be administrated to prevent or delay the progression of the disease (Kalia and Lang, 2015).

## 1.3 Vision and PD

### 1.3.1 The vertebrate retina

Among the non-motor symptoms of PD are visual disturbances, which may be linked to changes in the retinal signalling pathway. The vertebrate retina is composed of six principal cell types: photoreceptors, projection neurons, three types of interneurons (horizontal, amacrine and bipolar cells), and glial cells. These cell types are organised into histologically distinct layers; three nuclear layers containing cell bodies but no synapses that are separated by two plexiform layers containing synapses but no cells bodies (Sanes and Zipursky, 2010). From outside to in, the vertebrate retinal layers are; the outer nuclear layer (ONL); outer plexiform layer (OPL); inner nuclear layer

(INL); inner plexiform layer (IPL); and the ganglion cell layer (GCL; Figure 1.2). The ONL contains the photoreceptors that can be broadly categorised into rods and cones depending on their shape, distribution across the retina, the photopigments they contain, and their synaptic connections. Rods are responsible for low-light vision as they are very sensitive to light and can detect even single photons (Sakitt, 1972, Sampath and Rieke, 2004). Cones are not as sensitive to light as rods, however they have a much higher spatial resolution. Cones are responsible for bright-light, high acuity colour vision and each type of cone photoreceptor is most sensitive to a specific wavelength of light (Hoon et al., 2014). In the dark, photoreceptors exist in a depolarised state and are constantly releasing the neurotransmitter glutamate (Dowling and Ripps, 1973, Suryanarayanan and Slaughter, 2006). Unlike other neurons, light energy causes changes in membrane potentials of photoreceptors rather than causing them to produce action potentials. When stimulated by light, the photoreceptors become hyperpolarised and the release of glutamate is reduced (Archibald et al., 2009). Rod and cone photoreceptors synapse onto second-order glutamatergic bipolar cells at the OPL. The OPL is the simpler synaptic layer in the retina. Here, horizontal cells modulate the synaptic transmission between the photoreceptors and the bipolar cells. The bipolar cells can be sub-divided into rod and cone bipolar cells. Cone bipolar cells can either depolarise (ON-bipolar) or hyperpolarise (OFF-bipolar) in response to increments in light intensity (Hoon et al., 2014), whereas the rod bipolar cells are only ON-bipolar cells. The bipolar cells project into the IPL where they contact retinal ganglion cells (RGCs) and amacrine cells. The synaptic connections within the IPL can be organised into two structurally and functionally distinct layers: the inner lamina and the outer lamina (Archibald et al., 2009). The inner lamina contains synapses between the ON-bipolar cells, 'ON'-RGCs and amacrine cells. The outer lamina contains synapses between the OFF-bipolar cells, 'OFF'-RGCs and amacrine cells. The RGCs project their axons to more than ten areas of higher visual centres in the brain, making them the sole output neurons of the retina (Sanes and Zipursky, 2010). The optic tectum, known as the superior colliculus in mammals, is the main target of the RGCs in most vertebrates (Sanes and Zipursky, 2010). Amacrine cells modulate the excitation of RGCs through both feedfoward and feedback inhibition; amacrine cells that synapse onto RGC

dendrites generate feedforward inhibition, whilst amacrine cells that synapse onto axon terminals of bipolar cells generate feedback inhibition (Hoon et al., 2014).

**Figure 1.2 The organisation of the vertebrate retina**

A simplistic diagram indicating the principle cell types of the vertebrate retina (left) and the histologically distinct layers that these cell types are organised into (right). The amacrine neurons found at the border of the inner nuclear and inner plexiform layers are dopaminergic. Adapted with permission from Wilkinson-Berka (2004) and Webvision (2012).

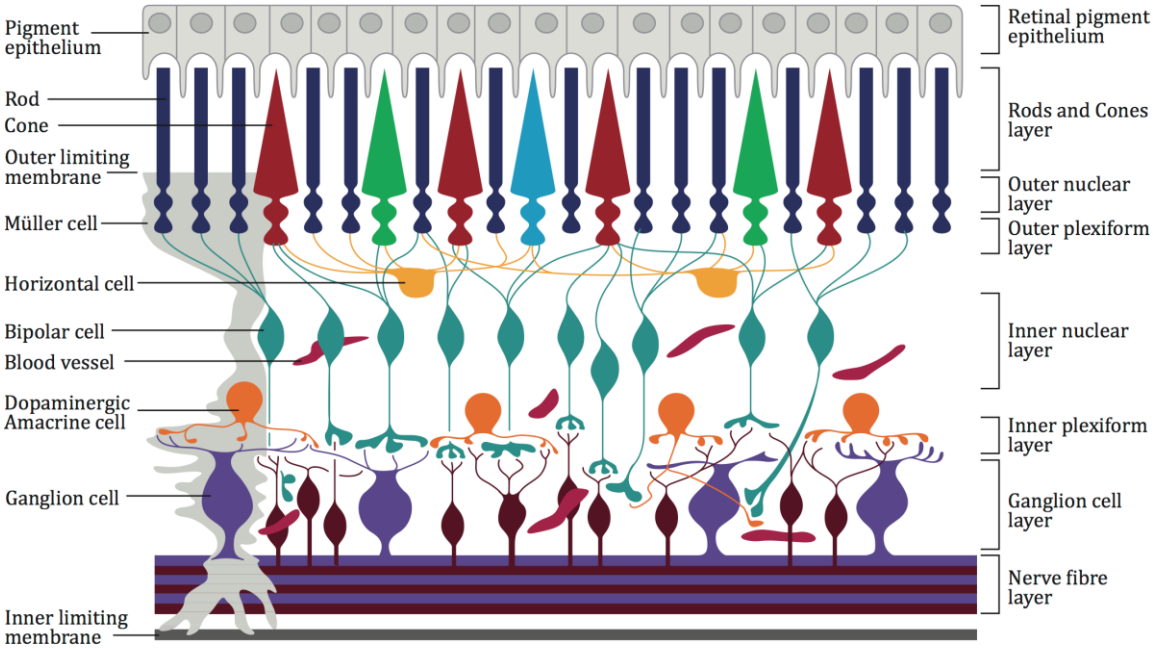

### 1.3.2 Dopamine in the human retina

In 1963, a role for catecholamines in the retinal function of rats was first highlighted (Malmfors, 1963). A subsequent study demonstrated that the rabbit retina contains DA neurons (Haeggendal and Malmfors, 1963). Further studies of the human retina have identified the A18 amacrine cells, located at the border of the inner nuclear and inner plexiform layers, as DA (Figure 1.2) (Frederick et al., 1982, Kolb et al., 1990). In the retina the density of these A18 neurons is low, however due to their widespread dendritic arborisation and long fine axons, a network with other amacrine and bipolar cells is established (Kolb et al., 1990, Dacey, 1990, Kolb et al., 1991, Archibald et al., 2009). DA neurons are depolarised under both low- and high-light levels suggesting that they receive input from both depolarising rod- and cone-bipolars (Zhang et al., 2007, Archibald et al., 2009).

DA neurons also contact the AII and A17 amacrine cells, both of which belong to the rod pathway. The AII amacrine cells are coupled to ON-bipolar cells via gap junctions, which allows rod signals to be transferred to cone circuits (Bloomfield and Dacheux, 2001). As well as being involved in the horizontal processing of retinal signalling, AII amacrine cells are also involved in the vertical signalling of visual information through the retina. The DA neurons also contain the neurotransmitter gamma-aminobutyric acid (GABA) (Wassle and Chun, 1988, Wulle and Wagner, 1990). The AII amacrine cells express D1-subtype dopamine receptors and $GABA_A$ receptors, suggesting that both dopamine and GABA are involved in modulating amacrine function (Wulle and Wagner, 1990, Archibald et al., 2009). DA neurons express $GABA_A$ receptors as well as AMPA sub-type glutamate receptors (Gustincich et al., 1999, Gabriel et al., 2002). It is clear that the retinal DA neurons receive both excitatory (glutamatergic) synaptic inputs from one or more type of bipolar cell and inhibitory (GABAergic and glycinergic) synaptic inputs from amacrine cells. The mix of excitatory and inhibitory inputs raise or lower the intrinsic firing rate of the neuron and in turn modify the rate of dopamine release (Witkovsky, 2004). Although DA neurons have a direct synaptic effect on certain amacrine cells, most retinal cells respond to dopamine via a paracrine effect with the diffusion of dopamine in the extracellular matrix of the retina extending over many microns (Witkovsky, 2004).

Dopamine acts through five receptor subtypes (D1-D5), which belong to the superclass of G-protein coupled receptors. The most common action of dopamine is to regulate the production of cyclic adenosine monophosphate. Receptors D1 and D5 are known as the D1-like receptors, whereas D1, D2 and D4 form the D2-like receptors. D1-like receptors are linked to the activation of adenylate cyclase and an increase in cAMP production. D2-like receptors are linked to the inhibition of adenylate cyclase and a decrease in cAMP production. When the D2-like receptors are activated they inhibit the rod and cone photoreceptors. When the D1-like receptors are activated they excite the RGCs, bipolar cells, horizontal cells, and the amacrine cells.

Dopamine is known to be an important neurotransmitter throughout the visual system and acts in both the outer and inner retinal layers at multiple levels. It is thought to function as a chemical messenger for light adaptation through promoting the flow of information through cone circuits and lessening that through rod circuits (Archibald et al., 2009). In addition, it is speculated that dopamine plays a role in the transition from a dark- to a light-adapted state because retinal dopamine concentrations show a tonic diurnal variation with low levels during the night and higher levels during the day (Doyle et al., 2002b).

### 1.3.3 Visual dysfunction in PD

It has previously been shown through *post-mortem* studies, that patients with PD, who were not receiving levodopa treatment at the time of death, had a significant reduction in the immunoreactivity of tyrosine hydroxylase (TH), the rate-limiting enzyme in dopamine production (Nguyen-Legros, 1988, Harnois and Di Paolo, 1990). In addition, treating monkeys with 1-methyl-1,2,3,6-tetrahydropyridine (MPTP) was shown to cause a dose-dependent but reversible reduction in amacrine cell TH immunoreactivity (Tatton et al., 1990). The amplitude of the electroretinogram (ERG) 'b' wave is reduced in PD patients under a number of different light conditions (Gottlob et al., 1987). This component of the ERG is thought to be an indicator of INL function, thus the reduction may reflect defects in visual processing that involve dopamine signalling. Gottlob et al. (1987) also utilised pattern response ERGs, which revealed that the amplitude of the response to a checkerboard stimulus is also

decreased in PD patients. Subsequent studies have suggested that a depletion of dopamine in the retina may result in attenuated ERG responses to peak stimuli and it has been shown that the pattern response ERG is sensitive to dopamine manipulation (Tagliati et al., 1994, Bodis-Wollner and Tzelepi, 1998). Although it is clear that dopamine plays an important role throughout the retina, it is not yet clear how the deficiency in dopamine levels, as seen in PD, affect the retina.

Visual dysfunction in PD can exist at several levels of the visual pathway including the retina and higher order visual cortical processing areas, reviewed by Armstrong (2015). PD generally affects older people meaning that a range of age-related visual pathologies including macular degeneration, cataracts and glaucoma must first be ruled out before the visual disturbances can be attributed to underlying PD. However, visual dysfunction is common in PD with patients suffering from problems with contrast discrimination, double or blurred vision, impaired motion perception, colour vision, and often, if dementia develops this can extend to complex hallucinations and perceptual disturbances (Bodis-Wollner et al., 1987, Regan and Maxner, 1987, Bulens et al., 1988, Haug et al., 1994, Trick et al., 1994, Diederich et al., 1998, Lieb et al., 1999, Pieri et al., 2000, Amick et al., 2003, Davidsdottir et al., 2005). Patients can also experience subtle changes in their control of eye movements (Shibasaki et al., 1979, White et al., 1983, Pinkhardt and Kassubek, 2011).

## 1.4 Animal models of PD

Due to the limitations of human experimentation, researchers have turned to animal models in order to study human diseases, including PD. The use of such animal models allows the study of cellular processes in the context of the whole organism, making them more reliable than cellular models. Over the past few decades, modelling PD in animals has proven to be invaluable in aiding researchers to better understand the pathology, etiology and molecular mechanisms of the disease. Typically, animal models of PD can be divided into two main groups: the neurotoxin models, which utilise environmental or synthetic toxins, and the genetic models, which utilise the *in vivo* expression of PD-related mutations. It is important to note that although animal models of PD have undoubtedly increased our understanding of the disease pathogenesis, none of the currently existing animal models can fully

recapitulate all of the key clinical and neuropathologic PD symptoms (Dawson et al., 2010).

### 1.4.1 Neurotoxin models

The classic neurotoxin-based model of PD utilises the administration of 6-hydroxydopamine (6-OHDA). Although 6-OHDA has a similar structure to dopamine, the addition of a hydroxyl group makes it toxic to DA neurons. This was first shown nearly 50 years ago when Ungerstedt (1968) injected 6-OHDA into the SNpc of the rat brain and observed a subsequent degeneration of the nigro-striatal DA system. Since this discovery, 6-OHDA has been extensively used in both rodent and primate models of PD. One of the main drawbacks of 6-OHDA is that it is unable to cross the BBB, meaning that direct injection into the brain is required. In general, 6-OHDA is injected into one of three locations in the brain: the SNpc, the median forebrain bundle, or the terminal region of the striatum (Duty and Jenner, 2011). Following injection, 6-OHDA is taken up into DA neurons via dopamine transporters. 6-OHDA also shows a high affinity for the noradrenaline transporter NET, therefore it is often used in conjunction with a noradrenaline reuptake inhibitor such as desipramine, which improves the specificity of the toxin to the DA neurons (Luthman et al., 1989, Duty and Jenner, 2011). Once inside DA neurons, 6-OHDA initiates degeneration through causing oxidative stress and mitochondrial dysfunction. Although the exact mechanisms behind this are still unclear, it is known that once in the cytosol, 6-OHDA readily oxidises giving rise to reactive oxygen species (ROS) such as hydrogen peroxide and quinones (Duty and Jenner, 2011). In addition, 6-OHDA has been shown to accumulate in the mitochondria where it interacts directly with both complexes I and IV of the mitochondrial electron transport chain, subsequently increasing oxidative stress further (Glinka et al., 1997). Although injection of 6-OHDA into the SNpc region of the rodent brain leads to the degeneration of approximately 60% of the TH-containing neurons and a subsequent loss of TH positive terminals in the striatum, this model is unable to recapitulate all of the clinical PD symptoms (Blandini et al., 2008, Jackson-Lewis et al., 2012). For example, administration of 6-OHDA does not induce Lewy-like inclusions or proteinaceous aggregates within neurons like those seen in PD, although 6-OHDA has been shown to interact with α-synuclein (Alves da Costa et al., 2006). Despite some limitations as a toxin to induce PD, the use

of 6-OHDA has contributed greatly to our understanding of PD pathology and will continue to be an important toxin to study the degeneration of nigro-striatal neurons within animal models and *in vitro*.

Another widely used neurotoxin model of PD involves the administration of MPTP. MPTP is able to replicate a number of key hallmarks of PD in monkeys and other higher mammals including oxidative stress, mitochondrial dysfunction, energy failure and inflammation (Langston et al., 1983, Burns et al., 1985, Jackson-Lewis et al., 2012). In addition, it can cause a significant number of these key symptoms in mice, although there is much variability in the sensitivity to the toxin in different mouse strains. Rats have been shown to be resistant to this compound (Chiueh et al., 1984). Similarly to 6-OHDA, administration of MPTP is unable to lead to the formation of LBs. Some studies have shown LB-like inclusions being produced after MPTP has been administered, however these results have been difficult to replicate (Jackson-Lewis et al., 2012).

The other neurotoxin models of PD involve the use of pesticides such as rotenone and paraquat. Rotenone is highly lipophilic, is able to cross the BBB, and similarly to MPTP, once in neurons it accumulates within mitochondria and inhibits complex I activity. Rotenone is able to reproduce almost all of the key hallmarks of PD including oxidative stress, inflammation, behavioural defects, and unlike MPTP and 6-OHDA, it induces synuclein aggregation and LB-like formation in mammalian models (Greenamyre et al., 2010). Paraquat is also able to induce the formation of LB-like inclusions in the DA neurons of the SNpc (Jackson-Lewis et al., 2012). Although MPTP- and 6-OHDA-induced models of PD have not yet been established in *Drosophila*, exposure to rotenone results in the selective loss of DA neurons in the brains of flies along with locomotor defects (Coulom and Birman, 2004). Paraquat has also been shown to lead to movement abnormalities in *Drosophila* including bradykinesia, resting tremors and rotational behaviours, which came as a result of the selective loss of DA clusters (Chaudhuri et al., 2007). Although these models are important, in particular to study the formation of the LB-like inclusions in DA neurons, they have drawbacks and the involvement of exposure to environmental toxins in the etiology of PD is still largely unknown. Furthermore, there are no recorded cases of rotenone-induced PD in humans.

### 1.4.2 Genetic models

The discovery of mutations in genes that cause PD such as *α-synuclein, parkin, LRRK2, PINK1* and *DJ-1*, has led to the development of genetic models of the disease. These models are valuable as they may help to shed light on specific molecular events that lead to the degeneration of the DA neurons in PD, as well as representing potential therapeutic targets (Jackson-Lewis et al., 2012). Three main types of cellular defects, namely abnormal protein aggregation, oxidative stress, and mitochondrial dysfunction, which are involved in the formation and/or progression of sporadic PD, have also been identified in genetic models. Thus we can speculate that the study of genetic models could lead to the identification of molecular and biochemical pathways that are involved in the pathogenesis of both sporadic and inherited PD. Having said this, autosomal-dominant transgenic models with mutations in *α-synuclein* or *LRRK2* and autosomal-recessive models with knockout of *PINK1*, *DJ-1* or *parkin* are often variable in their ability to display robust neurodegeneration and nigro-striatal pathology (Duty and Jenner, 2011).

Modelling PD using genetics has proven difficult in rodent models because they are inconsistent in their ability to capture key PD symptoms. For example, knockout, overexpression or transgenic *α-synuclein* mouse models have shown motor abnormalities, mitochondrial defects, α-synuclein-like inclusions, gliosis as well as other brain and spinal cord abnormalities, however there are no consistent reports of a progressive loss of the nigral DA neurons (Dawson et al., 2010). Despite this drawback, these mice models are very important to study α-synuclein-induced neurodegeneration. Transgenic rat models expressing the human *A30P* or *A53T α-synuclein* mutations under the TH promoter, also fail to show key PD symptoms (Lelan et al., 2011). However, these rats do show olfactory deficits that are also seen in the early phases of PD in humans. It is interesting to note that the *A53T α-synuclein* mutation causes PD in humans, whereas *53T* is the wild-type (WT) amino acid sequence in mice. Therefore, although mice are more closely related to humans in evolutionary terms than some of the invertebrate PD models, it still seems more appropriate to express the human genes to model PD. LRRK2 transgenic mouse and rat models are not very robust as there is little evidence to suggest that expression of the key *LRRK2* mutations cause DA neuron degeneration (Li et al., 2009, Li et al., 2010,

Dawson et al., 2010, Walker et al., 2014). However, most LRRK2 mouse models do display DA dysfunction such as alterations in DA neurotransmission, as well as behavioural defects that are levodopa responsive (Lin et al., 2009, Duty and Jenner, 2011). For example, bacterial artificial chromosome transgenic mice overexpressing WT *LRRK2* show an increase in dopamine release in the striatum accompanied by motor hyperactivity. Overexpressing the *LRRK2-G2019S* mutation causes an age-dependent reduction of striatal dopamine content and a decrease in striatal dopamine release and uptake, suggesting a role for LRRK2 in dopamine transmission (Li et al., 2010). *LRRK2* knockout mice are viable but they fail to show abnormalities in the DA system, DA neuronal loss, or susceptibility to MPTP (Andres-Mateos et al., 2009, Hinkle et al., 2012). In addition, *parkin*-mutant and *PINK1*-mutant mice models are also unable to show substantial DA or behavioural abnormalities (Itier et al., 2003, Perez and Palmiter, 2005, Gispert et al., 2009, Dawson et al., 2010).

Due to the difficulties of modelling PD in mice, alternative genetic models have emerged including the common fruit fly, *Drosophila melanogaster*, the nematode, *Caenorhabditis elegans*, and the zebrafish, *Danio rerio*. These models are advantageous over rodent models due to the ease of which their genome can be manipulated to model PD mutations. They also allow the identification of evolutionary conserved pathways and cellular processes implicated in the PD pathogenesis. Of these multicellular models, *Drosophila* has proven to be the most successful. Most *Drosophila* models are able to recapitulate DA neuron loss and motor defects with a good level of reproducibility. Furthermore, they have highly conserved orthologues of most of the PD-related genes including *parkin*, *PINK1*, *LRRK2*, *DJ-1* and *UCH-L1*. A variety of *Drosophila* models with mutations in these genes have been successfully developed. Although the *Drosophila* genome does not encode a clear *α-synuclein* orthologue, the first PD fly model created by Feany and Bender (2000) utilised overexpression of WT or mutant forms (*A30P* and *A53T*) of human *α-synuclein*. This resulted in a progressive loss of climbing ability, an age-dependent and selective loss of DA neurons, and filamentous intraneuronal α-synuclein inclusions. Subsequent studies have been able to confirm these phenotypes and although some discrepancies in DA neuron loss have been reported, this is likely due to differences in the sensitivity of the methods used (Munoz-Soriano and Paricio,

2011). Since the *parkin* gene is well conserved between flies and humans, a number of *parkin*-null fly models have been generated to understand its biological function. These studies have demonstrated that parkin is essential for the morphology, function and integrity of several clusters of DA neurons in the fly brain (Cha et al., 2005, Whitworth et al., 2005, Munoz-Soriano and Paricio, 2011). These *parkin* mutants also exhibit mitochondrial defects, severe deficits in motor ability, degeneration of the indirect flight muscles, reduced lifespan, and hypersensitivity to oxidative and environmental stress (Greene et al., 2003, Pesah et al., 2004, Cha et al., 2005, Munoz-Soriano and Paricio, 2011). The behavioural phenotype of these flies can be rescued with levodopa administration (Cha et al., 2005). *PINK1*-mutant flies show many phenotypic similarities to *parkin*-mutant flies including a reduction in the number of DA neurons, deficits in climbing ability and mitochondrial dysfunction (Clark et al., 2006, Park et al., 2006, Wang et al., 2006). Unlike humans, *Drosophila* has two DJ-1 orthologues, DJ-1α with its expression limited to the male germline and DJ-1β, which is ubiquitously expressed like its human counterpart (Menzies et al., 2005). Flies that are null for *DJ-1α*, *DJ-1β*, or both, are viable and do not have a reduced number of DA neurons or a reduced lifespan (Meulener et al., 2005, Park et al., 2005). Only two studies have shown that knockdown of *DJ-1*, utilising RNA interference (RNAi), can result in robust neurodegeneration and a selective age-dependent loss of DA neurons in the dorsomedial cluster (Yang et al., 2005, Lavara-Culebras and Paricio, 2007, Munoz-Soriano and Paricio, 2011). Although DJ-1 models can display PD-like phenotypes, they are more inconsistent than the other PD genetic fly models. Successful *Drosophila* models of LRRK2-linked PD have also been generated by a number of groups (see section 1.5.4).

## 1.5 Using *Drosophila* to model PD

Although attempts thus far have failed to produce a genetic model that is able to recapitulate all of the key neuropathologic and clinical features of human PD, the current models have provided us with valuable insights into PD pathogenesis. *Drosophila* has emerged as a valuable model organism in which to study PD. Flies are a promising system in which to identify evolutionary conserved genes that could be involved in the development or susceptibility of PD and therapeutic compounds that may be able to alleviate PD symptoms in both flies and humans (Dawson et al., 2010).

The next section will look at how *Drosophila* became to be such an important genetic model organism in which to study a plethora of human diseases, before focusing on *Drosophila* models of LRRK2-linked PD.

### 1.5.1 *Drosophila* as a model organism

At the beginning of the 20th century, Thomas Hunt Morgan carefully selected to use *Drosophila melanogaster* to study the chromosomal theory of inheritance. This pioneering work has helped to establish *Drosophila* as the most powerful genetic model organism. *Drosophila* is the model organism of choice in numerous groups for many reasons. Firstly, due to their small size and simple diet they can be maintained in large numbers relatively easily and inexpensively under laboratory conditions, although they do have to be continuously maintained because it is not possible to freeze them. Secondly, they are ideal for high-throughput experiments as they have a rapid generation time of 10-12 days at 25°C and females show high fecundity, producing large numbers of genetically identical progeny. The lifespan of *Drosophila* is between 40-120 days depending on environment, stress levels and diet, making them a suitable organism in which to study age-related disorders. Although flies and vertebrates diverged at the Protostome-Deuterostome split ~700 million years ago, a surprisingly large number of developmental processes are shared between *Drosophila* and humans (St Johnston, 2002). Since the entire *Drosophila* genome of ~13,600 genes across four chromosomes (the first sex chromosomes [X and Y], and the second, third and forth autosomal chromosomes) was sequenced in 2000, the extent of the similarities between *Drosophila* and humans has been revealed (Adams et al., 2000). For example, 75% of all human-related disease genes have orthologues in *Drosophila* (Reiter et al., 2001). Furthermore, *Drosophila* has orthologues of genes that when mutated cause a variety of human diseases including neurological disorders, cancer, developmental disorders, cardiovascular disease, and metabolic and storage disorders (Bier, 2005). Taken together, this shows the legitimacy of *Drosophila* as a complex multicellular organism in which to study a plethora of gene functions involved in human disease.

### 1.5.2 The genetic toolbox of *Drosophila*

The most important asset setting *Drosophila* aside from other animal models is its extensive and ever-increasing genetic toolbox, which enables manipulation of *Drosophila* in a way that is unrivalled in other model organisms. Before the genome of *Drosophila* was sequenced, Drosophilists predominantly utilised forward genetic approaches to achieve genetic manipulations. This approach involves the random generation of mutations, which can then be screened based upon specific phenotypes of interest. The technique of mutagenesis that is utilised depends on the kind of mutation that is required. Chemical mutagens are often favoured for inducing point mutations. The most efficient and commonly used chemical mutagen is ethyl methane sulphonate, an alkylating agent able to produce a high proportion of point mutations when fed to flies (Pastink et al., 1991). Radiation is favoured for producing chromosomal rearrangements. Radiation techniques, such as those using X-rays, induce chromosomal breaks, which can produce translocations, deletions, transpositions or inversions when repaired (Pastink et al., 1987). Insertional mutagenesis is favoured for rapid molecular cloning of the mutated gene. It involves the use of transposable elements that are "hopped" randomly into genes thereby disrupting their function (Ryder and Russell, 2003). The most commonly used transposons are *P*-elements, but *piggyBac*- and *hobo*-elements are also used. Although this is not the easiest form of mutagenesis and this approach alone cannot saturate the whole genome, the advantages of having a *P*-element as a tag to easily identify the affected gene can often outweigh the disadvantages (St Johnston, 2002). Forward genetic approaches have proven integral in understanding the nature and function of *Drosophila* genes. As researchers continue to develop them, these screens will remain important due to their ability to generate a variety of alleles of a gene, including nulls (amorphs) and weak partial LOF mutations (hypomorphs) (St Johnston, 2002).

With the sequencing of the *Drosophila* genome came an expansion in the *Drosophila* genetic toolbox to include reverse genetic approaches. This involves generating mutations in known genes and observing the resultant phenotypes in order to elucidate the function of that gene (Adams and Sekelsky, 2002). Reverse genetic approaches can be split into two classes. Firstly, those that utilise forward genetic

approaches, such as transposable element mutagenesis that have been modified to allow targeting of specific genes (Adams and Sekelsky, 2002). In this approach, *P*-elements inserted near to a gene of interest can be mobilised to generate specific null mutants through creating deletions in the nearby gene (Adams and Sekelsky, 2002). Homologous recombination can lead to loss of new mutations during chromosomal segregation, however balancer chromosomes have been developed and are widely used by Drosophilists to overcome this (see section 1.5.2.2). Various *P*-elements have been generated that are suitable for reverse genetic studies (Ryder and Russell, 2003). For example, *P*[PZ] and *P*[LacW] are enhancer-trap constructs, which allow characterisation of the spatial and temporal expression of genes and *P*[EP]-elements were designed for misexpression of genes (O'Kane and Gehring, 1987, Bier et al., 1989, Rorth et al., 1998). Enhancer-traps contain transformation markers, such as the *rosy* or *mini-White* constructs, which display an external phenotype (e.g. altered eye pigmentation) in the transformed fly to allow the identification of the transformants. *P*-elements also often contain a transposase recognition sequence at the 5' and 3' ends and an antibiotic resistance gene. The second class of reverse genetic approaches are those that use directed approaches to specifically alter the function of the relevant gene (Adams and Sekelsky, 2002). For example, RNAi can be utilised for targeted silencing of homologous genes (Hammond et al., 2001). This technique is based on the principle that double-stranded RNA will cause the degradation of endogenous mRNA when the sequence of the double-stranded RNA is derived from the coding sequence of the gene to be silenced.

### 1.5.2.1 The UAS/GAL4 system

A variation of the enhancer-trap technique known as the UAS/GAL4 system, revolutionised the way in which biological processes are studied in *Drosophila*. Initially developed in 1993 by Andrea Brand and Norbert Perrimon, the UAS/GAL4 system has become one of the most reliable and powerful genetic tools in *Drosophila* studies (Brand and Perrimon, 1993). This bipartite system allows the ectopic expression of any given sequence of interest, be it protein coding or noncoding RNA (e.g., RNAi), in a precise spatiotemporal pattern (Elliott and Brand, 2008). This system requires GAL4, a transcriptional activator derived from *Saccharomyces cerevisiae,* placed under the control of a tissue- or cell-specific promoter (Figure 1.3).

A transgene of choice can be placed under the control of a second component, the upstream activator sequence (UAS), to which GAL4 endogenously binds leading to the subsequent transcription of the downstream gene. These individual components can be expressed in two different fly lines, which when crossed together will result in progeny that ectopically express the gene of interest based on the expression pattern of the GAL4 line used. There is now a large collection of enhancer-trap lines publically available that express *GAL4* in a vast array of cell-type and tissue-specific patterns. In order to regulate the temporal expression of this system a second yeast protein, GAL80, can be utilised to selectively antagonise GAL4 (Elliott and Brand, 2008). GAL80 binds to the transactivation domain of GAL4 thereby preventing GAL4 from activating transcription (Lue et al., 1987, Ma and Ptashne, 1987, Lee and Luo, 1999). Temperature sensitive GAL80s have also been generated that allow a greater temporal control over the onset of expression (McGuire et al., 2003). Hormone inducible variants of GAL4 may also be used to regulate temporal expression (Han et al., 2000). When GAL4-hormone receptor chimeras are utilised, they are transcriptionally silent until bound by the appropriate ligand. This allows the onset of expression to be controlled through feeding the larvae or fly with the specific ligand at an appropriate time to activate transcription (Elliott and Brand, 2008).

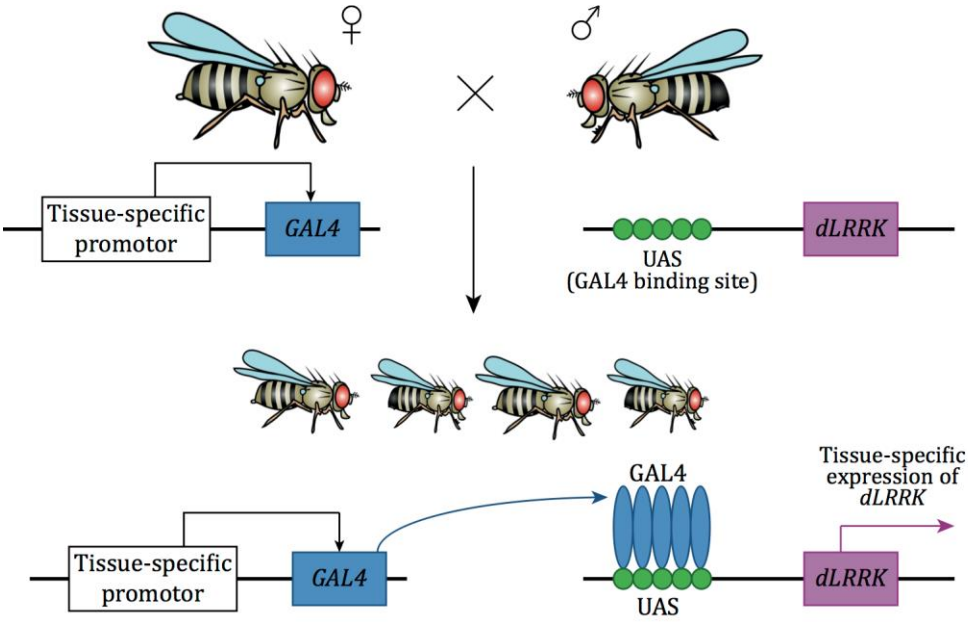


**Figure 1.3 The UAS/GAL4 system allows ectopic gene expression in a tissue-specific manner**

The UAS/GAL4 system is a bipartite system. A fly line that expresses *GAL4* under the control of a tissue-specific promotor is crossed to a second line that contains a gene of interest (in this example, *dLRRK*) downstream of the upstream activating sequence (UAS) to which GAL4 binds. When these two components are brought together in a crossing scheme, progeny will be generated in which the gene of interest is expressed only in those cells or tissue types that express the GAL4 protein. Fly images designed using the Genotype Builder from Roote and Prokop (2013).

### 1.5.2.2 Balancer chromosomes

Balancer chromosomes set fly genetics apart from genetics in all other model organisms making them one of the most important genetic tools in *Drosophila.* They contain an array of multiply inverted chromosomal segments thus preventing the correct alignment and homologous recombination during meiosis. In addition, these balancers carry recessive lethal or recessive sterile mutations, meaning that heterozygous mutations can be maintained in stable *Drosophila* stocks. Furthermore, balancer chromosomes carry dominant markers that produce a distinct external phenotype enabling the researcher to easily follow both the balancer and the mutation that is on the alternative allele during chromosomal segregation in the offspring (Figure 1.4). Due to their usefulness, balancers have been developed for the X, 2$^{nd}$ and 3$^{rd}$ chromosomes of *Drosophila*.

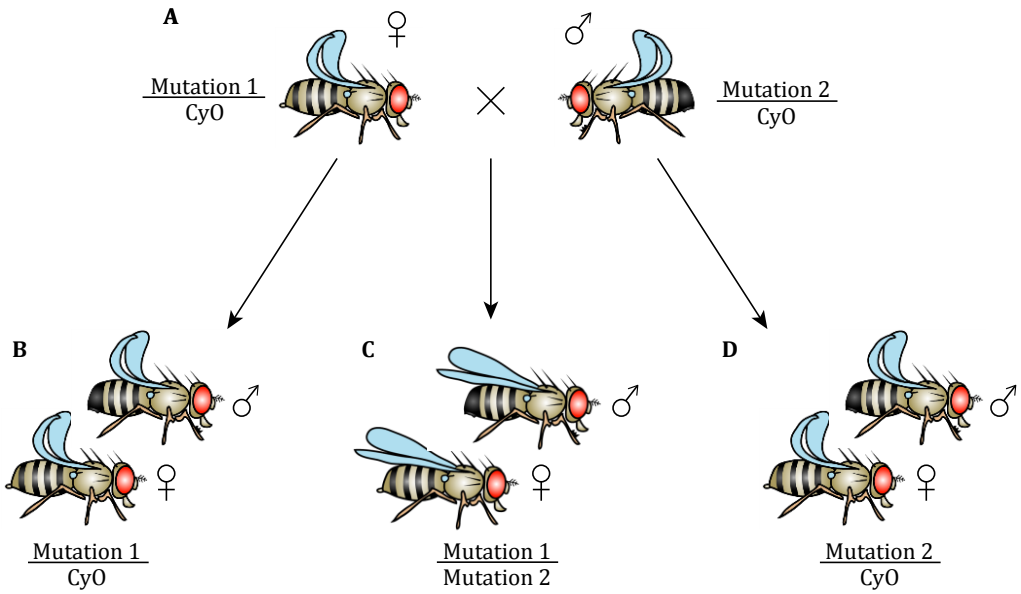


**Figure 1.4 Balancer chromosomes allow the tracking of mutations during chromosomal segregation**

Balancer chromosomes enable researchers to select flies of the desired genotype during crossing schemes. In this example, parent flies with the desired mutations are crossed together (A) to give progeny containing both mutations (C). The parent flies (A) each contain one of the desired mutations (Mutation 1 or Mutation 2) on one copy of the second chromosome and the balancer chromosome *CyO* on the alternative copy of the second chromosome. The *CyO* chromosome carries a dominant marker giving the adult fly curly wings. Therefore in this cross, chromosomal segregation will produce progeny with either curly (B and D) or straight wings (C). Progeny with curly wings must carry one of the mutations and the balancer chromosome, whilst those with straight wings must possess both Mutation 1 and Mutation 2 (one on each allele of chromosome 2) making them the desired genotype. As such, the use of balancers allows the researcher to follow alleles and confidently obtain flies of the desired genotype during crossing schemes. Fly images designed using the Genotype Builder from Roote and Prokop (2013).

### 1.5.3 Using *Drosophila* to study human neurodegenerative disorders

Neurodegenerative disorders are a subgroup of human diseases characterised by the progressive loss of structure or function of specific neuronal populations within the brain, which subsequently leads to cognitive, behavioural and physical defects. Examples of such disorders include Huntington's disease, Alzheimer's disease, PD, Amyotrophic lateral Sclerosis, and Lysosomal Storage Disorder's. Since advances in human genetics and genomics, researchers have been able to identify familial forms of these neurodegenerative disorders and thus pinpoint the disease-associated genes (Lu and Vogel, 2009). Human genetic studies have been crucial in the identification of genetic loci associated with neurodegenerative disorders, however due to both ethical and technical constraints they are of limited use for the elucidation of cellular processes and molecular pathways that contribute to the neurodegenerative development and progression (Lu and Vogel, 2009). Furthermore, neuropathological studies that utilise humans tend to occur *post-mortem,* thus they fail to provide any insight into the earliest stages of disease pathology. Animal models provide an excellent alternative in which to study the underlying pathogenic mechanisms of neurodegenerative disorders. *Drosophila* has proven to be an excellent model in which to study numerous neurodegenerative disorders for many reasons, reviewed in Cauchi and van den Heuvel (2006) and Hirth (2010) . Firstly, as previously mentioned the short lifespan of flies allows researchers to follow the progression of these age-related neurodegenerative disorders. Flies have a complex and well-characterised nervous system and are capable of displaying intricate neurological behaviours such as learning and memory. Furthermore, the fundamental cellular processes that are related to neurobiology are similar in flies and humans including synapse formation, neuronal communication, membrane trafficking and cell death (Hirth, 2010). Finally, the genetic toolbox of *Drosophila* allows the ectopic expression of human WT or mutant forms of neurodegenerative-associated disease genes; the ability to study the consequence of the loss- or gain-of function of the *Drosophila* orthologues of these disease genes; and genetic screens that can identify enhancers and suppressors that can modify a phenotype caused by the misexpression of neurodegenerative-associated disease genes (Hirth, 2010). Fly models can also be

useful in the screening of potential compounds to prevent or improve the symptoms of neurodegenerative disorders (Cauchi and van den Heuvel, 2006). This is achieved through the addition of a desired concentration of the compound to the fly food medium. The flies can either be raised on the drug-food or they can be transferred onto it during their adult stage.

### 1.5.4 *Drosophila* models of LRRK2-linked PD

As previously discussed, mutations in the *LRRK2* gene are the most common cause of genetic PD, thus several groups have exploited the vast genetic toolbox of *Drosophila* to model LRRK2-linked PD. Expressing WT or mutant forms of human *LRRK2* (*hLRRK2*) in flies has produced inconsistent results. For example, some groups have shown that flies expressing the LOF *R1441G* mutation in the ROC domain or the GOF *G2019S* mutation in the kinase domain of *hLRRK2,* have a reduction in climbing ability accompanied by a decrease in TH staining or the number of DA neurons, and retinal degeneration (Liu et al., 2008, Ng et al., 2009, Venderova et al., 2009). However, other groups have failed to find any significant neurodegeneration with *LRRK2* overexpression (Lee et al., 2007). A progressive, age-related loss of photoreceptor function has been observed with the selective expression of the *hLRRK2-G2019S* mutation specifically in the DA neurons (Hindle et al., 2013); there was no loss of photoreceptor function with DA expression of the WT *hLRRK2* transgene or other *hLRRK2* mutations. Although the external structure of the fly eye was uncompromised, the photoreceptors of old flies (28 days post eclosion [DPE]) showed extensive neurodegeneration including apoptosis, autophagy and mitochondrial disorganisation (Hindle et al., 2013). Increasing neuronal energy demands accelerated the neurodegeneration. This study suggests a spreading pathology of LRRK2-linked PD as the *hLRRK2-G2019S* mutation was expressed in the DA neurons but anatomical and functional degeneration was recorded in a different cell type, the photoreceptors. A further study demonstrated that young (1 DPE) flies with DA expression of *hLRRK2-G2019S* have increased neural activity, which could initiate an excitotoxic cascade thus leading to the degeneration of the photoreceptors reported in old flies expressing this mutation (Hindle et al., 2013, Afsari et al., 2014, West et al., 2015b). The impact of overexpressing WT *hLRRK2* or pathogenic *hLRRK2-G2019S* on the fly neuromuscular junction has also been investigated. The

postsynaptic expression of either of these transgenes does not lead to a significant alteration in mEJP frequency, amplitude, quantal content, or EJP amplitude. However presynaptic expression causes a significant increase in mEJP frequency and a reduced quantal content (Lee et al., 2010b, West et al., 2015b).

### 1.5.5 The *Drosophila* visual system as a model of the human visual system

Similarly to humans, *Drosophila* also has DA neurons that branch into the visual system (see section 1.5.5.3). The fly eye is composed of neuronal tissue and is much more accessible, easier to manipulate and easier to work with in general than the human visual system or the SNpc. Thus is provides an excellent platform for studying PD-related DA neuron loss. The following sections will describe the anatomy of the *Drosophila* visual system before comparing it with the visual system of humans.

#### 1.5.5.1 Anatomy of the *Drosophila* visual system

The visual system of *Drosophila* comprises the retina and the optic lobe, which contains approximately 60,000 cells that can be divided into four neuropiles termed the lamina, medulla, lobula and the lobula plate (Figure 1.5). The retina, or compound eye, is made up of 750 individual facets known as ommatidia that are arranged in a hexagonal crystalline array (Ting and Lee, 2007). Each ommatidium is physically separated from its neighbour and contains eight different photoreceptor (R) cells known as R1-R8 (Paulk et al., 2013). The R cells can be sub-divided in accordance with their morphology, the synaptic connections they make within the optic lobes of the brain, their position within the ommatidium, and the *opsin* genes they express (Salcedo et al., 1999, Ting and Lee, 2007). Each R cell contains a microvillar structure known as a rhabdomere that serves as the compartment for visual transduction. R1-R6 cells are the six outer photoreceptor cells; they have rhabdomeres that span the length of the ommatidium and express the Rh1 rhodopsin, which responds to a broad spectrum of light allowing light to be absorbed efficiently for their specialised function in motion detection (Salcedo et al., 1999). R7 and R8 are the inner photoreceptor cells; they have more complex patterns of *opsin* gene expression than R1-R6. R7 cells express either Rh3 or Rh4 both of which are ultra-violet absorbing

visual pigments. R8 cells express Rh5, a blue-sensitive opsin, or Rh6, a green-sensitive opsin. The R7 and R8 photoreceptors function as sensory receptors and they are required for colour vision. It is thought that R1-R6 are functionally equivalent to the vertebrate rod cells whilst R7 and R8 are the closest analogues of the vertebrate cone cells.

In contrast to the vertebrate retina, no synapses are made within the fly retina. Instead, the photoreceptors make synapses within the first optic brain region, which is located directly beneath the retina and is known as the lamina, or in the second optic brain region known as the medulla. The modular organisation of the retina is also seen in the lamina. Here, axons from R1-R6 cells target approximately 750 independent units known as cartridges and form the first synapses with downstream neurons that are involved in motion processing (Paulk et al., 2013). The lamina cartridges are composed of five different monopolar neuron cell types (L1-L5), as well as three classes of wide-field neurons including amacrine cells and centrifugal fibers from the medulla (T1, C2 and C3) (Sanes and Zipursky, 2010). The axons of R1-R6 project in a pattern that reflects the organisation of their rhabdomeres in order to bring together the visual input from six separate ommatidia (Ting and Lee, 2007). This is because the orientation of the photoreceptors within an individual ommatidium means that each R1-R6 neuron detects light from a different point in space, however due to the curvature of the eye, each R1-R6 neuron will detect light from the same point in space as one R1-R6 neuron in each of five neighbouring ommatidia (Sanes and Zipursky, 2010). This neural superposition enhances the visual sensitivity through increasing the signal-to-noise ratio of phototransduction. Pharmacological studies have revealed histamine as the photoreceptor neurotransmitter, which upon illumination of the photoreceptors binds to chloride channels causing a strong and transient hyperpolarisation of the lamina cell (Borst, 2009). As is seen in the vertebrate visual system, there are multiple contact synapses within the lamina, with a single presynaptic terminal (Meinertzhagen and O'Neil, 1991).

The R7 and R8 cells have axons that project through the lamina without making synapses here and terminate in specific layers of the medulla. The medulla is organised into layers and columns with the columns receiving input either directly

from R7 and R8, or indirectly from R1-R6 via L1-L5 (Ting and Lee, 2007). Each column is further divided into ten layers, M1-M10. The axons of R7 and R8 synapse with interneurons and transmedullary neurons in the M3 and M6 layers, respectively, whilst the lamina neurons connect to various M1-M5 layers. The axons from R7 and R8 from a single ommatidium, and lamina neurons from a single cartridge, are mostly restricted to a single column within the medulla, which maintains the retinotopic mapping of visual information within this higher optic region (Sanes and Zipursky, 2010). Approximately 50 subtypes of medulla neurons have been found that interconnect various medullary layers or they project from the medulla to specific layers of the higher visual ganglia known as the lobula and lobula plate (Fischbach and Dittrich, 1989, Ting and Lee, 2007). Like the medulla, the lobula and lobula plate are also organised into columns and layers. There are multiple pathways that link the lobula complex to regions within the central brain, although there is not yet a full account of this region of the *Drosophila* visual system.

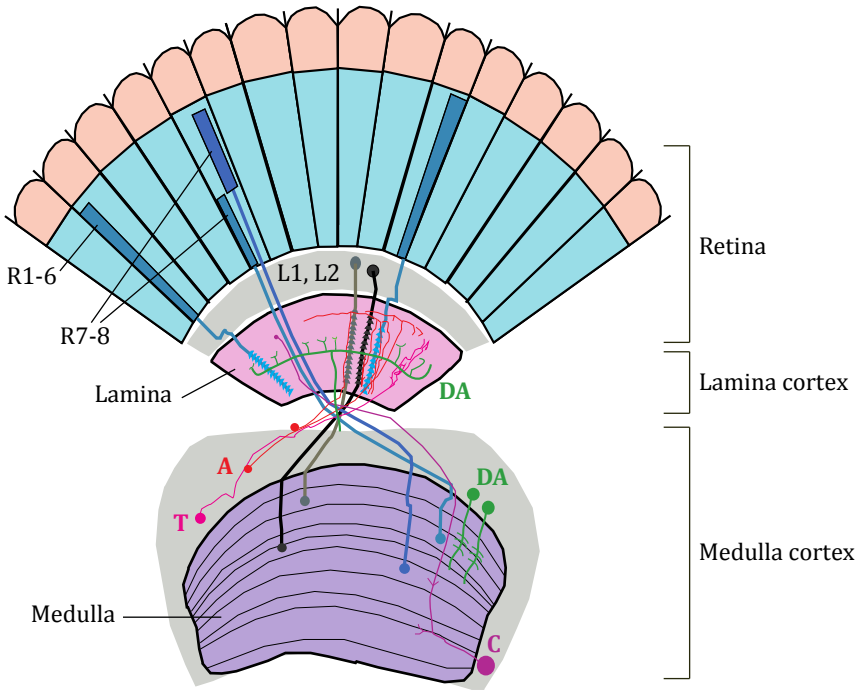


**Figure 1.5 The organisation of the *Drosophila* visual system**

A simplistic diagram of the *Drosophila* visual system showing the photoreceptors (R1-R8), the second-order lamina neurons (L1 and L2) and amacrine neurons (A), and two types of third-order medulla neurons (C and T). The diagram also shows dopaminergic neurons (DA) branching into the lamina and some that are intrinsic to the medulla. Adapted with permission from Afsari et al. (2014).

As well as the numerous neuronal types present within the fly optic lobe neuropiles, several distinct morphological types of glial cells have also been identified (Edwards and Meinertzhagen, 2010). Glia cells are non-neuronal cells that provide support and protection for the neuronal cells in both the central and peripheral nervous systems. Some of the important functions of glia include aiding neuronal development, acting as markers for axonal path-finding, providing cellular maintenance and insulation for neurons, and regulating the extracellular space of mature neurons by playing a part in neurotransmitter clearance and recycling. Within the lamina, there are six morphologically distinct types of glia, two surface glia (fenestrated and pseudocartridge glia), two types of cortex glia (distal and proximal satellite glia), and two types of neuropile glia (epithelial and marginal glia) (Edwards and Meinertzhagen, 2010). The fenestrated glia and epithelial glia are involved in endocytic clearance of excess neurotransmitters such as histamine and glutamate, the pseudocartridge glia are thought to function in the formation of the BBB, whilst the distal and proximal satellite glia and the marginal glia are important for ensheathing the monopolar neuronal cell bodies in the lamina and photoreceptor axonal projections (Edwards and Meinertzhagen, 2010). Although the glia within the medulla and lobula complex have been less well characterised than those found within the lamina, a number of major glial cell types have been identified including optic chiasm glia, cortex glia (medulla satellite glia and lobula plate satellite glia), and other neuropile glia.

### 1.5.5.2 Recording the visual response of *Drosophila*

Phototransduction is the process of converting light into electrical signals. Our understanding of the molecular mechanisms that underlie phototransduction in *Drosophila* has been achieved through a variety of molecular and genetic techniques. Both vertebrates and invertebrates carry out phototransduction via a specialised form of a G protein-coupled receptor cascade (Figure 1.6). *Drosophila* phototransduction represents one of the fastest known of these cascades with the fly photoreceptors being able to respond to single photons 10-100x faster than in vertebrate rod cells (Hardie and Juusola, 2015). Phototransduction in flies is initiated when a photon is absorbed by a molecule of visual pigments, which results in the isomerisation of the light-sensitive vitamin A derivative 11-cis 3-hydroxyretinal to

all-trans 3-hydroxyretinal; in vertebrates it is the isomerisation of the chromophore 2-dehydroretinal that is required instead of 3-hydroxyretinal. In both cases, this isomerisation results in the activation of rhodopsin, which forms metarhodopsin. In flies, metarhodopsin acts on the alpha subunit of a heterotrimeric G-protein (Gq), leading to the exchange of GDP for GTP and the activation of the G-alpha subunit. The active G-alpha subunit activates phospholipase C (PLC), which subsequently cleaves phosphatidyl inositol 4,5 bisphosphate into inositol triphosphate ($InsP_3$) and diacyl glycerol (DAG). There is an influx of calcium into the photoreceptors and two differing models have been suggested to explain how this influx occurs. One of these models proposes that the cation channels TRP and TRPL are activated when $InsP_3$ binds to the $InsP_3$-receptors, which are located in intracellular $Ca^{2+}$ stores. In turn, this leads to the release of $Ca^{2+}$ via a store-operated mechanism. The second model proposes that DAG indirectly gates the TRP and TRPL channels, which leads to an influx of $Ca^{2+}$ and $Na^{+}$ into the photoreceptors. The influx of $Ca^{2+}$ causes the photoreceptors to depolarise leading to a release of histamine at the synapse. This then triggers the hyperpolarisation of downstream neurons. Unlike *Drosophila,* vertebrate phototransduction does not utilise the inositol phospholipid signalling system. Instead, the effector for the G-protein is a phosphodiesterase that hydrolyses 3'-5' cyclic guanosine monophosphate (cGMP) to 5' GMP. This results in the closing of

cGMP-gated channels and hyperpolarisation (Hardie and Raghu, 2001, Hardie and Juusola, 2015).

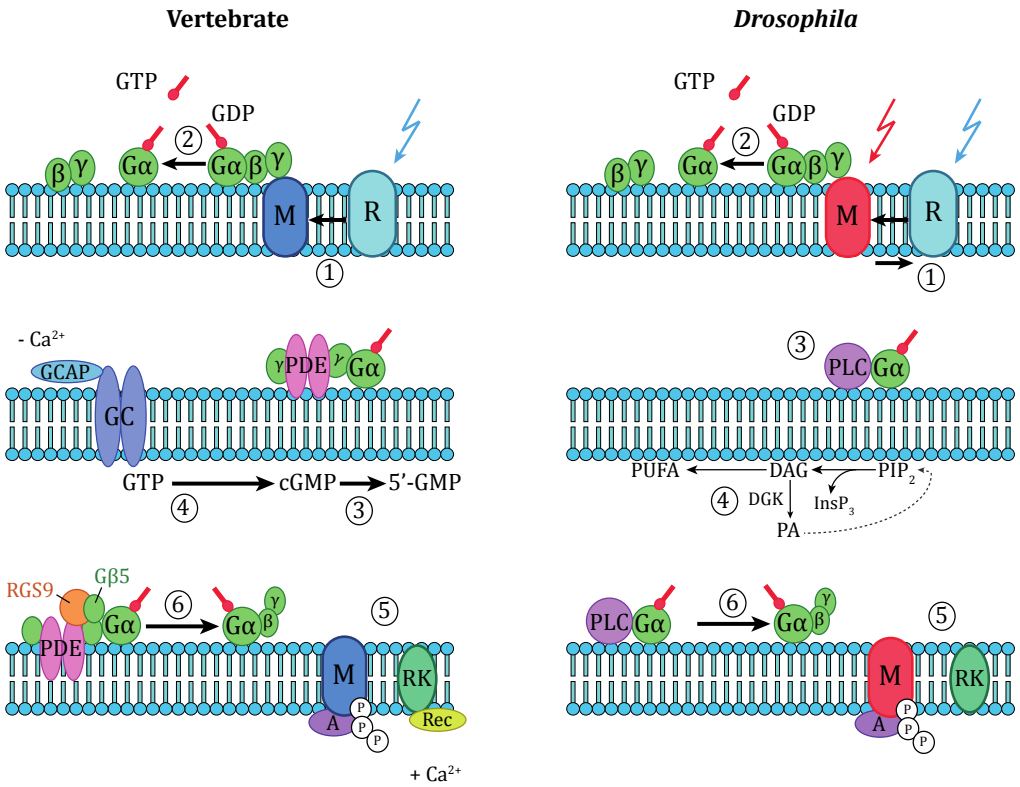


**Figure 1.6 Phototransduction cascades in vertebrates and *Drosophila***

The encircled numbers (1-6) refer to the following steps: (1) Photoisomerisation; rhodopsin (R) is photoisomerised to metarhodopsin (M). In *Drosophila,* M is stable and can be converted back to R by long-wavelength light; vertebrate M releases the bound chromophore *all-trans* retinal. (2) GTP/GDP exchange; M catalyses the exchange of GDP for GTP on the heterotrimeric G-protein (transducin in vertebrate rods, Gq in *Drosophila*), causing the active GTP bound α-subunit to dissociate. (3) Activation; Gα binds to and activates the effector enzyme (PDE in vertebrate rods, PLC in *Drosophila*). In vertebrates, activated PDE hydrolyses cGMP to 5'-GMP, which leads to the CNG channels closure. In *Drosophila,* activated PLC hydrolyses phosphatidyl inositol 4,5 bisphosphate ($PIP_2$) to diacyl glycerol (DAG) and inositol triphosphate ($InsP_3$). DAG is also a potential substrate for DAG lipase, which leads to the release of PUFAs. Two classes of channel (TRP and TRPL) are activated via an unknown mechanism. (4) Substrate resynthesis; in vertebrates, cGMP is resynthesised by guanylate cyclase (GC) and GC-activating protein (GCAP), which is inhibited by $Ca^{2+}$. In *Drosophila*, DAG is converted to phosphatidic acid (PA) by DAG kinase (DGK). PA is converted to $PIP_2$ via a multienzymatic pathway. (5) Metarhodopsin inactivation; M is phosphorylated by rhodopsin kinase (RK) and capped by arrestin (A). In vertebrates, RK is inhibited by recoverin (Rec) in

the presence of $Ca^{2+}$. (6) Inactivation of G protein and effector; the effector enzyme and Gα are inactivated by the GTPase activity of the G protein, which leads to the reassocation with Gβ, γ. This is accelerated by the activity of RGS9, Gβ5 and PDE in vertebrate rods, and by PLC in *Drosophila*. Adapted with permission from Hardie and Raghu (2001) and Hardie and Juusola (2015).

In both human and fly studies, the ERG is used to examine the visual transduction cascade. The ERG eye test in humans has been used since the late nineteen forties in order to detect abnormal function of the retina through recording the mass electrical reponse of the eye to light stimuli. The anatomy of the fly eye makes it relatively easy to record the ERG and this technique has been utilised in flies for over 50 years. The *Drosophila* ERG has proven to be invaluable in characterising many of the genes that are involved in phototransduction (Hotta and Benzer, 1969). Similarly to the human ERG, the *Drosophila* ERG uses an extracellular electrode that records the summed electrical response from the photoreceptors depolarising and the response of the lamina to the release of histamine. The depolarisation of the photoreceptors is reflected in the sustained negative component of the complex ERG waveform, whilst the hyperpolarisation and depolarisation of the lamina monopolar cells is thought to produce the on- and off-transient components, respectively (see Chapter 2 Figure 2.1) (Heisenberg, 1971, Coombe, 1986). The contributions of these cellular layers to the ERG waveform was determined through the use of mutants that selectively eliminate photoreceptor or lamina components. For example, null mutations of the histamine-gated $Cl^-$ channel gene *HisCl2* (*ort*) that causes the histamine A receptors on the second-order lamina neurons to become inactive, abolishes the synaptic transients of the ERG (Pantazis et al., 2008, Edwards and Meinertzhagen, 2010). Similarly, the $ora^{JK84}$ (outer rhabdomeres absent) mutant was isolated in which the R7 and R8 cells are the only functional receptors, meaning that the lamina receives no input as it is only the R1-R6 cells that synapse in the lamina (Harris et al., 1976). Again, in this mutant neither an on-transient nor off-transient is observed highlighting the importance of lamina signalling in the generation of the ERG synaptic transients.

A second and more sensitive visual assay that has been translated from humans (Candy et al., 2001, Tsai et al., 2012) to flies (Afsari et al., 2014) is the steady-state

visually evoked potential (SSVEP) assay. SSVEPs are natural responses generated by the brain in response to visual stimulation. Responses to flashing lights or flickering patterns generated at specific frequencies stimulates the visual system and causes this frequency to radiate throughout the brain, which produces signals at the same, or multiples of, the given frequency. This activity can be recorded via the electroencephalography method that utilises an array of electrodes placed along the scalp and the signals produced can be computed to determine visual sensitivity. The sensitivity of this assay is high because responses to many hundreds of stimulus events are averaged together and any out-of-band noise is eliminated from the analysis (Afsari et al., 2014).

An SSVEP assay has been developed for *Drosophila* through utilising a pre-programmed sequence of frequency-tagged flickering light stimuli (Afsari et al., 2014) (see Chapter 2 Figure 2.2). Through isolating the photoreceptor and neuronal responses, it has been possible to determine the contributions of the different layers of the fly visual system in generating the output frequency components (Afsari et al., 2014). For example, in *ort* null mutant flies (in which the histamine receptors are knocked out), the 1F1 response is still present but the 2F1 responses are completely abolished, suggesting that this component is a result of synaptic transient firing. The forth-order intermodulation term 2F1 + 2F2 is also completely abolished in these flies and in flies in which synaptic transmission has been eliminated through using *ort-GAL4* to drive the expression of tetanus toxin. This suggests that the 2F1 + 2F2 signal is entirely neuronal. Taken together, these data indicate that the 1F1 component arises from the photoreceptors whereas the 2F1 and 2F1 + 2F2 components depend on synaptic transmitter release from the photoreceptors, meaning that they arise from downstream signalling within the lamina and medulla. The *Drosophila* SSVEP assay also sweeps through different contrast levels allowing the analysis of population-level contrast verses response functions. It has been observed in a wide variety of previous experiments that when different contrast levels are applied to the input stimuli, there is a resultant typical rightward shift of the logarithmic input verses the output function of the neuron being observed (Phillips, 1990, Schneeweis and Schnapf, 1999, Candy et al., 2001, Busse et al., 2009, Asadollahi et al., 2010, Olsen et al., 2010, Louie et al., 2011). Some systems also show

a scaling of the outputs rather than the inputs known as response gain, which causes a downward compression of the response versus contrast curve. The contrast response functions of *Drosophila* closely resemble those seen in human and other vertebrate data with there being a clear reduction in the amplitude of the probe response when a constant mask contrast is presented at the same time (Afsari et al., 2014).

When recording the visual response of flies, the degree of pigmentation of the eye should be taken into consideration as this is known to alter the size and shape of the ERG response (Stark, 1973). In 1910, the first eye colour mutant was isolated by Thomas Hunt Morgan when he collected a white-eyed mutant male fly from a population of WT red-eyed flies (Morgan, 1910). The white eye colour was caused by a mutation in the *white* gene, which Morgan (1910) discovered as the first sex-linked gene. There are two pathways in *Drosophila* that give rise to the coloured eye pigments; these are the ommochrome pathway and the drosopterin pathway (see Chapter 5 for further details of these two pathways). Since the discovery of *white* mutant flies, numerous other eye pigment mutants have been isolated in both of these eye pigment pathways (Summers et al., 1982). Thus flies with shades of white, yellow, orange, red or brown eyes are all available. The powerful genetics of *Drosophila* enables Drosophilists to use the UAS/GAL4 system to drive the expression of a desired transgene within a specific eye colour background through exploiting mutations in one or both of the eye pigment pathways.

#### 1.5.5.3 Similarities between the *Drosophila* and human visual system

Over a century ago, the Spanish neuroanatomist Ramón y Cajal turned to the visual system of large flies in the hope of finding a much simpler sensory system than is seen in vertebrates in order to decipher the flow of information from anatomy (Sanes and Zipursky, 2010). However instead of discovering a simple visual system, Cajal found that flies have a complex and diverse visual system, which is strikingly similar to that of vertebrates. A study in *Drosophila* later showed that the complexity and cellular diversity seen in larger flies is maintained to a similar level in these smaller flies (Fischbach and Dittrich, 1989). Although noting fundamental differences, Cajal

argued that the neuronal organisation of the vertebrate and fly visual systems were essentially identical with the main design principles being maintained and only a small number of variations of adaptations. He wrote, "*if from the visual organ of the insect, we discount the crucial fact of the dislocation of the soma…then the analogy between the visual apparatus [of the vertebrates and insects] converts almost in identity*" (Sanes and Zipursky, 2010, Cajal, 1915). Cajal reinforced his argument through using silver staining to produce remarkable drawings of a fly and vertebrate visual system and a third drawing whereby he moved the cell bodies of the fly monopolar cells, without changing the positions of their synaptic contacts, so they corresponded with the position of the vertebrate retinal bipolar cells, this drawing has since been termed as the "Flertebrate" arrangement (Figure 1.7). A number of modern cytochemical and ultrastructural techniques have been utilised to compare the vertebrate and fly visual system and these have provided strong evidence in support of Cajal's view (Figure 1.8). Some of the structural similarities between the fly and vertebrate visual systems include; comprising a small number of main neuronal types (five in vertebrates; six in flies) that are further divided into numerous subtypes; having multiple cellular layers with an organised arrangement of neurons within each layer; multiple contact synapses with a single presynaptic terminal are found that adjoin multiple postsynaptic elements; and they both show a precise mapping of neuronal arrays at each level onto those within the next level (Sanes and Zipursky, 2010).

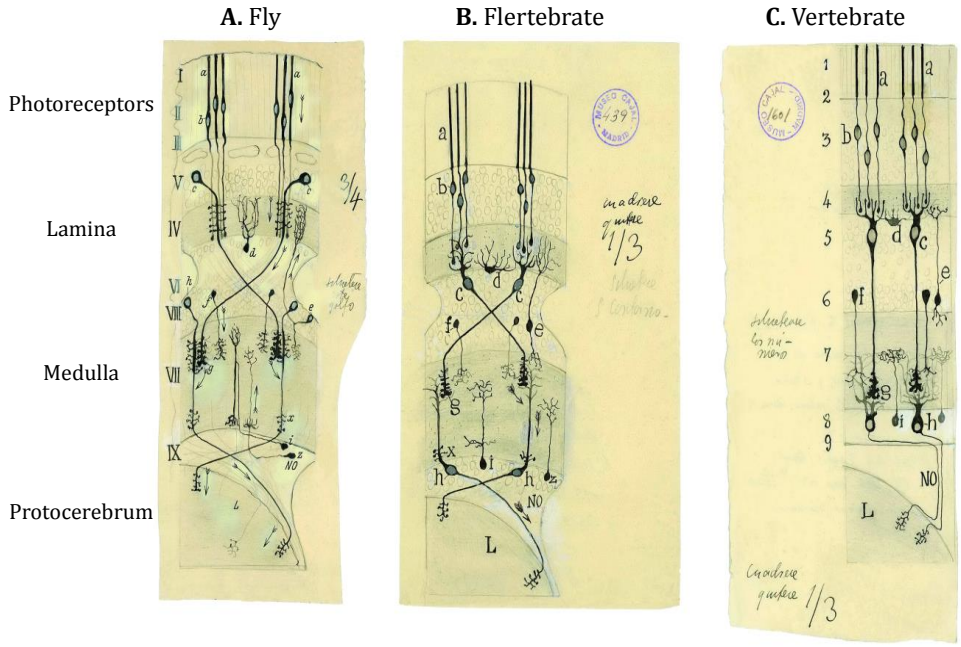


**Figure 1.7 The similarities between the neuronal networks of the fly and vertebrate visual systems**

Cajal recognised the similarities between the fly (A) and vertebrate (C) visual systems. (A) The fly visual system showing the retina (I-III), lamina (IV-V) medulla (VI-VIII) and the lobula region (L). (B) The flertebrate visual system. In this drawing of the insect visual system, Cajal redrew the cell bodies so that they correspond with their positions in vertebrates but without changing the positions of their synaptic contacts. As such, the lamina monopolar neurons take on the appearance of bipolar neurons (c); the amacrine cells take on the appearance of horizontal cells (d); and the transmedullary cells take on the appearance of retinal ganglion cells (h). (C) The vertebrate visual system showing the main cell types and their connections. Adapted with permission from Sanes and Zipursky (2010).

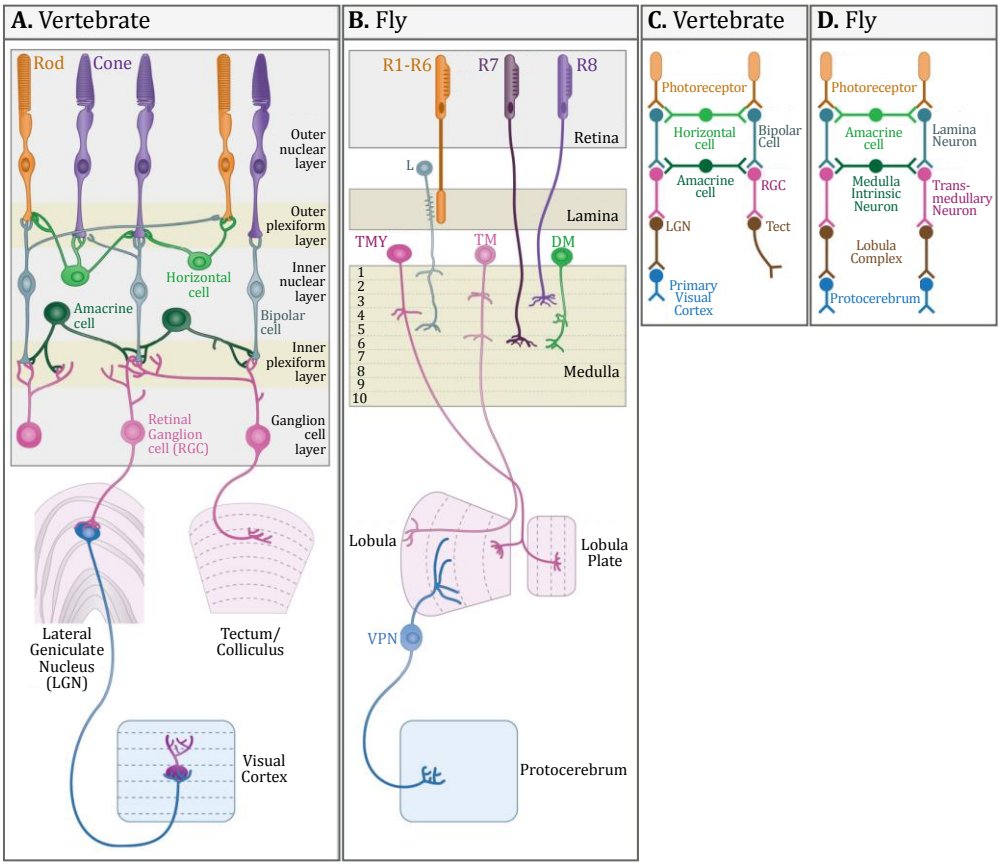


**Figure 1.8 A comparison between the structures underlying the first stages of visual processing in flies and vertebrates**

(A) The vertebrate visual system showing the retina with the main retinal cell types indicated: the lateral geniculate nucleus (LGN), the super colliculus (known as the optic tectum in lower vertebrates), and the primary visual cortex. (B) The *Drosophila* visual system showing the retina, lamina, medulla, the lobula complex comprising the lobula and lobula plate, and the protocerebrum. A few of the main cell types are shown. (C, D) Diagrammatic representation showing similar steps in transfer of information through the early stages of visual processing in vertebrates (C) and *Drosophila* (D). Adapted with permission from Sanes and Zipursky (2010).

Similarly to humans, *Drosophila* also has DA neurons with axons branching into their visual system (see Figure 1.5). Through staining with α-TH and utilising the UAS/GAL4 system to drive the expression of various GFP reporters under the control of two different DA GAL4 drivers (*TH*-GAL4 and *HL9*-GAL4), three different kinds of DA neurons have been found within the fly visual system: the PPL neurons, MC neurons and the LA neurons (Hindle et al., 2013). The cell bodies of the PPL neurons are found within the central brain and they send their axons into the lobula complex. The MC cell bodies are located on the surface of the medulla and their axons project into the medulla neuropil. The LA neuron cell bodies are in the lateral protocerebrum and their axons branch throughout the lamina. The functions of dopamine within the fly and vertebrate retina also overlap with a suggested role for dopamine in the adaptation to bright lights and in diurnal rhythms being shown in both (Chyb et al., 1999, Zimmerman et al., 2008, Hirsh et al., 2010).

## 1.6 Aims

In order for us to understand how mutations in *LRRK2* lead to PD, it is crucial that we first decipher the normal physiological function(s) of LRRK2 and the biology surrounding this protein. We may then be able to elucidate how this function is altered by pathogenic *LRRK2* mutations. The main aim of this study is to advance our understanding on the role of LRRK2 *in vivo* using the model organism *Drosophila melanogaster*. Through using a genetic model such as *Drosophila,* it is possible to exploit both LOF and GOF approaches to examine the function of LRRK2 in the visual response of flies. Studying the visual response provides us with a quantitative readout from both young and old flies, which has been difficult to achieve in other PD models. Although no stop or null mutations have been found in LRRK2, it is still important for us to determine the LOF of this protein because overexpression studies may explore the consequences of producing too much LRRK2 rather than investigating its normal physiological function. The specific contributing aims of this investigation are outlined below:

1. Determine if the LOF of *dLRRK*, the *Drosophila* orthologue of human *LRRK2*, leads to age-related visual defects in adult flies.

2. Establish if two chemically related compounds (UCA and UDCA) can rescue the visual response of flies expressing the GOF *hLRRK2-G2019S* mutation in the DA neurons.
3. Examine the interaction of eye colour and *dLRRK* genes with genetic and physiological approaches.

# 2 Materials and Methods

## 2.1 *Drosophila* husbandry and techniques

### 2.1.1 *Drosophila* stocks

*Drosophila* stocks used during this study were purchased from the Bloomington *Drosophila* Stock Centre (Indiana University, Bloomington, USA), the Vienna *Drosophila* RNAi Centre (VDRC; Institute of Molecular Biotechnology, Vienna, Austria), or were kindly donated from members of the *Drosophila* community. Rebalancing or recombining stocks already available in the Elliott and Sweeney labs also generated additional stocks. A detailed list of the stocks used during this research can be found in Table 2.1. Stocks that were obtained from outside sources were quarantined for at least two generations and were transferred to fresh media at least twice a week to ensure that they were free of mites.

Stocks were raised at either 18°C or 25°C and were transferred to fresh medium every 4 or 2 weeks, respectively. Experimental crosses were raised at 25°C, giving a generation time of ~10-12 days.

**Table 2.1 A list of *Drosophila* stocks used throughout this investigation including stock name, chromosome affected, a brief description and source from which the stock came**

| Stock | Chromosome | Description | Source |
|---|---|---|---|
| **Wild-type** | | | |
| *Canton-S* (*CS*) | n/a | Wild-type, red eyes | Elliott/Sweeney Lab Stock |
| $w^{1118}$ ($w^{-}$) | n/a | Wild-type, white eyes | Elliott/Sweeney Lab Stock |
| $w^{apricot}$ ($w^{a}$) | n/a | Wild-type, orange eyes | Bloomington Stock Centre 148 |
| **Balancer Stocks** | | | |
| *CyO*/sna$^{Sco}$ | Second | Second Chromosome Balancer | Elliott/Sweeney Lab Stock |
| TM3/TM6b | Third | Third Chromosome Balancer | Elliott/Sweeney Lab Stock |
| *CyO*-GFP/*If*; TM6b/MKRS | Second and Third | Second and Third Chromosome Balancer | Elliott/Sweeney Lab Stock |
| *CyO*/If; TM6b/MKRS | Second and Third | Second and Third Chromosome Balancer | Elliott/Sweeney Lab stock |

| Stock | Chromosome | Description | Source |
|---|---|---|---|
| **GAL4 Stocks** | | | |
| *Act*-GAL4/*CyO*-GFP | Second | Actin promoter; global driver | Elliott/Sweeney Lab Stock |
| *LongGMR*-GAL4/*CyO*-GFP | Second | Glass multimer reporter; eye specific driver | Elliott/Sweeney Lab Stock |
| *L1L2B*-GAL4/*CyO* | Second | Lamina monopolar cells L1 and L2 specific driver | (Rister et al., 2007) |
| *nSyb*-GAL4/*CyO*-GFP | Second | Neuronal Synaptobrevin promoter; pan-neuronal driver | Julie Simpson via Stephen Goodwin |
| [$w^+$]; *Rh1*-GAL4/*CyO;* MKRS/TM6B | Second | Rhodopsin 1 promoter; photoreceptor specific driver | Mikko Juusola |
| *Dmef2*-GAL4 | Second | Myocyte enhancing factor 2 promoter; somatic muscle specific driver | John Sparrow |
| *G14*-GAL4 | Second | Embryonic/larval somatic muscle specific driver | Akinao Nose, Tokyo |
| *TH*-GAL4/TM3 | Third | Tyrosine hydroxylase; DA neuron specific driver | Serge Birman via Stephen Goodwin |

| Stock | Chromosome | Description | Source |
|---|---|---|---|
| *Repo*-GAL4/TM3 | Third | Reversed polarity; Glial specific driver | Bloomington Stock Centre 7415 |
| *elav*$^{3e1}$-GAL4 | Third | Embryonic lethal abnormal vision; pan-neuronal specific driver | Elliott/Sweeney Lab Stock |
| **UAS Stocks** | | | |
| UAS-*hLRRK2*/*CyO* | Second | Human *LRRK2* transgene | H. Lundbeck A/S, Denmark |
| UAS-*hLRRK2-G2019S*/*CyO* | Second | Human *LRRK2-G2019S* mutant transgene | H. Lundbeck A/S, Denmark |
| UAS-*hLRRK2-D1994A*/*CyO* | Second | Kinase-dead human *LRRK2* transgene | H. Lundbeck A/S, Denmark |
| UAS-*Akt* | Second | Second chromosome *Akt* insertion | Bloomington Stock Centre 8191 |
| UAS-*Akt* RNAi | Second | *Akt* RNAi | Bloomington Stock Centre 31701 |
| UAS-*mLRRK1*/Sm6a | Second | Mouse *LRRK1* transgene | Generated during this study |
| UAS-*brown* | Second | Second chromosome *brown* insertion | Stephan Schneuwly |

| Stock | Chromosome | Description | Source |
|---|---|---|---|
| UAS-*cinnabar*/Sm6a | Second | Second chromosome *cinnabar* insertion | Generated during this study |
| UAS-*dLRRK* RNAi | Third | *dLRRK* RNAi | Bloomington Stock Centre 32457 |
| UAS-*hLRRK2* | Third | Human *LRRK2* transgene | (Liu et al., 2008) |
| UAS-*hLRRK2-G2019S* | Third | Human *LRRK2-G2019S* mutant transgene | (Liu et al., 2008) |
| **Mutant Stocks** | | | |
| $dLRRK^{e03680}$ | Third | PBac{RB} P-element disruption of *dLRRK*, generating a *dLRRK* null mutant | (Wang et al., 2008) |
| $dLRRK^{ex1}$/TM6b | Third | *dLRRK* loss of function, imprecise P-element excision | Bloomington Stock Centre 34750 |
| $Akt1^{04226}$/TM3 | Third | Mutant *Akt1*, derived by Insertional mutagenesis using the P-element construct P{PZ} | Bloomington Stock Centre 11627 |
| $bw^{1}$ | Second | *brown* null mutant | Bloomington Stock Centre 245 |

| Stock | Chromosome | Description | Source |
|---|---|---|---|
| *cn*$^{3}$ | Second | *cinnabar* null mutant | Flaviano Giorgini |
| *cn*$^{1}$*bw*$^{1}$/*CyO* | Second | Mutations in both *cinnabar* and *brown* generating loss of function of both genes | Bloomington Stock Centre 264 |

### 2.1.2 *Drosophila* media

Stocks were maintained in 25x95 mm plastic vials (Dutscher Scientific, UK) plugged with cotton wool (Fisher Scientific, UK) containing ~7 ml standard yeast-sucrose-agar media: 25 g/l sucrose, 3.75 g/l agar, 0.125 g/l $CaCl_2$, 0.125 g/l $FeSO_4$, 0.125 g/l $MnCl_2$, 0.125 g/l NaCl, 2 g/l $KNaC_4H_4O_6 \cdot 4H_2O$; following autoclaving and cooling for 1 hr to ~45°C, the antifungal agents Bavistin (1.5 mg/l in 100% ethanol [EtOH]; BASF, Auckland, New Zealand) and Nipagin (0.7 mg/l in 100% EtOH; Sigma, UK) were added. Experimental flies kept on this media were transferred to fresh vials every 3-4 days.

Drug experiments were performed on 4-24® instant *Drosophila* medium (Carolina Biological Supply Company, USA). The instant media was prepared by mixing 50:50 with $dH_2O$. 10 mM stocks of the drug dissolved in 100% EtOH were kept at -20°C. The appropriate volumes of these stocks were added to $dH_2O$ to give a desired concentration of 2.5 µM, before the $dH_2O$ was mixed with the instant media. Control food had the appropriate volume of 100% EtOH added with no drug. Experimental flies kept on this media were transferred to fresh media every 2-3 days.

Unless otherwise stated, experimental crosses were maintained in 1/3 pint glass bottles on a richer maize-based medium: 119.0 g/l maize meal, 17.5 g/l yeast, 15.9 g/l agar, 103.2 g/l sucrose; following cooking and cooling to ~45°C, the antifungal agents Nipagin (0.4 mg/l in 100% EtOH; Sigma, UK) and propionic acid (0.4% v/v; Arcos Organics, Geel, Belgium) were added. Once the media was transferred to 1/3 pint bottles, the bottles were bunged using sponge stoppers and were autoclaved at 121°C for 20 mins. During cooling, the media in the bottles was swirled to prevent an agar layer setting on the surface. To enhance egg-laying, dried yeast pellets were added to the surface of the bottled maize medium before the introduction of experimental crosses. The sponge stoppers were replaced with Flugs® (Dutscher Scientific, UK) after crosses were transferred to the bottled media to provide a more secure bung to prevent entry of mites. Experimental flies were maintained on the maize-based media until eclosion at which time female flies were transferred to vials containing standard yeast-sucrose-agar medium or 4-24® instant *Drosophila* media.

Experimental flies were then aged at 29°C in constant darkness or with continuous flashing blue LED lights, depending on the experimental protocol.

### 2.1.3 *Drosophila* anaesthesia

To identify gender and genotype, adult *Drosophila* were anaesthetised on a porous gas pad using continuous administration of $CO_2$. Anaesthetised adult flies were observed using a dissecting microscope (Zeiss Stemi-2000, Carl Zeiss AG, Germany).

### 2.1.4 *Drosophila* crossing techniques

Crosses were established through adding adult males to virgin female mates. As female *Drosophila* are capable of storing sperm it is essential for female flies to be collected as virgins to ensure a controlled genetic cross. At 25°C female flies should not mate within 8 hrs of eclosion, thus they can be regarded as virgins during this time period. Virgin females can be identified because newly eclosed flies have pale pigmentation, display a meconium that is visible through the abdominal cuticle, and they have unexpanded wings. Based on these principles, virgin females were collected in the morning through completely emptying vials and isolating virgins based on the presence of the aforementioned features, and then collecting any further females that eclosed within the following 8 hrs. Adult males and virgin females were crossed in a fresh vial or bottle. $F_0$ flies were removed and transferred to fresh vials or were euthanised after 7 days to prevent over-crowding and specific selection of $F_1$ flies for further crosses or experiments.

### 2.1.5 Recombinations

Homologous chromosomal recombination in female flies was utilised to generate stocks in which two genetic components were present on the same chromosomal arm. This allows for the use of three or more genetic components on a single chromosome. For example, this approach was used to recombine the *dLRRK*$^{e03680}$ *piggyBac* mutation with both *TH*-GAL4 and *Repo*-GAL4 (see Figure 2.3). Recombination is achieved through mating individual stocks with each other and selecting against balancers to identify virgin female offspring that carry the two desired genetic components. Individual flies that carry two genetic components often

have a darker eye colour, thus can be easily recognised and selected. These offspring were then crossed to males from balancer stocks for the relevant chromosome and potential recombinant offspring were selected. Where possible, these selections were made based on eye colour as well as other characteristic phenotypes. The presence of the desired genetic components was confirmed via PCR or confirmation of GFP (see section 2.3.2).

## 2.2 Physiological analyses

### 2.2.1 Flash Electroretinograms (ERGs)

Unanaesthetised adult female flies were aspirated into shortened 200 µl Gilson pipette tips so just the head was left protruding from the tip. The fly was restrained using nail varnish (Creative Nail Design). Glass pipette electrodes were filled with a simple *Drosophila* saline (130 mM NaCl, 4.7 mM KCl, 1.9 mM $CaCl_2$; (Heisenberg, 1971)). A recording electrode was placed on the surface of the eye and a second reference electrode was placed on the mouthparts using micromanipulators (Figure 2.1A). Once in position, flies were dark-adapted for 2 mins. ERGs were recorded in response to three to five stimuli (10 sec apart, 0.5 sec long) from the blue component of an LED light (Kingbright, KAF-5060PBESEEVGC, maximum emission wavelength 465 nm, Taipei, Taiwan) placed ~6 cm in front of the fly. Stimuli were monitored with a BPX65 photodiode (Centronics) placed next to the pipette tip. The photodiode current was 0.5 nA in the darkened laboratory and 400 nA during the light stimuli. DASY*Lab* software was used to record the ERGs and DASY*View* (Version 2.1.6) was used for analysis (DASY*lab* customised software, C. J. H. Elliott, University of York). The three to five stimuli were averaged for each fly. Each genotype/time-point sample is the average (±SEM) from at least ten flies. An example ERG trace is shown in (Figure 2.1B) indicating the on-transient, photoreceptor response and off-transient components.

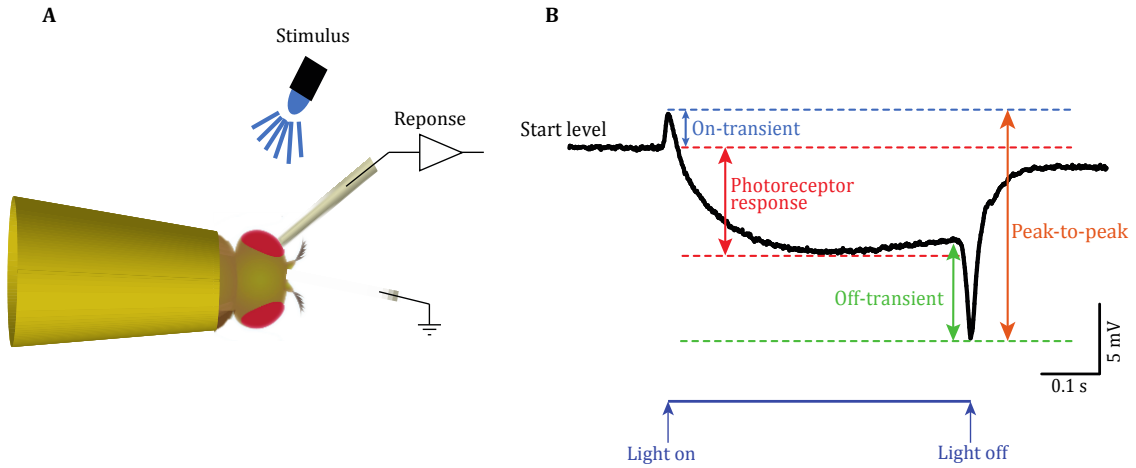


**Figure 2.1 Recording the visual response of *Drosophila* using the flash ERG**

(A) Flies are restrained in shortened Gilson pipette tips and exposed to 500 ms pulses of light from the blue component of an LED light. An electrode filled with a simple saline solution is placed on the surface of the eye to record the response of the visual network, whilst a second electrode is placed within the mouthparts to act as a reference. (B) A typical recording from a WT fly with the three main ERG components indicated. The on-transient was determined as the potential difference between the starting potential and the maximum value of the ERG trace. The photoreceptor response was determined as the potential difference between the starting level and the potential about halfway along the recording. The off-transient was determined as the potential difference between the end of the photoreceptor response and the minimum value of the ERG trace. The peak-to-peak response was determined as the potential difference between the maximum value and minimum value.

### 2.2.2 Steady-State Visually Evoked Potential (SSVEP) assay

The SSVEP assay combines features of the flash ERG (see section 2.2.1) with a computational approach that is based on human visual experiments, in which flickering stimulation is linked to the analysis of 'frequency-tagged' responses. The SSVEP assay was carried out as described in Afsari et al. (2014). Briefly, adult female flies were prepared for flash ERGs as described in section 2.2.1 and their photic responses were verified (Figure 2.2A). Flies that failed to show robust photic responses, or a high quality contact between the electrode and fly eye could not be maintained, were rejected immediately. The fly was illuminated by a separate blue light LED channel (Prizmatix) centred at a wavelength of 467 nm (Gaussian spectral profile, FWHM 34 nm). The intensity of the light was controlled by a sequence generator encoded in Matlab (Version 2013a; Mathworks, Natick, MA; Source code at http://github.com/wadelab/flyCode), with the Data Acquisition Toolbox installed. In some parts of the sequence, a single square wave flickering about the mean illumination at a frequency of 12 Hz was delivered. In other parts of the sequence, two square wave modulations with different frequencies were added together and delivered (Figure 2.2B). One of the frequencies was at 12 Hz and the other frequency was at 15 Hz. The different frequency components that are generated are referred to using previously adopted nomenclature: [harmonic]F[input], where [input] refers to the different input categories (1 = 12 Hz, referred to as the 'probe', 2 = 15 Hz, referred to as the 'mask'), and [harmonic] is the multiple of each input category. The responses to 11 different contrast levels of the probe were also recorded. The contrast levels ranged from 0 to 69% contrast in equal steps. The effect of adding in the mask was also examined. The mask was present in half of the trials and had a constant contrast of 30%. Trials containing different contrast levels were randomised across presentations and the entire sequence of 22 trials was repeated 5 times. The total data acquisition time for each fly was approximately 25 mins. Each stimulus sweep gave a signal above the system noise meaning that phase-locked responses are evident. A Fourier transform of the waveform was computed (http://github.com/wadelab/flyCode) to obtain a frequency-domain representation of the data (Figure 2.2C). Contrast response function (CRF) data were calculated and fitted using a 3-parameter hyperbolic ratio function to achieve statistical

independence as described in Afsari et al. (2014). All CRF data throughout this thesis are multiplied 1000 times so that whole numbers can be plotted on graphs.

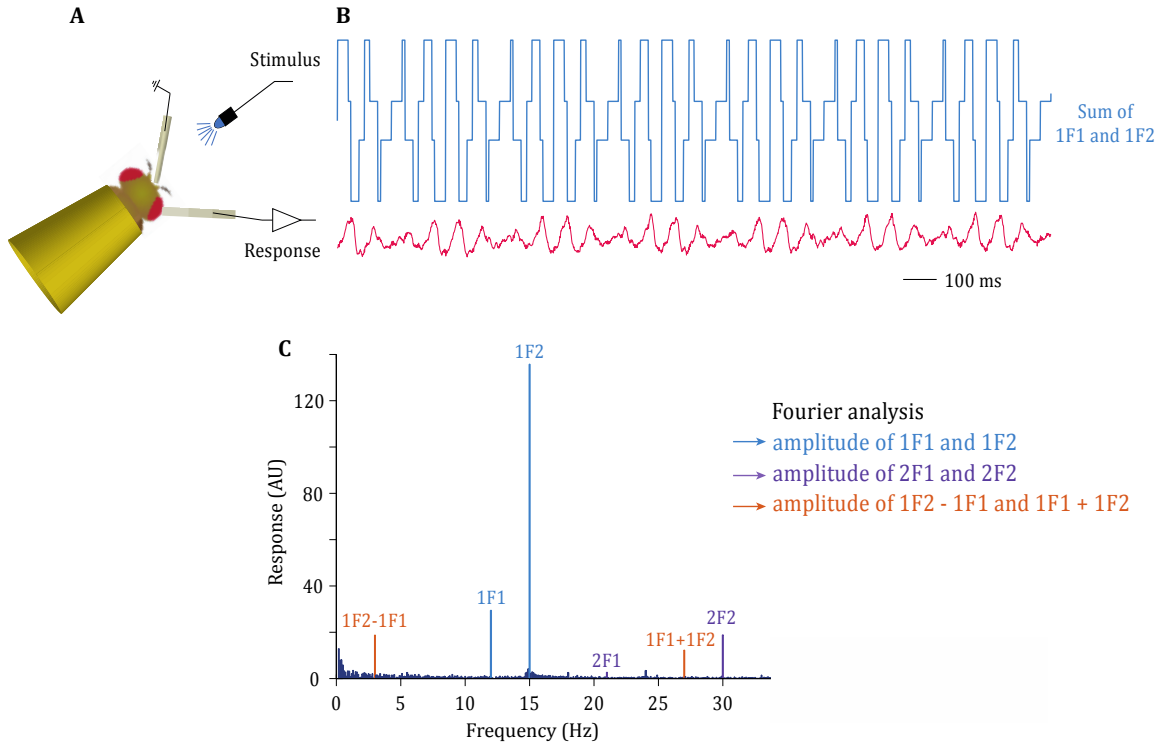


**Figure 2.2 Recording and analysing the visual response of *Drosophila* using the SSVEP**

(A) Flies are restrained in shortened Gilson pipette tips and illuminated by a blue LED that is driven by a continuously flickering wave. An electrode filled with a simple saline solution is placed on the surface of the eye to record the response of the visual network, whilst a second electrode is placed within the mouthparts to act as a reference. (B) The blue line represents the stimulus, which is the sum of two square waves of 12 Hz and 15 Hz known as 1F1 and 1F2, respectively. The red line represents a typical response (1 second of data from a single trial) to this stimulus from a white-eyed fly. (C) A Fourier analysis is used to separate the response into parts depending on frequency, which can then be plotted. Harmonics of the input frequencies (12 Hz and 15 Hz) are shown in the Fourier transform of the signal as blue (first harmonic) and purple (second harmonic) bars. Low-order intermodulation terms (1F2-1F1 and 1F1+1F2) are shown in orange.

## 2.3 Molecular biology

### 2.3.1 Extraction of genomic DNA

DNA was extracted from single adult flies through homogenisation in a 1.5 ml Eppendorf tube with 50 µl DNA extraction buffer (25 mM NaCl, 10 mM Tris-HCl pH 8.2, 1 mM EDTA) supplemented with fresh Proteinase K (200 µg/ml). The homogenate was incubated at 37°C for 30 mins before being incubated at 85°C for 10 mins to inactivate the Proteinase K. To allow separation of particulates, the homogenate was centrifuged at 13000*g* for 3 mins in a benchtop centrifuge. 1-2 µl of the supernatant was used as a PCR template. Increased concentrations of DNA could be obtained through using multiple flies for the extraction.

Alternatively, to obtain higher concentrations of DNA, genomic DNA was extracted from 15 adult flies using the Gentra Puregene DNA purification kit (Qiagen, UK) as per the manufacturer's instructions (Qiagen, 2010). 1-2 µl of genomic DNA was used per PCR reaction.

### 2.3.2 Polymerase Chain Reaction (PCR)

To amplify genomic DNA, PCR reactions were run using PCR mastermix (Promega, UK; 25 U/ml *Taq* DNA polymerase, *Taq* Reaction buffer, 200 µM of each dNTP, 1.5 mM $MgCl_2$) with 1 µM of each primer and 0.5-1 mg of genomic DNA or 1-2 ng of plasmid DNA. Reactions were run as a total volume of 20 µl in a Techne TC512 PCR thermocycler (CamLab, UK) for 30 cycles. Annealing temperatures were calculated as 5°C lower than the lowest primers melting temperature ($T_m$) with an extension time of 1 min per kb (no less than 30 secs). Primers were designed and checked using Primer3 software and were synthesised by Eurogentec (UK). A list of primers used throughout this investigation can be found in Table 2.2.

**Table 2.2 Primer sequences**

| Primer | Sequence |
|---|---|
| 3'SPLNK-PB-SEQ | ACG CAT GAT TAT CTT TAA C |
| 3'SPLNK-PB2 | CGA TAA AAC ACA TGC GTC |
| dLRRKe03680-Reverse | GGC TAA CCG ATG CAG AGG AA |
| 3'pUAST | ATC TCT GTA GGT AGT TTG TCC A |
| 5'pUAST | CTG CAA CTA CTG AAA TCT GC |

### 2.3.3 DNA agarose gel electrophoresis

Agarose gel electrophoresis was utilised to analyse DNA products from PCR or restriction enzyme digests. 0.7% and 1% agarose gels in TAE buffer (40 mM Tris acetate, 1 mM EDTA, pH 8.3) were used for large and small (<1kb) DNA products, respectively. SYBR® safe (Invitrogen, UK; 10 µl/100 ml) was added to the gels to allow visualisation of DNA using a blue light transilluminator. Before loading, bromophenol blue loading dye (0.25% w/v bromophenol blue, 30% glycerol v/v in $dH_2O$) was added to the DNA. Depending on the expected DNA product size, either a 1 kb or 100 bp DNA ladder (0.5 µg/lane; NEB, UK) was loaded alongside the DNA. Gels were run at ~80–100 V. PCR followed by gel electrophoresis were used to screen stocks for the presence of the *dLRRK*$^{e03680}$ *piggyBac*-element following recombination or standard crossing procedures. One primer was designed from the PBac{RB} P-element sequence and the other from the *dLRRK* sequence. An example gel with WT (*w*$^{1118}$), homozygous *dLRRK*$^{e03680}$ and successfully recombined *Repo*-GAL4, *dLRRK*$^{e03680}$/TM6b stocks is shown in Figure 2.3.

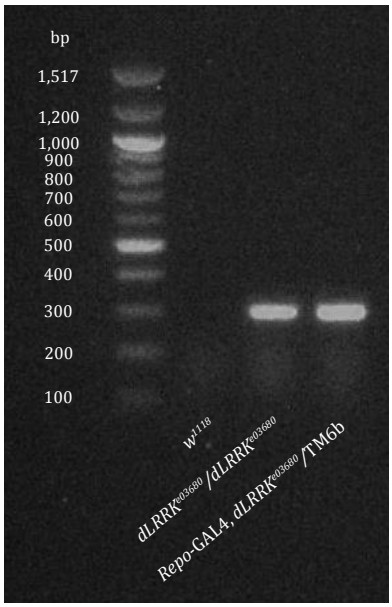


**Figure 2.3 PCR of mutant *dLRRK*$^{e03680}$ recombinants**

Primers designed to detect the presence of the PBac{RB} P-element in the *dLRRK* gene were used during PCR to determine if *dLRRK*$^{e03680}$ and *Repo*-GAL4 had successfully recombined. The WT (*w*$^{1118}$) stock was used as a negative control and the homozygous *dLRRK*$^{e03680}$ stock was used as a positive control. The PCR products were run on a 1% agarose gel in parallel with a 100 bp DNA ladder (NEB, UK). There is no band present in the *w*$^{1118}$ stock but the expected 300 bp band is present in both the homozygous *dLRRK*$^{e03680}$ stock and the *Repo*-GAL4, *dLRRK*$^{e03680}$ recombined stock, suggesting a successful recombination. Of note, the presence of *Repo*-GAL4 in this stock was determined by confirmation of GFP expression.

### 2.3.4 DNA purification; Gel extraction

DNA fragments required for cloning were excised from agarose gels, placed on a blue light transilluminator box for visualisation, using a sharp sterile scalpel. Gel slices were transferred to 1.5 ml Eppendorf tubes and processed in accordance with the QIAquick® Gel Extraction kit (Qiagen, UK) via the manufacturer's instructions (Qiagen, 2015). The DNA concentration was determined using a NanoDrop ND-1000 spectrophotometer (Thermo Scientific, DE, USA).

### 2.3.5 Restriction endonuclease digestion

Restriction enzymes are used to specifically cleave plasmids that contain restriction sites, typically in multiple cloning sites. This allows for the excision and insertion of

DNA fragments during sub-cloning. This approach was used to excise *mLRRK1* and c*innabar* from their donor plasmids and cleave the recipient plasmid, in both cases pUAST attB, for their insertion. Restriction enzymes were also used to cleave plasmid DNA from transformed clones to check for the presence of the plasmid and sub-cloned gene by gel electrophoresis. The required restriction enzymes were added to the plasmid along with the appropriate buffer with a total reaction volume of 20 µl. The DNA was used at a concentration that would provide at least 20 ng of the smallest fragment post-digestion. Reactions were incubated for at least 2 hrs at 37°C followed by a 20 min incubation at 80°C to inactivate the enzymes. Restriction products were run on an electrophoresis gel (see section 2.3.3) to ensure correct cleavage of the restriction enzymes.

### 2.3.6 DNA ligation

DNA fragments previously cleaved with restriction endonucleases, were ligated into cleaved vector plasmids using T4 DNA ligase. Ligation reactions were set up to give a 3:1 insert : vector (ng) ratio, determined using the following formula: Insert mass (ng) = 3 x (insert length bp/vector length bp) x vector mass (ng). DNA concentrations were determined using a NanoDrop ND-1000 spectrophotometer (Thermo Scientific, DE, USA). The DNA was mixed with 0.2 µl of T4 ligase (Fermentas, UK) and 2 µl T4 buffer (Fermentas, UK) in a total reaction volume of 20 µl. Reactions were incubated at 15°C overnight followed by a 10 min incubation at 65°C to inactivate the enzyme.

### 2.3.7 *E .coli* transformation and amplification of plasmid DNA

In order to generate new transgenic *Drosophila* lines, XL-1 Blue supercompetent *E. coli* cells (Stratagene, CA, USA) were used to amplify plasmid DNA. Transformation was achieved via heat-shock, mostly in accordance with the manufacturer's instructions (Stratagene, 2004). However, the protocol was modified and scaled to use 50 µl of cells instead of the recommended 100 µl. Furthermore, instead of SOC media, Luria broth (L-Broth: 10 g/l tryptone, 10 g/l NaCl, 5 g/l yeast extract) was used. For the transformation of plasmid from a ligation mix, 1 µl of the ligation reaction was utilised as recommended. For transformation of a plasmid from a Whatman® FTA® disc, 50 µl of cells were added directly to the disc following TE

washing. Post transformation cells were plated on L-Broth agar plates (20 g/l agar in L-Broth) containing the antibiotic ampicillin (200 µg/ml) for antibiotic selection. Plates were incubated at 37°C overnight.

A sterile pipette tip was used to pick individual colonies and then transferred into a sterile 15 ml falcon tube containing 5 ml sterile L-Broth and ampicillin (200 µg/ml). Cultures were incubated at 37°C for 12-16 hrs with vigorous shaking. Stocks of transformed *E. coli* were stored in 50% v/v glycerol at -80°C. Glycerol stocks were used to streak fresh plates when required.

To check for the presence of an insert within transformed colonies following a ligation during sub-cloning, the plasmid DNA must first be purified by miniprep (see section 2.3.9.1). For minipreps, 1.5 ml of each overnight culture was pelleted at 13000*g* for 2 mins in a bench-top microcentrifuge. After removal of the supernatant, pellets were frozen at -20°C. To reduce the number of minipreps required and to ascertain those colonies most likely to have taken up the insert, the colony cracking method could be performed through using 15 µl of the overnight culture (see section 2.3.8).

### 2.3.8 Colony cracking

Colony cracking was used as a quick method to screen large numbers of colonies to determine those most likely to have taken up the insert. It relies upon cell lysis using alkaline conditions and the identification of positive clones based on the electrophoretic mobility variance between supercoiled DNA plasmids containing the insert and those that do not. Plasmids carrying the insert will run slower than those that don't. Inserts as small as 200 bp can be detected.

50 µl bromophenol blue loading dye and 1 ml resuspension buffer (50 mM Tris-HCl pH 8.0, 10 mM EDTA, 100 µg/ml RNaseA) was added to 1 ml of 5x cracking buffer (25 g sucrose, 5 ml 5 M NaOH, 2.5 ml 10% SDS, 40 ml $dH_2O$). 10 µl of this was mixed with 15 µl of overnight culture. The mixture was then loaded and run on an electrophoresis gel (see section 2.3.3). An uncut empty pUAST attB plasmid was used as control, no ladder is required. Alternatively, single colonies can be patched and used directly for cracking instead of 15 µl of overnight culture. Colonies that carry the

plasmid containing the insert will run slower on the electrophoresis gel than the control plasmid. These colonies were identified and the overnight culture from which they came was purified via miniprep (see section 2.3.9.1).

## 2.3.9 Plasmid purification

### 2.3.9.1 MiniPrep purification

Frozen pellets, produced by centrifugation of 1.5 ml of overnight cultures (see section 2.3.7), were purified using the QIAprep spin miniprep kit (Qiagen, UK) in accordance with the manufacturer's instructions (Qiagen, 2010). This method allows the purification of up to 20 µg molecular biology grade plasmid DNA from *E.* coli. Concentrations of purified plasmid DNA was ascertained using a NanoDrop ND-1000 spectrophotometer (Thermo Scientific, DE, USA). The purified plasmid DNA was stored at -20°C.

Minipreps were used to check for the presence of the insert within the transformed plasmids by restriction enzyme digest (see section 2.3.5) and/or by PCR (see section 2.3.2), followed by gel electrophoresis (see section 2.3.3).

### 2.3.9.2 MidiPrep purification

To provide a greater purity of plasmid DNA (up to 200 µg of transfection-grade plasmid DNA) and greater yields for microinjection of *Drosophila* embryos, plasmids were purified using the QIAGEN HiSpeed Plasmid Midi kit (Qiagen, UK).

Having confirmed the presence of the appropriate insert via colony cracking, miniprep, restriction enzyme digest, PCR and gel electrophoresis, 100 µl of the appropriate overnight culture (see section 2.3.7) was used to inoculate 100 ml of L-Broth containing ampicillin (200 µg/ml). 100 ml cultures were incubated at 37°C overnight with vigorous shaking. Alternatively, for optimal results a single colony could be picked from patched plates (see section 2.3.8) or a freshly streaked plate, streaked from the appropriate glycerol stock, and used to inoculate a 5 ml starter culture of L-Broth containing ampicillin (200 µg/ml). Starter cultures were incubated at 37°C for 8 hrs with vigorous shaking before being used to inoculate a 100 ml

culture (100 µl in 100 ml) and incubated as above. Following incubation, 100 ml cultures were centrifuged at 6000 rpm for 15 mins at 4°C. After removal of the supernatant, the pellet was frozen before being processed in accordance with the QIAGEN HiSpeed Plasmid Midi kit protocol.

## 2.4 Generation of transgenic *Drosophila* lines

To allow the ectopic expression of the mouse *LRRK1* (*mLRRK1*) transgene or of the *cinnabar* transgene by the UAS/GAL4 system, *mLRRK1*-pUAST attB and *cinnabar*-pUAST attB were micro-injected into *Drosophila* embryos to generate two separate transgenic stocks.

### 2.4.1 Generation of *mLRRK1* pUAST attB constructs

*mLRRK1*-pUAST attB was generated through the excision of the *mLRRK1* cDNA insert from the pYX-Asc vector (cDNA clone: IRAVp968H02134D; Source BioScience, UK) using NotI and SalI restriction endonucleases in buffer D (Promega, UK; see section 2.3.5). The host pUAST attB vector was excised using NotI-HF and XhoI restriction endonucleases in buffer 4 (NEB, UK). The excised 5284 bp *mLRRK1* cDNA insert was ligated into the excised pUAST attB vector (see section 2.3.6). The ligation reaction was used to transform XL-1 Blue supercompetent *E. coli* cells (Stratagene, CA, USA), which were plated onto L-Broth-agar plates containing 200 µg/ml ampicillin and incubated at 37°C overnight. Single colonies were picked for amplification in 5 ml 8 hr cultures (see section 2.3.7). Colonies that were most likely to contain the insert were determined via colony cracking (see section 2.3.8). Those identified via colony cracking were purified by MiniPrep (see section 2.3.9.1). The presence of the insert was determined by restriction endonuclease assessment using NotI-HF and KpnI-HF in cutsmart buffer (NEB, UK; see section 2.3.5) and by PCR using pUAST primers. After confirming the presence of the insert, 100 µl of the original 8 hr culture was used to seed a 100 ml overnight culture incubated at 37°C with shaking (see section 2.3.9.2). Cultures were centrifuged at 6000 rpm for 15 mins at 4°C and the pellet was used to purify the plasmid using the QIAGEN Midi/Maxi kit (see section 2.3.9.2).

### 2.4.2 Generation of *cinnabar* pUAST attB constructs

Before the *cinnabar* cDNA insert could be excised from the pFLC-I vector, the cDNA clone first needed to be transformed from a Whatman® FTA® disc. This was achieved through quickly washing the Whatman® FTA® disc with sterile TE (pH 8.0), then transforming the plasmid using 50 µl XL-1 Blue supercompetent *E. coli* cells (Stratagene, CA, USA; see section 2.3.7). The transformed cells were plated onto L-Broth-agar plates containing 200 µg/ml ampicillin and incubated at 37°C overnight. Single colonies were picked for amplification and purification using the MiniPrep method (see section 2.3.9.1). Restriction endonuclease digest with NotI-HF and KpnI-HF in cutsmart buffer (NEB, UK) was used to ensure the pFLC-I containing the *cinnabar* cDNA insert had been successfully transformed (see section 2.3.5). After confirming this, the excised 1900 bp *cinnabar* cDNA insert was ligated into an excised pUAST-attB vector (NotI-HF, KpnI-HF; NEB, UK; see section 2.3.6). The ligation was used to transform XL-1 Blue supercompetent *E. coli* cells (Stratagene, CA, USA; see section 2.3.7). Colonies that were most likely to contain the insert were determined via colony cracking (see section 2.3.8). Those identified via colony cracking were purified by miniprep (see section 2.3.9.1). The presence of the insert was determined by restriction endonuclease assessment using NotI-HF and KpnI-HF in cutsmart buffer (NEB, UK; see section 2.3.5) and by PCR using pUAST primers. After confirming the presence of the insert, 100 µl of the original 8 hr culture was used to seed a 100 ml overnight culture incubated at 37°C with shaking (see section 2.3.9.2). Cultures were centrifuged at 6000 rpm for 15 mins at 4°C and the pellet was used to purify the plasmid using the QIAGEN Midi/Maxi kit (see section 2.3.9.2).

### 2.4.3 Ethanol precipitation of DNA

Following midipreps (see section 2.3.9.2), the plasmid DNA concentration of both *mLRRK1*-pUAST attB and *cinnabar*-pUAST attB was determined using a NanoDrop ND-1000 spectrophotometer (Thermo Scientific, DE, USA). For microinjections into *Drosophila* embryos, a plasmid concentration of 0.4 µg/µl is required. To achieve this concentration, pUAST attB constructs were precipitated with a 1/10$^{th}$ volume of NaOAc + 3 volumes 100% ice cold EtOH (calculated after addition of NaOAc), and incubated at -20°C overnight. Precipitated DNA was pelleted by centrifugation at

13000*g* for 30 mins at 4°C in a bench-top microcentrifuge. The supernatant was decanted and the pellet was washed with 1 ml 70% EtOH followed by centrifugation at 13000*g* for 10 mins. The supernatant was decanted and the pellet was air dried for ~5-10 mins. Pellets were re-suspended in the appropriate volume of sterile nuclease-free $H_2O$. The concentration of the precipitated plasmid DNA was determined using a NanoDrop ND-1000 spectrophotometer (Thermo Scientific, DE, USA).

### 2.4.4 Microinjection of *Drosophila* embryos

For microinjections, the *mLRRK1*-pUAST attB and c*innabar*-pUAST attB constructs were sent to the University of Cambridge, Department of Genetics, Fly Facility. The phiC31 integrase system was utilised for microinjections. The phiC31 integrase is a sequence-specific recombinase that is encoded within the genome of the phiC31 bacteriophage. The phiC31 integrase mediates recombination between two 34 bp sequences known as attachment sites (att), one found within the donor plasmid (attB) and the other found within the target genome (attP). In the presence of phiC31 integrase an attB- containing donor plasmid can be unidirectionally integrated into the target genome through recombination with the attP site. The phiC31 fly stock used for microinjections during this investigation was the Bloomington stock 24482, (genotype: y[1] M{vas-int.Dm}ZH-2A w*; M{3xP3-RFP.attP'}ZH-51C) which has an attP site on the 2$^{nd}$ chromosome (51C), marked with RFP to make it easier to identify those stocks in which plasmid integration was successful. Successful lines were balanced over a 2$^{nd}$ chromosomal balancer and the integrase was removed before being sent back from Cambridge.

## 2.5 Western blotting

Western blotting was used to assess the levels of total Akt and phosphorylated Akt in flies expressing WT *hLRRK2, hLRRK2*-G2019S and control flies. The method used for western blotting was adapted from Abcam (2016).

### 2.5.1 Protein extraction

Protein was extracted from whole adult fly heads as previously described (Emery, 2007). Flies were collected in 15 ml falcon tubes and were snap frozen on dry ice. The

15 ml falcon tubes were placed into 50 ml falcon tubes containing a small amount of dry ice and vortexed 2-3 times to remove the heads from the bodies. 30 heads per genotype were collected and transferred to 1.5 ml Eppendorf tubes on dry ice. Fly heads were stored at -80°C until all genotypes had been collected. To extract protein, one complete mini protease inhibitor cocktail tablet (cOmplete tablet, Mini EDTA-free, *EASYpack*; Roche) was dissolved in 7 ml RIPA buffer (150 mM NaCl, 1.0% IGEPAL® CA-630, 0.5% sodium deoxycholate, 0.1% SDS, 50 mM Tris, pH 8.0; Sigma, UK) and 2X Halt™ phosphatase inhibitor cocktail (Thermo Fisher Scientific Pierce, UK) was added. 30 µl of this protease/phosphatase inhibitor cocktail was added to tubes of 30 fly heads placed on ice. Heads were homogenised using a sterile plastic pestle before being centrifuged at 13000*g* for 15 mins at 4°C. The supernatant was removed and the protein concentration was quantified using the Bradford assay (see Section 2.5.2).

### 2.5.2 Quantification of protein concentration: Bradford assay

Binding of protein to the Coomassie dye in the Bradford reagent leads to a colour shift from red/brown to blue. The absorbance of the reagent-protein complex can be recorded at 595 nm. Bovine serum albumin (BSA) standards (0, 25, 125, 250, 500, 750 and 1000 µg/ml) were prepared and 10 µl of each standard was loaded in duplicate into a 96-well plate. Protein samples were diluted 2 µl in 23 µl $dH_2O$ (1:12.5). 10 µl of diluted protein sample were loaded into the 96-well plate in paired duplicates. 200 µl of Coomassie Plus reagent (Thermo Fisher Scientific Pierce, UK), warmed to room temperature (RT), was added to both the standards and the protein samples. The absorbance was then recorded on a Multiskan Ascent 96/384 plate reader (Thermo Scientific, UK). A BSA standard curve was produced through measuring the absorbance of the known concentrations of BSA. The protein concentrations of the unknown samples were calculated using this standard curve.

### 2.5.3 Sodium Dodecyl Sulphate Polyacrylamide Gel Electrophoresis (SDS-PAGE)

Known amounts of protein sample were mixed in a 3:1 ratio with sample buffer (100 µl β-mercaptoethanol in 900 µl 4x laemmli buffer) before heating to 85°C for 5 mins.

Protein samples and a protein ladder (6 µl Color Prestained Protein Standard, Broad Range [11-245 kDa]; NEB, UK) were loaded into a 10% Mini-PROTEAN® TGX™ pre-cast gel (BIO-RAD, UK) placed in a tank containing running buffer (25 mM Tris, 192 mM glycine, 0.1% SDS). Protein samples were separated through running the gel at 100 V on ice for ~1.5 hrs.

### 2.5.4 Protein transfer to a PVDF membrane

Following SDS-PAGE, a Mini-Trans-Blot® Cell was used to transfer the proteins from the gel to a PVDF membrane (Amersham Hybond 0.45 µm PVDF; GE Healthcare, UK). Foam pads, 4 pieces of Whatman® gel blot paper (0.8 mm thick; Thermo Fisher Scientific Pierce, UK) and the SDS-PAGE gel were soaked in transfer buffer (25 mM Tris, 192 mM glycine, 20% [v/v] methanol, 0.1% [w/v] SDS). PVDF membrane was cut to the same size as the gel then activated in 100% methanol for 30-60 secs followed by a quick dip into the transfer buffer. One of the soaked foam pads was placed onto the negative (black) side of a Mini Gel Holder Cassette followed by 2 pieces of soaked Whatman® gel blot paper, the gel, the activated PVDF membrane, the remaining two pieces of Whatman® gel blot paper and the remaining foam pad, ensuring no bubbles were trapped between the layers. The cassette was then placed into the tank along with the transfer buffer and a Bio-Ice Cooling unit that had been stored at -80°C. Proteins were transferred to the PVDF membrane by applying 100 V for 1 hr at 4°C.

### 2.5.5 Probing of PVDF membrane

Following the transfer of proteins to the PVDF membrane, the membrane was blocked for 1 hr in 5% (w/v) BSA or 3% (w/v) Marvel milk in TBS-T (Tris buffered saline [10 mM Tris, pH 7.6, 150 mM NaCl] supplemented with 0.1% [v/v] Tween™-20). This was followed by primary antibody incubation in either 5% (w/v) BSA or 3% (w/v) Marvel milk in TBS-T overnight at 4°C. Membranes were subsequently washed (5 x 3 min) in TBS-T. The appropriate species of secondary antibody (conjugated to HRP) was added in either 5% (w/v) BSA or 3% (w/v) Marvel milk in TBS-T for 1 hr at RT. Excess secondary antibody was removed via washing membranes (5 x 3 min) in TBS-T. All washes and antibody incubations were performed on a rocking platform.

Membranes were incubated in ECL reagent (GE Healthcare, UK) for 1 min. CL-XPosure™ x-ray film (Thermo Fisher Scientific Pierce, UK) was placed on the blot for 5 sec (α-myosin) or 20 sec (α-Akt or α-phospho-Akt). Exposed film was developed in Carestream® Kodak® autoradiography GBX Developer/Replenisher (Sigma, UK) for 1 min, rinsed in $H_2O$ for 30 secs, then fixed in Carestream® Kodak® autoradiography GBX Fixer/Replenisher (Sigma, UK) for 1 min. Antibody concentrations can be found in (Table 2.3).

**Table 2.3 Antibody Species, Source and Dilutions used for Western Blotting**

| Antibody | Species | Source | Dilution |
|---|---|---|---|
| α-Akt (pan) (C67E7) | Rabbit monoclonal | Cell Signaling Technology | 1/1000 |
| α-Phospho-Akt (Ser473) (D9E) XP® | Rabbit monoclonal | Cell Signaling Technology | 1/1000 |
| α-Myosin (MAC147) | Rat monoclonal | Abcam | 1/50000 |
| α-Rabbit IgG HRP-linked | Goat | Cell Signaling Technology | 1/1000 |
| α-Rat IgG HRP-linked | Goat | Cell Signaling Technology | 1/1000 |

## 2.6 Measurement of mitochondrial complex activity

### 2.6.1 Isolation of mitochondria

Mitochondria-enriched fragments were prepared from the heads of adult female flies (7 DPE) with the indicated genotype, that had been kept in a 29°C flashing light incubator on food containing drug or no drug, as previously described in Pogson et al. (2014). A total of 30 fly heads were used for each genotype/drug combination. Fly heads were removed from bodies by snap freezing flies on dry ice followed by vortexing at high speed. The separated fly heads were collected in 1.5 ml Eppendorf tubes and stored at -80°C. Fly heads were gently crushed in 200 µl chilled isolation buffer (250 mM sucrose, 10 mM Tris-HCl pH 7.4, 0.15 mM $MgCl_2$) using a sterile plastic pestle. Homogenised samples were centrifuged twice at 500x*g* for 5 min at 4°C to remove debris, the supernatant was transferred to a fresh tube between each cycle. The supernatant was centrifuged at 5000x*g* for 5 min at 4°C. The resulting pellet containing mitochondrial-enriched fragments was re-suspended in 20 µl isolation buffer and stored at -80°C. The protein concentration of each sample was quantified using the Bradford assay (see section 2.5.2).

### 2.6.2 Preparation of samples for recording mitochondrial complex activity

The same sample was used for all mitochondrial complex assays (Complex I, II, III, IV and the citrate synthase assay), and three repeats of each genotype/drug treatment sample was used per assay. 250 µl assay buffer (25 mM $KH_2PO_4$, 5 mM $MgCl_2$, pH 7.2) was added to each sample followed by three cycles of rapid freeze-thawing in liquid nitrogen. Samples were briefly vortexed to ensure an even distribution of mitochondrial-enriched fragments. Diluted samples were used on the day that they were defrosted. The methods used for recording the activity of complexes I-IV and the citrate synthase assay (described in detail below) have been previously published by Birch-Machin et al. (1994) and Pogson et al. (2014).

### 2.6.3 Complex I activity

Complex I activity was determined by following the oxidation of NADH at 340 nm with a reference wavelength of 425 nm ($\varepsilon$ = 6.22 $mM^{-1}$ $cm^{-1}$) at 30°C using a BMG Labtech FLUOStar plate reader. The complex I assay buffer contained 3 mM KCN, 2.5 mg/ml BSA, 50 µM ubiquinone, and 2 µg/ml antimycin A that were added fresh daily to the stock assay buffer (25 mM $KH_2PO_4$, 5 mM $MgCl_2$, pH 7.2). 190 µl complete assay buffer minus X µl mitochondrial extract was added per well of a 96-well plate. For each sample, 0 µl, 5 µl, 7.5 µl, 10 µl and 12.5 µl of mitochondrial extract were used; these volumes were added to the appropriate volume of complete assay buffer. The baseline was recorded for 10 cycles before the reaction was started with addition of 250 µM NADH and recorded for a further 80 cycles. To inhibit the reaction, 3 µg/ml rotenone was added and measured for 10-15 cycles. The results are expressed as µmol NADH oxidised/min/citrate synthase activity.

### 2.6.4 Complex II activity

Complex II activity was measured by following the reduction of DCPIP at 600 nm ($\varepsilon$ = 19.2 $mM^{-1}$ $cm^{-1}$) at 30°C using a BMG Labtech FLUOStar plate reader. The electron acceptor ubiquinone is linked to the dye DCPIP to increase the sensitivity of the assay. The complex II assay buffer contained 3 mM KCN and 20 mM succinate added fresh

daily to the stock assay buffer (25 mM $KH_2PO_4$, 5 mM $MgCl_2$, pH 7.2). 195 µl complete assay buffer minus X µl mitochondrial extract was added per well of a 96-well plate. For each sample, 0 µl, 5 µl, 7.5 µl, 10 µl and 12.5 µl of mitochondrial extract were used; these volumes were added to the appropriate volume of complete assay buffer. After a 10 min incubation at RT, 50 µM DCPIP, 2 µg/ml antimycin A, and 3 µg/ml rotenone were added to each used well. After a 2 min incubation at RT, the baseline was recorded for 10 cycles. The reaction was started with the addition of 50 µM ubiquinone and recorded for a further 80 cycles. The results are expressed as µmol DCPIP reduced/min/citrate synthase activity.

### 2.6.5 Complex III activity

Complex III activity was measured by following the reduction of cytochrome c at 550 nm with a reference wavelength of 580 nm in a BMG Labtech FLUOStar plate reader at 30°C. A 1 mM stock of ubiquinol was made from adding EtOH, acidified with pH 2.0 6 M HCl, to ubiquinone followed by the addition of excess sodium borohydride. This was left overnight on ice then centrifuged for 10 min at 2000*g* at 4°C. The complex III assay buffer contained 2.5 mg/ml BSA, 2 mM KCN, 15 µM cytochrome c, 2 µg/ml rotenone and 0.6 mM n-Dodecyl β-D-maltoside added fresh daily to the stock assay buffer (25 mM $KH_2PO_4$, 5 mM $MgCl_2$, pH 7.2). 193 µl complete assay buffer minus X µl mitochondrial extract was added per well of a 96-well plate and a baseline was recorded for 10 cycles. 35 µM ubiquinol was added to each well and the non-enzymatic reaction was recorded for 10 cycles. For each sample, 0 µl, 10 µl, 15 µl, 20 µl and 30 µl of mitochondrial extract were used; these volumes were added to the appropriate volume of complete assay buffer containing ubiquinol and the reaction was recorded for a further 80 cycles. To fully reduce the cytochrome c, a few grains of ascorbate was added to each well and the reaction recorded for a further 10-15 cycles. The rates were calculated as a first order constant and the results are expressed as K/min/citrate synthase activity.

### 2.6.6 Complex IV activity

Complex IV activity was measured by following the oxidation of reduced cytochrome c at 550 nm, with a reference wavelength of 580 nm in a BMG Labtech FLUOStar plate

reader at 30°C. A 15 mM stock of cytochrome c was made in assay buffer (20 mM $KH_2PO_4$, pH 7.2) followed by the addition of excess ascorbate. 50 ml assay buffer was run through a 25G sephadex column before the 15 mM cytochrome c stock was added to the column. The fractions of reduced cytochrome c were collected dependent on colour (darker red fractions were preferable) and stored at -80°C. The absorbance of reduced cytochrome c fractions was measured at 550 nm and 565 nm to check for full reduction, and the stock concentration was calculated using the extinction coefficient 27.7 $mM^{-1}$ $cm^{-1}$. The complex IV assay buffer contained 150 µg/ml n-Dodecyl β-D-maltoside added fresh daily to the stock assay buffer. 197.5 µl complete assay buffer minus X µl mitochondrial extract was added to each well of a 96-well plate. For each sample, 0 µl, 12.5 µl, 15 µl, 17.5 µl and 20 µl of mitochondrial extract were used; these volumes were added to the appropriate volume of complete assay buffer and the baseline was recorded for 10 cycles. Dependent upon the earlier calculation, the appropriate volume of cytochrome c was added to each well and the reaction was recorded for 80 cycles. To fully oxidise the cytochrome c, a few grains of potassium fericyanide was added to each well and the reaction was recorded for 10-15 cycles. The rates were calculated as a first order constant and the results are expressed as K/min/citrate synthase activity.

### 2.6.7 Citrate synthase assay

Citrate synthase is an enzyme that is unique to mitochondria. Therefore, measuring the citrate synthase activity gives an estimate of the mitochondrial content of a sample. The assay follows the production of 5 thio-2-nitrobenzoate at 30°C using a BMG Labtech FLUOStar plate reader. The citrate synthase assay buffer contains 50 µM acetyl coenzyme A, 0.1 mM DTNB and 0.1% Triton X-100 added fresh daily to 100 mM Tris HCl (pH 8.0). 197.5 µl complete assay buffer minus X µl mitochondrial extract was added per well of a 96-well plate. For each sample, 0 µl, 5 µl, 7.5 µl, 10 µl and 12.5 µl of mitochondrial extract were used; these volumes were added to the appropriate volume of complete assay buffer and the baseline was recorded for 10 cycles. The reaction was started by the addition of 0.5 mM oxaloacetic acid and recorded for 80 cycles.

## 2.7 Statistical analysis

All statistical analyses were carried out in IBM SPSS Statistics v22. Student's t-test was performed to test for statistical significance between two groups; univariate ANOVA followed by a Bonferroni post-hoc test was performed to test for statistical significance between multiple groups; and univariate ANOVA followed by a post-hoc Dunnett's comparison was performed when comparing genotypes to a WT control. Although the visual neurons are all linked in the same neural network, the responses from the photoreceptors, lamina and medulla were treated as independent events, with separate univariate ANOVAs as previously described in Afsari et al. (2014), rather than a multivariate approach. This decision was based on the idea that the visual network would use feedback to regulate signalling in each layer of the network (Zheng et al., 2006, Tuthill et al., 2014, Hu et al., 2015). Statistical significance was defined as $p<0.05$ throughout.

# 3 Transcellular Signalling is Key to LRRKs *in vivo* Role

## 3.1 Introduction

### 3.1.1 *Drosophila* LRRK

*Drosophila* has a single orthologue (CG5483) of the *hLRRK2* and *hLRRK1* genes known as *Drosophila LRRK* (*dLRRK*; Figure 3.1). dLRRK is composed of ~2400 amino acids and shares 24% identity and 38% similarity at the amino acid level with hLRRK2 (Wang et al., 2008, Langston et al., 2016). dLRRK contains ankyrin repeats, several leucine-rich repeats, a kinase domain and a GTPase domain, but it does not have a WD40 domain (Wang et al., 2008). Interestingly, hLRRK1 also lacks the WD40 domain making the overall domain structure of dLRRK more similar to the smaller hLRRK1 protein (1981 amino acids) than to the larger hLRRK2 (2527 amino acids). The GTPase domain of dLRRK shows 33% and 30% identity to the GTPase domain of hLRRK2 and hLRRK1, respectively, and the dLRRK kinase domain shows 36% and 38% identity to the respective kinase domains of hLRRK2 and hLRRK1 (Langston et al., 2016).

There are broad similarities between *dLRRK* and *hLRRK2*. For example, like *hLRRK2*, *dLRRK* is also ubiquitously expressed and the dLRRK protein has been shown to associate with membranous structures including exosomes, lysosomes, synaptic vesicles and mitochondria (Imai et al., 2008, Lee et al., 2010b, Dodson et al., 2012, Lee et al., 2012b, Lin et al., 2015). In addition, the critical residues that are mutated in LRRK2-linked PD are conserved between flies and humans (Imai et al., 2008). There also appears to be at least partial conservation of function between dLRRK and hLRRK2; both are active kinases capable of autophosphorylation (Imai et al., 2008, Greggio et al., 2009, Kamikawaji et al., 2009, Gloeckner et al., 2010); both are suggested to interact with multiple Rab proteins (Shin et al., 2008, Dodson et al., 2012, MacLeod et al., 2013, Dodson et al., 2014, Yun et al., 2015, Steger et al., 2016) and to associate with Argonaute-1 of the RNA-induced silencing complex (Gehrke et al., 2010); and there is evidence to suggest that they can both phosphorylate some of

the same substrates (Lee et al., 2010b, Matta et al., 2012, Martin et al., 2014, Arranz et al., 2015). Furthermore, *dLRRK* knockdown and *hLRRK2* overexpression show reciprocal effects (Matta et al., 2012, Martin et al., 2014), whilst overexpression of *dLRRK* or overexpression of *hLRRK2* have the same effect (Lin et al., 2010). Several studies using flies have also shown that transgenic expression of either mutant *dLRRK* or mutant *hLRRK2* in the DA neurons results in the loss of DA neurons (Imai et al., 2008, Liu et al., 2008, Gehrke et al., 2010, Lin et al., 2010). However, other studies have failed to recapitulate the reduction in the number of DA neurons with expression of mutant *hLRRK2* (Ng et al., 2009, Hindle et al., 2013).

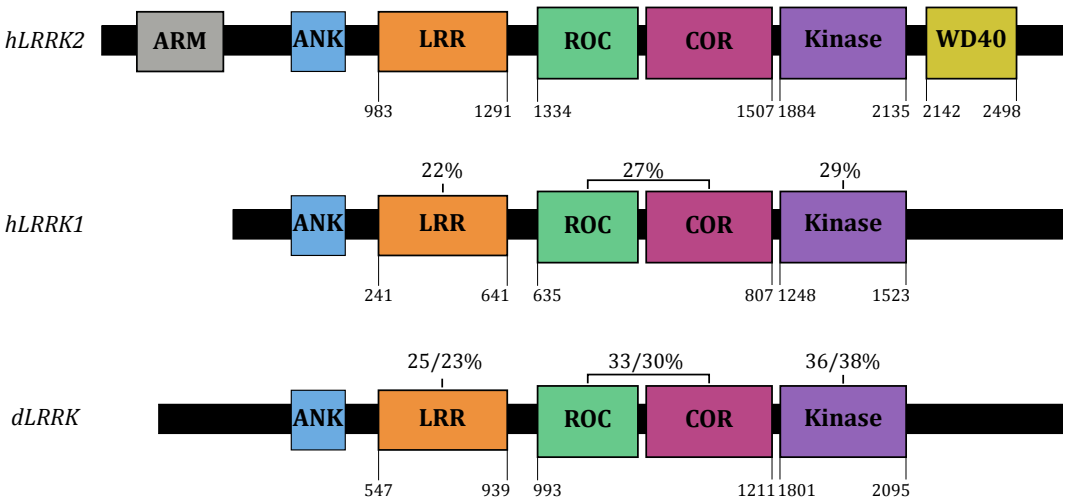


**Figure 3.1 Schematic diagrams of human *LRRK2*, the homologous human *LRRK1* and the single *Drosophila* orthologue *dLRRK***

The labelled boxes indicate the predicted domains of each LRRK protein. Percentage identities based on Clustal 2.1 multiple sequence alignment are given for the LRR, ROC-COR and kinase domains. These percentages are written above the appropriate domain. For *hLRRK1,* percentages are given relative to *hLRRK2;* for *dLRRK* percentages are given relative to *hLRRK2* (left) and *hLRRK1* (right). Adapted with permission from (Langston et al., 2016).

Several studies have attempted to study the role of dLRRK using flies in which the expression of *dLRRK* has been ablated, however opposing results have been found from different laboratories. Imai et al. (2008) and Wang et al. (2008) suggested that dLRRK is not required for the survival and maintenance of DA neurons because they found that loss of dLRRK function did not lead to changes in the number or patterns of the DA neurons. In one of these studies, although the overall DA neuron number was unchanged, the dopamine content was increased in the brains of *dLRRK*$^{-}$ LOF flies compared with WTs (Imai et al., 2008). As this could not be attributed to changes in DA neuron number, it was thought that alterations in dopamine transmission, storage or metabolism were the cause. Controversially, Lee et al. (2007) found that loss of dLRRK function caused a severe reduction in TH staining and a shrunken morphology of the DA neurons, as well as impaired locomotor activity, suggesting DA neuron degeneration.

Inconsistent results have also been found when exposing *dLRRK*$^{-}$ LOF mutants to oxidative stress agents with some mutants being sensitive to hydrogen peroxide but not to rotenone, paraquat or β-mecaptoethanol whilst others were significantly more resistant to hydrogen peroxide (Imai et al., 2008, Wang et al., 2008). Biochemical and genetic analyses have provided evidence to suggest that dLRRK phosphorylates the eukaryotic initiation factor 4E-binding protein (4E-BP), a negative regulator of protein translation and a key mediator in survival responses to cellular stress. Therefore, it is possible that dLRRK modulates the survival of DA neurons through regulating protein synthesis, whereas pathogenic forms of dLRRK or hLRRK2 lead to a deregulation or mis-regulation of cell survival pathways (Imai et al., 2008, Dawson et al., 2010).

Contrasting results have also been found when studying synaptic transmission in *dLRRK*$^{-}$ LOF mutants; Lee et al. (2010b) found that *dLRRK*$^{-}$ LOF flies have a significant depletion in EJP amplitudes causing deficits in synaptic transmission, whereas Matta et al. (2012) found no difference in the EJP amplitude between *dLRRK*$^{-}$ LOF mutants and WT flies. This discrepancy may be attributed to the fact that different *dLRRK*$^{-}$ LOF mutant alleles were utilised by the two different groups (West et al., 2015b).

In light of these discrepancies, the role of dLRRK needs to be further clarified. The visual system of *Drosophila* provides an excellent representative model of the human visual system as previously discussed in Chapter 1. Furthermore, the anatomy of the fly eye makes it relatively easy to record the ERG. Thus, in this study we have utilised the ERG as a rapid assay to study the role of dLRRK within the fly visual system whilst taking advantage of the powerful genetic toolbox of *Drosophila.*

## 3.2 Aims

1. Examine the role of dLRRK in the visual response through recording the ERG of flies with the LOF of *dLRRK.*
2. Determine where *dLRRK* expression is required for normal visual function.
3. Establish if *dLRRK* orthologues can substitute as effectively as *dLRRK* in the visual response.

## 3.3 Results

### 3.3.1 Loss of *dLRRK* causes an age-related, progressive loss of synaptic signalling from the photoreceptors to the lamina

In order to determine if dLRRK plays a key role within the visual system, the ERG was utilised to record the visual response of flies in which the expression of *dLRRK* had been lost. As previously discussed in Chapter 1, ERGs measure the extracellular potential that is generated by the summed neuronal activity from the photoreceptors and the underlying second-order lamina neurons in response to pulses of light. *Drosophila* ERGs were recorded through placing a glass capillary electrode, filled with a simple saline solution, on the surface of one eye and a second reference electrode against the mouthparts (see Chapter 2, Figure 2.1). The potential difference between the two electrodes was recorded in response to 3-5 pulses of light. The R1-R6 photoreceptors show a maximum response to blue light (Harris et al., 1976), thus a blue LED was used to deliver the light pulses.

Two different *dLRRK*$^{-}$ LOF fly lines were tested. The first fly line, *dLRRK*$^{e03680}$ (referred to as *dLRRK*$^{-}$/*dLRRK*$^{-}$ throughout this thesis), is a kinase-null mutant of *dLRRK* due to a *piggyBac*-element insertion in the intron between exon five and six (Wang et al.,

2008). This fly line has a truncated form of the dLRRK protein consisting of ANK, LRR and Rac domains. Homozygous *dLRRK$^{e03680}$* mutant flies are viable, fertile and do not develop with any obvious external abnormalities. They also show a similar, albeit slightly reduced, lifespan to their WT counterparts. The second *dLRRK*$^{-}$ LOF fly line was the *dLRRK$^{ex1}$* line (Lee et al., 2007). This fly line was generated through imprecise excision of an EP-element in a separate transgenic insertion stock known as *dLRRK$^{G7459}$*. This imprecise excision results in a 464 bp deletion that includes the stop codon of the *dLRRK* coding sequence, which gives rise to the *dLRRK$^{ex1}$* LOF line. Homozygous *dLRRK$^{ex1}$* mutants show an age-related reduction in fertility, fecundity and impaired locomotive activity (Lee et al., 2007). For these reasons and to eliminate possible second-site mutations, the *dLRRK$^{ex1}$* mutant was not used as a homozygous line but was crossed to the *dLRRK$^{e03680}$* line to generate a *dLRRK*$^{-}$ LOF transheterozygote line (referred to as *dLRRK$^{ex1}$*/*dLRRK*$^{-}$ throughout this thesis). The *Canton-S* (*CS*) fly line was outcrossed to a second WT line, *w$^{1118}$*, to generate the *CS*/*w$^{1118}$* line that was used as the WT control for these experiments. Outcrossing these two WT lines to each other ensured that possible second-site mutations due to inbreeding were eliminated. *CS* and *w$^{1118}$* flies were also outcrossed to *dLRRK$^{e03680}$* flies to generate two heterozygote *dLRRK*$^{-}$ LOF lines referred to as *CS*/*dLRRK*$^{-}$ and *w$^{1118}$*/*dLRRK*$^{-}$, respectively. All of these flies were raised on standard yeast-sucrose-agar media and aged at 29°C.

To determine if there is an age-dependent deterioration in the visual response of mutant or control flies, ERGs were recorded from adult flies at 3, 7, 14 and 21 days post eclosion (DPE). The degree of pigmentation of the eye is known to affect the size of the ERG due to the absorbance of light by the pigment (Stark, 1973). Due to the variation in eye colour between the genotypes used here (red for *CS*/*w$^{1118}$* and *CS*/*dLRRK*$^{-}$; orange for *dLRRK*$^{-}$/*dLRRK*$^{-}$; light orange for *dLRRK$^{ex1}$*/*dLRRK*$^{-}$ and *w$^{1118}$*/*dLRRK*$^{-}$), the average peak-to-peak responses (see Chapter 2 Figure 2.1) for each time-point were plotted as a percentage of the 3 DPE responses for each genotype (Figure 3.2). The peak-to-peak responses of WT (*CS*/w$^{1118}$) and heterozygote (*CS*/*dLRRK*$^{-}$ and *w$^{1118}$*/*dLRRK*$^{-}$) flies showed a reduction of between 5-8% from 3 to 21 DPE, and there were no significant differences in the responses from these genotypes at any age. However, *dLRRK*$^{-}$ LOF flies (*dLRRK*$^{-}$/*dLRRK*$^{-}$ and

*dLRRK*$^{ex1}$/*dLRRK*$^{-}$) showed a 24% and 20% reduction in their peak-to-peak responses from 3 to 14 DPE, and a 44% and 37% reduction from 3 to 21 DPE, respectively. At 14 DPE, the responses of *dLRRK*$^{-}$/*dLRRK*$^{-}$ flies were significantly lower than the WT responses ($p$<0.05), and at 21 DPE the responses of both *dLRRK*$^{-}$/*dLRRK*$^{-}$ and *dLRRK*$^{ex1}$/*dLRRK*$^{-}$ flies were significantly lower than WTs (both $p$<0.001). This suggests that *dLRRK*$^{-}$ LOF flies have a progressive, age-dependent deterioration in their visual response.

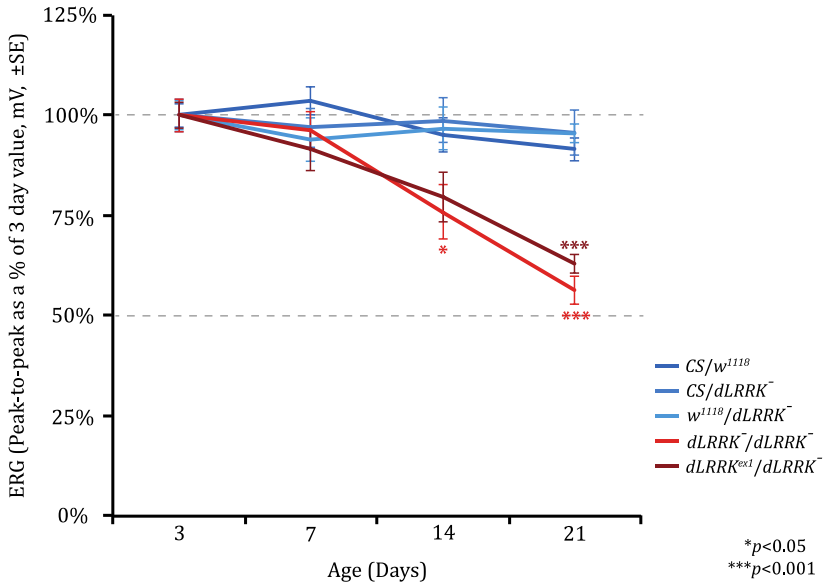


**Figure 3.2 *dLRRK*⁻ LOF flies show an age-related, progressive deterioration in their visual response**

The 3, 7, 14 and 21 DPE ERG peak-to-peak responses as a percentage of the 3 DPE value recorded from WTs (*CS*/*w*$^{1118}$), *dLRRK*⁻ heterozygotes (*CS*/*dLRRK*⁻ and *w*$^{1118}$/*dLRRK*⁻), and *dLRRK*⁻ LOF mutants (*dLRRK*⁻/*dLRRK*⁻ and *dLRRK*$^{ex1}$/*dLRRK*⁻). The peak-to-peak responses of WT and *dLRRK*⁻ heterozygote flies were maintained from 3 to 21 DPE, showing only a 5-8% decrease in amplitude. The *dLRRK*⁻ LOF mutants showed an age-dependent, progressive loss of their visual response with the peak-to-peak responses decreasing by 24% (*dLRRK*⁻/*dLRRK*⁻) and 20% (*dLRRK*$^{ex1}$/*dLRRK*⁻) from 3 to 14 DPE, and a further 20% (*dLRRK*⁻/*dLRRK*⁻) and 17% (*dLRRK*$^{ex1}$/*dLRRK*⁻) decrease from 14 to 21 DPE. At 14 DPE, the peak-to-peak responses were significantly lower in *dLRRK*⁻/*dLRRK*⁻ flies compared with WTs (ANOVA with post-hoc Dunnett's comparison to WT control, *$p$<0.05). At 21 DPE, both *dLRRK*⁻/*dLRRK*⁻ and *dLRRK*$^{ex1}$/*dLRRK*⁻ flies had significantly reduced responses compared with WTs (ANOVA with post-hoc Dunnett's comparison to WT control, both ***$p$<0.001). The responses of *dLRRK*⁻ heterozygotes did not differ significantly from WT controls at any age. n≥15 for each genotype/age combination. Data presented are mean ± SEM bars.

As previously discussed in Chapter 1, individual components of the ERG trace represent output of certain components of the phototransduction cascade in the visual system. Therefore, valuable information can be gained through studying the individual components of the ERG trace and the integrity of synaptic transmission between the photoreceptors and the underlying lamina can be determined. Figure 3.3 shows representative ERG traces from each genotype at 3, 14 and 21 DPE. The traces are set to the same scale to aid comparison between genotypes. The difference in size of the ERG traces between genotypes reflects the difference in eye colour; $w^{1118}$/*dLRRK*$^{-}$ flies have the lightest coloured eyes and show the biggest ERG responses and *CS*/*dLRRK*$^{-}$ flies have the darkest coloured eyes and show the smallest ERG responses. The genotypes with lighter coloured eyes ($w^{1118}$/*dLRRK*$^{-}$, *dLRRK*$^{-}$/*dLRRK*$^{-}$ and *dLRRK*$^{ex1}$/*dLRRK*$^{-}$) also show the characteristic negative voltage deflection that immediately follows the on-transient, which has been suggested to be caused by an increased initial photoreceptor response in the absence of dark screening pigment (Vilinsky and Johnson, 2012). At 3, 14 and 21 DPE, all components of the ERG (on-transient, off-transient and photoreceptor response) were maintained in the control and heterozygote genotypes. Although all components of the ERG were evident in 3 DPE *dLRRK*$^{-}$ LOF flies, by 14 DPE the off-transient component was severely reduced and by 21 DPE it was almost completely absent. A deterioration of the photoreceptor response and on-transient also became evident by 21 DPE in these flies. The off-transient component reflects the depolarisation of the lamina in response to the release of histamine from the photoreceptors following light-onset. The initial loss of this component by 14 DPE suggests that *dLRRK*$^{-}$ LOF flies have an age-related loss of synaptic transmission from the photoreceptors, which further deteriorates by 21 DPE.

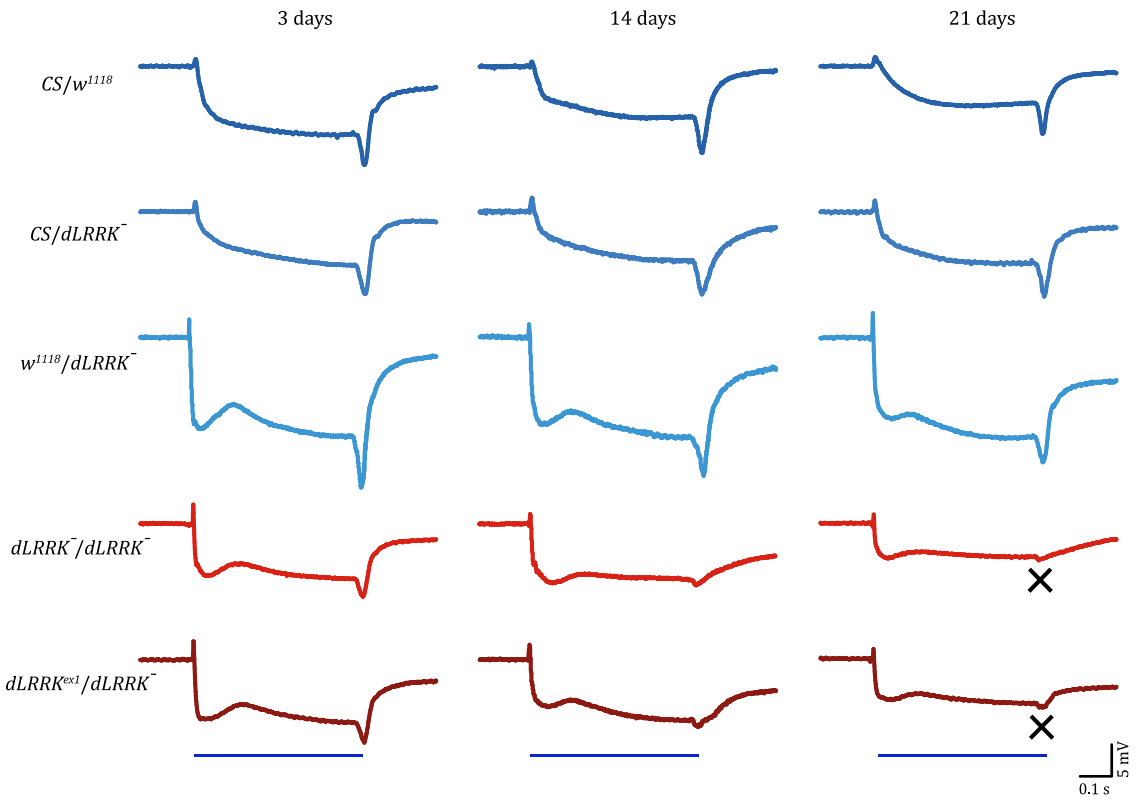


**Figure 3.3 *dLRRK*⁻ LOF flies show an age-related, progressive loss of synaptic signalling from the photoreceptors to the underlying lamina**

Representative ERG traces from 3 (left), 14 (middle) and 21 (right) DPE WT (*CS*/$w^{1118}$; dark blue), *dLRRK*⁻ heterozygote (*CS*/*dLRRK*⁻ and $w^{1118}$/*dLRRK*⁻; shades of blue), and *dLRRK*⁻ LOF flies (*dLRRK*⁻/*dLRRK*⁻ and $dLRRK^{ex1}$/*dLRRK*⁻; shades of red). ERGs are recorded in response to 0.5 second blue light pulses. The blue lines drawn below the bottom ERG traces represent the duration of the light pulse. The on-transient, photoreceptor response and off-transient components were maintained in the WT and *dLRRK*⁻ heterozygote flies at all ages. The off-transient component of the *dLRRK*⁻ LOF flies was severely reduced by 14 DPE and was almost completely absent by 21 DPE (indicated by the black crosses). The on-transient and photoreceptor responses were also reduced in the *dLRRK*⁻ LOF flies at 21 DPE. Scale bars for time (seconds) and potential (mV) are shown. Each trace is the average of the fly's response to at least three flashes of light.

Each component of the ERG was quantified separately for each genotype using DASY *View* software and the average values were plotted for 3, 14 and 21 DPE (Figure 3.4A-D, white bars, grey bars, and coloured bars, respectively). As indicated by the example ERG traces, there were no significant differences between any of the individual ERG components from 3 to 21 DPE for *CS*/*w*$^{1118}$ and *CS*/*dLRRK*$^{-}$ flies. However, the ERG off-transient recorded from *w*$^{1118}$/*dLRRK*$^{-}$ flies showed a 26% decrease in the size from 3 to 21 DPE, which was found to be significant ($p$<0.01); the on-transient and photoreceptor components were maintained with age in these flies. The peak-to-peak responses of both *dLRRK*$^{-}$ LOF lines were significantly reduced from 3 to 14 DPE (*dLRRK*$^{-}$/*dLRRK*$^{-}$: 24% decrease [$p$<0.01]; *dLRRK*$^{ex1}$/*dLRRK*$^{-}$: 20% decrease [$p$<0.001]), 3 to 21 DPE (*dLRRK*$^{-}$/*dLRRK*$^{-}$: 44% decrease [$p$<0.001]; *dLRRK*$^{ex1}$/*dLRRK*$^{-}$: 37% decrease [$p$<0.001]), and 14 to 21 DPE (*dLRRK*$^{-}$/*dLRRK*$^{-}$: 26% decrease [$p$<0.05]; *dLRRK*$^{ex1}$/*dLRRK*$^{-}$: 21% decrease [$p$<0.05]). At 14 DPE, the decrease in the ERG amplitude recorded from the *dLRRK*$^{-}$ LOF fly lines was due to a significant reduction in the off-transient component (*dLRRK*$^{-}$/*dLRRK*$^{-}$: 56% decrease [$p$<0.001]; *dLRRK*$^{ex1}$/*dLRRK*$^{-}$: 45% decrease [$p$<0.001]), as all other components were maintained at this time-point. By 21 DPE, both *dLRRK*$^{-}$ LOF fly lines also showed significant reductions in the on-transient (both ~30% decrease [$p$<0.01]) and photoreceptor responses (both ~30% decrease [$p$<0.001]), and the off-transient component had reduced even further (*dLRRK*$^{-}$/*dLRRK*$^{-}$: 70% decrease [$p$<0.001]; *dLRRK*$^{ex1}$/*dLRRK*$^{-}$: 62% decrease [$p$<0.001]). The off-transient component showed a greater reduction in size from 3 to 21 DPE in the *dLRRK*$^{-}$ LOF flies compared to the *w*$^{1118}$/*dLRRK*$^{-}$ flies (62-70% vs 26%, respectively). As previously mentioned, the loss of the off-transient component indicates that these flies have a deficit in synaptic transmission from the photoreceptors to the underlying lamina.

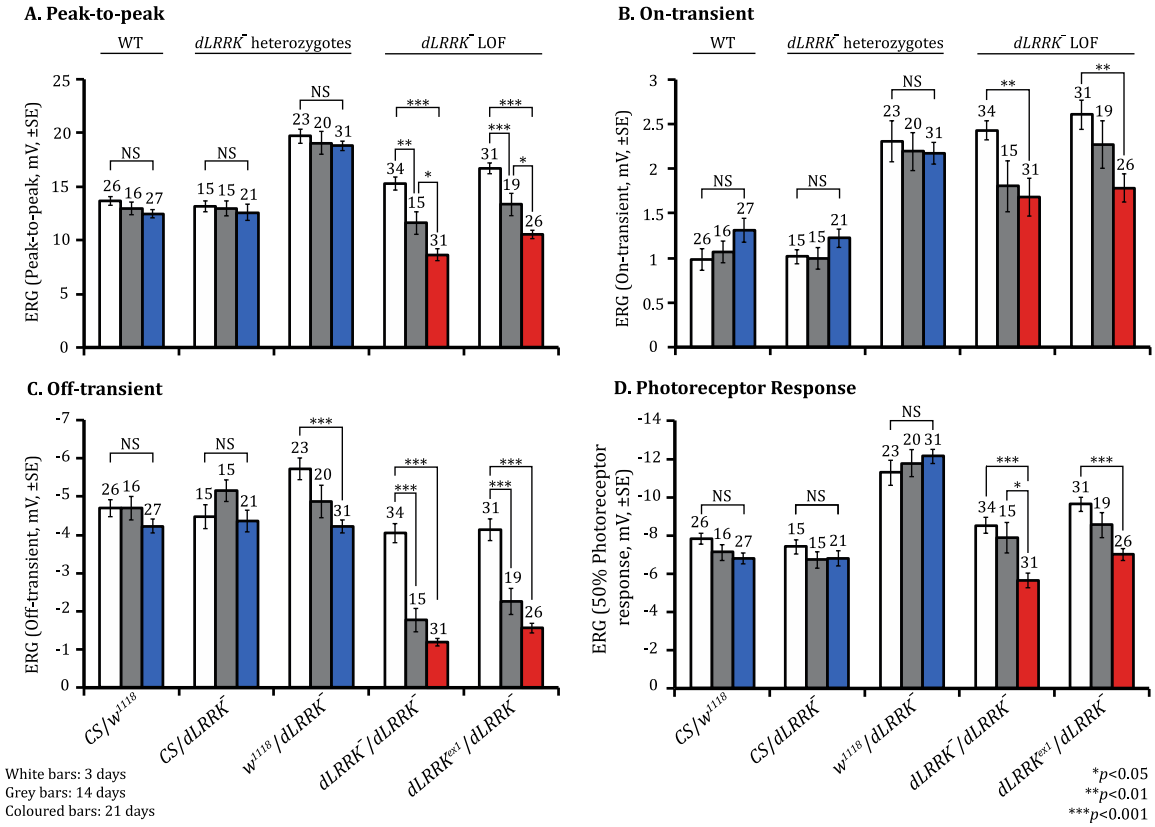


**Figure 3.4 Quantification of the individual ERG components showing the progressive deterioration in visual function of *dLRRK*⁻ LOF flies**

ERG peak-to-peak responses (A), on-transient (B), off-transient (C) and photoreceptor responses (D) were quantified for WT (*CS*/*w*$^{1118}$), *dLRRK*⁻ heterozygote (*CS*/*dLRRK*⁻ and *w*$^{1118}$/*dLRRK*⁻), and *dLRRK*⁻ LOF flies (*dLRRK*⁻/*dLRRK*⁻ and *dLRRK*$^{ex1}$/*dLRRK*⁻) at 3 (white bars), 14 (grey bars) and 21 (coloured bars) DPE. (A-D) All ERG components were significantly reduced by 21 DPE in *dLRRK*⁻ LOF flies. The off-transient was the first component to be lost, showing a significant reduction by 14 DPE, which was followed by the loss of the on-transient and photoreceptor responses at 21 DPE. The off-transient component of *w*$^{1118}$/*dLRRK*⁻ flies was also significantly reduced by 21 DPE. Apart from the off-transient of *w*$^{1118}$/*dLRRK*⁻ flies, all ERG components were maintained from 3 to 21 DPE for WT and *dLRRK*⁻ heterozygotes. All statistics are ANOVA with post-hoc Bonferroni correction: ***$p$<0.001, **$p$<0.01, *$p$<0.05, NS, no significant difference, $p$>0.05. Data presented are mean ± SEM bars; n numbers are displayed above the bars.

### 3.3.2 Reduced gene expression of *dLRRK* leads to a loss of synaptic signalling from the photoreceptors

To confirm that the age-related deterioration of visual function was due to the loss of dLRRK activity, *dLRRK*-RNAi was utilised to generate flies with reduced gene expression of *dLRRK*. The UAS/GAL4 system was used to drive expression of *dLRRK*-RNAi either ubiquitously with *Actin*-GAL4 or pan-neuronally with *elav*-GAL4 (these flies are referred to as *Actin*-GAL4>UAS-*dLRRK*-RNAi and *elav*-GAL4>UAS-*dLRRK*-RNAi, respectively). As before, these flies were raised on standard yeast-sucrose-agar media and aged at 29°C before ERGs were recorded at 3 and 21 DPE.

Figure 3.5 shows representative ERG traces from flies expressing *dLRRK*-RNAi at each time-point, as well as representative traces previously recorded from WT and *dLRRK*$^{-}$ LOF flies for comparison. These ERG traces show that when *dLRRK*-RNAi was expressed either ubiquitously or pan-neuronally there was a severe reduction in the size of the ERG off-transient and overall ERG amplitude from 3 to 21 DPE. However, the 21 DPE off-transient recorded form the *dLRRK*-RNAi fly lines was observed to be larger than the off-transient recorded from the *dLRRK*$^{-}$ LOF flies, suggesting that *dLRRK*-RNAi was not being driven hard enough to generate a complete loss of dLRRK function.

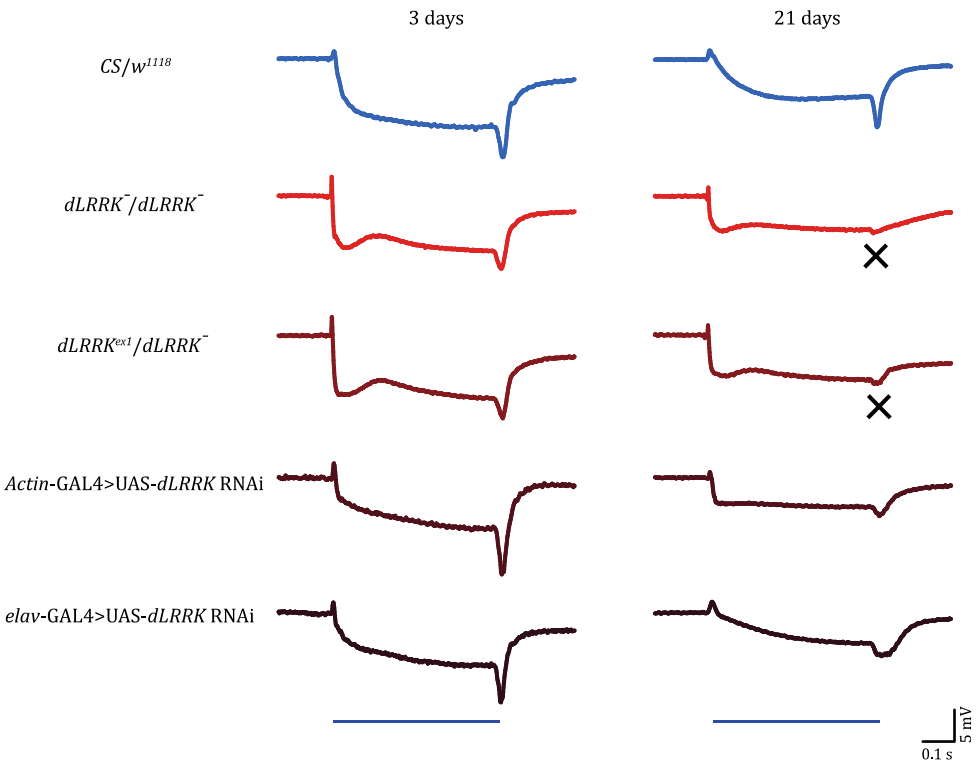


**Figure 3.5 Flies with ubiquitous or pan-neuronal expression of *dLRRK*-RNAi show an age-related loss of synaptic signalling**

Representative ERG traces from 3 (left) and 21 (right) DPE WT flies (*CS*/$w^{1118}$; dark blue), *dLRRK*⁻ LOF mutants (*dLRRK*⁻/*dLRRK*⁻ and $dLRRK^{ex1}$/*dLRRK*⁻; shades of red), and flies with ubiquitous or pan-neuronal expression of *dLRRK*-RNAi (*Actin*-GAL4>UAS-*dLRRK*-RNAi and *elav*-GAL4>UAS-*dLRRK*-RNAi, respectively; shades of dark red). ERGs are recorded in response to 0.5 second blue light pulses. The blue line drawn below the bottom ERG traces represents the duration of the light pulse. As previously shown in Figure 3.3 and Figure 3.4, all components of the WT ERG were maintained, whereas all components of the *dLRRK*⁻ LOF ERG were reduced by 21 DPE. All ERG components recorded from *Actin*-GAL4>UAS-*dLRRK*-RNAi and *elav*-GAL4>UAS-*dLRRK*-RNAi flies were reduced by 21 DPE, but to a lesser extent than those recorded from *dLRRK*⁻ LOF mutants. Scale bars for time (seconds) and potential (mV) are shown. Each trace is the average of the fly's response to at least three flashes of light. The black crosses indicate the absence of the off-transient component.

Again, each component of the ERG was quantified separately and the average values plotted for 3 and 21 DPE (Figure 3.6A-D). The ubiquitous expression of *dLRRK*-RNAi caused a significant reduction in each component of the ERG from 3 to 21 DPE, similarly to that observed in the *dLRRK*$^{-}$ LOF mutant flies (peak-to-peak: 38% decrease [$p$<0.001]; on-transient: 30% decrease [$p$<0.05]; off-transient: 54% decrease [$p$<0.001]; photoreceptor response: 25% decrease [$p$<0.01]). The pan-neuronal expression of *dLRRK*-RNAi caused a significant reduction in the overall peak-to-peak response (35% decrease [$p$<0.001]) the off-transient (36% decrease [$p$<0.001]) and the photoreceptor response (33% decrease [$p$<0.001]), but not in the on-transient. There were no significant differences between any of the ERG components recorded at 21 DPE from *Actin*-GAL4>UAS-*dLRRK*-RNAi flies and *elav*-GAL4>UAS-*dLRRK*-RNAi flies.

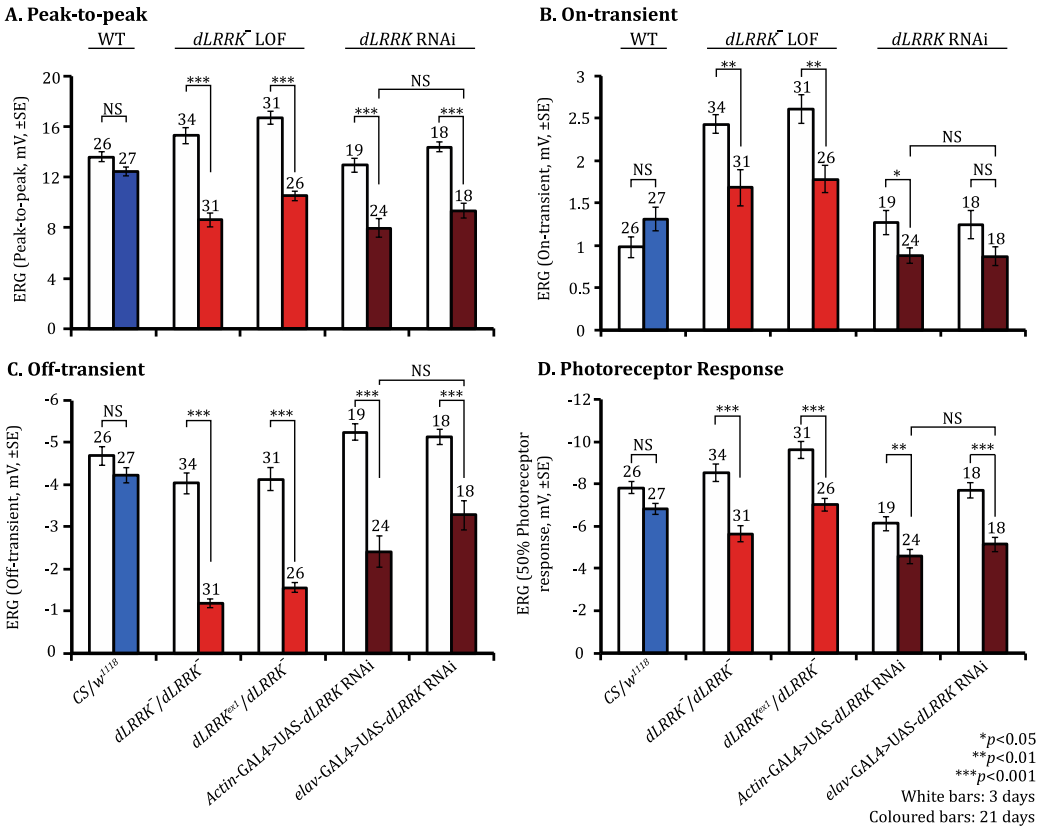


**Figure 3.6 Quantification of the individual ERG components showing the age-related loss in visual function of flies with ubiquitous or pan-neuronal expression of *dLRRK*-RNAi**

The ERG peak-to-peak response (A), on-transient (B), off-transient (C) and photoreceptor response (D) were quantified for WT flies (*CS*/$w^{1118}$), *dLRRK*⁻ LOF mutants (*dLRRK*⁻/*dLRRK*⁻ and $dLRRK^{ex1}$/*dLRRK*⁻), and flies with ubiquitous or pan-neuronal expression of *dLRRK*-RNAi (*Actin*-GAL4>UAS-*dLRRK*-RNAi and *elav*-GAL4>UAS-*dLRRK*-RNAi, respectively) at 3 (white bars) and 21 (coloured bars) DPE. (A-D) Similarly to *dLRRK*⁻ LOF mutants, *Actin*-GAL4>UAS-*dLRRK*-RNAi flies showed significant reductions in all ERG components by 21 DPE. *elav*-GAL4>UAS-*dLRRK*-RNAi flies showed significant reductions in the peak-to-peak, off-transient and photoreceptor responses by 21 DPE, but not in the on-transient response. WT flies did not show significant differences in any of the ERG components from 3 to 21 DPE. There were no significant differences between any of the 21 DPE ERG components between flies with ubiquitous or pan-neuronal expression of *dLRRK*-RNAi. All statistics are Student's t-tests: ***$p$<0.001, **$p$<0.01, *$p$<0.05, NS, no significant difference, $p$>0.05. Data presented are mean ± SEM bars; n numbers are displayed above the bars.

### 3.3.3 Tissue-specific expression of *dLRRK* rescues the loss of synaptic signalling in *dLRRK*¯ LOF flies

To determine where *dLRRK* is required within the visual system for correct function, the UAS/GAL4 system was utilised to allow tissue-specific expression of *dLRRK* within a *dLRRK*$^{e03680}$ homozygous mutant background. The *long glass multimer reporter*-GAL4 driver (*LongGMR*-GAL4) was used to drive the expression of *dLRRK* specifically in the eye. The *glass* gene encodes a zinc finger protein that is required for the normal development of photoreceptor cells and is expressed in all cell types of the developing eye (Moses and Rubin, 1991). The *lamina monopolar cell 1 and 2* B-GAL4 driver (*L1L2B*-GAL4) was used to drive the expression of *dLRRK* within the lamina neurons. *L1L2B*-GAL4 has previously been shown to drive GFP expression specifically in the L1 and L2 monopolar cells and to a lesser extent in the L5 neurons (Rister et al., 2007). The *tyrosine hydroxylase*-GAL4 driver (*TH*-GAL4) was used to drive the expression of *dLRRK* specifically in the DA neurons (Friggi-Grelin et al., 2003). As previously mentioned in Chapter 1, *TH* encodes the enzyme that is required for the rate-limiting step in the synthesis of dopamine (Nguyen-Legros, 1988, Harnois and Di Paolo, 1990). The *Rhodopsin1*-GAL4 driver (*Rh1*-GAL4) was used to drive the expression of *dLRRK* specifically in the R1–R6 photoreceptor cells (Mollereau et al., 2000). The *reversed polarity*-GAL4 driver (*Repo*-GAL4) was used to drive the expression of *dLRRK* specifically in the glial cells. The *repo* gene encodes a glial-specific homeo-domain protein (Xiong et al., 1994). All of these fly lines were kept in the same conditions as previous experiments and ERGs were recorded at 3 and 21 DPE.

Interestingly, when expression of *dLRRK* was driven specifically in the somatic muscle with *Dmef2*-GAL4 (Ranganayakulu et al., 1996) or *G14*-GAL4 (Shishido et al., 1998), no progeny eclosed, though balancer flies were viable. Thus, both of these proved lethal in combination with the homozygous *dLRRK*$^{e03680}$ mutation, and the visual response of these flies could not be tested.

Figure 3.7 shows representative 3 and 21 DPE ERG traces from flies expressing *dLRRK* specifically in the eyes, lamina neurons, DA neurons, photoreceptors or glial cells in a *dLRRK*¯ LOF background alongside representative ERG traces previously

recorded from *dLRRK*$^{-}$ LOF flies for comparison. At 21 DPE, there was little or no deterioration observed in the visual response recorded from flies with tissue-specific expression of *dLRRK* in the eyes, lamina neurons, DA neurons, photoreceptors or glial cells. Unlike in the *dLRRK*$^{-}$ LOF ERG, the on-transients, photoreceptor responses and off-transients were all maintained at 21 DPE for all of these genotypes. The difference in the size of the ERG traces between genotypes reflects the difference in eye colour; *LongGMR*-GAL4 produces flies with dark red eyes thus the ERG amplitude recorded from these flies is always lower than for other genotypes; the *L1L2B*-GAL4, *Rh1*-GAL4 and *Repo*-GAL4 produce flies with red eyes whilst the *TH*-GAL4 produces flies with orange eyes.

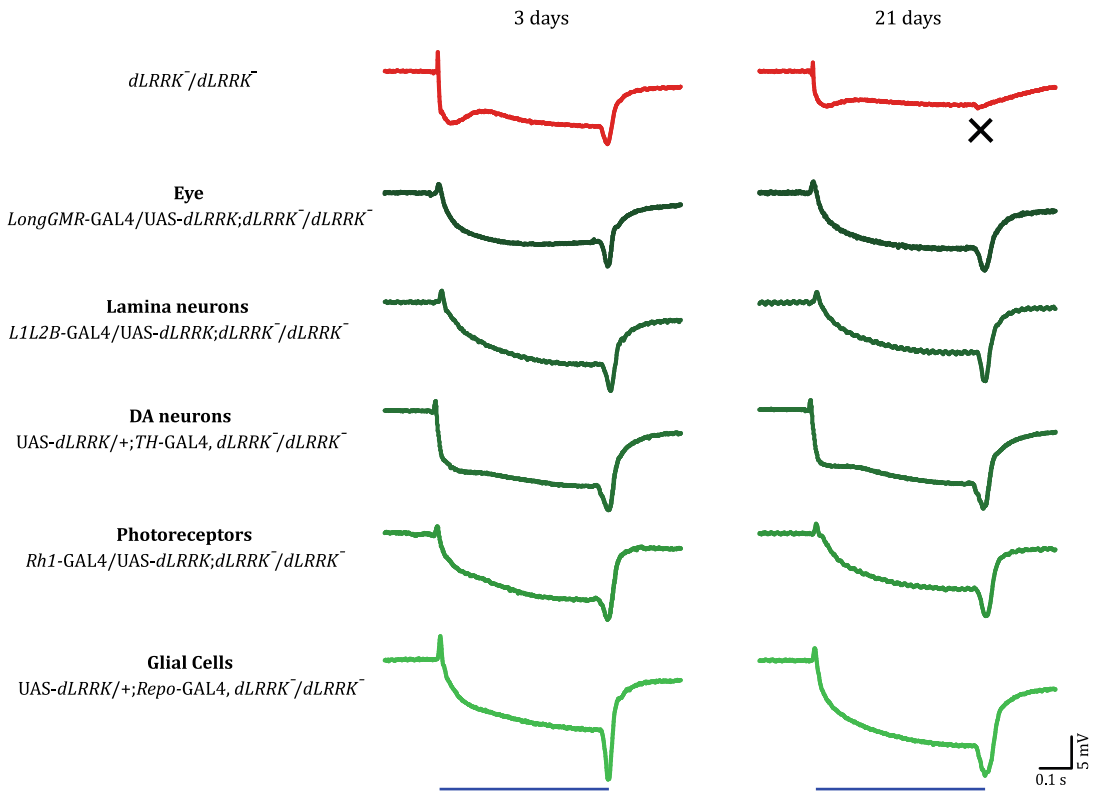


**Figure 3.7 *dLRRK* expression in the eye, lamina neurons, DA neurons, photoreceptors or glial cells in a *dLRRK*⁻ LOF background rescues the loss of visual function**

Representative ERG traces from 3 (left) and 21 (right) DPE *dLRRK*⁻ LOF mutants (*dLRRK*⁻/*dLRRK*⁻; red) and flies expressing *dLRRK* specifically in the eye (*LongGMR*-GAL4), lamina neurons (*L1L2B*-GAL4), DA neurons (*TH*-GAL4), photoreceptors (*Rh1*-GAL4) or glial cells (*Repo*-GAL4) in a *dLRRK*⁻ LOF background (shades of green). ERGs are recorded in response to 0.5 second blue light pulses. The blue lines drawn below the bottom ERG traces represent the duration of the light pulse. All components of the ERG were maintained at 21 DPE with *dLRRK* expression in the eye, lamina neurons, DA neurons, photoreceptors or glial cells. Scale bars for time (seconds) and potential (mV) are shown. Each trace is the average of the fly's response to at least three flashes of light.

Each component of the ERG was quantified separately and the average values plotted for 3 and 21 DPE (Figure 3.8A-D). There were no significant differences from 3 to 21 DPE in any of the individual ERG components recorded from flies expressing *dLRRK* in the eye, lamina neurons, DA neurons or photoreceptors in a *dLRRK*$^{-}$ LOF background. Flies with glial expression of *dLRRK* showed a significant reduction in both the on- and off-transient components at 21 DPE (both ~24% [$p$<0.01]), whereas the photoreceptor response of these flies was significantly increased at 21 DPE (29% increase [$p$<0.05]). Although there were significant differences between the 3 and 21 DPE ERG components with the glial expression of *dLRRK*, each component was still evident in the ERG traces (see Figure 3.7).

To compare the visual response of experimental rescue genotypes with the WT visual response, the variation in eye colour between genotypes must be taken in account. Therefore, the average 21 DPE peak-to-peak and off-transient responses were plotted as a percentage of the 3 DPE responses for each genotype (Figure 3.9A-B). As previously described, by 21 DPE the peak-to-peak response of WT flies decreased by 8% whereas the peak-to-peak response of *dLRRK*$^{-}$/*dLRRK*$^{-}$ flies decreased by 44% ($p$<0.001 compared to WT). The 21 DPE peak-to-peak responses from flies with expression of *dLRRK* in the eye, lamina neurons, photoreceptors or glial cells showed a decrease of 2-9%, and expression of *dLRRK* in the DA neurons caused no decrease (all $p$>0.05 compared to WT; Figure 3.9A). Similarly, by 21 DPE the off-transient component of WT flies showed a 10% decrease whereas in *dLRRK*$^{-}$/*dLRRK*$^{-}$ flies it decreased by 70% ($p$<0.001 compared to WT). The 21 DPE off-transients recorded from flies with expression of *dLRRK* in the eye, lamina neurons or DA neurons showed a decrease of 3-11%, and expression of *dLRRK* in the photoreceptors caused no reduction (all $p$>0.05 compared to WT; Figure 3.9B). This suggests that the visual response of these flies is equivalent to WT flies. The 21 DPE off-transient of flies with glial expression of *dLRRK* showed a decrease of 25%, but this was not significantly different compared to WTs. Taken together, these data suggest that expressing *dLRRK* in the eye, lamina neurons, DA neurons or photoreceptors is sufficient to restore synaptic signalling from the photoreceptors to the lamina neurons, whilst glial expression of *dLRRK* may only partially restore synaptic signalling.

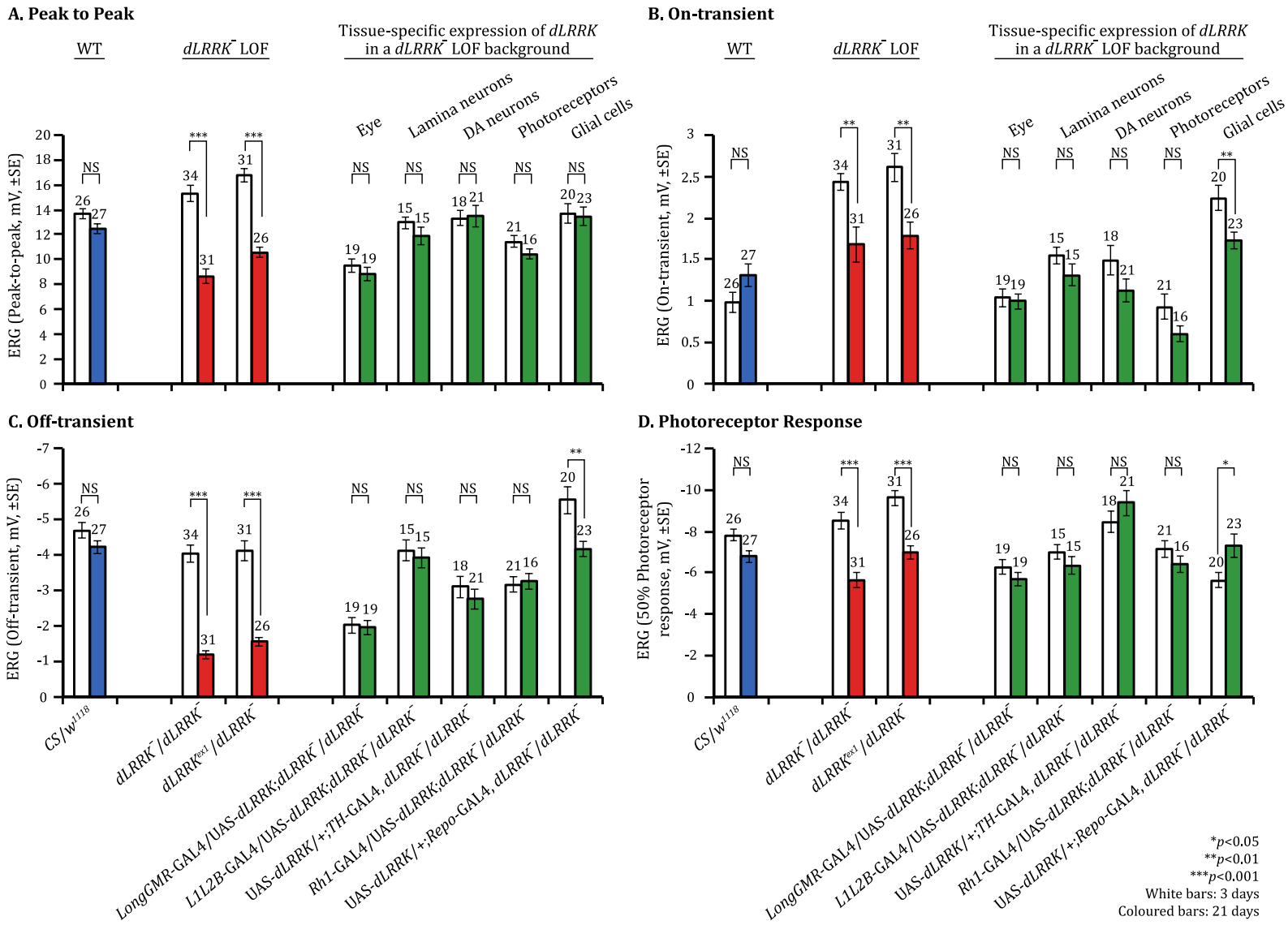


**Figure 3.8** Figure legend overleaf.

**Figure 3.8 Quantification of the individual ERG components showing the rescue of visual function of *dLRRK*⁻ LOF flies with *dLRRK* expression in the eye, lamina neurons, DA neurons, photoreceptors and glial cells**

The ERG peak-to-peak response (A), on-transient (B), off-transient (C) and photoreceptor response (D) were quantified for WT flies (*CS*/*w*$^{1118}$), *dLRRK*⁻ LOF mutants (*dLRRK*⁻/*dLRRK*⁻) and flies expressing *dLRRK* specifically in the eye (*LongGMR*-GAL4), lamina neurons (*L1L2B*-GAL4), DA neurons (*TH*-GAL4), photoreceptors (*Rh1*-GAL4) or glial cells (*Repo*-GAL4) in a *dLRRK*⁻ LOF background at 3 (white bars) and 21 (coloured bars) DPE. (A-D) Expressing *dLRRK* in the eye, lamina neurons, DA neurons or photoreceptors rescued the loss of all ERG components at 21 DPE. Expressing *dLRRK* in the glial cells offered a partial rescue, as both the on- and off-transient components were significantly lower at 21 DPE, whereas the photoreceptor responses were significantly higher. All Statistics are Student's t-test: ***$p$<0.001, **$p$<0.01, *$p$<0.05, NS, no significant difference, $p$>0.05. Data presented are mean ± SEM bars; n numbers are displayed above the bars.

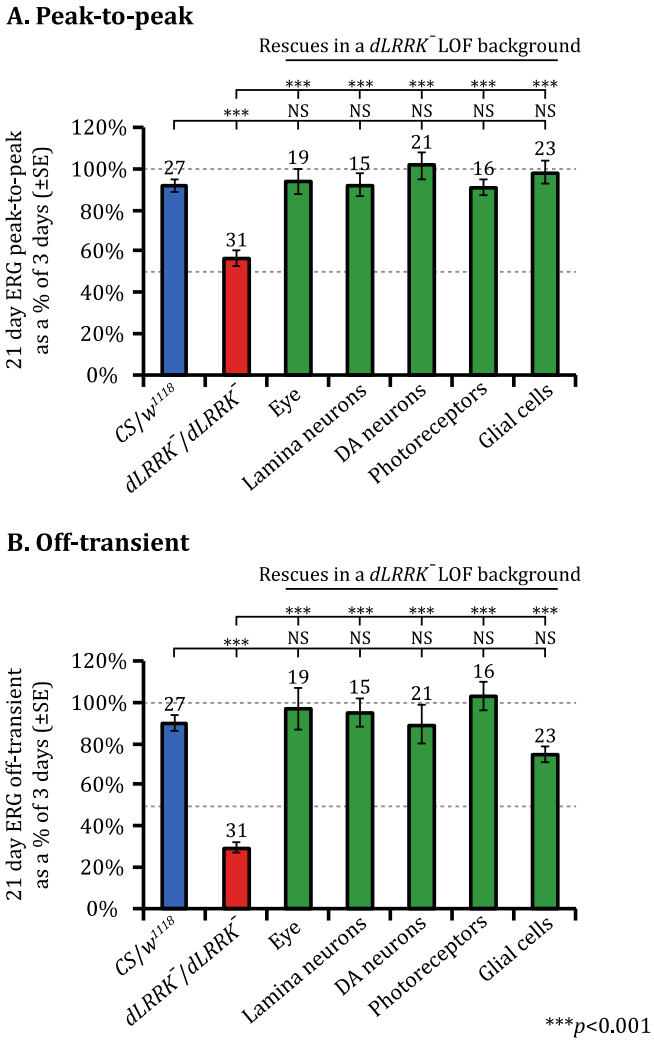


**Figure 3.9 The visual response of flies with tissue-specific expression of *dLRRK* in a *dLRRK*⁻ LOF background is equivalent to the visual response of WT flies**

The 21 DPE peak-to-peak (A) and off-transient (B) responses as a percentage of the 3 DPE response for WT flies (*CS*/*w*$^{1118}$; blue), *dLRRK*⁻ LOF mutants (*dLRRK*⁻/*dLRRK*⁻; red) and flies expressing *dLRRK* in the eye (*LongGMR*-GAL4), lamina neurons (*L1L2B*-GAL4), DA neurons (*TH*-GAL4), photoreceptors (*Rh1*-GAL4) or glial cells (*Repo*-GAL4) in a *dLRRK*⁻ LOF background (Green). (A-B) There were no significant differences between the 21 DPE peak-to-peak or off-transient responses of WT flies and rescue genotypes, whereas both were significantly reduced in *dLRRK*⁻ LOF mutants compared with WTs (ANOVA with post-hoc Dunnett's comparison to WT control, ***$p$<0.001, NS, no significant difference, $p$>0.05). There were no significant differences in the peak-to-peak and off-transient responses between rescue genotypes (statistics not shown), but all rescue genotypes showed significantly bigger peak-to-peak and off-transient responses than *dLRRK*⁻ LOF mutants (ANOVA with post-hoc Bonferroni correction, ***$p$<0.001). Data presented are mean ± SEM bars; n numbers are displayed above the bars.

The UAS/GAL4 system can sometimes cause the "leaky" expression of the associated gene in tissues others than those expressing the GAL4. To determine if any of the GAL4 drivers used for tissue-specific expression of *dLRRK* (*LongGMR*-GAL4, *L1L2B*-GAL4, *TH*-GAL4, *Rh1*-GAL4 and *Repo*-GAL4) allow low levels of expression or leak in the absence of the UAS, each GAL4 line was crossed into the $dLRRK^{e03680}$ homozygous background. The UAS-*dLRRK* transgene was also crossed into the $dLRRK^{e03680}$ homozygous background in the absence of any GAL4 (UAS-*dLRRK*/+; $dLRRK^{-}/dLRRK^{-}$). Collectively, all of these genotypes will be referred to as negative controls because none of them should exhibit *dLRRK* expression. ERGs were recorded from these flies at 3 and 21 DPE.

Figure 3.10 shows representative ERG traces from all negative control genotypes alongside representative ERG traces previously recorded from $dLRRK^{-}$ LOF flies at 3 and 21 DPE. All negative controls showed robust ERG responses at 3 DPE, however by 21 DPE the ERG amplitude of each genotype was observed to be severely reduced and the off-transient component was almost completely absent; except for the flies expressing *Repo*-GAL4 in a $dLRRK^{-}$ LOF background (+/+; *Repo*-GAL4, $dLRRK^{-}/dLRRK^{-}$), where a small off-transient was maintained.

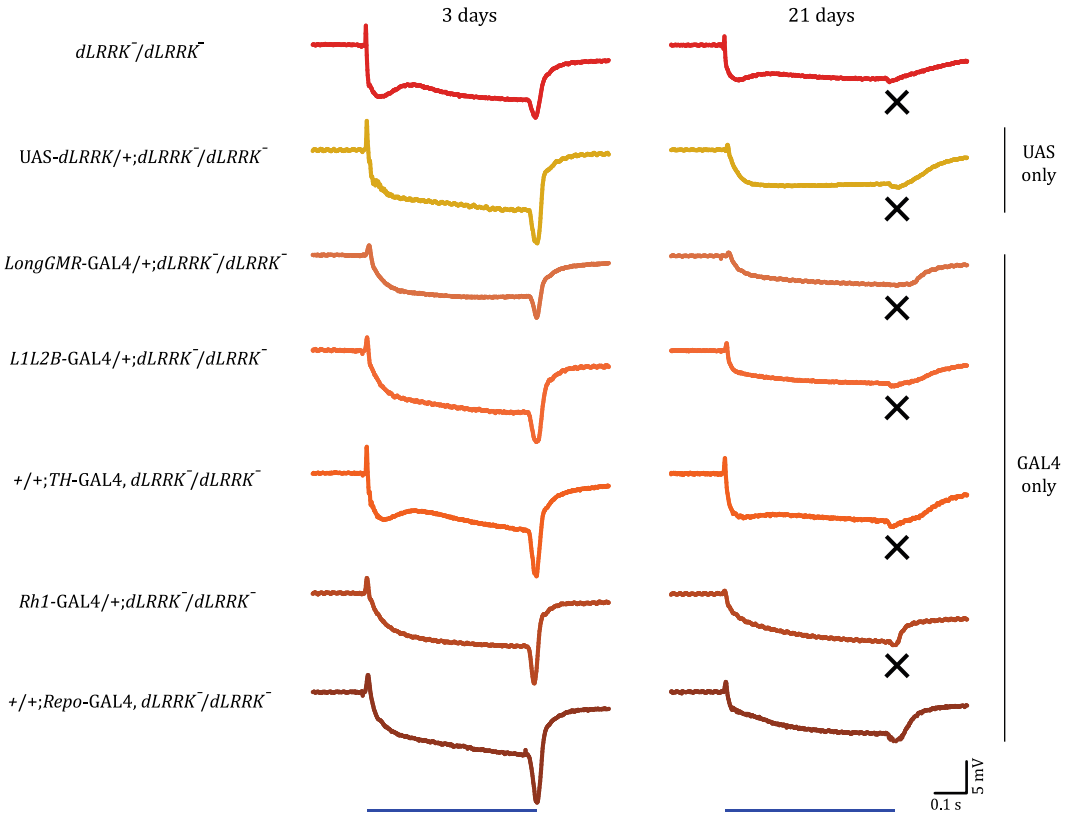


**Figure 3.10 Visual function is not restored when only one component of the UAS/GAL4 system is expressed in a *dLRRK*⁻ LOF background**

Representative ERG traces from 3 (left) and 21 (right) DPE *dLRRK*⁻ LOF mutants (*dLRRK*⁻/*dLRRK*⁻; red), flies with the UAS-*dLRRK* component only in a *dLRRK*⁻ LOF background (yellow), and flies with the GAL4 component only (*LongGMR*-GAL4; *L1L2B*-GAL4; *TH*-GAL4; *Rh1*-GAL4; *Repo*-GAL4) in a *dLRRK*⁻ LOF background (shades of orange). ERGs are recorded in response to 0.5 second blue light pulses. The blue line below the bottom ERG traces represents the duration of the light pulse. Similarly to the *dLRRK*⁻ LOF mutants, flies expressing only one component of the UAS/GAL4 system failed to maintain the individual components of the ERG at 21 DPE. The off-transient component was almost completely absent in all of these flies (indicated by the black crosses), apart from in flies expressing *Repo*-GAL4 only, where a small off-transient response was still observed. Scale bars for time (seconds) and potential (mV) are shown. Each trace is the average of the fly's response to at least three flashes of light.

Each component of the ERG was quantified separately and the average values plotted for 3 and 21 DPE (Figure 3.11A-D). Similarly to *dLRRK*$^{-}$ LOF flies, the peak-to-peak responses recorded from all of the negative control genotypes showed a significant reduction from 3 to 21 DPE (35%-49% decrease [all $p<0.001$]). All ERG components recorded from UAS-*dLRRK*/+; *dLRRK*$^{-}$/*dLRRK*$^{-}$ flies were significantly reduced by 21 DPE, but the off-transient component was most severely reduced (on-transient: 45% decrease [$p<0.01$]; off-transient: 68% decrease [$p<0.001$]; photoreceptor response: 24% decrease [$p<0.05$]). All fly lines expressing a GAL4 in the absence of UAS-*dLRRK* in a *dLRRK*$^{-}$ LOF background also showed significant reductions in the ERG on-transient (27%-72% decrease [$p\leq0.001$ or $p<0.01$ dependent upon genotype]), off-transient (56%-70% decrease [all $p<0.001$]), and photoreceptor responses (19%-37%, decrease [$p\leq0.001$ or $p<0.01$ dependent upon genotype]) by 21 DPE.

To compare the visual responses of the negative controls with the WT and *dLRRK*$^{-}$ LOF visual responses, the average 21 DPE peak-to-peak and off-transient responses were plotted as a percentage of the 3 DPE responses for each genotype (Figure 3.12A-B). Both the peak-to-peak and off-transient amplitudes of all negative controls were equivalent to *dLRRK*$^{-}$ LOF flies (all $p>0.05$) and were significantly lower than those recorded from WT controls (all $p<0.001$). There were no significant differences between the 21 DPE ERG responses recorded from the negative control genotypes. Taken together, these data suggest that the UAS/GAL4 system was not allowing leaky gene expression because there was no rescue of visual function when only one of these components was present in a *dLRRK*$^{-}$ LOF background. Thus, these flies all showed a similar age-related loss of synaptic signalling to the *dLRRK*$^{-}$ LOF mutant flies. Importantly, the expression of *dLRRK* in a WT background using the same GAL4 drivers as for the *dLRRK*$^{-}$ LOF mutant flies, or expression of the GAL4s in the absence of UAS-*dLRRK* in a WT background did not cause any significant difference in the visual response compared to WT controls (see Appendix 1 and Appendix 2).

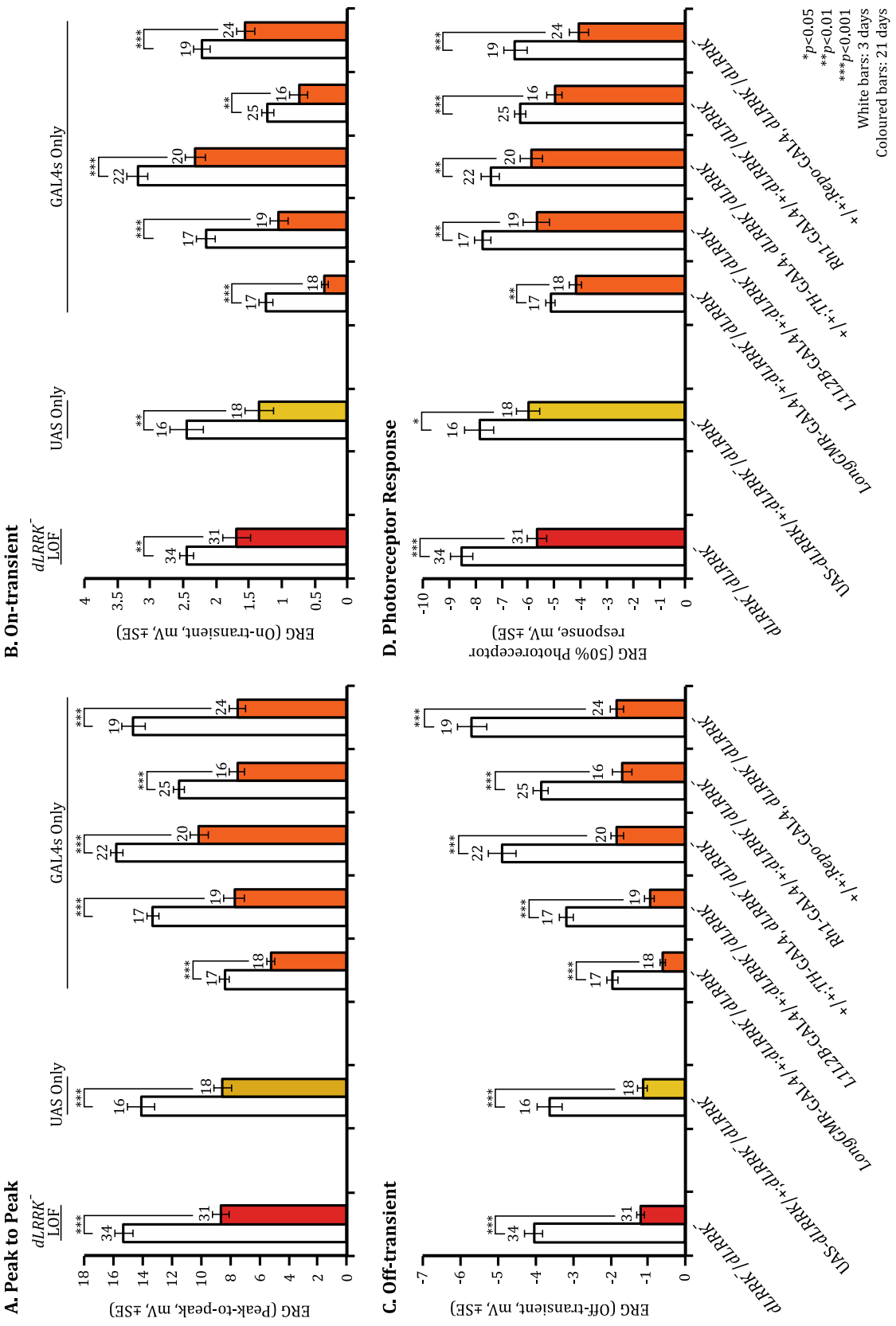


**Figure 3.11** Figure legend overleaf.

**Figure 3.11 Quantification of the individual ERG components showing the progressive deterioration of visual function when only one component of the UAS/GAL4 system is expressed in a *dLRRK*$^{-}$ LOF background**

The ERG peak-to-peak response (A), on-transient (B), off-transient (C) and photoreceptor response (D) were quantified for *dLRRK*$^{-}$ LOF mutants (*dLRRK*$^{-}$/*dLRRK*$^{-}$), flies with the UAS-*dLRRK* component only in a *dLRRK*$^{-}$ LOF background, and flies with the GAL4 component only in a *dLRRK*$^{-}$ LOF background (*LongGMR*-GAL4; *L1L2B*-GAL4; *TH*-GAL4; *Rh1*-GAL4; *Repo*-GAL4) at 3 (white bars) and 21 (coloured bars) DPE. (A-D) All components of the ERG were significantly reduced in flies with only one component of the UAS/GAL4 present in a *dLRRK*$^{-}$ LOF background. All statistics are Student's t-test: ***$p$<0.001, **$p$<0.01, *$p$<0.05, NS, no significant difference, $p$>0.05. Data presented are mean ± SEM bars; n numbers are displayed above the bars.

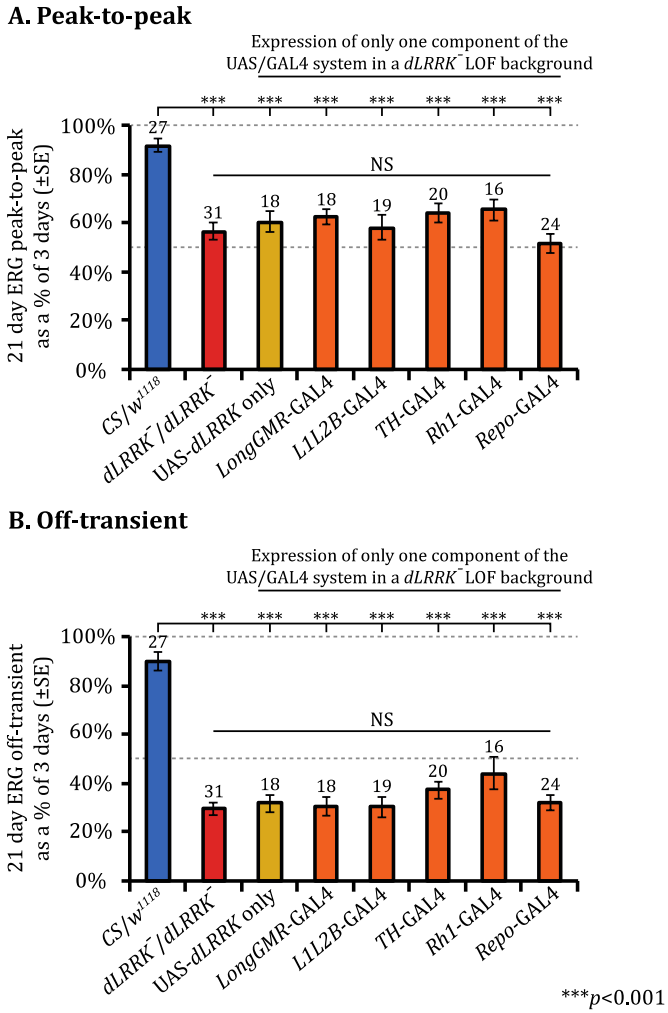


**Figure 3.12 The visual response of flies with expression of only one component of the UAS/GAL4 system in a *dLRRK*⁻ LOF background is equivalent to that of *dLRRK*⁻ LOF flies**

The 21 DPE peak-to-peak (A) and off-transient (B) responses as a percentage of the 3 DPE responses for WT flies (*CS*/*w*$^{1118}$; blue), *dLRRK*⁻ LOF mutants (*dLRRK*⁻/*dLRRK*⁻; red), flies with the UAS-*dLRRK* component only in a *dLRRK*⁻ LOF background (UAS-*dLRRK* only; yellow), and flies with the GAL4 component only in a *dLRRK*⁻ LOF background (*LongGMR*-GAL4; *L1L2B*-GAL4; *TH*-GAL4; *Rh1*-GAL4; *Repo*-GAL4; orange). (A-B) The 21 DPE peak-to-peak and off-transient amplitudes were significantly higher in WT flies than in all other genotypes (ANOVA with post-hoc Dunnett's comparison to WT control, ***$p$<0.001). There were no significant differences in the 21 DPE peak-to-peak or off-transient responses between *dLRRK*⁻/*dLRRK*⁻ flies and flies with expression of only one component of the UAS/GAL4 system in a *dLRRK*⁻ LOF background; there were also no significant differences between any of the negative control genotypes (ANOVA with post-hoc Bonferroni correction, NS, no significant difference, $p$>0.05). Data presented are mean ± SEM bars; n numbers are displayed above the bars.

### 3.3.4 DA expression of *dLRRK* orthologues rescues the loss of synaptic signalling from the photoreceptors in *dLRRK¯* LOF flies

As previously discussed in Chapter 1, *dLRRK* is the fly orthologue of *hLRRK2* and *hLRRK1*. To determine if various *LRRK2* or *LRRK1* orthologues can substitute for the fly's own version of *LRRK,* these transgenes were expressed in the DA neurons or glial cells of *dLRRK¯* LOF flies using *TH*-GAL4 or *Repo*-GAL4, respectively, and ERGs were recorded at 3 and 21 DPE.

Fly lines expressing the WT *hLRRK2* gene, the PD-related *hLRRK2-G2019S* mutant gene or a kinase-dead version of *hLRRK2* (*hLRRK2-D1994A*), were all a kind gift from Kenneth Vielsted Christensen, at the Lundbeck pharmaceutical company in Denmark. At Lundbeck, these transgenes were cloned into a pUAST attB vector, which was microinjected into the phiC31 *vas-int; attp'-51C* fly line (Bloomington Stock 24482) at Bestgene. When the expression of these transgenes is driven using the same GAL4 driver, both the WT and mutant *hLRRK2* transgenes are expressed at the same level making them directly comparable to each other.

At the time of this study, human *LRRK1* cDNA was unavailable, but mouse *LRRK1* (*mLRRK1*) was already available as cDNA. Thus, a fly line expressing *mLRRK1* was generated during this study (see Chapter 2 section 2.4.1). *mLRRK1* cDNA was sub-cloned into the pUAST attB vector using standard sub-cloning techniques before being microinjected into the same phiC31 *vas-int; attp'-51C* fly line as the *hLRRK2* constructs at the University of Cambridge, Department of Genetics, Fly Facility. Again, this means that *mLRRK1* is expressed at the same level as the *hLRRK2* transgenes when being driven by the same GAL4 enabling direct comparisons to be made. In addition, all of these flies have the same orange eye colour meaning that differences in the amount of screening pigment, which alter the shape and size of the ERG, were eliminated.

Figure 3.13 shows representative ERG traces from flies expressing *hLRRK2*, *hLRRK2-G2019S*, *hLRRK2-D1994A* or *mLRRK1* in the DA neurons (*TH*-GAL4) in a *dLRRK¯* LOF background at 3 and 21 DPE. Representative ERG traces previously recorded from

flies with DA expression of their own version of *dLRRK* in a *dLRRK*$^{-}$ LOF background are also shown for comparison. As previously described in section 3.3.3, DA expression of *dLRRK* rescued the age-related loss of synaptic signalling caused by the loss of dLRRK activity, evidenced by the presence of the off-transient component and other components of the ERG trace at both 3 and 21 DPE. Similarly, all ERG components were maintained at 21 DPE with DA expression of WT *hLRRK2*. The on-transient, off-transient and photoreceptor responses were evident in the 21 DPE ERG traces from flies with DA expression of *hLRRK2-G2019S*, *hLRRK2-D1994A* or *mLRRK1*. However, the off-transient component recorded from these genotypes was reduced from that observed at 3 DPE, which may suggest that the mutant forms of *hLRRK2* or *mLRRK1* only offer a partial rescue of visual function.

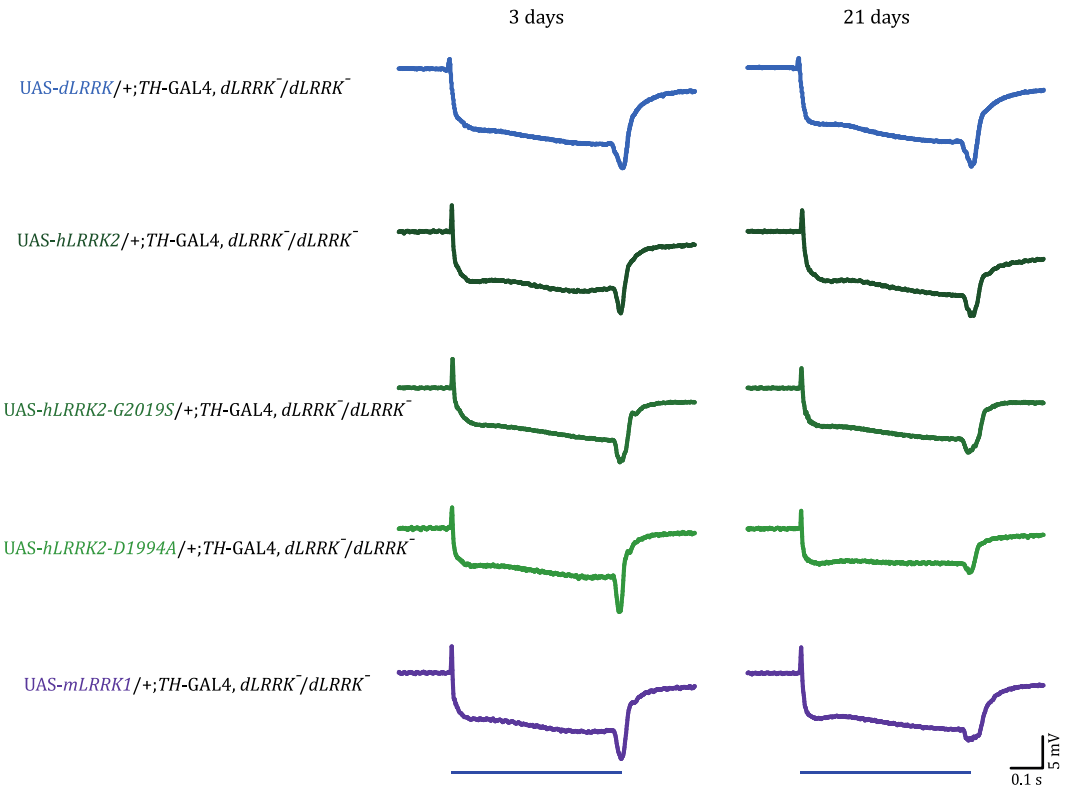


**Figure 3.13 Visual function is completely or partially rescued with DA expression of *dLRRK* orthologues in a *dLRRK*⁻ LOF background**

Representative ERG traces from 3 (left) and 21 (right) DPE flies with DA expression of *dLRRK* (blue), human versions of *LRRK2:* WT *hLRRK2* (dark green), PD-mutant *hLRRK2-G2019S* (lighter green), kinase-dead *hLRRK2-D1994A* (lightest green), or a mouse version of *LRRK1: mLRRK1* (purple) in a *dLRRK*⁻ LOF background. ERGs are recorded in response to 0.5 second blue light pulses. The blue line below the bottom ERG traces represents the duration of the light pulse. All components of the ERG were maintained at 21 DPE with DA expression of *dLRRK* or *hLRRK2*. All ERG components were also evident at 21 DPE with DA expression of *hLRRK2-G2019S, hLRRK2-D1994A* or *mLRRK1,* but the off-transient component was slightly reduced. Scale bars for time (seconds) and potential (mV) are shown. Each trace is the average of the fly's response to at least three flashes of light.

In order to determine if any of the ERG components were significantly reduced from 3 to 21 DPE, the individual ERG components were quantified separately for each genotype (Figure 3.14A-D). As previously described, there were no significant differences between any of the 3 and 21 DPE ERG components recorded from flies with DA expression of *dLRRK* in a *dLRRK*$^{-}$ LOF background. DA expression of WT *hLRRK2* in a *dLRRK*$^{-}$ LOF background also completely rescued the loss of synaptic signalling, as there were no significant differences in any of the ERG components by 21 DPE. This suggests that *hLRRK2* is able to rescue the visual response of *dLRRK*$^{-}$ LOF flies as effectively as the fly's own version of *LRRK*. Flies with DA expression of *hLRRK2-G2019S* had significantly decreased peak-to-peak responses by 21 DPE (20% decrease [$p$<0.001]); the on- and off-transient components were also significantly reduced by 21 DPE (on-transient: 20% decrease [$p$<0.05]; off-transient: 39% decrease [$p$<0.001]). Flies with DA expression of *hLRRK2-D1994A* also showed significantly reduced peak-to-peak responses by 21 DPE (22% decrease [$p$<0.001]); again, the on-transient and off-transient components of these flies were also significantly reduced by 21 DPE (on-transient: 21%decrease [$p$<0.01]; off-transient: 48% decrease [$p$<0.001]). The photoreceptor responses of these two genotypes were maintained at 21 DPE. DA expression of *mLRRK1* caused a small, but significant, reduction in the peak-to-peak responses at 21 DPE (12% decrease [$p$<0.05]), which was caused by a significant reduction of the off-transient component (33% decrease [$p$<0.001]); neither the on-transient nor photoreceptor responses showed significant reductions at 21 DPE in these flies. Although flies with DA expression of *hLRRK2-G2019S, hLRRK2-D1994A* or *mLRRK1* all showed significant reductions in the 21 DPE off-transient amplitudes, the representative ERG traces from these genotypes indicated that the off-transient component was not completely absent (see Figure 3.13). This suggests that DA expression of these transgenes partially restores the loss of synaptic signalling from the photoreceptors in *dLRRK*$^{-}$ LOF flies.

At 21 DPE, the off-transient amplitude was significantly lower in flies with DA expression of *mLRRK1* compared with flies with DA expression of *hLRRK2* ($p$<0.001). The other ERG components did not differ significantly between these two genotypes. Although DA expression of *mLRRK1* partially rescued visual function in *dLRRK*$^{-}$ LOF mutants, DA expression of *hLRRK2* completely rescued visual function, suggesting

that the function of *hLRRK2* is more similar to the function of the fly's own version of *LRRK*.

Flies with DA expression of *hLRRK2-G2019S* had significantly reduced peak-to-peak and off-transient responses at 21 DPE compared with flies expressing WT *hLRRK2* ($p<0.05$ and $p<0.01$, respectively; Figure 3.14). The photoreceptor and on-transient responses did not differ between these genotypes. All components of the ERG were significantly reduced in flies with DA expression of *hLRRK2-D1994A* compared with those expressing WT *hLRRK2* at 21 DPE (peak-to-peak, on-transient and off-transient: all $p<0.001$; photoreceptor response: $p<0.05$). This suggests that only the WT *hLRRK2* transgene is able to completely rescue the loss of synaptic signalling when expressed in a $dLRRK^{-}$ LOF background. Both the gain-of-kinase-function (*hLRRK2-G2019S*) and loss-of-kinase-function (*hLRRK2-D1994A*) transgenes partially rescued the visual response of $dLRRK^{-}$ LOF flies and there were no significant differences in any of the 21 DPE ERG components between these two genotypes. This suggests that the kinase domain may not be the key domain in mediating this rescue.

Comparisons were also made between flies expressing their own version of *dLRRK* and those expressing the WT *hLRRK2* transgene (Figure 3.14). Neither the peak-to-peak amplitude nor the off-transient amplitude was significantly different between these two genotypes at 21 DPE. However, the 21 DPE on-transient was significantly reduced in flies expressing *dLRRK* ($p<0.001$) and the photoreceptor response was significantly increased ($p<0.001$) compared with flies expressing *hLRRK2*. The UAS-*dLRRK* and UAS-*hLRRK2* transgenes were generated at different times and were microinjected into different regions of the fly genome. This means that they will likely be expressed at differing levels, even when driven by the same GAL4 (*TH*-GAL4 in this case), which may result in some of the differences seen between these two genotypes.

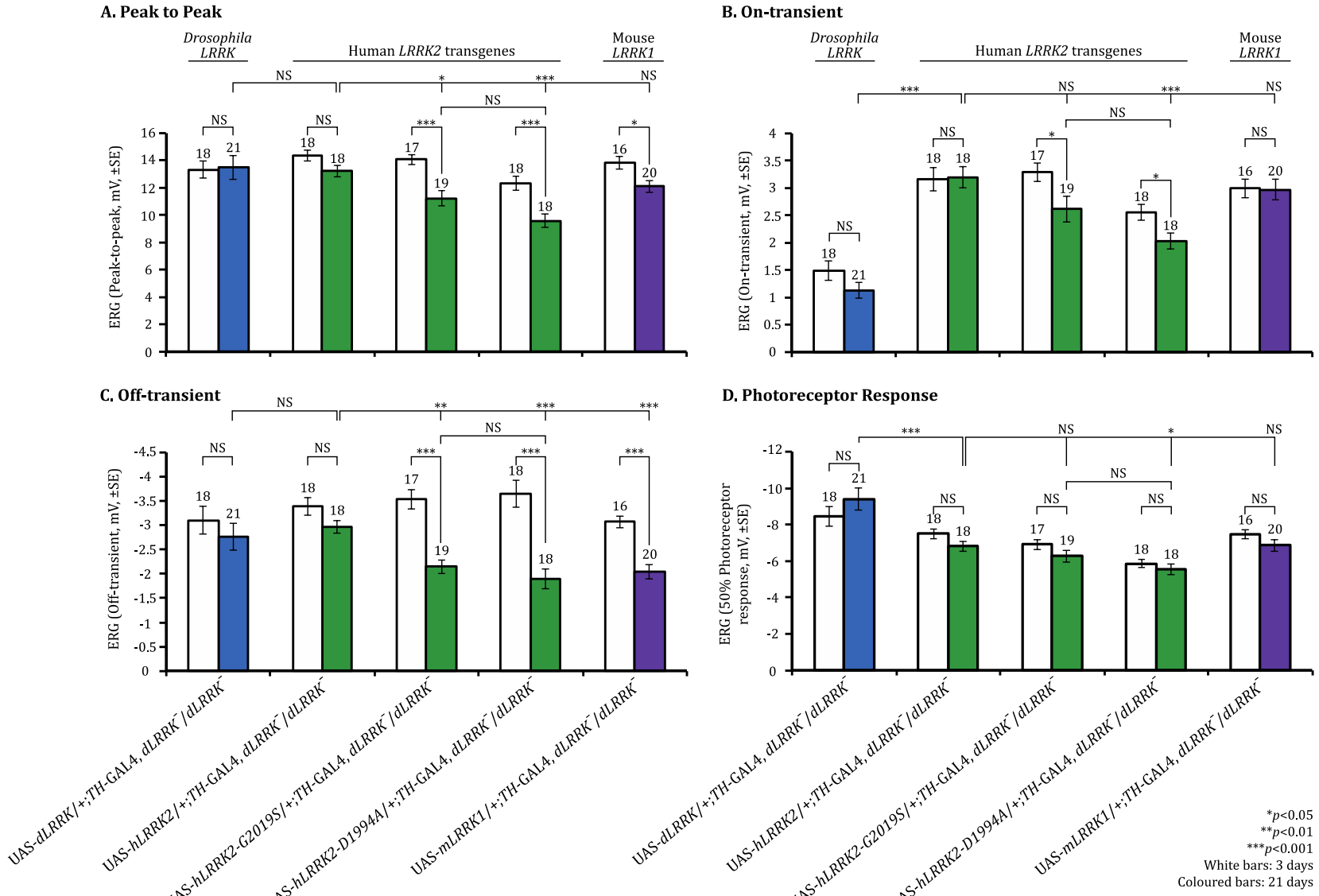


**Figure 3.14** Figure legend overleaf.

**Figure 3.14 Quantification of the individual ERG components showing the complete or partial rescue of visual function with DA expression of *dLRRK* orthologues in a *dLRRK*⁻ LOF background**

The ERG peak-to-peak response (A), on-transient (B), off-transient (C) and photoreceptor response (D) were quantified for flies with DA expression of *dLRRK,* WT *hLRRK2, hLRRK2-G2091S, hLRRK2-D1994A* or *mLRRK1* in a *dLRRK*⁻ LOF background at 3 (white bars) or 21 (coloured bars) DPE. (A-D) All ERG components were maintained from 3 to 21 DPE with DA expression of *dLRRK* or *hLRRK2*. All ERG components, apart from the photoreceptor response, were significantly lower at 21 DPE than at 3 DPE with DA expression of *hLRRK2-G2019S* or *hLRRK2-D1994A.* Only the peak-to-peak and off-transient responses were significantly reduced at 21 DPE with DA expression of *mLRRK1*. At 21 DPE, the on-transient and photoreceptor responses were significantly different with DA expression of *hLRRK2* compared with DA expression of *dLRRK*. Some or all of the ERG components were significantly higher with DA expression of *hLRRK2* compared with DA expression of *hLRRK2-G2019S* (peak-to-peak and off-transient)*, hLRRK2-D1994A* (all ERG components) or *mLRRK1* (off-transient only) at 21 DPE. Statistics within genotypes are Student's t-test; statistics between multiple genotypes are ANOVA with post-hoc Bonferroni correction: ***$p$<0.001, **$p$<0.01, *$p$<0.05, NS, no significant difference, $p$>0.05. Data presented are mean ± SEM bars; n numbers are displayed above the bars.

### 3.3.5 Glial expression of *dLRRK* orthologues partially rescues the loss of synaptic signalling from the photoreceptors in *dLRRK*⁻ LOF flies

Figure 3.15 shows representative ERG traces from flies expressing *hLRRK2*, *hLRRK2-G2019S*, *hLRRK2-D1994A* or *mLRRK1* in the glial cells (*Repo*-GAL4) in a *dLRRK*⁻ LOF background at 3 and 21 DPE. Representative ERG traces previously recorded from flies expressing their own version of *LRRK* in a *dLRRK*⁻ LOF background are also shown for comparison. For each of these genotypes, all 3 and 21 DPE ERG components were evident in the ERG traces. However, the size of each individual ERG component was reduced by 21 DPE in all genotypes, suggesting that the expression of these transgenes in the glial cells only partially restores synaptic signalling.

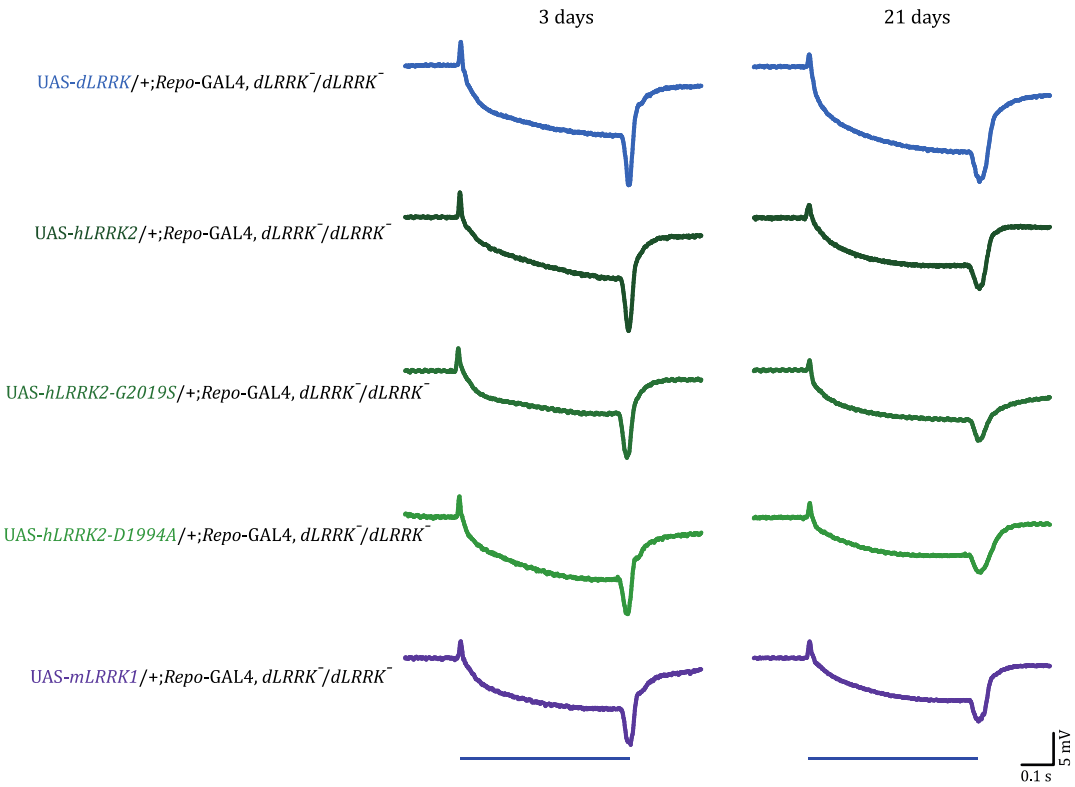


**Figure 3.15 Visual function is partially rescued with glial expression of *dLRRK* orthologues in a *dLRRK*⁻ LOF background**

Representative ERG traces from 3 (left) and 21 (right) DPE flies with glial expression of *dLRRK* (blue), human versions of *LRRK2:* WT *hLRRK2* (dark green), PD-mutant *hLRRK2-G2019S* (lighter green), kinase-dead *hLRRK2-D1994A* (lightest green), or a mouse version of *LRRK1: mLRRK1* (purple) in a *dLRRK*⁻ LOF background. ERGs are recorded in response to 0.5 second blue light pulses. The blue line below the bottom ERG traces represents the duration of the light pulse. Although all components of the ERG were maintained at 21 DPE for each genotype, the overall size of the response was smaller than at 3 DPE. Scale bars for time (seconds) and potential (mV) are shown. Each trace is the average of the fly's response to at least three flashes of light.

The individual components of the ERG were quantified separately for each genotype and the 3 and 21 DPE averages plotted (Figure 3.16A-D). As previously mentioned, flies with glial expression of *dLRRK* showed significant reductions in the on- and off-transient responses by 21 DPE (both $p<0.01$), whereas the photoreceptor response was significantly increased ($p<0.05$; Section 3.3.3); the overall peak-to-peak amplitude of these flies was maintained at 21 DPE. In contrast, the peak-to-peak amplitude of flies with glial expression of WT *hLRRK2* was significantly reduced by 21 DPE (19% decrease [$p<0.01$]). The off-transient responses of these flies were also significantly decreased (33% decrease [$p<0.01$]), but both the on-transient and photoreceptor responses were maintained at 21 DPE. Flies with glial expression of mutant forms of *hLRRK2* (*hLRRK2-G2019S* or *hLRRK2-D1994A*) also showed significant reductions in their peak-to-peak amplitudes by 21 DPE (27% and 36% decrease, respectively, [both $p<0.001$]). The *hLRRK2-G2019S* flies also had significantly reduced on- and off-transient components (25% decrease [$p<0.01$] and 49% decrease [$p<0.001$], respectively). The *hLRRK2-D1994A* flies showed significant reductions in all three of the ERG components (on- and off-transients: 34% decrease and 51% decrease, respectively [both $p<0.001$]; photoreceptor response: 23% decrease [$p<0.05$]). Similarly to the flies with glial expression of *hLRRK2*, flies expressing *mLRRK1* in the glial cells showed significantly reduced peak-to-peak amplitudes by 21 DPE (19% decrease [$p<0.001$]). These *mLRRK1* flies also had significantly reduced on- and off-transient components by 21 DPE (15% decrease [$p<0.05$] and 35% decrease [$p<0.001$], respectively), but the photoreceptor response was maintained.

At 21 DPE, there were no significant differences between any of the ERG components recorded from flies with glial expression of *hLRRK2* or *mLRRK1* (Figure 3.16), suggesting that the partial rescue of visual function was similar with glial expression of either of these two transgenes. WT *hLRRK2* was more efficient at rescuing the visual function compared with the mutant forms of *hLRRK2*; the peak-to-peak ($p<0.01$), on-transient ($p<0.05$) and off-transient ($p<0.001$) responses were all significantly lower with glial expression of *hLRRK2-G2019S* compared with glial expression of WT *hLRRK2*; all ERG components were significantly reduced with glial expression of *hLRRK2-D1994A* compared with glial expression of WT *hLRRK2* (peak-

to-peak: $p<0.001$; on-transient: $p<0.01$; off-transient: $p<0.001$; photoreceptor response: $p<0.05$). There were no significant differences between any of the 21 DPE ERG components recorded from flies with glial expression of *hLRRK2-G2019S* or *hLRRK2-D1994A.* These data indicate that the kinase domain may not the key domain for rescuing visual function, which was also suggested with DA expression of these transgenes (see section 3.3.4).

Comparisons were also made between flies expressing their own version of *dLRRK* and those expressing the WT *hLRRK2* transgene (Figure 3.16). At 21 DPE, the peak-to-peak and photoreceptor responses were significantly higher with glial expression of *dLRRK* compared with glial expression of *hLRRK2* ($p<0.05$ and $p<0.01$ respectively). Neither the on- nor off-transient responses were significantly different between these two genotypes. However, as previously mentioned the expression levels of these two transgenes may not be directly comparable to one another (see section 3.3.4).

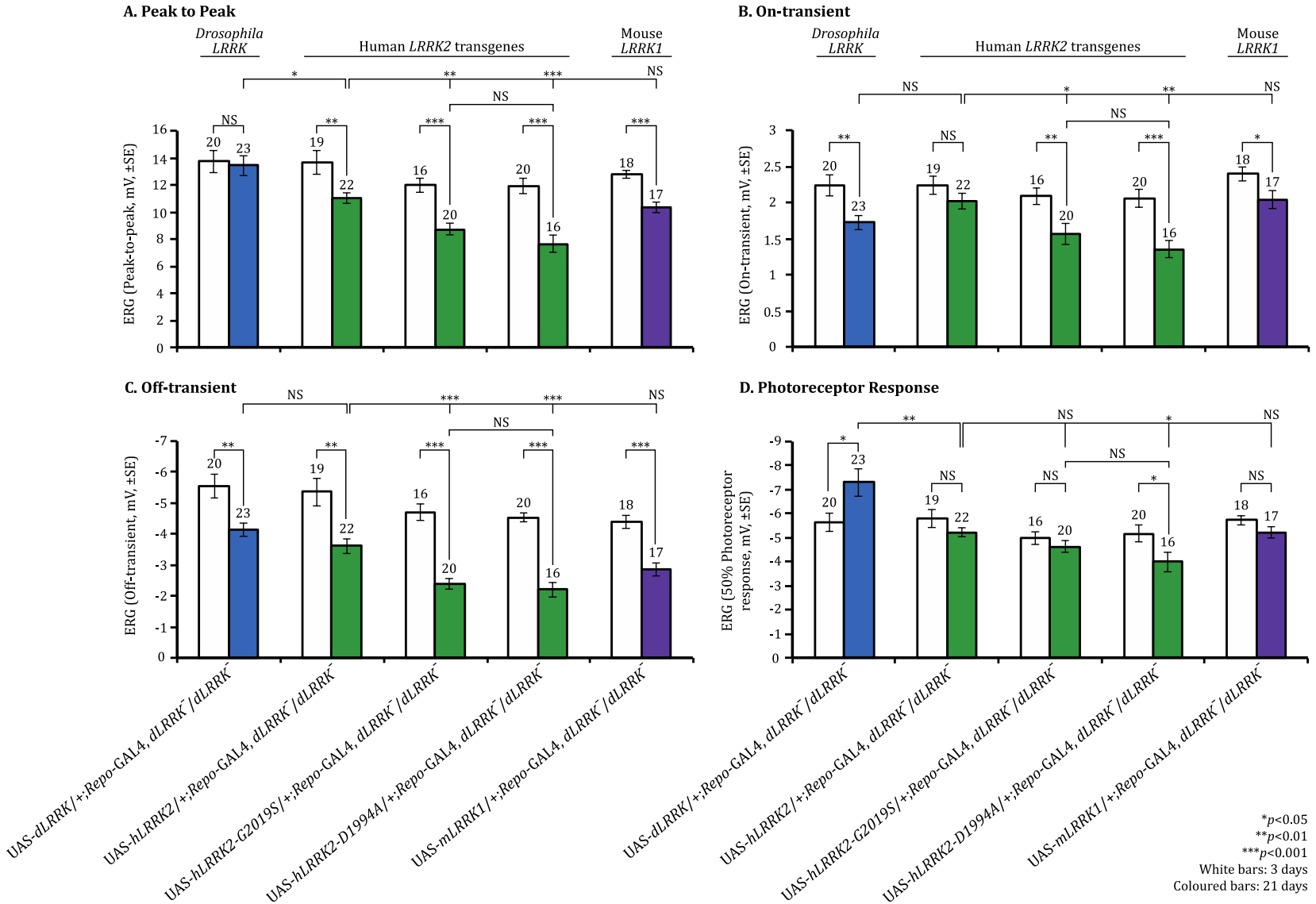


**Figure 3.16** Figure legend overleaf.

**Figure 3.16 Quantification of the individual ERG components showing the partial rescue of visual function with glial expression of *dLRRK* orthologues in a *dLRRK*⁻ LOF background**

The ERG peak-to-peak response (A), on-transient (B), off-transient (C) and photoreceptor response (D) were quantified for flies with glial expression of *dLRRK,* WT *hLRRK2, hLRRK2-G2091S, hLRRK2-D1994A* or *mLRRK1* in a *dLRRK*⁻ LOF background at 3 (white bars) or 21 (coloured bars) DPE. (A-D) For all genotypes, some or all of the ERG components were significantly reduced from 3 to 21 DPE (for *dLRRK*: on-transient, off-transient and photoreceptor response; for *hLRRK2*: peak-to-peak and off-transient; for *hLRRK2-G2019S*: peak-to-peak, on-transient and off-transient; for *hLRRK2-D1994A*: all components; for *mLRRK1*: peak-to-peak, on-transient and off-transient). At 21 DPE, there were significant differences in the peak-to-peak and photoreceptor responses between flies with glial expression of *hLRRK2* or *dLRRK*. Some or all of the ERG components were significantly higher with glial expression of *hLRRK2* compared with glial expression of *hLRRK2-G2019S* (peak-to-peak, on-transient and off-transient) or *hLRRK2-D1994A* (all ERG components). There were no significant differences between any of the 21 DPE ERG components with glial expression of *hLRRK2* or *mLRRK1*. Statistics within genotypes are Student's t-test; statistics between multiple genotypes are ANOVA with post-hoc Bonferroni correction: ***$p$<0.001, **$p$<0.01, *$p$<0.05, NS, no significant difference, $p$>0.05. Data presented are mean ± SEM bars; n numbers are displayed above the bars.

## 3.4 Discussion

### 3.4.1 Expression of *dLRRK* is essential to maintain synaptic signalling from the photoreceptors in aged flies

The first key observation in this chapter was that LRRK is essential for the maintenance of normal visual function in aged flies. It was shown that old *dLRRK*⁻ LOF flies have severely reduced ERG responses compared with old WT flies. The loss of the ERG off-transient component in *dLRRK*⁻ LOF flies suggests that the flaw is in the adaption of lower-order visual neurons, possibly the L1 and L2 interneurons, rather than in the photoreceptors (see Chapter 1 Figure 1.5). In order to explain these observations, we propose two hypotheses: (1) that dLRRK regulates axonal growth

and retraction of the L1 and L2 interneurons or of the photoreceptors, and (2) that dLRRK regulates dopamine transmission.

#### 3.4.1.1 Hypothesis 1: LRRK activity regulates the axonal growth and retraction of the L1 and L2 interneurons or of the photoreceptors

As previously mentioned in Chapter 1, LRRK2 has been implicated in axonal outgrowth. Indeed, this was one of the first phenotypes reported in primary neuronal cultures whereby overexpression of PD-associated mutations in *LRRK2* caused a dramatic reduction in neurite length and branching (MacLeod et al., 2006, Plowey et al., 2008, Li et al., 2009, Parisiadou et al., 2009, Heo et al., 2010, Ramonet et al., 2011, Winner et al., 2011). Conversely, silencing or knockout of *LRRK2* has the opposite effect leading to prominent increases in neurite length and branching compared with controls (MacLeod et al., 2006, Parisiadou et al., 2009). Therefore, it is possible that LRRK has a role in mediating the growth and retraction of the L1 and L2 axons within the fly visual system. As knockout of *LRRK2* has previously been reported to increase axon length, it is possible that the L1 and L2 axons in the *dLRRK*$^{-}$ LOF fly model are unable to shrink during the course of the day. This may cause the visual response of these flies to remain in an active state, unlike WT flies. This would likely increase the energy demands on the visual system and in particular on the lamina neurons, which may over time cause degeneration leading to the eventual loss of synaptic signalling that was observed in the old, but not young, *dLRRK*$^{-}$ LOF flies. In support of this idea, it has previously been shown that increasing the energy demands of the visual system accelerates the visual degeneration caused by DA expression of *hLRRK2-G2019S* (Hindle et al., 2013). However, *hLRRK2-G2019S* induced visual degeneration originates in the photoreceptors not the lamina, but this could be due to the *hLRRK2-G2019S* mutation having the opposite effect on the L1 and L2 axonal growth than the *dLRRK*$^{-}$ LOF mutation. *LRRK2*$^{-/-}$ knockout mice also display altered synaptic transmission in striatal projection neurons, such that the amplitude of glutamatergic miniature excitatory postsynaptic currents (mEPSCs) are significantly increased whereas the frequency of mEPSCs are significantly reduced compared with controls (Parisiadou et al., 2014). Interestingly, these *LRRK2*$^{-/-}$ mice also show defects in

neurite outgrowth as they exhibit a significant decrease of dendritic spines, and the dendritic spines that are present are significantly longer but the spine heads are significantly smaller compared with WTs (Parisiadou et al., 2014). Although axonal length was not recorded in the *LRRK2*$^{-/-}$ mouse, this study provides support for our hypothesis, that removal of LRRK causes alterations in neurite outgrowth and consequently effects synaptic transmission.

In the fly, circadian rhythms in the structure of photoreceptors (Chen et al., 1992) and the underlying lamina (Pyza and Meinertzhagen, 1999) have been reported, so neurite outgrowth and retraction occurs here on a daily basis. Notably, within the first optic neuropil the axons of the monopolar cell interneurons, L1 and L2, show daily rhythmic size and shape changes; the axons swell at the beginning of the day and night and later shrink during the course of the day and night, respectively (Pyza and Meinertzhagen, 1999). These axonal changes persist under constant darkness conditions but are absent in the null mutant of the clock gene *period* (*per*$^{01}$), indicating a circadian origin for these rhythms. As well as this happening in *Drosophila*, these neuron types have also been shown to change the size of their axons in two other fly species, namely *Musca domestica* (Pyza and Meinertzhagen, 1995) and *Calliphora vicina* (Pyża and Cymborowski, 2001). The pattern of daily changes of L1 and L2 axon sizes correlates with the pattern of locomotor activity and is specific to each species (Pyża and Cymborowski, 2001). Interestingly, recent data from our lab has also suggested that there is a circadian rhythm in WT *Drosophila* ERG responses, with responses being low at night and in the middle of the day and high in the morning and early evening (Nippe and Elliott, unpublished). Again, the daily pattern of ERG responses correlates with the daily pattern of L1 and L2 axon swelling and shrinking. Therefore, it is possible that shrinking of the L1 and L2 axons during the course of the day and night leads to reduced synaptic transmission between the photoreceptors and the lamina, causing the observed reduction in the ERG response during these hours.

To test this hypothesis, electron microscopy could be utilised as previously described (Pyza and Meinertzhagen, 1999) to observe axonal growth and retraction in the visual system of our *dLRRK*$^{-}$ LOF flies. In addition, flies could be kept under arrhythmic conditions before the visual response is recorded.

### 3.4.1.2 Hypothesis 2: LRRK regulates dopamine transmission

The loss of synaptic signalling in the lamina suggests that LRRK may have a role in regulating dopamine transmission because it is known that dopamine regulates visual responses in both flies and humans (Chyb et al., 1999, Witkovsky, 2004). This idea was initially attractive because dopamine regulates the kinetics of the individual photoreceptor responses to light, and because hLRRK2 has previously been suggested to regulate DA transmission in several rodent studies. It has been shown that mice overexpressing a murine WT *LRRK2* BAC have elevated striatal dopamine release and are hyperactive, whereas mice overexpressing a murine *LRRK2* BAC containing the *G2019S* mutation have an age-dependent decrease in striatal dopamine content, release, and uptake (Li et al., 2010). Murine *G2019S* BAC mutants also have reduced extracellular dopamine levels, which can be detected without pharmacological intervention (Melrose et al., 2010). ROC domain mutant human *R1441G* BAC and *R1441C* knock-in mice, both show impaired dopamine transmission and dopamine receptor function (Li et al., 2009, Tong et al., 2009, Melrose et al., 2010). LRRK2 has been shown to regulate dopamine receptor activation through modulation of protein kinase A activity in a mouse model (Parisiadou et al., 2014). However, other mouse modes have failed to find an interaction between LRRK2 and dopamine transmission, suggesting the need for further research to resolve these discrepancies (Hinkle et al., 2012). In *Drosophila*, transgenic expression of PD-related mutant *dLRRK* significantly reduced brain dopamine content, whereas dopamine content was elevated in *dLRRK*$^{-}$ LOF flies compared with WT controls (Imai et al., 2008). There was no difference in the number of DA neurons in control and *dLRRK*$^{-}$ LOF flies, suggesting that dLRRK negatively regulates steady-state dopamine levels through affecting dopamine transmission, storage or metabolism (Imai et al., 2008). On the other hand, a separate study found a reduction in TH staining in *dLRRK*$^{-}$ LOF flies as well as evidence of DA neuron degeneration (Lee et al., 2007). Overall, there is increasing evidence to suggest a link between LRRK2 and dopamine transmission in both mouse and fly models.

Dopamine is a well-known neurotransmitter and neuromodulator in the vertebrate and invertebrate retina. In the vertebrate retina, light input and the retinal circadian clock regulate the synthesis and release of dopamine, such that dopamine activity is

higher during light exposure and/or during daylight hours (Iuvone et al., 1978, Doyle et al., 2002b). A number of mammalian studies have reported daily rhythms in steady-state levels of dopamine and its major retinal metabolite, 3,4-dihydroxyphenylacetic acid, with levels being higher during the day than at night (Melamed et al., 1984, Nowak and Zurawska, 1989, Pozdeyev and Lavrikova, 2000, Doyle et al., 2002a, Doyle et al., 2002b). These studies suggest that dopamine mediates light-adaptive mechanisms and day-phase circadian processes in retinal function. In support of this, mice in which the expression of *TH* is selectively disrupted in the retina exhibit deficits in light-adapted ERG responses, contrast sensitivity, acuity and retinal circadian rhythms (Jackson et al., 2012). Furthermore, mammalian visual contrast sensitivity shows a circadian rhythm, which is regulated through interactions of the retinal dopamine D4 receptor with the clock gene *Npas2* and the clock-controlled gene *adenylyl cyclase-1* (Hwang et al., 2013). Dopamine is also a key neurotransmitter of the fly visual system and flies deficient in dopamine show visual defects. For example, long-term blockade of dopamine release impairs visual attention-like behaviour in *Drosophila* (Ye et al., 2004). The DA system of *Drosophila* is also highly rhythmic and has been implicated in circadian photoreception; neural dopamine is required for entrainment of activity rhythms to low ambient light (Hirsh et al., 2010). This is further evidenced by the *Drosophila* TH gene, *ple*, exhibiting rhythmic transcription (Ceriani et al., 2002). Thus, dopamine is a key neurotransmitter in maintaining circadian rhythms in both the vertebrate and fly visual systems and altered levels of dopamine can lead to visual deficits.

Putting these ideas together, it is hypothesised that the loss of dLRRK function affects dopamine release within the fly visual system causing deficits in circadian photoreception. Thus, the loss of visual function observed in *dLRRK*$^{-}$ LOF flies may be the consequence of altered dopamine signalling causing these flies to experience nocturnal visual acuity during the day. However, it would be surprising if this was linked to DA transmission because the lamina neurons and photoreceptors do not release dopamine and it was observed during this study that specific expression of *dLRRK* in these tissues rescued the visual response. Thus, we would have to postulate that expression of *dLRRK* within these tissues would somehow be able to affect the levels of dopamine within the visual system and this may prove difficult to explain.

However, in order to explore this hypothesis further, *TH*-RNAi or overexpression of an extra copy of *TH* in the *dLRRK*$^{-}$ LOF flies could be utilised to decrease or increase the levels of dopamine synthesis, respectively. ERGs could then be recorded from these flies. In addition, the release of dopamine from vesicles could be manipulated through altering the expression levels of the *Drosophila* vesicular monoamine transporter, a protein that transports monoamines including dopamine and histamine into the synaptic vesicles of presynaptic neurons (Chang et al., 2006). It should be noted that hypotheses one and two are not necessarily mutually exclusive, because LRRK may influence DA transmission whilst also having a role in axonal outgrowth, and a combination of these might disrupt normal visual function.

### 3.4.2 LRRK is exported and secreted in exosomes

The second key observation in this chapter was that expression of *dLRRK* in the DA neurons or photoreceptors was as effective at rescuing the visual response as expression in the lamina neurons. Expressing *dLRRK* in the glial cells also improved the visual response of *dLRRK*$^{-}$ LOF flies, but this rescue was incomplete with components of the ERG still showing reductions from 3 to 21 DPE. Expression of UAS-*dLRRK* in the absence of GAL4 or expression of GAL4 in the absence of UAS-*dLRRK* did not offer any rescue to the visual response of *dLRRK*$^{-}$ LOF flies. This suggests that the UAS/GAL4 system was functioning as desired and the expression of *dLRRK* was limited to the specific neurons of our choice. Taken together, these data indicates a role for transcellular signalling by LRRK or by a downstream molecule. Interestingly, DA expression of the *hLRRK2-G2019S* mutation in flies has previously been shown to cause a progressive loss of photoreceptor function (Hindle et al., 2013). Again, this suggests a role for transcellular signalling by LRRK as the expression of *hLRRK2-G2019S* in one kind of neuron (DA neuron) leads to loss-of-function and degeneration of a different type (photoreceptor), thus the degeneration spreads from cell-to-cell. Braak et al. (2003) and Braak et al. (2004) have previously proposed the idea of a spreading pathology in PD, based on the observation that α-synuclein deposits spread throughout the brain of PD patients (see Chapter 1, section 1.2.5.2). Our data are in keeping with Braak's idea of a spreading pathology in PD.

One possibility, which could explain how LRRKs action spreads from cell-to-cell in the fly visual system, is that LRRK is exported in exosomes, as it is already known that LRRK2 is released in exosomes by the mammalian kidney (Gonzales et al., 2009, Fraser et al., 2013). Exosomes are a class of small (30-120 nm) extracellular vesicles originating from the endomembrane system when membrane derived from multivesicular bodies (MVBs) fuses with the plasma membrane. They are thought to play key roles in cell-to-cell communication, reviewed in Bang and Thum (2012). A number of cell types including cells in the kidney, brain and immune system (all of which natively express LRRK2) secrete exosomes as a mechanism to export potentially toxic proteins to avoid their build up in the lysosomal system (Bellingham et al., 2012). In PD, there is increasing evidence to suggest an exosomal role in cell-cell transmission of α-synuclein (Desplats et al., 2009, Emmanouilidou et al., 2010, Alvarez-Erviti et al., 2011). Importantly, a number of studies have placed LRRK2 in the right places to be exported in exosomes; for example, LRRK2 has been shown to interact with a number of vesicle types, including endosomes, lysosomes, autophagosomes, the Trans-Golgi-Network and intraluminal vesicles within MVBs (Biskup et al., 2006, Alegre-Abarrategui et al., 2009, Higashi et al., 2009, Herzig et al., 2011, Dodson et al., 2012). Consistent with this, there is a lot of evidence to suggest a role for LRRK2 in the endocytic pathway including retrograde vesicle trafficking from endosomes to the Trans-Golgi-Network and modifying chaperone-mediated autophagy (Biskup et al., 2006, Alegre-Abarrategui et al., 2009, Dodson et al., 2012). LRRK2 also associates with, or physically interacts with, a number of the Rab GTPases. Rab proteins are small GTPases and comprise ~70 family members. They are localised to the cytoplasmic surface of specific subcellular compartments of the endocytic and exocytic pathways and have key roles in all forms of intracellular vesicular trafficking events. As previously mentioned in Chapter 1, LRRK2 has been implicated in regulating synaptic endocytosis via an association with Rab5b (Shin et al., 2008, Yun et al., 2015). In *Drosophila*, dLRRK was found to localise to the membranes of late endosomes and lysosomes where it was shown to physically interact with the late endosomal protein Rab7 (Dodson et al., 2012). Consistent with this, a physical interaction between mammalian LRRK2 and Rab7L1, an orthologue of Rab7, has also been found (MacLeod et al., 2013, Beilina et al., 2014). Deficiency of *Rab7L1* in primary rat neurons, or of the *Rab7L1* orthologue in *Drosophila,* caused DA

neuron denegation, whereas overexpression of *Rab7L1* was able to rescue DA neuron loss and reduced lifespan caused by *LRRK2* mutations in *Drosophila* (MacLeod et al., 2013). PD-associated defects in either *LRRK2* or *Rab7L1* were also shown to cause deficiency of VPS35 and Golgi apparatus sorting defects, which could be rescued through expression of WT *VPS35* (MacLeod et al., 2013). VPS35 is a core component of the retromer complex and is involved in retrograde trafficking of cargos from the endocytic pathway to the Trans-Golgi-Network. Interestingly, *Rab7L1* is a genetic risk factor for sporadic PD and mutations in *VPS35* have been identified in PD families (Vilarino-Guell et al., 2011, Zimprich et al., 2011), further implicating disruption of the retrograde pathway as potentially leading to PD. *Drosophila* LRRK has also been shown to interact with Rab9 (Dodson et al., 2014). *dLRRK*$^{-}$ LOF flies show defects in the endolysosomal and autophagy pathways including an accumulation of enlarged lysosomes, autophagosomes, and early endosomes laden with mono-ubiquitylated cargo proteins. These lysosomal abnormalities are suppressed through expression of a constitutively active form of *Rab9* (Dodson et al., 2014). Furthermore, a recent study utilised modern phosphoproteomics coupled with biochemical and pharmacological approaches to identify a subset of Rab GTPases as bona-fide LRRK2 targets, these included Rab10, Rab1b and Rab8a (Steger et al., 2016). LRRK2 phosphorylates these substrates on an evolutionary conserved threonine residue found in the switch II domain in human and murine cells and in the mouse brain. All of the PD-associated missense mutations in *LRRK2* have been shown to increase the phosphorylation of at least three Rab GTPases, which strongly decreases their affinity for regulatory proteins (Steger et al., 2016). It would be interesting to overexpress some of the Rab proteins in our *dLRRK*$^{-}$ LOF fly model to determine if they are able to rescue the visual dysfunction observed in these flies, or to use flies that are mutant in certain Rab proteins to examine if this causes visual dysfunction. In addition to an association with Rab GTPases, LRRK and LRRK2 have also been shown to phosphorylate *Drosophila* endophilin A and the mammalian orthologue EndoA1, respectively, which is a protein involved in clathrin-mediated endocytosis (Matta et al., 2012, Arranz et al., 2015).

Putting these ideas together, it is hypothesised that in the *dLRRK*$^{-}$ LOF fly model the spread of dLRRK action is mediated by exosomal release, as LRRK secretion from

exosomes provides a possible mechanism by which LRRK action can extend to cells that lack autonomous LRRK expression. It has previously been shown that exosomes mediate the progression of prion diseases (Fevrier et al., 2004, Vella et al., 2007, Coleman et al., 2012) and a similar mechanism has been suggested in a number of other forms of neurodegeneration (Rajendran et al., 2006, Emmanouilidou et al., 2010, Saman et al., 2012). Therefore, *hLRRK2-G2019S* induced degeneration could spread by the release of prion-like proteins in exosomes, either *hLRRK2-G2019S* itself, or by the *G2019S* mutation affecting exosomal release of some other component that leads to neuronal dysfunction and degeneration. To explore this hypothesis further the genetic toolbox of *Drosophila* could be exploited to introduce genes that are known to manipulate exosomal release including *Ykt6* (Gross et al., 2012), *Rab35* (Hsu et al., 2010), *Rab27a/b* (Ostrowski et al., 2010) and *Evi*/*Wntles* (Korkut et al., 2009) into both the *dLRRK*$^{-}$ LOF and *hLRRK2-G2019S* mutant backgrounds. In addition, flies that are transgenic for *dLRRK-, hLRRK2-* or *hLRRK2-G2019S*-tagged with a fluorescent reporter could be generated to determine if LRRK2 is secreted and found in exosomes. It will also be interesting to determine if the expression of *dLRRK* in a cell type that is not found within the visual system is also able to rescue visual function. Unfortunately, as previously mentioned, initial attempts at this using *Dmef2*-GAL4 or *G14*-GAL4 to drive expression in somatic muscle were unsuccessful.

### 3.4.3 The function of dLRRK in the fly visual system is more similar to the function of LRRK2 than LRRK1

In this study it was shown that DA expression, or to a lesser extent glial expression, of the human *LRRK2* gene was as effective as the fly's own version of *LRRK* in rescuing the visual response of *dLRRK*$^{-}$ LOF flies. As previously shown in Figure 3.1, many of the residues present in hLRRK2 are conserved in dLRRK and the two proteins share 24% identity and 38% similarity overall (Wang et al., 2008, Langston et al., 2016). Some of the suggested functions and substrates of hLRRK2 have also been described for dLRRK, suggesting at least partial conservation of function between these two proteins (see section 3.1.1). Thus, it is perhaps unsurprising that *hLRRK2* was able to substitute as effectively as *dLRRK* in our fly model, and our data certainly indicates a conserved functional role of *hLRRK2* and *dLRRK* within the visual response. Although

*hLRRK2* rescued visual dysfunction in the *dLRRK*¯ LOF fly model, there were some differences in the ERG response between flies expressing *hLRRK2* and those expressing *dLRRK* at 21 DPE. As previously mentioned, these two transgenic lines were generated at different times and by different laboratories meaning that the differences in ERG responses may be a consequence of differing expression levels of these two transgenes even in combination with the same GAL4. To test this, western blot analysis could be performed to detect differences in expression levels of *hLRRK2* and *dLRRK* in our *dLRRK*¯ LOF fly model.

Unlike the DA expression of *hLRRK2*, DA expression of *mLRRK1* was unable to completely rescue the visual response of *dLRRK*¯ LOF flies. This suggests that the function of *dLRRK* may be more similar to *hLRRK2* than *mLRRK1*, at least in terms of the visual response. This is slightly surprisingly as structural and phylogenetic analyses suggest that *dLRRK* is actually more closely related to *LRRK1* than *LRRK2* (Marin, 2006, Marin, 2008). However, as shown in Figure 3.1 multiple sequence alignments at the amino acid level demonstrate that the GTPase domain and the leucine-rich repeat domain of *dLRRK* shows more similarity to *hLRRK2* (33% and 25%, respectively) than to *hLRRK1* (30% and 23%, respectively), but the kinase domain shows more similarity to *hLRRK1* than to *hLRRK2* (38% and 36%, respectively). Rare variants in LRRK1 have been proposed to segregate with PD, however there is no genetic support for a causal involvement of LRRK1 in the disease pathogenesis (Schulte et al., 2014). Unfortunately, due to the non-pathogenic nature of LRRK1 it has not been as intensively studied as LRRK2 and a comparison between transgenic expression of *LRRK1* and *LRRK2* has not previously been investigated in flies to our knowledge. Therefore, further studies are needed to determine if the function of LRRK1 and the proteins that it interacts with are conserved between humans and flies.

### 3.4.4 Is the GTPase domain, rather than the kinase domain, the key domain for maintenance of normal visual function?

Here, it was shown that neither DA nor glial expression of the GOF *hLRRK2-G2019S* transgene or the kinase-dead *hLRRK2-D1994A* transgene were able to completely rescue the loss of synaptic signalling of *dLRRK*¯ LOF flies. Interestingly, although these

two mutations are opposing (one increases kinase activity whilst the other decreases kinase activity) they showed similar ERG responses at 21 DPE with no significant differences found between the two. This suggests that the kinase domain may not be the key domain in maintaining the visual response. As briefly mentioned in Chapter 1, there is increasing evidence to suggest that decreased GTPase activity due to mutations in *LRRK2* also plays a key role in PD pathogenesis. For example, the *LRRK2-R1441C/G* mutations consistently lead to decreased GTP hydrolysis but cause either an increase or no obvious effect on GTP binding (Lewis et al., 2007, Li et al., 2007, West et al., 2007, Xiong et al., 2012b). The *LRRK2-G2019S* mutation has also been shown to cause a decrease in the GTPase activity of the protein (Liu et al., 2011a, Xiong et al., 2012b). The *LRRK2-Y1699C* mutation found within the COR domain also leads to decreased GTPase activity, which is thought to be as a consequence of weakening the dimerisation of LRRK2 at the ROC-COR tandem interface (Daniels et al., 2011, Xiong et al., 2012a). Due to the lack of reproducible LRRK2 substrates, it has been suggested that the GTPase domain, which contains autophosphorylation sites, might be the only *in vivo* target for LRRK2 kinase activity (Berwick and Harvey, 2011). This model proposes that autophosphorylation would be required for the GTPase domain function, and the LRRK2 GTPase activity might be the more likely output of this protein than the kinase activity (Berwick and Harvey, 2011). There is controversy surrounding this hypothesis because other studies have failed to find an effect of the *LRRK2-G2019S* mutation on GTPase activity (Xiong et al., 2010). It would be expected that the higher autophosphorylation levels of the *LRRK2-G2019S* mutation would cause a decrease in the activity of the GTPase domain and elicit a very similar effect to the ROC and COR mutations *R1441C* and *Y1699C,* which it fails to do (Berwick and Harvey, 2011). It would be interesting to examine how PD-related mutations in the GTPase domain of *LRRK2* affect the visual response of flies. This may help to reveal if the kinase or the GTPase domain is the key domain for maintaining normal visual function.

### 3.4.5 Mutations in *white* cause visual defects

During this present study, heterozygote $w^{1118}/dLRRK^{-}$ flies showed a significant reduction in the off-transient component of the ERG by 21 DPE. It has previously been suggested that mutations in *white* cause neurodegeneration within the visual system;

data collected from our lab (Petridi and Elliott, unpublished) and by a separate group have shown a reduction in the ERG response of *white* mutant flies with age (Perez et al., 2014). Furthermore, although *white* mutants are positively phototactic they have been shown to lack optomotor responses (Kalmus, 1943) and to have abnormal ERGs (Wu and Wong, 1977). It is thought that these defects are in part attributable to an inability to screen stray light due to the absence of screening pigments, because albino mammals also lacking screening pigments show similar neurological and retinal defects (Guillery, 1986, Jeffery, 1997, Dorey et al., 2003, Thomas et al., 2005). Thus, the $w^{1118}$ mutation may cause the reduction of the 21 DPE off-transient seen here in the $w^{1118}/dLRRK^{-}$ flies, rather than the presence of only one mutant copy of *dLRRK*. This is possible because the visual response was maintained in the alternative $CS/dLRRK^{-}$ heterozygous line.

## 3.5 Conclusion

Flies that lack expression of *dLRRK* develop severe visual defects with age. Tissue-specific expression of *dLRRK* in the eye, lamina neurons, DA neurons, photoreceptors or glial cells is sufficient to rescue the age-related loss of visual function observed in $dLRRK^{-}$ LOF flies. This suggests a key role for transcellular signalling of LRRK *in vivo*, which may be linked to exosomes. The WT human orthologue of *dLRRK* can also rescue the loss of visual function of $dLRRK^{-}$ LOF flies and is able to substitute as effectively as the fly's own version of *LRRK*. Mouse *LRRK1* or kinase-mutant forms of human *LRRK2* only partially restore visual function, suggesting that the function of *dLRRK* in the fly visual system is more similar to the function of *hLRRK2* than *mLRRK1*. This also suggests that the kinase domain may not be the key domain of LRRK in maintaining the visual response.

# 4 Investigating Potential Therapeutic Compounds for Their Rescue of Dopaminergic Expression of *hLRRK2-G2019S in vivo*

## 4.1 Introduction

### 4.1.1 Mitochondrial dysfunction in PD

One of the most common observations of PD and animal models is mitochondrial dysfunction. Mitochondria are oval-shaped semi-continuous organelles of approximately 1-2 μm long and 0.5-1 μm wide. They are often referred to as the 'powerhouse of the cell' as they are responsible for producing adenosine triphosphate (ATP), which is the cells primary energy currency. Two highly specialised membranes enclose mitochondria, the inner and outer membranes, which have differing functions (Figure 4.1A-B). Together, these two membranes form two separate mitochondrial compartments; a narrow intermembrane space enclosed between the outer and inner membrane, and the internal matrix, enclosed by the inner membrane. The inner membrane is usually highly convoluted forming a number of infoldings known as cristae that project into the matrix, thus greatly increasing the surface area. Mitochondria utilise pyruvate and fatty acids as fuel. Pyruvate is produced during glycolysis, a series of cytosolic reactions that oxidises glucose and lipid metabolites in the absence of molecular oxygen. During glycolysis, a glucose molecule of six carbon atoms is converted into two molecules of pyruvate. During the early steps of this process, two molecules of ATP are hydrolysed to provide the required energy, but four ATP molecules are generated during the later steps, meaning there is a net gain of two ATP molecules for each glucose molecule that is broken down. Two energy-rich activated carrier molecules known as NADH are also produced per molecule of glucose. Glycolysis is the key pathway to produce ATP in many anaerobic organisms. In the mitochondria, the metabolism of sugars can be completed and this allows approximately 15 times more ATP to be produced than by glycolysis alone. Both pyruvate and fatty acids are transported across the inner

mitochondrial membrane into the matrix where they are converted to acetyl CoA. Acetyl CoA then enters into the citric acid cycle (also known as the tricarboxylic acid cycle or the Krebs cycle) where the carbon atoms of the acetyl groups are completely oxidised to produce $CO_2$. The acetyl groups are not directly oxidised, rather this group is transferred to oxaloacetate to form a six-carbon tricarboxylic acid known as citric acid, for which the subsequent cycle of reactions is named. The citric acid molecule is then gradually oxidised through a series of reactions giving rise to three molecules of NADH, one molecule of $FADH_2$ and one molecule of GTP. The high-energy molecules that are carried by NADH and $FADH_2$ are transferred to the inner mitochondrial membrane, where they enter the electron transport chain (ETC; Figure 4.1B). NADH is oxidised by complex I (also known as NADH dehydrogenase) of the ETC and $FADH_2$ is oxidised by complex II (also known as succinate dehydrogenase) to produce $NAD^+$ and FAD, respectively. The freed electrons are then passed along the ETC through the respiratory complexes that undergo a series of redox reactions. As electrons move along the respiratory chain, protons ($H^+$) are pumped across the inner membrane into the intermembrane space, thus energy is stored as an electrochemical proton gradient across the inner membrane. This electrochemical proton gradient drives the synthesis of ATP, via the membrane-bound enzyme ATP synthase, in a process known as oxidative phosphorylation.

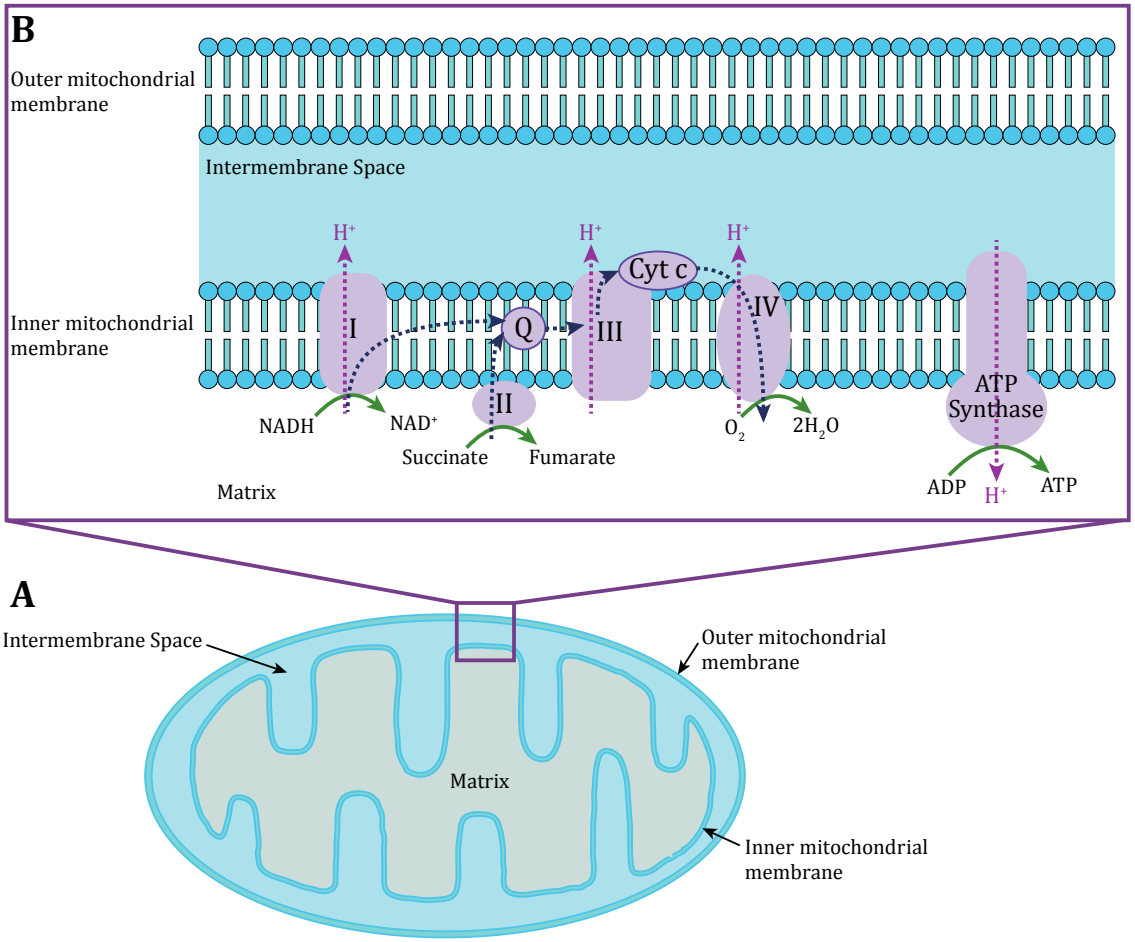


**Figure 4.1 The mitochondrial electron transport chain**

A diagrammatic representation of (A) a mitochondrion and (B) the flow of electrons through mitochondrial complexes I-IV, ubiquinone (Q) and cytochrome c (Cyt c), and the flow of protons ($H^+$) from the matrix to the intermembrane space then through the ATP synthase complex to drive the synthesis of ATP. Dashed blue lines show the flow of electrons, dashed pink lines show the flow of protons and green arrows show the products of reactions with respiratory complexes.

Early evidence for a link between mitochondrial dysfunction and PD came in the 1980's after a group of drug users intravenously injected the neurotoxin MPTP (Langston et al., 1983, Burns et al., 1985). This subsequently caused them to develop Parkinsonism-like symptoms with inhibited mitochondrial respiration. MPTP is a highly lipophilic compound that is able to rapidly cross the BBB upon administration (Duty and Jenner, 2011). In the brain it is taken up by astrocytes where it is metabolised to its active metabolite 1-methyl-4-phenylpyridinium ($MPP^+$). When $MPP^+$ is released from astrocytes, it is taken up in the DA neurons via the dopamine transporter (Blandini and Armentero, 2012). Here, it utilises vesicular monoamine transporters to be taken up and stored in vesicles. It is thought that the storage of $MPP^+$ in vesicles causes dopamine to be ousted due to the limited capacity of the vesicle. Once in the intercellular space, dopamine can be metabolised to a number of toxic compounds. In the neuron, the majority of MPTP accumulates in the mitochondria where it inhibits complex I of the ETC leading to an increase in reactive oxygen species (ROS) and a decrease in ATP production (Nicklas et al., 1987). This is likely to lead to the initiation of cell death-related signalling pathways such as p38-mitogen activated kinase and c-Jun N-terminal kinase, which have both been shown to be activated upon MPTP administration (Saporito et al., 2000, Karunakaran et al., 2008, Duty and Jenner, 2011). Subsequent studies and *post-mortem* analysis reveal that the activity of complex I is also significantly reduced (by approximately 30%) in the SN of sporadic PD patients (Schapira et al., 1989, Exner et al., 2012). Complex I deficiencies have also been found in the frontal cortex of PD *post-mortem* brains (Parker et al., 2008).

Several of the PD-related genes including *PINK1*, *parkin*, *DJ-1*, *α-synuclein* and *LRRK2* have been linked to the mitochondria. For example, mutations in *PINK1* have been shown to cause a plethora of mitochondrial defects including decreases in mitochondrial membrane potential (MMP), reduced activity of complexes I and IV, reduced ATP production, decreased mitochondrial import and mtDNA levels, increased production of ROS, and abnormal mitochondrial morphologies (Exner et al., 2007, Hoepken et al., 2007, Gautier et al., 2008, Piccoli et al., 2008, Dagda et al., 2009, Gegg et al., 2009, Gispert et al., 2009, Grunewald et al., 2009, Morais et al., 2009, Winklhofer and Haass, 2010). There are also consistent findings from *parkin*-mutant

patient tissue, which shows decreases in complex I activity (up to 45%), MMP (up to 30%) and ATP production (up to 58%), as well as altered mitochondrial morphology (Mortiboys et al., 2008). PINK1 and parkin operate within the same pathway; PINK1 recruits parkin to the outer mitochondrial membrane, which induces mitophagy as a way for the cell to dispose of damaged mitochondria. The PINK1-parkin pathway has also been implicated in mitochondrial transport (Weihofen et al., 2009, Wang et al., 2011, Liu et al., 2012).

There is less known about the impact that LRRK2 has on the mitochondria. Approximately 10% of overexpressed LRRK2 has been found to be in association with the outer mitochondrial membrane (West et al., 2005). Confocal imaging, subcellular fractionation, and electron microscopy have been utilised to show the localisation of endogenous LRRK2 to mitochondria in mammalian brain tissue (Biskup et al., 2006, Exner et al., 2012). Mitochondrial pathology has been observed in transgenic mice expressing the *LRRK2-G2019S* mutation (Ramonet et al., 2011). Furthermore, skin fibroblasts derived from patients carrying the *LRRK2-G2019S* mutation show decreases in MMP and overall ATP production, as well as increased mitochondrial interconnectivity (Mortiboys et al., 2010). Fragmented mitochondria have also been observed in mammalian cultured cells and primary cortical neurons upon overexpression of WT *LRRK2* or pathogenic *LRRK2* mutants via increased mitochondrial recruitment of dynamin-related protein, Drp1 (Wang et al., 2012). Although these studies suggest a link between LRRK2 pathology and mitochondrial dysfunction, further studies are needed to determine whether these effects are direct or indirect and the underlying mechanisms that are involved.

### 4.1.2 Bile acid mitochondrial rescue agents

A recent *in vitro* drug screen performed in fibroblasts derived from *parkin*-mutant PD patients identified a number of compounds that were able to rescue reduced MMP and cellular ATP levels (Mortiboys et al., 2013). Two of these compounds, namely ursocholanic acid (UCA), a bile acid derivative, and dehydro (11,12) ursolic acid lactone (DUA), a pentacyclic triterpene, were selected for further assessment to determine their effect on the activities of complexes I-IV of the ETC (Figure 4.2A-B). Both UCA and DUA were found to significantly rescue and increase the activities of

complexes I-IV by 200-500%. DUA and UCA show structural similarities to glucocorticoids, so it is perhaps unsurprising that inhibition or knockdown of the glucocorticoid receptor completely abolished the mitochondrial rescue effects of these compounds (Mortiboys et al., 2013).

Neither DUA nor UCA are FDA-licensed drugs, and there is little information available concerning their bioavailability and safety in humans. Following a literature search, the chemically related compounds, ursodeoxycholic acid (UDCA), a bile acid, and ursolic acid (UA), a pentacyclic triterpene, were identified (Figure 4.2C-D). Unlike DUA and UCA, the clinical pharmacokinetics of UDCA are well characterised and it has been used in the clinical treatment of primary biliary cirrhosis for over 30 years (Poupon et al., 1994). In addition, UDCA is now considered as the first-line of treatment for other cholestatic conditions including primary sclerosing cholangitis and intrahepatic cholestasis of pregnancy (Sepe et al., 2014). UDCA has a high safety profile, and its clinical history reveals minimal side effects. The derivative of UDCA, tauroursodeoxycholic acid (TUDCA), is able to prevent neuropathology in animal models of Huntington's disease and Stroke, and also improves the survival and function of nigral transplants in a rat model of PD (Duan et al., 2002, Keene et al., 2002, Rodrigues et al., 2003). Another study has revealed that UDCA is neuroprotective in DA neurons via the modulation of anti-oxidative molecules and attenuation of mitochondria-mediated programmed cell death pathways (Chun and Low, 2012). UA is a naturally occurring compound that is present in many plants. The bioavailability of UA and its dose-dependent increase in mouse brain tissue has been well characterised (Yin et al., 2012). Like DUA and UCA, both UDCA and UA were able to significantly rescue and increase intracellular ATP levels and MMP of *parkin*-mutant fibroblasts. UCA and UDCA were also shown to rescue mitochondrial dysfunction in parkin-deficient neurons (Mortiboys et al., 2013). Furthermore, UCA and UDCA are able to completely rescue cellular ATP levels in *LRRK2-G2019S*-mutant fibroblasts with a similar effect to that observed in *parkin*-mutant patient tissue (Mortiboys et al., 2013). Therefore, the beneficial effect of these compounds is not limited to *parkin*-associated PD thus increasing the relevance of these compounds for potential therapeutic use in the treatment of PD.

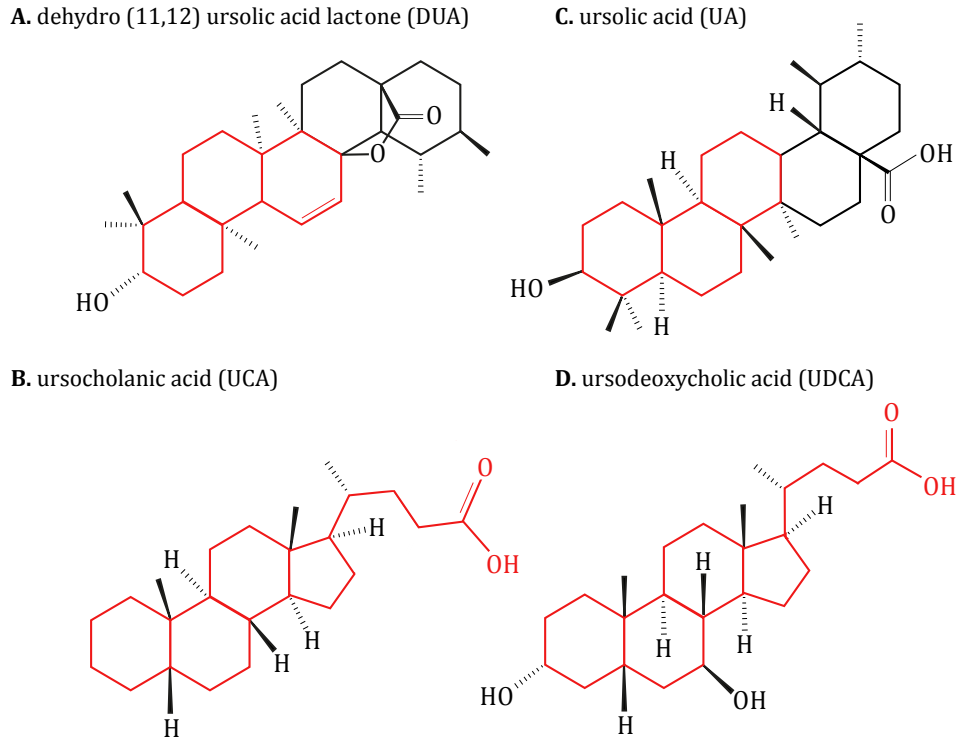


**Figure 4.2 Structures of four chemically related bile acid derivatives**

(A) dehydro (11,12) ursolic acid lactone (DUA) and (B) ursocholanic acid (UCA) were identified during the initial drug screen, whilst a literature search identified (C) ursolic acid (UA) and (D) ursodeoxycholic acid (UDCA) as two structurally similar compounds. The structural similarities are shown in red. All structures are represented in standard chemical format and the 3D-orientation of the groups are displayed. Hydrogens are only displayed if they affect the 3D-orientation of the molecule. Where no group is shown, a methyl group is attached. Adapted with permission from Mortiboys et al. (2013).

The *LRRK2-G2019S* mutation shows an age-dependent, reduced penetrance, suggesting the presence of biological rescue mechanisms in some individuals. If suitable biological targets can be identified, it may be possible to reduce the risk or even prevent currently asymptomatic or non-manifesting *LRRK2-G2019S* (NM-*LRRK2-G2019S*) carriers from undergoing phenotypic conversion and developing clinically manifest PD (M-*LRRK2-G2019S*). We recently reported that intracellular ATP levels and basal mitochondrial oxygen consumption are similarly decreased in both M-*LRRK2-G2019S* and NM-*LRRK2-G2019S* carriers (Mortiboys et al., 2015). Treatment with UDCA was able to recover intracellular ATP levels in NM-*LRRK2-G2019S* fibroblasts similarly to that previously seen in M-*LRRK2-G2019S* fibroblasts (Mortiboys et al., 2013, Mortiboys et al., 2015). Unlike in *parkin*-mutant patient tissue, the activities of complexes I and II were normal in both M-*LRRK2-G2019S* and NM-*LRRK2-G2019S* carriers compared with controls, whereas complex IV activity was markedly decreased in both. A significant decrease in complex III activity was recorded in M-*LRRK2-G2019S* carriers, and an intermediate non-significant decrease was recorded in NM-*LRRK2-G2019S* carriers. The specific impairment of complex IV activity in *LRRK2-G2019S*-associated PD delineates this form of familial PD from the early-onset forms of PD (EOPD), caused by mutations in *parkin* or *PINK1*, which show specific dysfunction of complex I. This suggests that although different mechanisms may lead to mitochondrial dysfunction in EOPD and *LRRK2-G2019S*-associated PD, UDCA is an effective therapeutic compound in both scenarios.

### 4.1.3 DUA and UCA rescue mitochondrial function through increasing the phosphorylation of Akt$^{Ser473}$

Akt (or protein kinase B) is a serine/threonine kinase that was first discovered as a proto-oncogene (Bellacosa et al., 1991). Since its discovery, Akt has become a major focus of attention because it has been implicated in the regulation of diverse cellular functions including metabolism, growth, proliferation, survival, transcription and protein synthesis. The Akt pathway is activated in response to insulin, growth factors, cytokines and cell stress that induce the production of phosphatidylinositol (3,4,5) trisphosphates by phosphatidylinositol 3-kinase (PI3K). These lipids serve as docking sites and recruit Akt and its upstream activator PDK1 to the plasma

membrane. PDK1 phosphorylates Akt at $Thr^{308}$, which leads to partial activation of Akt. mTORC2 phosphorylates Akt at $Ser^{473}$ stimulating full enzymatic activity. Mis-regulation of this pathway has been implicated in a variety of human diseases including cancer, cardiovascular disease, diabetes and neurological diseases such as Alzheimer's and Huntington's disease (Colin et al., 2005, Griffin et al., 2005). More recently, defective Akt signalling has been implicated in the neurodegenerative process of PD, with a number of studies reporting that drugs used to treat PD through targeting the DA system are neuroprotective via Akt activation (Sagi et al., 2007, Chen et al., 2008, Lim et al., 2008, Nair and Olanow, 2008, Yu et al., 2008). Furthermore, the expression of constitutively active Akt protects against DA cell death induced by intrastriatal 6-OHDA (Ries et al., 2006). It has also been reported that Akt signalling is promoted by parkin (Fallon et al., 2006, Yang et al., 2005) and DJ-1 (Kim et al., 2005, Yang et al., 2005), both of which are implicated in autosomal recessive forms of PD. Finally, the expression of *Akt* and *phospho$^{Ser473}$-Akt*, which are both normally expressed at high levels in the DA neurons of human brains, are found to be significantly decreased in the PD brain (Timmons et al., 2009).

UA has previously been reported to reduce muscle atrophy and stimulated muscle hypertrophy in mice through increasing the phosphorylation of Akt at $Ser^{473}$ (Kunkel et al., 2011). UDCA has been reported to suppress mitochondria-dependent cell death in SH-SY5Y cells and similarly to UA, it was found to exert its protective effect through Akt activation (Chun and Low, 2012). In accordance with this, DUA and UCA were found to significantly increase $Akt^{Ser473}$ phosphorylation in *parkin*-mutant fibroblasts, but interestingly not in control fibroblasts (Mortiboys et al., 2013). Selective inhibition of Akt phosphorylation or PI3K activity abolished the therapeutic effects of DUA and UCA in *parkin*-mutant fibroblasts, thus further implicating the Akt pathway in the mitochondrial rescue effect exerted by these compounds (Mortiboys et al., 2013).

### 4.1.4 Mitochondrial dysfunction in the *hLRRK2-G2019S* fly model

The selective expression of the *hLRRK2-G2091S* transgene in the DA neurons of flies (*TH>G2019S*) leads to a progressive, age-related loss of photoreceptor function (Hindle et al., 2013). The functional decline in the ERG response of old (28 DPE)

*TH>G2019S* flies was accompanied by severe neurodegeneration throughout the internal structure of the retina. Antibody staining reveals clear evidence of increased autophagy and apoptosis around the microvilli of the photoreceptors, whilst electron micrographs show that the photoreceptor mitochondria are also compromised. These dysfunctional mitochondria became swollen (70% increase in area) with wider cristae (~80% wider), and are increasingly more broken, fragmented and rounded (Hindle et al., 2013). The degeneration caused by the DA expression of *hLRRK2-G2019S* is accelerated through increasing the demands on the visual system to adapt, or through increasing the activity of the DA neurons. *TH>G2019S* flies kept in vials with the light pulsed on and off at random intervals show a significant reduction in ERG amplitude by 10 DPE compared with flies with DA expression of the WT *hLRRK2* transgene. Mitochondrial degeneration has also been reported in the flight muscles of flies expressing the *hLRRK2-G2019S* transgene under the control of a muscle-specific driver (Ng et al., 2012).

As previously described in Chapter 1, a more sensitive assay based on the SSVEP method was developed for recording the visual response of flies (Afsari et al., 2014). This highly sensitive assay allows the isolation of the responses from the photoreceptors, second-order lamina neurons and third-order medulla neurons. The fly SSVEP is designed to deliver stimuli that sweep through different contrast levels, enabling the measurement and analysis of contrast response functions (CRFs; see Chapter 2, section 2.2.2 for a complete description of this assay). The SSVEP assay has proved sensitive enough to be able to detect abnormal visual phenotypes caused by DA expression of *hLRRK2-G2019S* in 1 DPE flies. Raising larvae on the previously published LRRK2-IN-1 kinase inhibitor or a novel kinase inhibitor, BMPPB-32, rescued the SSVEP of *hLRRK2-G2019S* 1 DPE flies (Afsari et al., 2014). Thus, this assay provides a robust and stable platform to assess the visual response of flies and to determine the effectiveness and selectivity of potential therapeutic compounds (Afsari et al., 2014). The SSVEP assay was used throughout this chapter to meet the following aims.

## 4.2 Aims

1. Determine the *in vivo* effects of two mitochondrial rescue agents, namely UCA and UDCA, on neuronal function in flies with DA expression of the *hLRRK2-G2019S* mutation.
2. Assess the effects that UCA and UDCA have on the activities of complexes I-IV of the mitochondrial respiratory chain in the *hLRRK2-G2019S* fly model.
3. Establish whether UCA and UDCA interact with Akt *in vivo* as previously described *in vitro*.
4. Asses whether overexpression of *parkin* in the DA neurons provides protection against *hLRRK2-G2019S* induced visual dysfunction.
5. Determine if the kinase inhibitor, BMPPB-32, can rescue *hLRRK2-G2019S* induced visual dysfunction after being administrated to adult flies.

Some of the data presented in this chapter are already published in:

Mortiboys H, Furmston R, Bronstad G, Aasly J, Elliott C, Bandmann O. UDCA exerts beneficial effect on mitochondrial dysfunction in $LRRK2^{G2019S}$ carriers and in vivo. *Neurology* 2015;10(85):846–52

West RJ, Furmston R, Williams CA, Elliott CJ. Neurophysiology of *Drosophila* models of Parkinson's disease. *Parkinsons Dis.* 2015;381281

## 4.3 Results

### 4.3.1 Increasing the energy demands of the visual system leads to a rapid loss of visual function in flies with DA expression of *hLRRK2-G2019S* by 7 DPE

Here, the sensitive SSVEP assay was used to determine the *in vivo* effects of the bile acid derivatives UCA and UDCA when they were fed to *hLRRK2-G2019S* transgenic flies. First, the progression of visual degeneration of flies expressing the mutant *hLRRK2-G2019S* transgene in the DA neurons (*TH>G2019S*) was compared to flies expressing the WT *hLRRK2* transgene (*TH>hLRRK2*) or to control flies expressing no transgene ($TH/w^{apricot}$). DA expression of *hLRRK2-G2019S* or WT *hLRRK2* was

achieved as previously described (Hindle et al., 2013, Afsari et al., 2014). Both the WT and mutant *hLRRK2* transgenic fly lines have orange eyes, therefore the non-transgenic $w^{apricot}$ fly line, also with orange eyes, was chosen as an eye-colour matched control (Figure 4.3). This eliminated differences in the amount of screening pigment between genotypes, which is known to alter the shape and size of the ERG, and enabled direct comparisons to be made between genotypes.

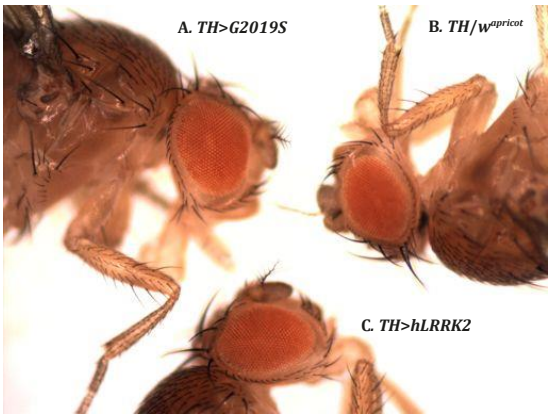


**Figure 4.3 A comparison between the eye colour of flies with DA expression of *hLRRK2-G2019S*, WT *hLRRK2* or no transgene**

Flies with DA expression of (A) the PD-associated *hLRRK2-G2019S* transgene (*TH>G2019S*), (B) no transgene ($TH/w^{apricot}$), or (C) the WT *hLRRK2* transgene (*TH>hLRRK2*) all have a similar orange eye colour. The amount of screening pigment between these three genotypes is similar, thus any differences in the CRFs between genotypes should not be due to eye colour.

To speed up the life cycle and to accelerate visual degeneration, newly emerged female flies were transferred to instant food supplemented with 100% EtOH and were kept in a pulsating light incubator at 29°C. To ensure the food didn't dry out, flies were transferred to fresh vials every 2-3 days. Flies were prepared for ERG analysis as previously described (see Chapter 2, section 2.2.2). After dark adaption, the photic responses of flies were verified through the presence of a robust response to six flashes of the blue component of an LED light. If a fly failed to respond during the flash ERG, the fly was discarded. If a robust response was recorded, the SSVEP assay was run using a pre-programmed sequence of frequency-tagged flickering stimuli as described in Afsari et al. (2014). The temporal contrast of the probe stimuli (12 Hz) was swept through a range of values (0-69%). The visual response to this stimulus was measured both in isolation, and in the presence of a 30% contrast mask at a different temporal frequency (15 Hz). This enabled the effects of the stimulus and mask contrast to be measured in isolation. To observe the progression of visual degeneration, CRFs were measured by SSVEP at 3, 7 and 14 DPE for each genotype. Signalling from the photoreceptors (1F1) and the lower-order lamina (2F1) and medulla (2F1+2F2) neurons, were separated and plotted on individual graphs against the probe contrast level. Graphs were plotted on the same scale for each age and genotype tested to aid comparisons between data sets.

At 3 DPE, robust CRFs were recorded from $TH/w^{apricot}$ controls and from transgenic *TH>hLRRK2* and *TH>G2019S* flies (Figure 4.4Ai-iv). The grey curve on each graph shows the response when the mask is absent (unmasked) whilst the pink curve shows the response in the presence of the constant 30% contrast mask (masked) as the contrast of the probe increases from 0 to 69%. For each genotype, the unmasked responses from both the 1F1 and 2F1 harmonic components of the swept probe increased monotonically with contrast. The intermodulation (2F1+2F2) response showed a maximum level at around the point where the contrast of the mask and probe are equal (30% contrast), which has previously been described in Afsari et al. (2014). In these intermodulation graphs, the grey line provided an estimate of baseline noise level as it represents the response when the second input frequency is not present and thus appears as a flat line. The CRFs recorded from $TH/w^{apricot}$, *TH>hLRRK2* and *TH>G2019S* flies were also plotted on the same graph to aid

comparisons between genotypes. (Figure 4.4B). These graphs show that at 3 DPE, the CRFs recorded from control and transgenic flies were very similar.

The average peak CRFs for the unmasked 1F1, unmasked 2F1 and masked and unmasked 2F1+2F2 responses were plotted for each genotype (Figure 4.5A-D). These plots show that there were no significant differences in the peak CRFs recorded from control and *TH>G2019S* flies at 3 DPE (all $p>0.05$). There were no significant differences observed for the 2F1+2F2 unmasked responses between genotypes, suggesting that the baseline noise level was similar between experiments (Figure 4.5D).

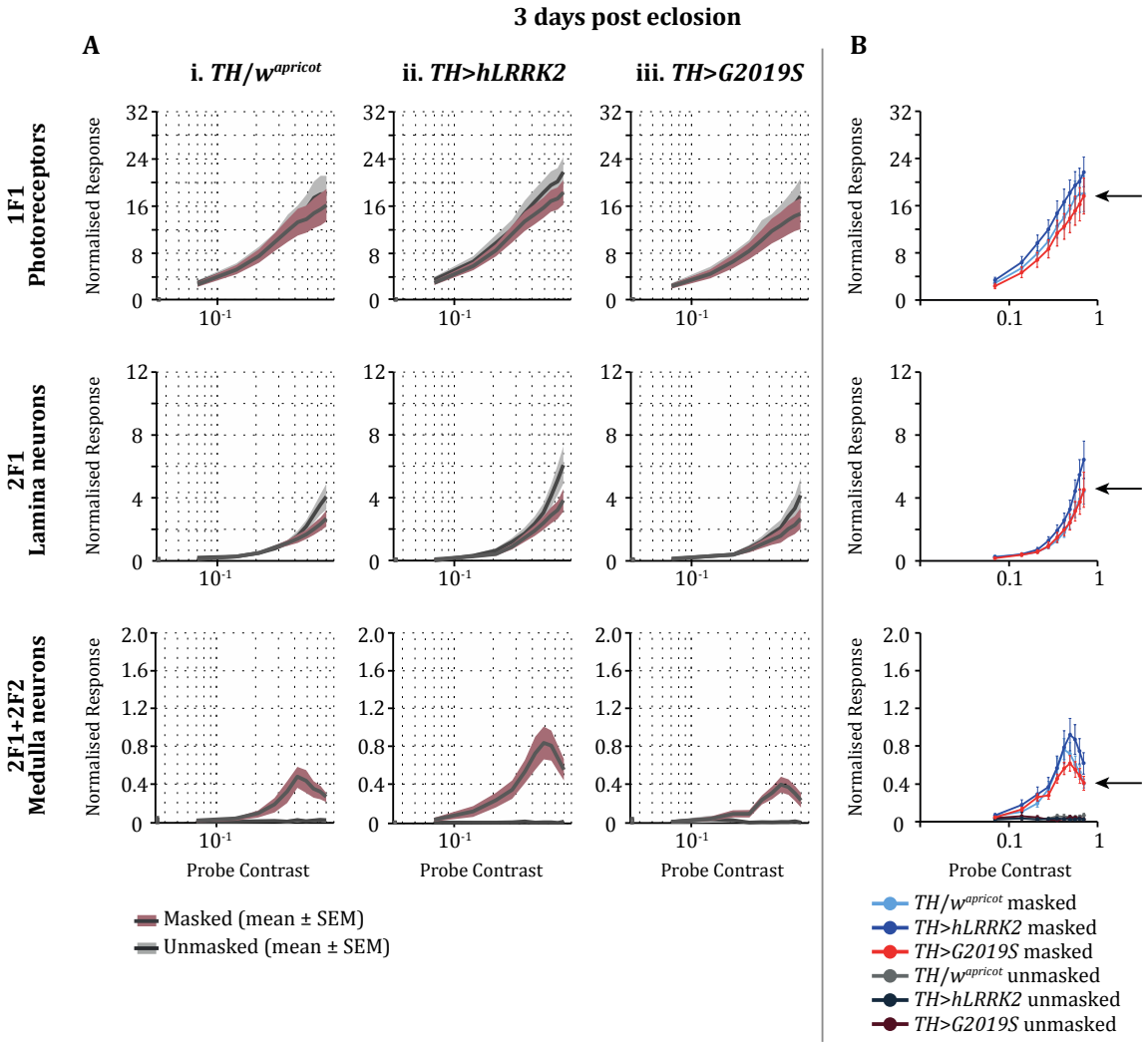


**Figure 4.4 Neural responses to swept contrast flicker recorded at 3 DPE are similar between flies with DA expression of *hLRRK2-G2019S* and controls**

(A) 3 DPE CRFs recorded from (i) *TH/w*$^{apricot}$, (ii) *TH>hLRRK2* and (iii) *TH>G2019S* flies for 1F1 (first row), 2F1 (second row) and 2F1+2F2 (third row) with (pink) and without (grey) a 30% mask as the probe contrast is increased from 0 to 69%. (B) Combined plots of all genotypes for the corresponding rows in (A). In (A) the solid lines indicate the mean response and the shaded area indicates ± SEM. In (B) data are mean ± SEM bars. The black arrows point to the responses from flies with DA expression of *hLRRK2-G2019S*, which indicate that the responses of these flies were similar to control flies. n≥8 for each genotype.

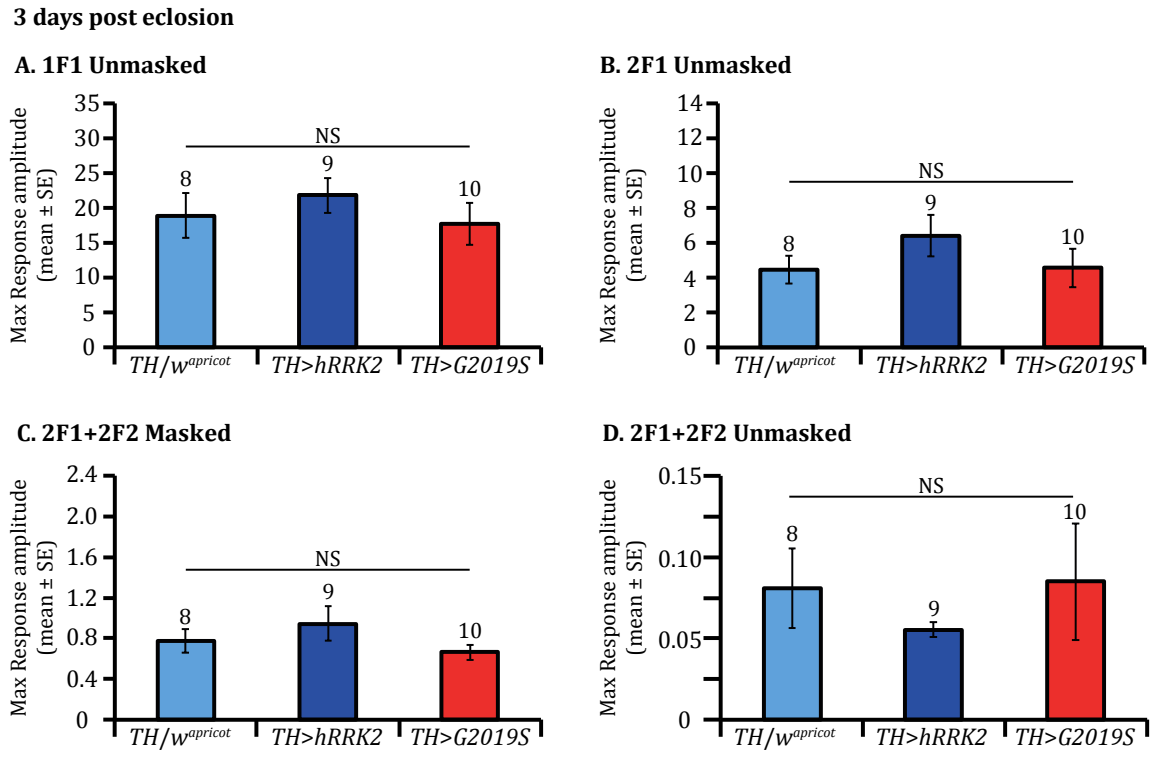


**Figure 4.5 At 3 DPE, peak CRFs do not differ between flies with DA expression of *hLRRK2-G2019S* or controls**

The 3 DPE peak CRFs recorded from flies expressing no transgene (*TH/w*$^{apricot}$: light blue), WT *hLRRK2* (*TH>hLRRK2*: dark blue) or *hLRRK2-G2019S* (*TH>G2019S*: red) in the DA neurons for (A) 1F1 photoreceptors, (B) 2F1 lamina, (D) 2F1+2F2 medulla, without a 30% mask and (C) 2F1+2F2, with a 30% mask as the probe contrast is increased from 0 to 69%. (A-C) The peak CRFs recorded from the three neuronal layers were comparable between genotypes. (D) There were no significant differences in the unmasked 2F1+2F2 responses between genotypes, thus the baseline noise level was similar between experiments. All statistics are ANOVA with post-hoc Bonferroni correction: NS, no significant difference, $p>0.05$. Data presented are mean ± SEM bars; n numbers are displayed above the bars.

At 7 DPE, CRFs recorded from control *TH/w*$^{apricot}$ and *TH>hLRRK2* flies remained robust and were similar, if not slightly increased, compared to those recorded at 3 DPE (Figure 4.6Ai-ii). In contrast, CRFs recorded from 7 DPE *TH>G2019S* flies were dramatically reduced compared with those recorded at 3 DPE (photoreceptors: 59% decrease; lamina: 64% decrease; medulla: 55% decrease; Figure 4.6Aiii). The 7 DPE *TH>G2019S* CRFs were also considerably lower than the CRFs recorded from *TH>hLRRK2* and *TH/w*$^{apricot}$ flies (Figure 4.6B).

Plotting the average peak CRFs for each genotype (Figure 4.7A-D) revealed that the photoreceptor responses of *TH>G2019S* flies were reduced to 24% of *TH/w*$^{apricot}$ flies ($p$<0.001) and 33% of *TH>hLRRK2* flies ($p$<0.001). The responses recorded from the neuronal layers of *TH>G2019S* flies were even more reduced compared with control flies (lamina response: 15% of *TH/w*$^{apricot}$ flies, $p$<0.001 and 22% of *TH>hLRRK2* flies, $p$<0.01; medulla response: 17% of *TH/w*$^{apricot}$ flies, $p$<0.001 and 29% of *TH>hLRRK2* flies, $p$<0.05). The CRFs recorded from *TH>hLRRK2* flies were slightly reduced compared with those recorded from *TH/w*$^{apricot}$ flies, although only the photoreceptor responses showed a significant difference ($p$<0.05). *TH>hLRRK2* flies are likely to have slightly higher LRRK2 kinase activity compared with non-transgenic *TH/w*$^{apricot}$ flies because they express a copy of the *hLRRK2* gene in addition to their own version *LRRK*. Increased LRRK2 kinase activity may have caused the reduced photoreceptor responses observed in these flies.

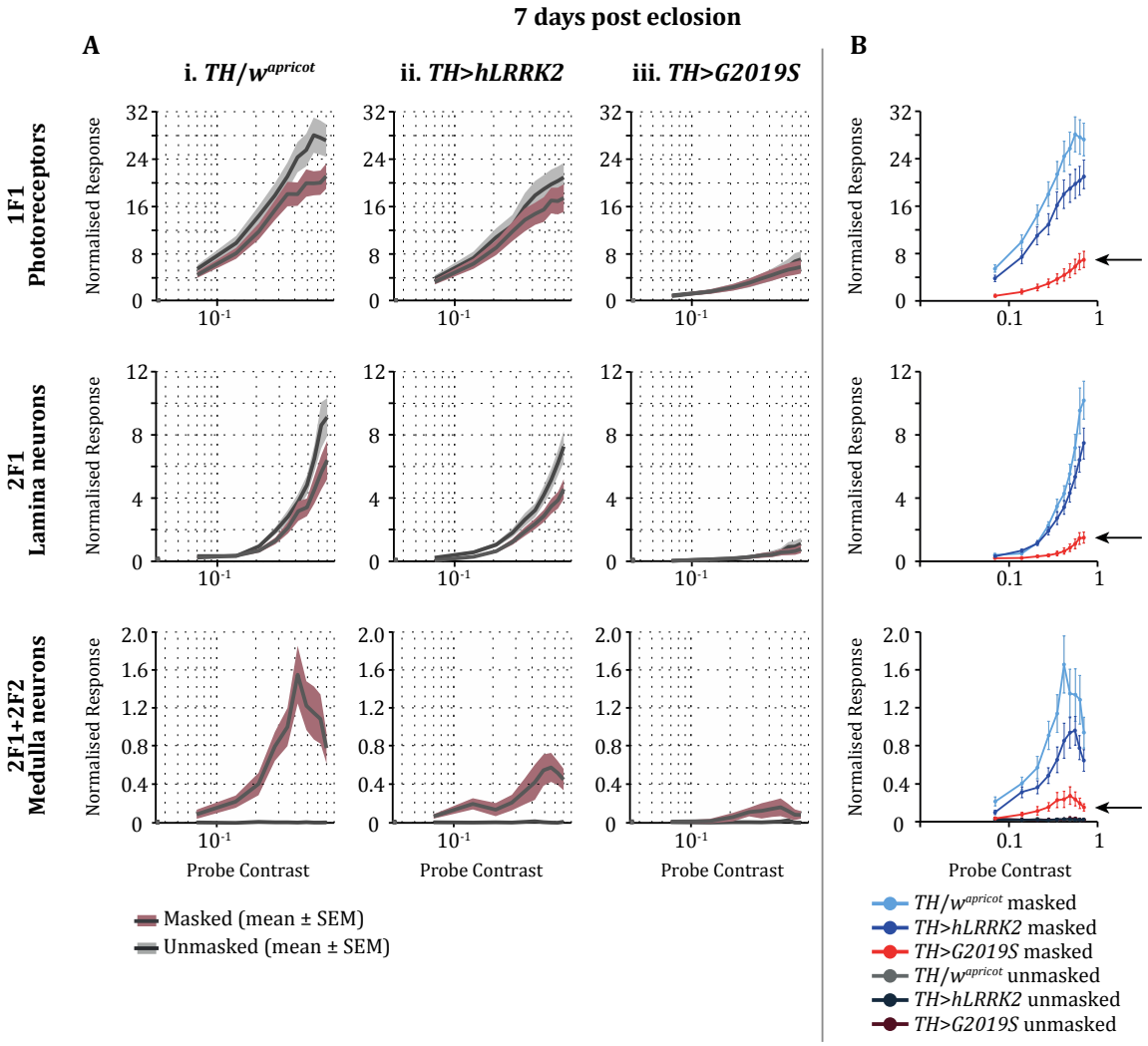


**Figure 4.6 Neural responses to swept contrast flicker recorded at 7 DPE are dramatically reduced in flies with DA expression of *hLRRK2-G2019S* compared with controls**

(A) 7 DPE CRFs recorded from (i) *TH/w*$^{apricot}$, (ii) *TH>hLRRK2* and (iii) *TH>G2019S* flies for 1F1 (first row), 2F1 (second row) and 2F1+2F2 (third row) with (pink) and without (grey) a 30% mask as the probe contrast is increased from 0 to 69%. (B) Combined plots of all genotypes for the corresponding rows in (A). In (A) the solid lines indicate the mean response and the shaded area indicates ± SEM. In (B) data are mean ± SEM bars. The black arrows point to the responses from flies with DA expression of *hLRRK2-G2019S*, which indicate the severe reduction in the visual response of these flies compared to controls. n≥11 for each genotype.

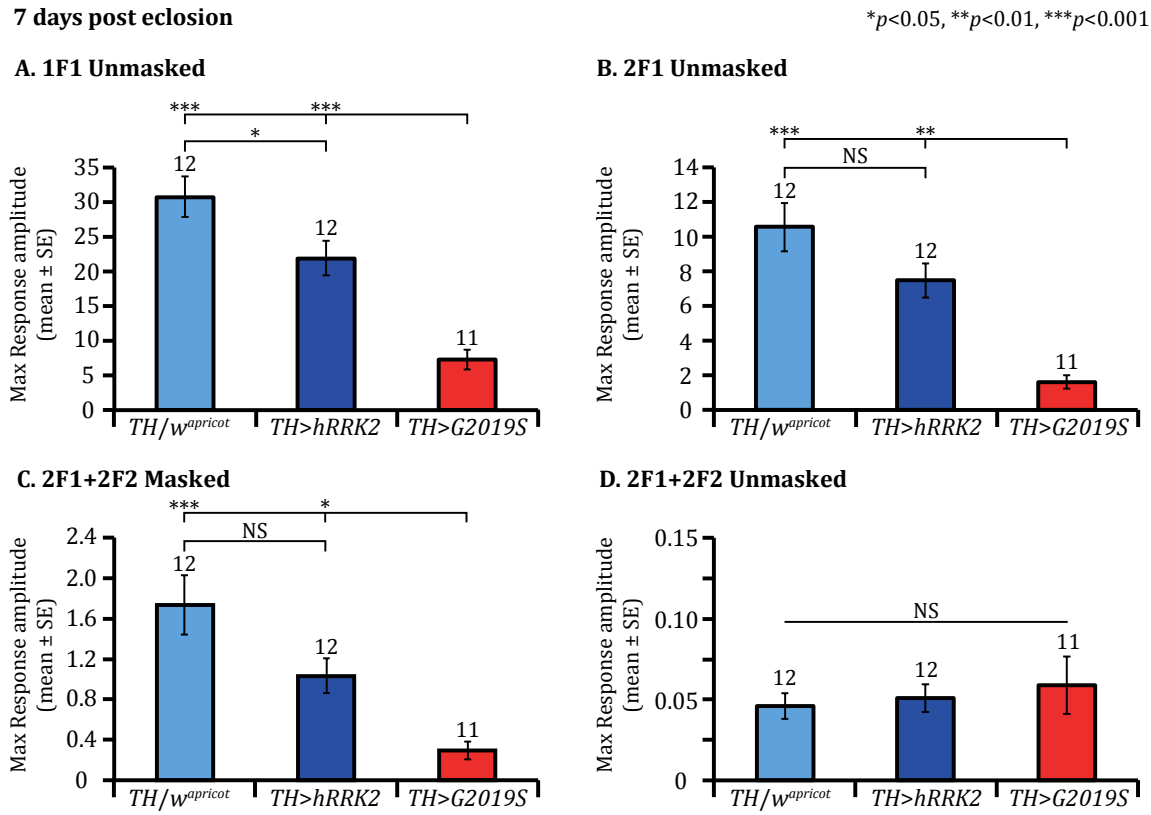


**Figure 4.7 At 7 DPE, peak CRFs recorded from flies with DA expression of *hLRRK2-G2019S* are significantly lower than controls**

The 7 DPE peak CRFs recorded from flies expressing no transgene (*TH/w*$^{apricot}$: light blue), WT *hLRRK2* (*TH>hLRRK2*: dark blue) or *hLRRK2-G2019S* (*TH>G2019S*: red) in the DA neurons for (A) 1F1 photoreceptors, (B) 2F1 lamina, (D) 2F1+2F2 medulla, without a 30% mask and (C) 2F1+2F2, with a 30% mask as the probe contrast is increased from 0 to 69%. (A-C) The peak CRFs recorded from all three neuronal layers were significantly lower in flies expressing *hLRRK2-G2019S* compared with flies expressing no transgene or those expressing WT *hLRRK2*. The photoreceptor responses of *TH>hLRRK2* flies were also significantly lower than those recorded from *TH/w*$^{apricot}$ flies. (D) There were no significant differences in the unmasked 2F1+2F2 responses between genotypes, thus the baseline noise level was similar between experiments. All statistics are ANOVA with post-hoc Bonferroni correction: ***$p$<0.001, **$p$<0.01, *$p$<0.05, NS, no significant difference, $p$>0.05. Data presented are mean ± SEM bars; n numbers are displayed above the bars.

At 14 DPE, the visual responses recorded from *TH*/$w^{apricot}$ and *TH>hLRRK2* flies had deteriorated, evidenced by the reduction in the CRFs from those recorded at 7 DPE (Figure 4.8Ai-ii). The CRFs recorded from *TH>G2019S* flies remained very low and were almost indistinguishable from those recorded at 7 DPE (Figure 4.8Aiii). The 14 DPE CRFs were similar between genotypes (Figure 4.8B). Plotting the peak CRFs revealed that the photoreceptor, lamina and medulla responses were not significantly different between the three genotypes (Figure 4.9A-D). The reduced visual response of control flies at 14 DPE suggested that prolonged exposure to pulsating lights at 29˚C caused adverse effects, therefore 7 DPE was chosen as the latest time-point to record the visual response of flies under these conditions for all subsequent experiments.

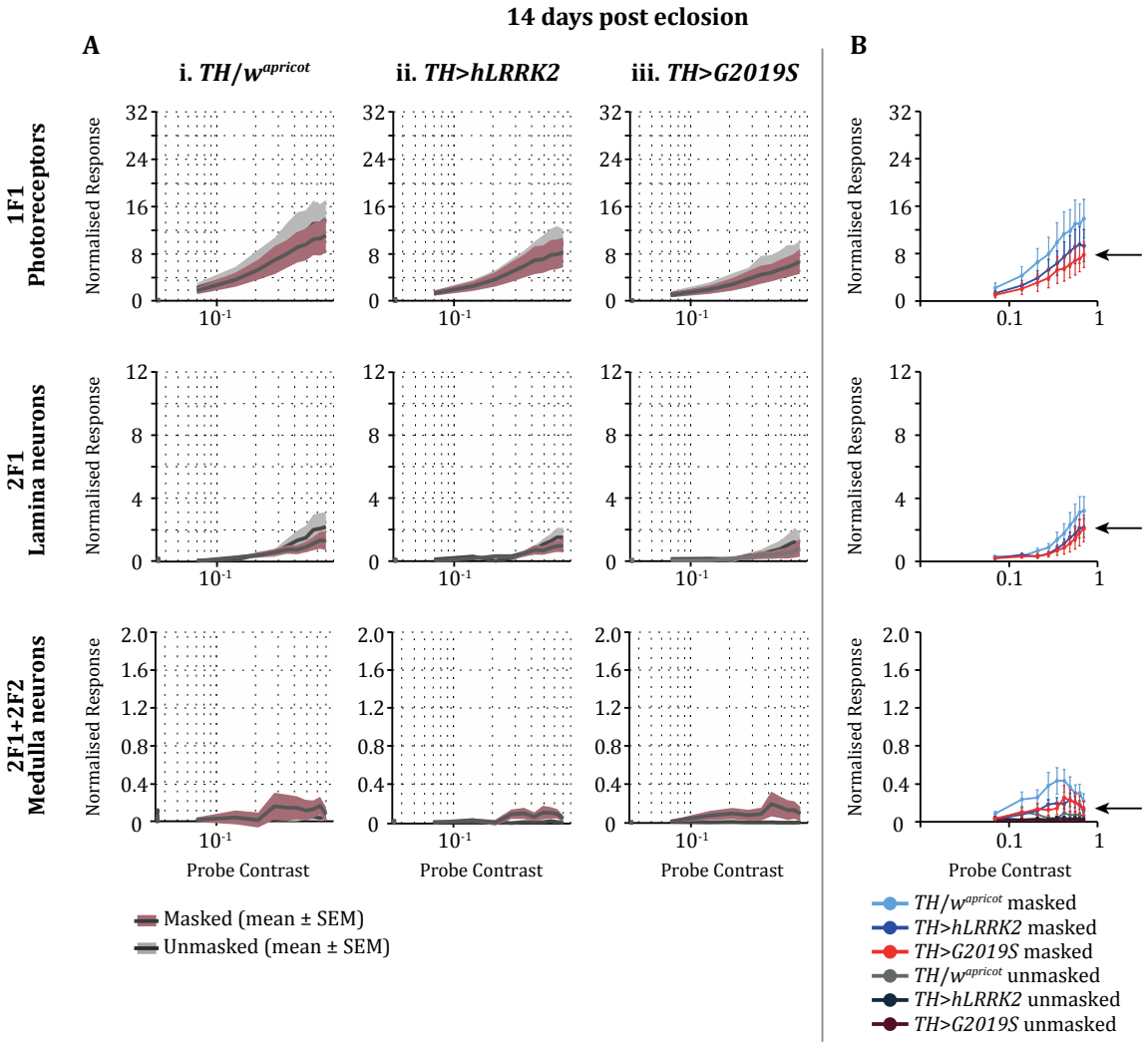


**Figure 4.8 Neural responses to swept contrast flicker recorded at 14 DPE are dramatically reduced in flies with DA expression of *hLRRK2-G2019S* and in controls**

(A) 14 DPE CRFs recorded from (i) *TH/w*$^{apricot}$, (ii) *TH>hLRRK2* and (iii) *TH>G2019S* flies for 1F1 (first row), 2F1 (second row) and 2F1+2F2 (third row) with (pink) and without (grey) a 30% mask as the probe contrast is increased from 0 to 69%. (B) Combined plots of all genotypes for the corresponding rows in (A). In (A) the solid lines indicate the mean response and the shaded area indicates ± SEM. In (B) data are mean ± SEM bars. The black arrows point to the responses from flies with DA expression of *hLRRK2-G2019S,* which indicate that the reduced visual response recorded from these flies was comparable to the reduced visual responses recorded from control flies. n≥9 for each genotype.

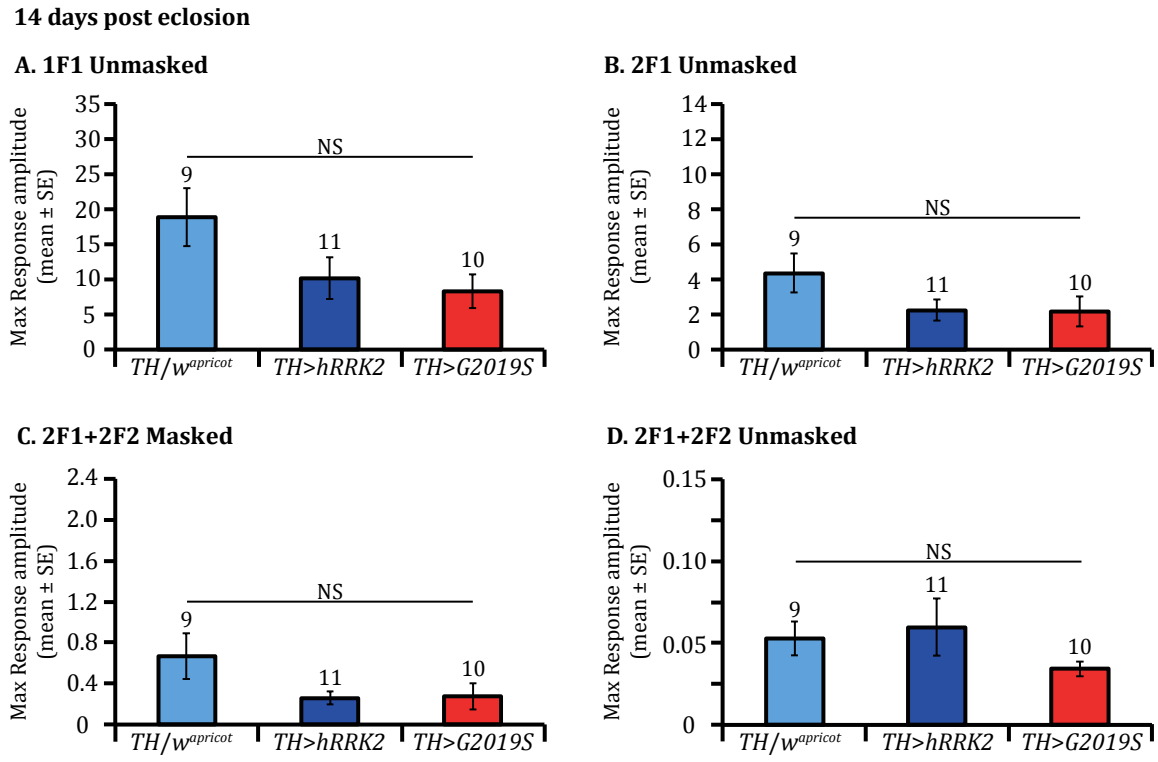


**Figure 4.9 At 14 DPE, peak CRFs do not differ between flies with DA expression of *hLRRK2-G2019S* or controls**

The 14 DPE peak CRFs recorded from flies expressing no transgene (*TH/w$^{apricot}$*: Light blue), WT *hLRRK2* (*TH>hLRRK2*: Dark blue) or *hLRRK2-G2019S* (*TH>G2019S*: Red) in the DA neurons for (A) 1F1 photoreceptors, (B) 2F1 lamina, (D) 2F1+2F2 medulla, without a 30% mask and (C) 2F1+2F2, with a 30% mask as the probe contrast is increased from 0 to 69%. (A-C) All 14 DPE peak CRFs recorded from the three neuronal layers were very low and were similar between genotypes. (D) There were no significant differences in the unmasked 2F1+2F2 responses between genotypes, thus the baseline noise level was similar between experiments. All statistics are ANOVA with post-hoc Bonferroni correction: NS, no significant difference, $p>0.05$. Data presented are mean ± SEM bars; n numbers are displayed above the bars.

### 4.3.2 Treatment with UCA or UDCA rescues visual dysfunction in flies with DA expression of *hLRRK2-G2019S* at 7 DPE

To determine the *in vivo* effects of UCA and UDCA on neuronal function, these compounds were fed to *TH>G2019S*, *TH>hLRRK2* and *TH/w*$^{apricot}$ flies. Food containing UCA or UDCA was made through dissolving the appropriate compound in 100% EtOH and then diluting into deionised water to achieve a final concentration of 2.5 μM. The drug solution was then mixed with instant fly food. The visual responses of flies fed with these drugs were measured by SSVEP at 3 and 7 DPE and were compared to the visual responses of flies that had been fed on food containing no drug but supplemented with 100% EtOH (this food will henceforth be referred to as 'control food'). To try and mimic the situation of a PD patient, who is unlikely to start taking drugs until later in their adult life, larvae were raised on drug-free food and female adult flies were transferred to food containing 2.5 μM UCA, 2.5 μM UDCA or control food on the day of eclosion. Once eclosed, all flies were maintained at 29˚C in a pulsating light incubator; these are the same conditions previously used when examining the visual response of flies fed control food in section 4.3.1.

At 3 DPE, CRFs were robust for each genotype/drug combination (Figure 4.10A-C). For each genotype, CRFs showed no significant differences between flies that had been fed control food or those that had been fed food containing UCA or UDCA (all $p>0.05$; Figure 4.11A-C). As previously shown in Figure 4.5, there were no significant differences between the 3 DPE CRFs recorded from untreated *TH>G2019S, TH>hLRRK2* and *TH/w*$^{apricot}$ flies. Treatment with UCA or UDCA also caused no significant differences in the CRFs recorded from these genotypes (all $p>0.05$).

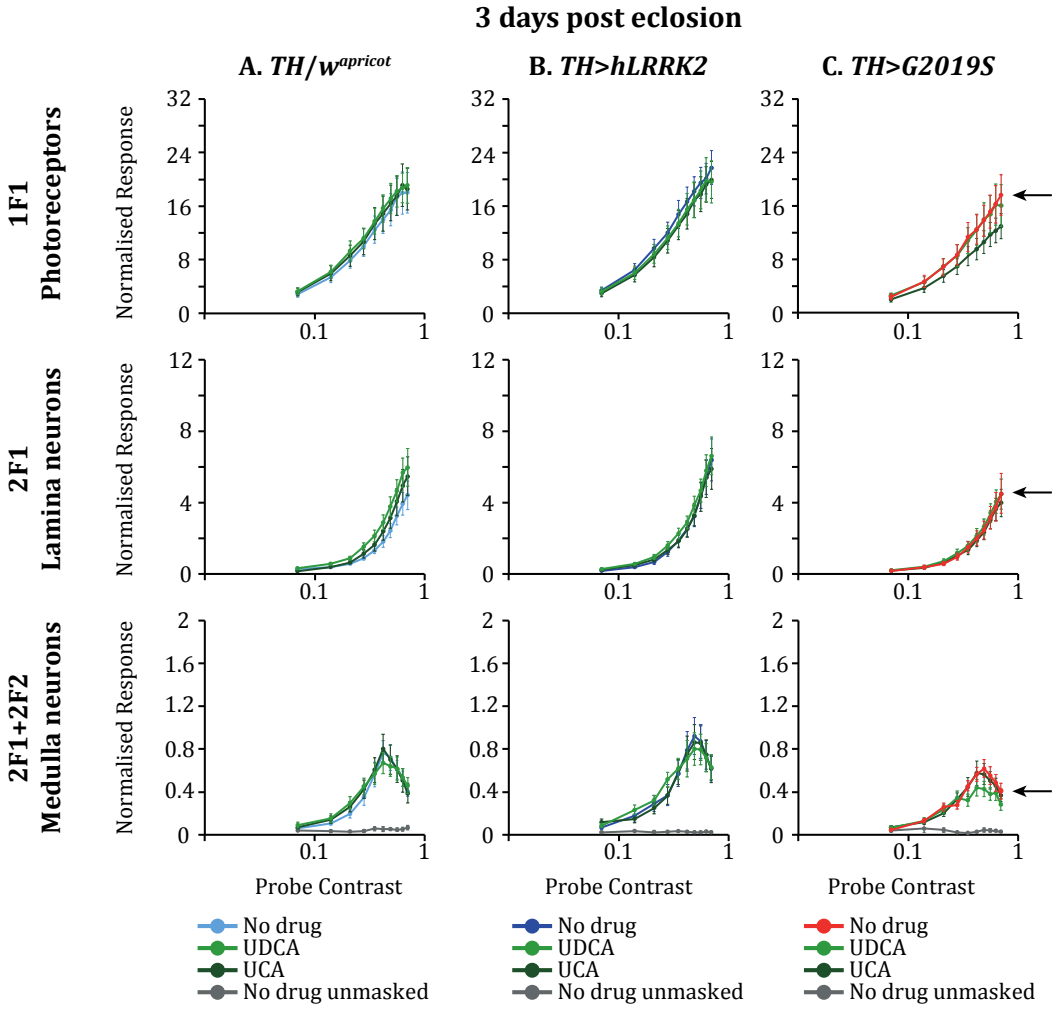


**Figure 4.10 Treatment with UCA or UDCA does not affect the CRFs of flies with DA expression of *hLRRK2-G2019S*, WT *hLRRK2* or no transgene at 3 DPE**

3 DPE CRFs recorded from flies with DA expression of (A) no transgene, (B) WT *hLRRK2* or (C) *hLRRK2-G2019S,* after being fed food containing no drug (blue or red lines) or food supplemented with UCA (dark green lines) or UDCA (light green lines). CRFs are shown for the photoreceptors (1F1 unmasked, first row), lamina neurons (2F1 unmasked, second row), and medulla neurons (2F1+2F2 masked and unmasked, third row). At 3 DPE, treatment with UCA or UDCA did not affect the CRFs recorded from any genotype. Data presented are mean ± SEM bars. In (C) the black arrows point to the responses from *TH>G2019S* flies fed on food containing no drug. n≥8 for each genotype/drug combination.

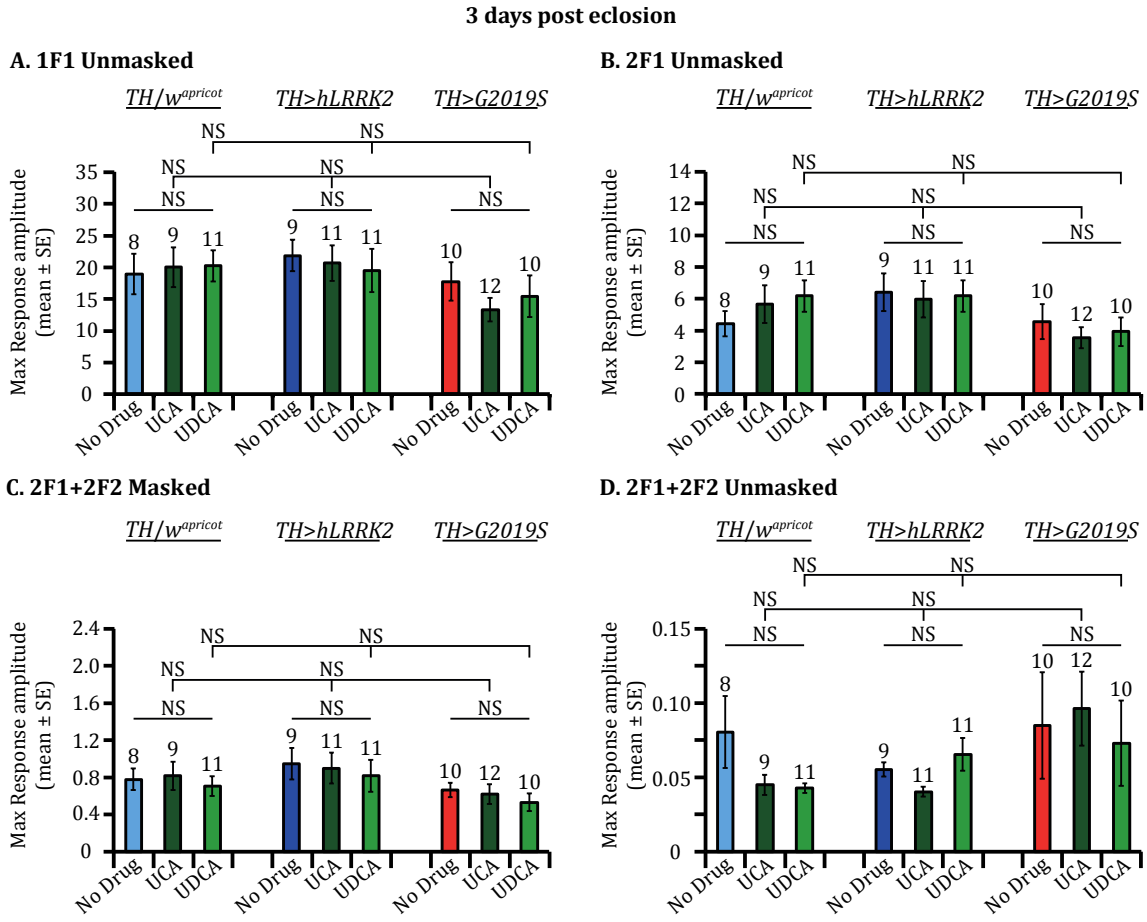


**Figure 4.11 At 3 DPE, peak CRFs from flies with DA expression of *hLRRK2-G2019S,* WT *hLRRK2* or no transgene do not differ following treatment with UCA or UDCA**

The 3 DPE peak CRFs recorded from flies expressing no transgene (light blue), WT *hLRRK2* (dark blue) or *hLRRK2-G2019S* (red) in the DA neurons, after being fed control food or food supplemented with UCA (dark green) or UDCA (light green). Peak CRFs are shown for (A) 1F1, (B) 2F1, (D) 2F1+2F2, without a 30% mask and (C) 2F1+2F2, with a 30% mask as the probe contrast is increased from 0 to 69%. (A-C) Treatment with UCA or UDCA did not cause any significant changes to the CRFs within genotypes or between genotypes. (D) The unmasked 2F1+2F2 responses were not significantly different between genotypes, thus the baseline noise level was similar between experiments. Statistics within and between genotypes are all ANOVA with post-hoc Bonferroni correction: NS, no significant difference, $p>0.05$. Data presented are mean ± SEM bars; n numbers are displayed above the bars.

At 7 DPE, treatment with UCA or UDCA did not affect the CRFs recorded from *TH/w*$^{apricot}$ or *TH>hLRRK2* flies (Figure 4.12A-B). In contrast, feeding UCA or UDCA to *TH>G2019S* flies substantially increased all three components of the neuronal visual response (Figure 4.12C). When *TH>G2019S* flies were fed UCA, the photoreceptor response was increased by 136% (Figure 4.13A; $p<0.05$), the lamina response was increased by 203% (Figure 4.13B; $p<0.05$) and the medulla response was increased by 176% (Figure 4.13C; $p<0.05$) compared with untreated *TH>G2019S* flies. When *TH>G2019S* flies were fed UDCA, the photoreceptor response was increased by 117% (Figure 4.13A; $p<0.05$), the lamina response was increased by 217% (Figure 4.13B; $p<0.05$), and the medulla response was increased by 105% compared with untreated *TH>G2019S* flies. However, the medulla response was not significantly different from untreated flies, possibly due to the variability of the data (Figure 4.13C; $p>0.05$). The peak CRFs recorded from *TH/w*$^{apricot}$ or *TH>hLRRK2* flies did not differ significantly between treatments (Figure 4.13A-C).

Although both UCA and UDCA showed a powerful beneficial effect on neuronal signalling in flies with DA expression of *hLRRK2-G2019S*, the rescue of visual function was incomplete. A comparison between *TH>G2019S* flies fed UCA with control flies fed UCA revealed that the rescue was ~70% (photoreceptor response: 69% and 67% of *TH/w*$^{apricot}$ and *TH>hLRRK2* flies; lamina response: 58% and 66% of *TH/w*$^{apricot}$ and *TH>hLRRK2* flies; medulla response: 58% and 85% of *TH/w*$^{apricot}$ and *TH>hLRRK2* flies), however these differences were not significant ($p>0.05$). A comparison between *TH>G2019S* flies fed UDCA with control flies fed UDCA revealed that the rescue was ~65%, slightly lower than for UCA (photoreceptor response: 66% and 64% of *TH/w*$^{apricot}$ and *TH>hLRRK2* flies; lamina response: 69% and 73% of *TH/w*$^{apricot}$ and *TH>hLRRK2* flies; medulla response: 51% and 64% of *TH/w*$^{apricot}$ and *TH>hLRRK2* flies). Again, these differences were not found to be significant ($p>0.05$). It is possible that the variability in the data masked any significant differences between these genotypes. The data is perhaps more variable when flies are fed on drug-containing food due to individual flies consuming different amounts of food, thus different amounts of the drug.

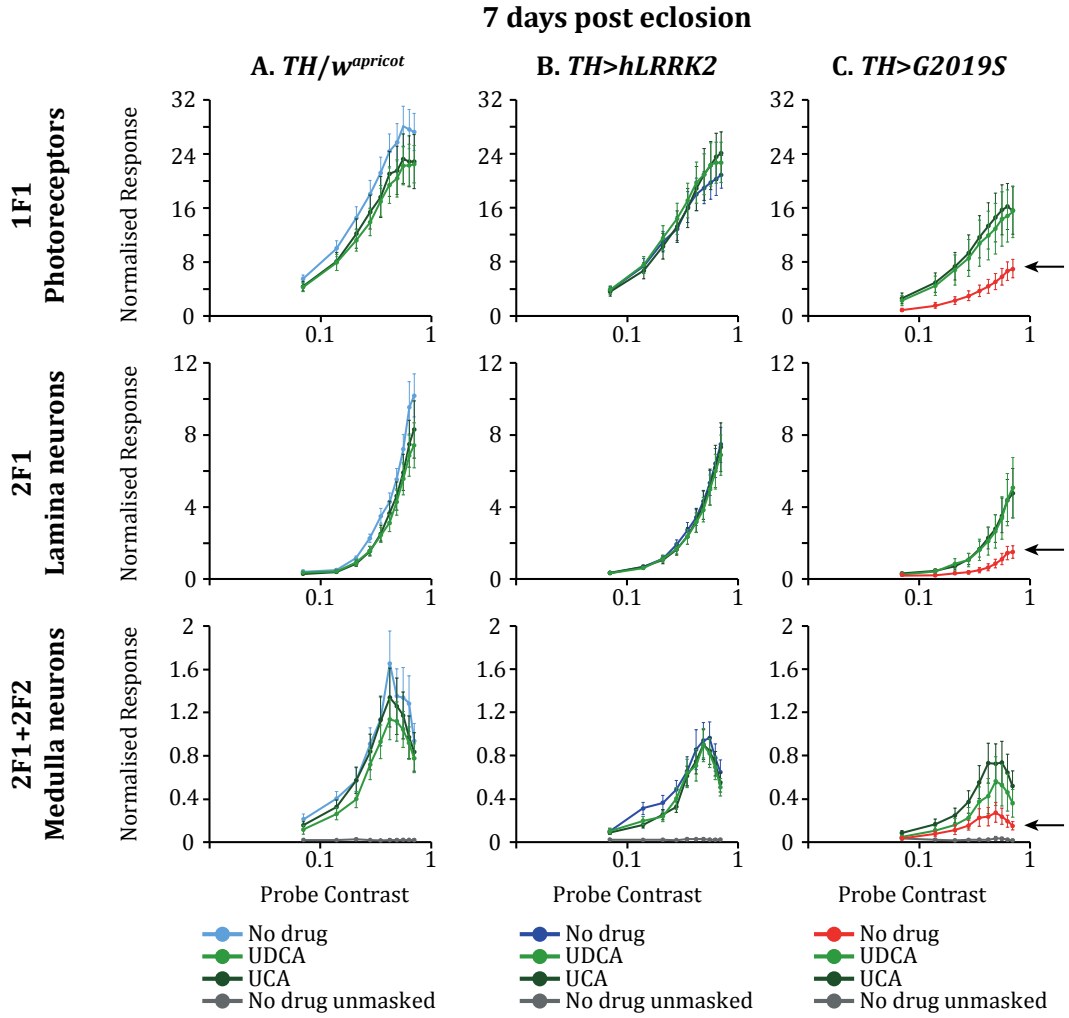


**Figure 4.12 Treatment with UCA or UDCA dramatically improves the CRFs of flies with DA expression of *hLRRK2-G2019S* at 7 DPE**

7 DPE CRFs recorded from flies with DA expression of (A) no transgene, (B) WT *hLRRK2* or (C) *hLRRK2-G2019S,* after being fed food containing no drug (blue or red lines) or food supplemented with UCA (light green lines) or UDCA (dark green lines). CRFs are shown for the photoreceptors (1F1 unmasked, first row), lamina neurons (2F1 unmasked, second row), and medulla neurons (2F1+2F2 masked and unmasked, third row). At 7 DPE, CRFs recorded from untreated *TH>G2019S* flies were considerably lower than those recorded from untreated control genotypes (indicated by the black arrows), but were markedly improved after treatment with either UCA or UDCA. The CRFs recorded from *TH>hLRRK2* or *TH/w*$^{apricot}$ flies were unaffected following UCA or UDCA treatment. Data presented are means ± SEM bars. n≥10 for each genotype/drug combination.

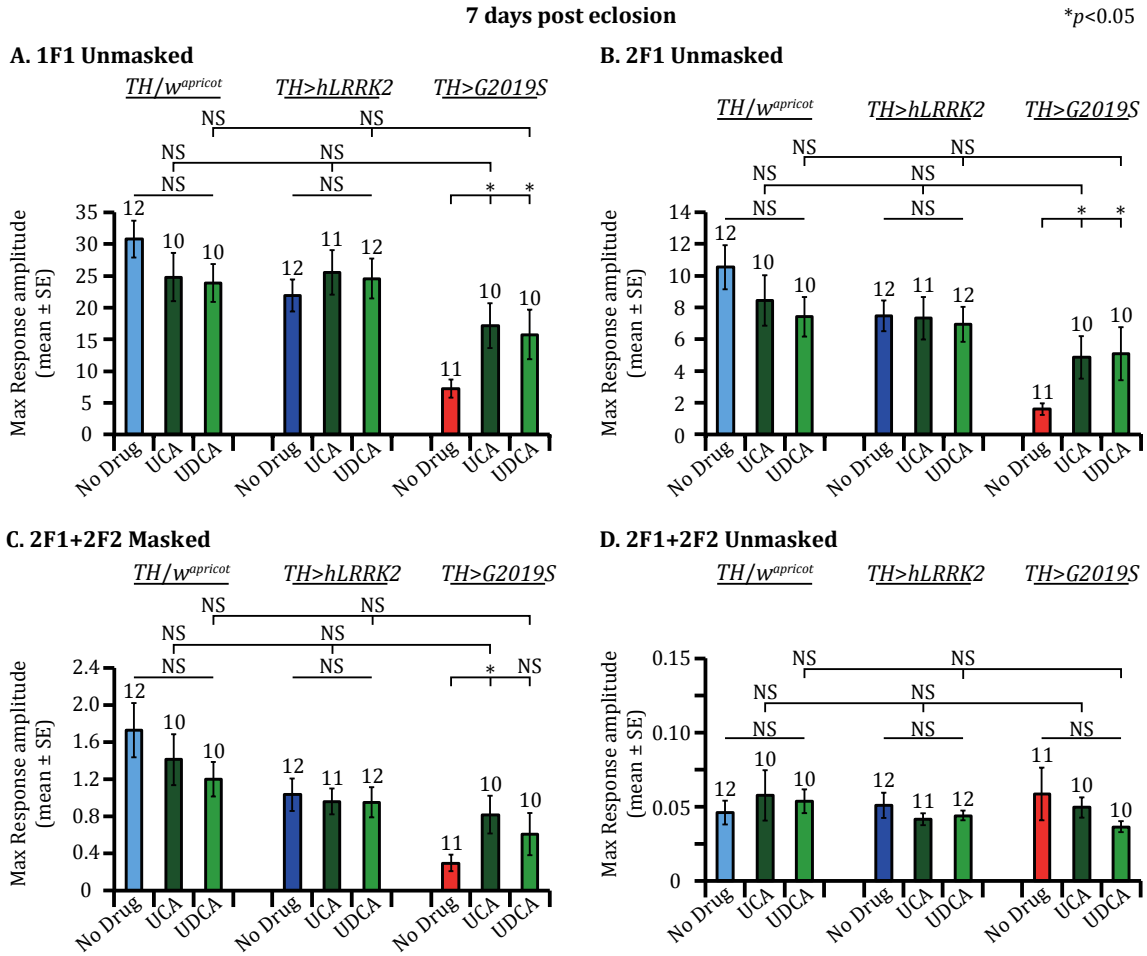


**Figure 4.13 At 7 DPE, peak CRFs from flies with DA expression of *hLRRK2-G2019S* are significantly improved following treatment with UCA or UDCA**

The 7 DPE peak CRFs recorded from flies expressing no transgene (light blue), WT *hLRRK2* (dark blue) or *hLRRK2-G2019S* (red) in the DA neurons, after being fed control food or food supplemented with UCA (dark green) or UDCA (light green). Peak CRFs are shown for (A) 1F1, (B) 2F1, (D) 2F1+2F2, without a 30% mask and (C) 2F1+2F2, with a 30% mask as the probe contrast is increased from 0 to 69%. (A-C) Treatment with UCA significantly increased all CRFs recorded from *TH>G2019S* flies. Treatment with UDCA significantly increased the 1F1 and 2F1 CRFs recorded from *TH>G2019S* flies. Both UCA and UDCA increased the CRFs of *TH>G2019S* flies to levels that were comparable with those recorded from control flies also treated with these compounds. Neither UCA nor UDCA increased the CRFs of *TH>hLRRK2* or *TH/w^apricot* flies. (D) The unmasked 2F1+2F2 responses were not significantly different between genotypes, thus the baseline noise level was similar between experiments. Statistics within and between genotypes are all ANOVA with post-hoc Bonferroni correction: *$p$<0.05, NS, no significant difference, $p$>0.05. Data presented are mean ± SEM bars; n numbers are displayed above the bars.

### 4.3.3 The activity of mitochondrial complexes I, II and IV are similar in flies with DA expression of *hLRRK2-G2019S* and controls

Although it was evident that UCA and UDCA had a beneficial effect on the neuronal visual response in flies with DA expression of *hLRRK2-G2019S*, we wanted to determine if this was due to a rescue of mitochondrial dysfunction. Thus, the activities of complexes I-IV of the mitochondrial respiratory chain were measured. Mitochondria-enriched fragments were extracted from the heads of 7 DPE $TH/w^{apricot}$, *TH>hLRRK2* and *TH>G2019S* flies, all of which had been fed control food or food supplemented with UCA or UDCA. Samples were transported to the Sheffield Institute of Translational Neuroscience (SITraN) on dry ice and the assays were performed alongside our collaborators. After each sample was prepared, individual assays were used to measure the activity of complexes I-IV (see Chapter 2, section 2.6). The specific activity of each complex was normalised to that of citrate synthase. Each assay was repeated three times, and five different volumes of mitochondrial extract from each sample were used per repeat. Unfortunately, we were unable to record the activity of complex III during any of the three repeats so these data are not presented. For both complexes I and IV, the activity was only successfully recorded in two out of the three repeats, so data from the third repeat were not included in the analysis.

There were no significant differences recorded in the activities of complex I (Figure 4.14A), complex II (Figure 4.14B) or complex IV (Figure 4.14C) between genotypes. Treatment with UCA or UDCA also had no significant effect on the activities of complexes I, II or IV when fed to $TH/w^{apricot}$, *TH>hLRRK2* or *TH>G2019S* flies.

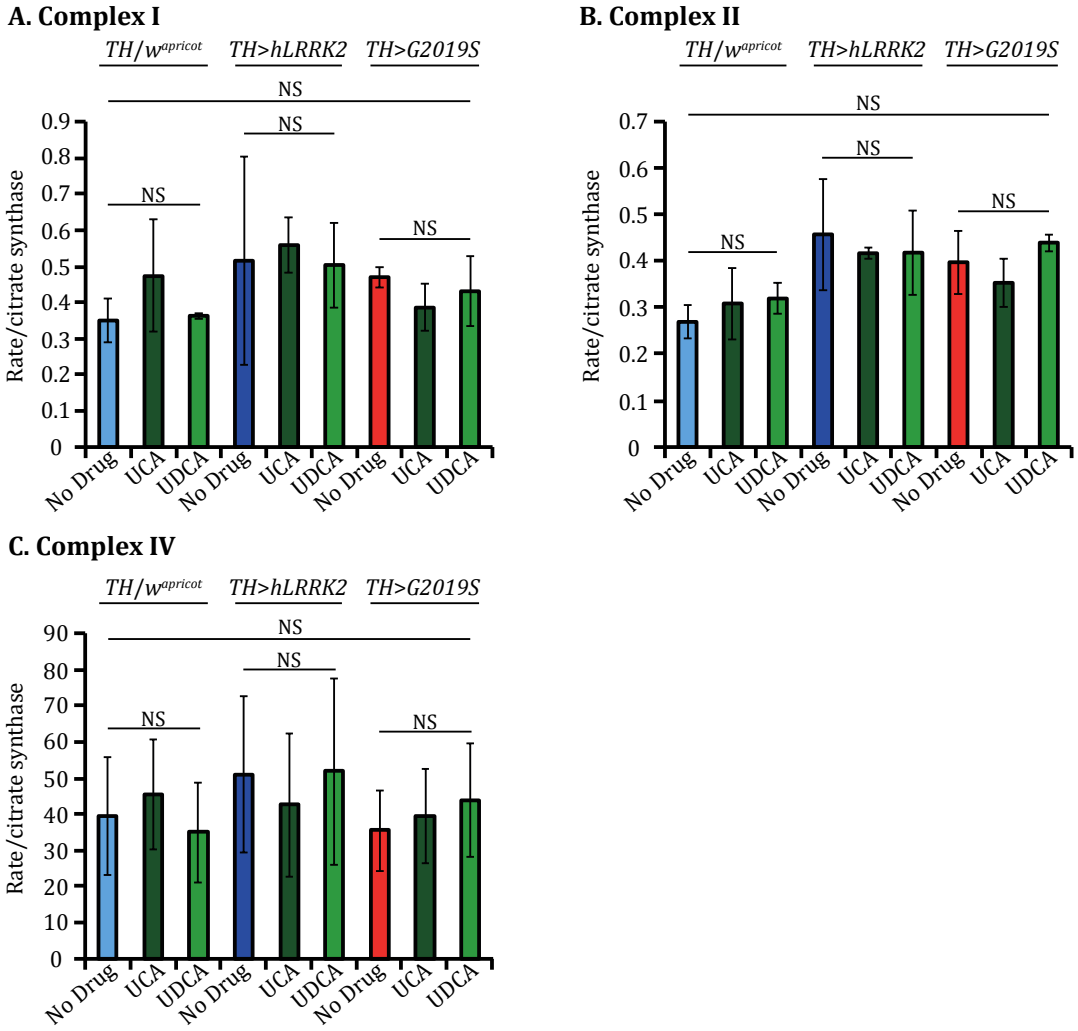


**Figure 4.14 The activities of complexes I, II or IV do not differ between flies with DA expression of *hLRRK2-G2019S* or controls or following treatment with UCA or UDCA**

The activities of complexes I (A), II (B) and IV (C) normalised to citrate synthase, recorded from 7 DPE flies expressing no transgene (light blue), WT *hLRRK2* (dark blue) or *hLRRK2-G2019S* (red) in the DA neurons, after being fed control food or food supplemented with UCA (dark green) or UDCA (light green). (A-C) There were no significant effects of genotype or drug treatment on the activities of complex I, II or IV. Statistics within and between genotypes are all ANOVA with post-hoc Bonferroni correction: NS, no significant difference, $p>0.05$. Data presented are mean ± SEM bars. The number of repeats for each genotype in (A) and (C) was two and in (B) was three.

### 4.3.4 Do UCA and UDCA increase the phosphorylation of Akt$^{Ser473}$?

As previously mentioned, DUA and UCA were found to exert their beneficial effects through significantly increasing Akt$^{Ser473}$ phosphorylation in *parkin*-mutant fibroblasts (Mortiboys et al., 2013). The *Drosophila* genome contains a single *Akt1* gene encoding a protein that is ~76.5% similar to the mammalian Akt1 protein (Franke et al., 1994). All of the components known to be involved in the mammalian Akt signalling pathway have also been implicated in the *Drosophila* Akt signalling pathway, and this pathway functions as an anti-apoptotic pathway in flies, as in mammals (Scanga et al., 2000). Furthermore, several studies have suggested that inactivation of Akt results in apoptotic death of DA neurons in both flies and humans (Yang et al., 2005, Timmons et al., 2009). Thus Akt1 appears to be conserved between flies and humans, which suggests that UCA and UDCA may also increase the phosphorylation of Akt1 in flies.

#### 4.3.4.1 Treatment with UCA or UDCA increases the visual response of flies with reduced expression of *Akt*

To determine if UCA and UDCA improved the visual responses of *TH>G2019S* flies through an interaction with the Akt pathway, SSVEPs were recorded from flies with reduced gene expression of *Akt* following treatment with no drug, UCA or UDCA. If UCA and UDCA do exert their beneficial effects through increasing the phosphorylation of Akt, it would be expected that the visual responses of flies with reduced expression of *Akt* would be compromised, but would be improved following treatment with these compounds. The UAS/GAL4 system was used to drive the expression of *Akt*-RNAi using either *elav*-GAL4 or *neuronal synaptobrevin*-GAL4 (*nsyb*-GAL4) to achieve pan-neuronal expression. CRFs were measured by SSVEP at 3 and 7 DPE. As with previous experiments, newly emerged female flies were transferred to control food or food containing 2.5 μM UCA or 2.5 μM UDCA. These flies were maintained in a 29˚C pulsating light incubator.

At 3 DPE, CRFs recorded from flies expressing *Akt*-RNAi pan-neuronally using *elav*-GAL4 (*elav*-GAL4>*Akt-RNAi*) did not differ significantly between drug treatments (Figure 4.15Ai-iv). When *Akt*-RNAi was expressed using the *nsyb*-GAL4 driver (*nsyb*-

GAL4>*Akt*-RNAi), treatment with either UCA or UDCA improved the CRFs, however significant differences were only recorded in the photoreceptor (Figure 4.15Ai; $p<0.05$) and lamina responses (Figure 4.15Aii; $p<0.05$) following treatment with UDCA. Although both the photoreceptor and lamina responses of untreated *nsyb*-GAL4>*Akt*-RNAi flies were slightly reduced compared with untreated *elav*-GAL4>*Akt*-RNAi flies, these differences were not found to be significant (Figure 4.15Ai-iv). *nsyb*-GAL4>*Akt*-RNAi flies have a very dark red eye colour whereas *elav*-GAL4>*Akt*-RNAi flies have a much brighter red eye colour. Therefore, the slightly reduced CRFs recorded from *nsyb*-GAL4>*Akt*-RNAi flies at 3 DPE compared with those recorded from *elav*-GAL4>*Akt*-RNAi flies may be due to the difference in eye colour.

At 7 DPE, feeding *elav*-GAL4>*Akt*-RNAi flies UDCA significantly increased all three components of the neuronal visual response compared with untreated *elav*-GAL4>*Akt*-RNAi flies (Figure 4.15Bi-iii; photoreceptor response: 66% increase; lamina response: 80% increase; medulla response: 93% increase; all $p<0.05$). Feeding *elav*-GAL4>*Akt*-RNAi flies UCA also increased the visual response, but not significantly (photoreceptor response: 23% increase; lamina response: 23% increase; medulla response: 28% increase; all $p>0.05$). Similarly, treatment with UCA or UDCA significantly increased all three components of the neuronal visual response of *nsyb*-GAL4>*Akt*-RNAi flies compared with untreated *nsyb*-GAL4>*Akt*-RNAi flies (Figure 4.15Bi-iii; photoreceptor response: 188% increase with UCA, 186% increase with UDCA; lamina response: 156% increase with UCA, 193% increase with UDCA; medulla response: 135% increase with UCA, 146% increase with UDCA; all $p<0.05$).

At 7 DPE, *nsyb*-GAL4>*Akt*-RNAi flies showed a more severe reduction in their visual response compared with *elav*-GAL4>*Akt*-RNAi flies. A comparison of untreated *nsyb*-GAL4>*Akt*-RNAi flies with untreated *elav*-GAL4>*Akt*-RNAi flies revealed that the visual response of *nsyb*-GAL4>*Akt*-RNAi flies was ~35% of *elav*-GAL4>*Akt*-RNAi flies (photoreceptor response: 31% of *elav*-GAL4>*Akt*-RNAi flies, $p<0.01$; lamina response: 33% of *elav*-GAL4>*Akt*-RNAi flies, $p<0.05$; medulla response: 41% of *elav*-GAL4>*Akt*-RNAi flies, $p<0.05$). Although *nsyb*-GAL4>*Akt*-RNAi flies have darker eyes than *elav*-GAL4>*Akt*-RNAi flies, it is likely that *nsyb*-GAL4 drives the expression of *Akt*-RNAi more strongly than *elav*-GAL4; if the differences between these two

genotypes were due to eye colour alone, then feeding UCA or UDCA to these flies would not be expected to have caused such a beneficial neuronal rescue.

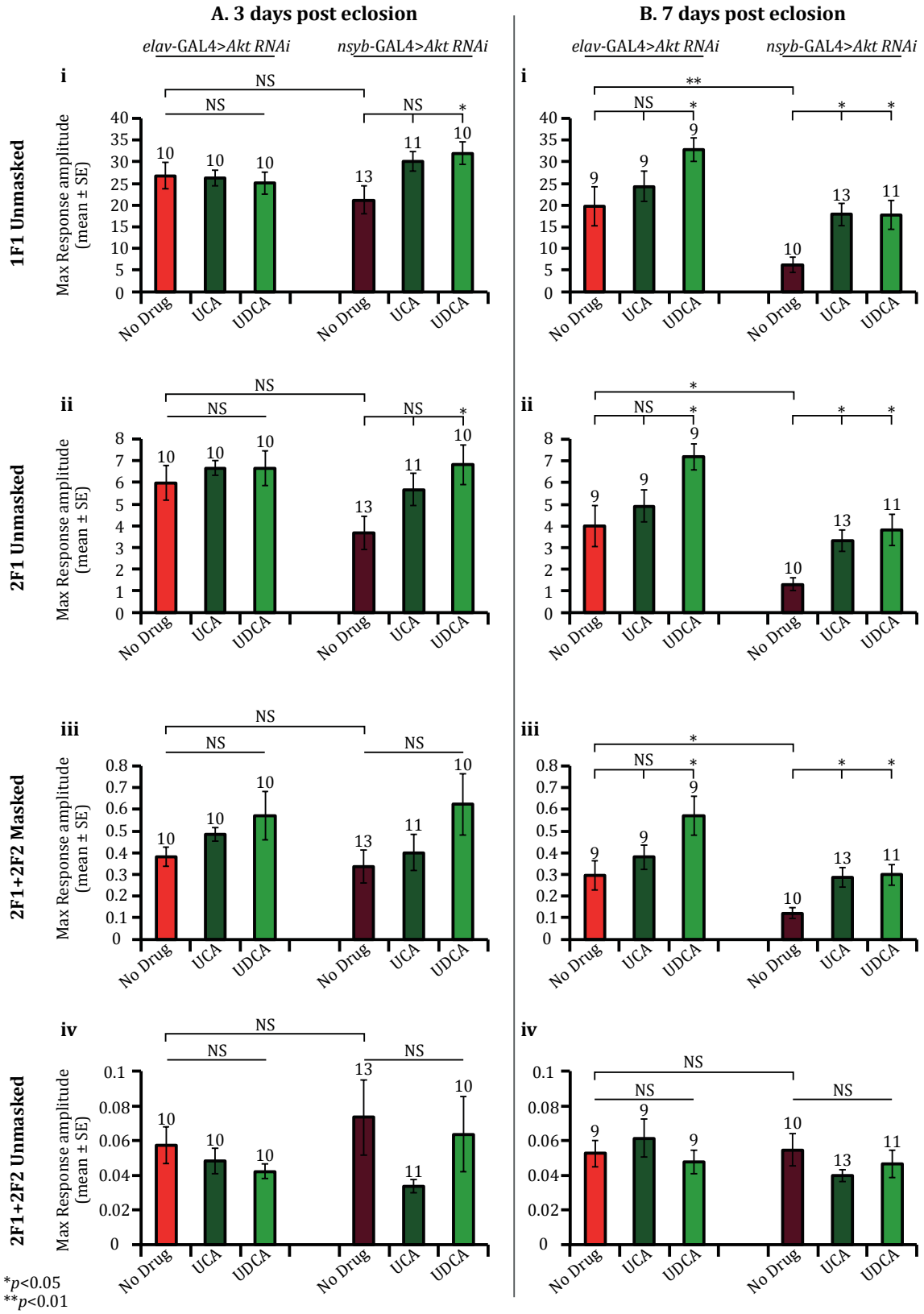


**Figure 4.15 At 7 DPE, treatment with UDCA or UCA increases the CRFs of flies with reduced expression of *Akt***

Figure legend overleaf.

**Figure 4.15 At 7 DPE, treatment with UDCA or UCA increases the CRFs of flies with reduced expression of *Akt***

Peak CRFs recorded from flies expressing *Akt*-RNAi pan-neuronally with *elav*-GAL4 (red) or *nsyb*-GAL4 (dark red) after being given food containing no drug, UCA (dark green) or UDCA (light green) at (A) 3 DPE and (B) 7 DPE. Peak CRFs are shown for (i) 1F1, (ii) 2F1, (iv) 2F1+2F2, without a 30% mask and (iii) 2F1+2F2, with a 30% mask as the probe contrast is increased from 0 to 69%. (Ai-iii) At 3 DPE, treatment with UCA or UDCA did not significantly alter the CRFs recorded from *elav*-GAL4>*Akt*-RNAi flies. UCA did not significantly increase any of the CRFs recorded from *nsyb*-GAL4>*Akt*-RNAi flies, whereas UDCA significantly increased the 1F1 and 2F1 CRFs. (Bi-iii) At 7 DPE, treatment with UDCA significantly increased all CRFs recorded from *elav*-GAL4>*Akt*-RNAi and *nsyb*-GAL4>*Akt*-RNAi flies. Treatment with UCA only significantly increased CRFs recorded from *nsyb*-GAL4>*Akt*-RNAi flies. The CRFs of *nsyb*-GAL4>*Akt*-RNAi flies were significantly lower than *elav*-GAL4>*Akt*-RNAi flies. (Aiv and Biv) There were no significant differences in the unmasked 2F1+2F2 responses between genotype/drug combinations, suggesting that the baseline noise level was similar between experiments. Statistics within genotypes are ANOVA with post-hoc Bonferroni correction and statistics between two different genotypes are Student's t-tests: $^{**}p<0.01$, $^{*}p<0.05$, NS, no significant difference, $p>0.05$. Data presented are mean ± SEM bars; n numbers are displayed above the bars.

### 4.3.4.2 Treatment with UCA or UDCA increases the visual response of flies with DA expression of both *hLRRK2-G2019S* and a mutant copy of *Akt1*

The LOF P{PZ}Akt1$^{04226}$ fly line (Bloomington Stock 11627), derived by insertional mutagenesis (Spradling et al., 1999), was also used to determine if UCA and UDCA interact with the Akt pathway in flies. This mutant *Akt1* gene is inserted on the third chromosome of *Drosophila*, the same chromosome that UAS-*G2019S* and *TH*-GAL4 are inserted. After numerous failed attempts to recombine UAS-*G2019S* and the mutant *Akt1*, possibly because they are inserted too closely together on chromosome three, a fly line was generated in which UAS-*G2019S* and *TH*-GAL4 had been recombined. Mutant *Akt1* was then crossed into the recombined UAS-*G2019S, TH*-GAL4 background (these flies are referred to as *TH>G2019S/Akt1* throughout this thesis). Homozygous *Akt1* flies are not viable, thus the flies that we tested only expressed one mutant copy of the *Akt1* gene. CRFs of female *TH>G2019S/Akt1* flies that had been fed control food or food containing 2.5 μM UCA or 2.5 μM UDCA from the day of emergence were measured by SSVEP at 3 and 7 DPE. These flies were kept under the same conditions as previous experiments (29˚C, pulsating light incubator).

Figure 4.16Ai-iv shows the peak 3 DPE CRFs recorded from *TH>G2019S/Akt1* flies fed control, UCA or UDCA food. To aid comparisons, the peak CRFs previously recorded from 3 DPE *TH>G2019S* flies fed control, UCA or UDCA food are also plotted on the same graphs. The photoreceptor and lamina responses of all *TH>G2019S/Akt1* flies were robust at 3 DPE and were not significantly affected by drug treatment (Figure 4.16Ai-ii; both $p>0.05$). The medulla responses of untreated *TH>G2019S/Akt1* flies were weak, however treatment with UCA increased these responses by 80% (Figure 4.16Aiii; $p<0.05$). Treatment with UDCA also increased the medulla responses, but not significantly (56% increase). Surprisingly, the photoreceptor responses of untreated *TH>G2019S* flies were only 34% of untreated *TH>G2019S/Akt1* flies ($p<0.001$). There were no differences in the lamina responses between these two genotypes ($p>0.05$), but the medulla responses of *TH>G2019S* flies were 57% higher than those recorded from *TH>G2019S/Akt1* flies ($p<0.001$). A comparison between *TH>G2019S/Akt1* and *TH>G2019S* flies both treated with UCA revealed that the

photoreceptor and lamina responses of *TH>G2019S* flies were 39% ($p$<0.001) and 56% ($p$<0.01) of those recorded from *TH>G2019S/Akt1*, respectively; the medulla responses were not significantly different. A similar result was observed with a comparison between *TH>G2019S/Akt1* and *TH>G2019S* flies both treated with UDCA; *TH>G2019S* flies showed photoreceptor responses that were 48% of those recorded from *TH>G2019S/Akt1* flies ($p$<0.001) and lamina responses that were 62% of those recorded from *TH>G2019S/Akt1* flies ($p$<0.05). Again, the medulla responses were not significantly different.

Figure 4.16Bi-iv shows the peak 7 DPE CRFs recorded from *TH>G2019S/Akt1* flies fed control, UCA or UDCA food. As before, the peak CRFs previously recorded from 7 DPE *TH>G2019S* flies fed control, UCA or UDCA food are also plotted on the same graphs to help with comparisons. The CRFs recorded from untreated *TH>G2019S/Akt1* flies fed control food were reduced compared with those recorded at 3 DPE (Figure 4.16Bi-iii; photoreceptor response: 70% decrease; lamina response: 68% decrease; medulla response: 37% decrease). Treatment with UCA increased all three components of the visual response in *TH>G2019S/Akt1* flies compared with untreated *TH>G2019S/Akt1* flies, but only the photoreceptor responses were significantly different (photoreceptor response: 113% increase, $p$<0.05; lamina response: 123% increase, $p$>0.05; medulla response: 66% increase, $p$>0.05). Treatment with UDCA showed a more beneficial effect than UCA as it significantly increased all three components of the neuronal visual response of *TH>G2019S/Akt1* flies compared with untreated *TH>G2019S/Akt1* flies (photoreceptor response: 169% increase, $p$<0.01; lamina response: 262% increase, $p$<0.001; medulla response: 164% increase, $p$<0.01).

There were no significant differences in the CRFs recorded from 7 DPE untreated *TH>G2019S/Akt1* and untreated *TH>G2019S* flies (Figure 4.16Bi-iv). There were slight differences in the photoreceptor and lamina responses recorded from *TH>G2019S/Akt1* flies fed UCA compared with those recorded from *TH>G2019S* flies also fed UCA, but these differences were not significant. However, the medulla response recorded from *TH>G2019S/Akt1* flies fed UCA was only 36% of the medulla response recorded from *TH>G2019S* flies also fed UCA ($p$<0.01). Similarly, there were slight differences in the photoreceptor, lamina and medulla responses recorded from

*TH>G2019S/Akt1* flies fed UDCA compared with those recorded from *TH>G2019S* flies also fed UDCA, but none of these differences were significant.

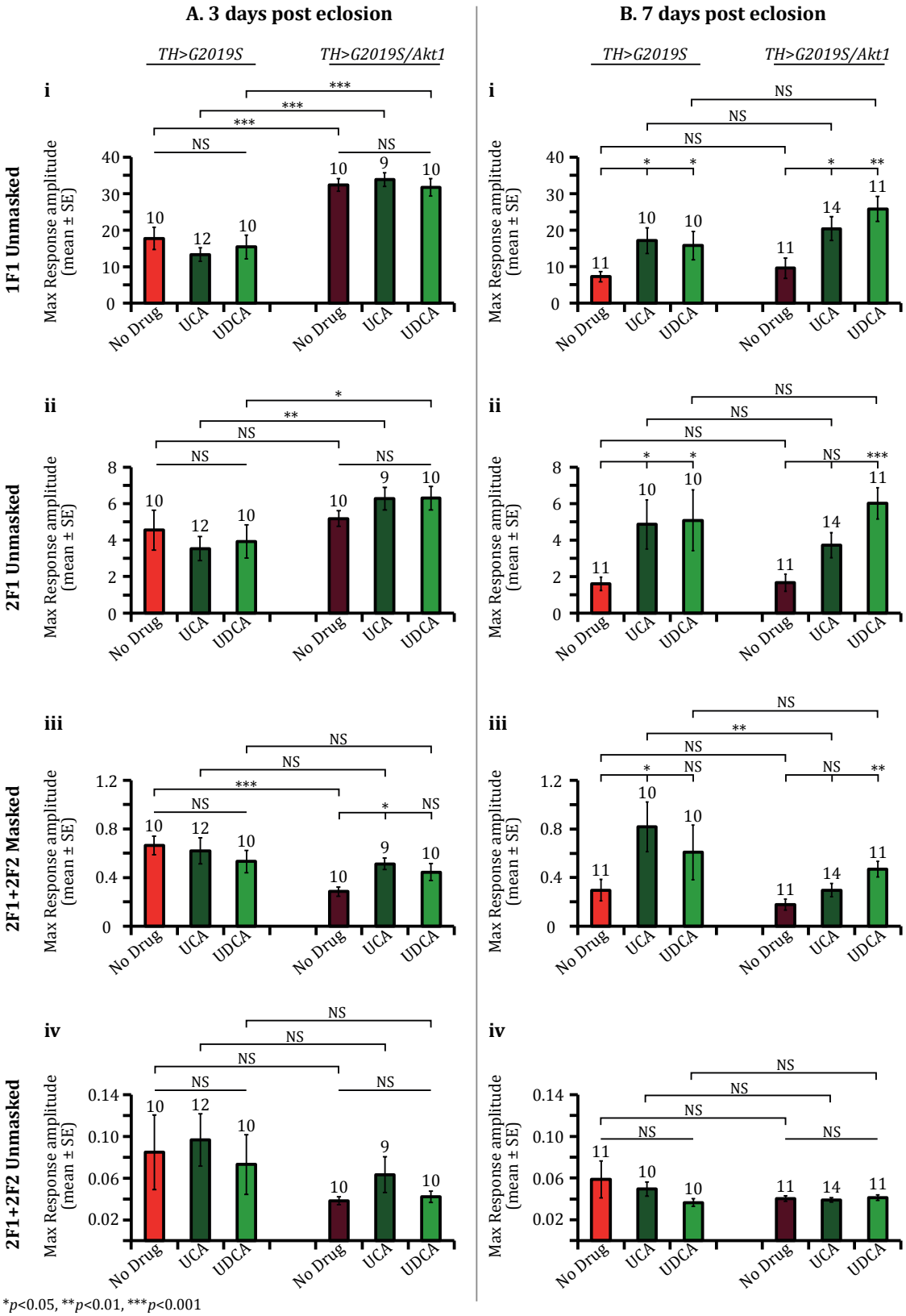


**Figure 4.16 At 7 DPE, treatment with UDCA, or to a lesser extent UCA, improves the CRFs of flies with DA expression of both *hLRRK2-G2019S* and mutant *Akt1***

Figure legend overleaf.

**Figure 4.16 At 7 DPE, treatment with UDCA, or to a lesser extent UCA, improves the CRFs of flies with DA expression of both *hLRRK2-G2019S* and mutant *Akt1***

Peak CRFs recorded from flies with DA expression of *hLRRK2-G2019S* with (*TH>G2019S*/*Akt1*; dark red) and without (*TH>G2019S*; red) a mutant copy of *Akt1* in the background recorded at (A) 3 DPE or (B) 7 DPE. Flies had been fed control food or food supplemented with UCA (dark green) or UDCA (light green). Peak CRFs are shown for (i) 1F1, (ii) 2F1, (iv) 2F1+2F2, without a 30% mask and (iii) 2F1+2F2, with a 30% mask as the probe contrast is increased from 0 to 69%. (Ai-iii) At 3 DPE, the 1F1 responses recorded from *TH>G2019S*/*Akt1* flies were significantly higher than those recorded from *TH>G2019S* flies, whereas the masked 2F1+2F2 responses were significantly lower. The 2F1 responses were not significantly different between genotypes. Treatment with UDCA caused no significant changes to the CRFs and treatment with UCA only caused a slight increase to the masked 2F1+2F2 response recorded from *TH>G2019S*/*Akt1* flies. (Bi-iii) At 7 DPE, there were no significant differences in the CRFs recorded from untreated *TH>G2019S*/*Akt1* and *TH>G2019S* flies. Treatment with UCA or UDCA significantly increased some, or all, of the CRFs recorded from *TH>G2019S*/*Akt1* and *TH>G2019S* flies. (Aiv and Biv) At both 3 and 7 DPE, there were no significant differences in the unmasked 2F1+2F2 responses between genotypes/drug treatments, suggesting that the baseline noise level was similar between experiments. Statistics within genotypes are ANOVA with post-hoc Bonferroni correction and statistics between two genotypes are Student's t-tests: ***$p<0.001$, **$p<0.01$, *$p<0.05$, NS, no significant difference, $p>0.05$. Data presented are mean ± SEM bars; n numbers are displayed above the bars.

#### 4.3.4.3 Overexpression of *Akt* in the DA neurons increases the visual response of flies with DA expression of *hLRRK2-G2019S*

To determine if the overexpression of Akt could rescue the visual response of *TH>G2019S* flies without feeding them UCA or UDCA, the UAS/GAL4 system was utilised. The UAS-*Akt* transgene is on the second chromosome and thus was crossed into the *TH>G2019S* background (these flies are referred to as *TH>Akt; G2019S* from hereon in). As controls, UAS-*Akt* was also crossed into the *TH>hLRRK2* (*TH>Akt; hLRRK2*) and $TH/w^{apricot}$ ($TH>Akt/w^{apricot}$) backgrounds. Although these flies were not given any drug, females were transferred to instant fly food supplemented with 100% EtOH on the day of emergence and kept under the same conditions (29˚C, pulsating light incubator) as previous experiments to enable direct comparisons to be viable. CRFs were measured by SSVEPs at 3 and 7 DPE. The presence of the extra UAS-*Akt* transgene in the $TH/w^{apricot}$, *TH>hLRRK2* or *TH>G2019S* backgrounds caused a darker eye colour (Figure 4.17A-C), so when comparisons were made to flies that did not express the extra UAS-*Akt* transgene, the difference in eye colour was taken into consideration.

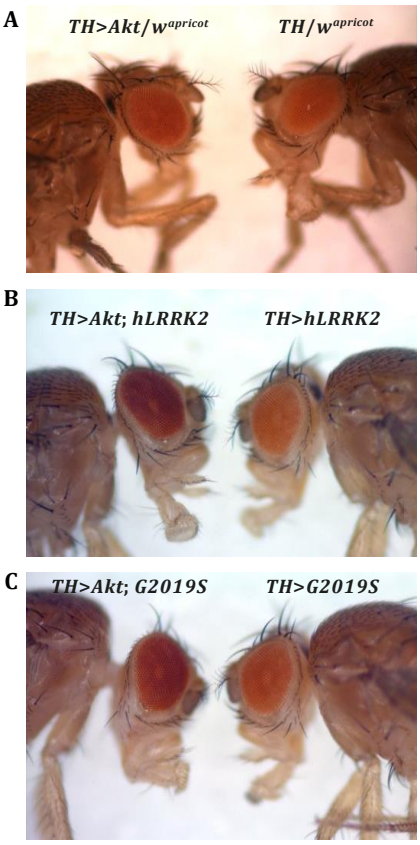


**Figure 4.17 Flies with DA expression of UAS-*Akt* and a second transgene have darker coloured eyes than flies with DA expression of one or no transgenes**

Example images of (A) flies with DA expression of UAS-*Akt* (left) compared to flies expressing no transgene (right), (B) flies with DA expression of UAS-*Akt* and UAS-*hLRRK2* (left) compared to flies expressing UAS-*hLRRK2* only (right), and (C) flies with DA expression of UAS-*Akt* and UAS-*hLRRK2-G2019S* (left) compared to flies expressing UAS-*hLRRK2-G2019S* only (right). Flies expressing two transgenes had darker coloured eyes than those expressing just one or no transgene.

Figure 4.18Ai-iv shows the peak CRFs recorded from 3 DPE *TH>Akt; G2019S*, *TH>Akt; hLRRK2* and *TH>Akt/w$^{apricot}$* flies. To aid comparisons, the 3 DPE CRFs previously recorded from *TH>G2019S*, *TH>hLRRK2* and *TH/w$^{apricot}$* flies are plotted on the same graphs. At 3 DPE, the photoreceptor and medulla responses recorded from *TH>Akt; G2019S* and *TH>Akt/w$^{apricot}$* flies were not significantly different (Figure 4.18Ai,iii). However, the lamina responses recorded from *TH>Akt/w$^{apricot}$* flies were 66% of those recorded from *TH>Akt1; G2019S* flies (Figure 4.18Aii; $p<0.05$). Surprisingly, all of the CRFs recorded from *TH>Akt; hLRRK2* were significantly lower than those recorded from *TH>Akt; G2019S* flies (photoreceptor response: 60% of *TH>Akt; G2019S* flies; lamina response: 54% of *TH>Akt; G2019S* flies; medulla response: 54% of *TH>Akt; G2019S* flies; all $p<0.01$). The medulla responses recorded from *TH>Akt; hLRRK2* flies were also significantly lower than those recorded from *TH>Akt/w$^{apricot}$* flies ($p<0.05$). The 3 DPE CRFs recorded from *TH>Akt/w$^{apricot}$* and *TH/w$^{apricot}$* flies did not differ significantly from each other. Conversely, a comparison between *TH>Akt; hLRRK2* and *TH>hLRRK2* flies revealed that all CRFs recorded from *TH>Akt; hLRRK2* flies were reduced (photoreceptor response: 63% of *TH>hLRRK2* flies; lamina response: 51% of *TH>hLRRK2* flies; medulla response: 56% of *TH>hLRRK2* flies; all $p<0.05$). The photoreceptor and lamina responses did not significantly differ between *TH>Akt; G2019S* and *TH>G2019S* flies, but the medulla responses recorded from *TH>G2019S* flies were slightly reduced (67% of *TH>Akt; G2019S* flies; $p<0.05$).

Figure 4.18Bi-iv shows the peak CRFs recorded from 7 DPE *TH>Akt; G2019S*, *TH>Akt; hLRRK2* and *TH>Akt/w$^{apricot}$* flies. 7 DPE CRFs previously recorded from *TH>G2019S*, *TH>hLRRK2* and *TH/w$^{apricot}$* flies are also shown for comparison. At 7 DPE, there were no significant differences in any of the CRFs recorded from *TH>Akt; G2019S*, *TH>Akt; hLRRK2* and *TH>Akt/w$^{apricot}$* flies (Figure 4.18Bi-iv). A comparison between *TH>Akt/w$^{apricot}$* and *TH/w$^{apricot}$* flies revealed that all CRFs recorded from *TH>Akt/w$^{apricot}$* flies were reduced (photoreceptor response: 51% of *TH/w$^{apricot}$* flies, $p<0.001$; lamina response: 42% of *TH/w$^{apricot}$* flies, $p<0.001$; medulla response: 46% *TH/w$^{apricot}$* flies, $p<0.01$). A comparison between *TH>Akt; hLRRK2* with *TH>hLRRK2* flies revealed that all CRFs recorded from *TH>Akt; hLRRK2* flies were reduced (photoreceptor response: 67% of *TH>hLRRK2* flies, $p<0.05$; lamina response: 42% of *TH>hLRRK2* flies, $p<0.01$; medulla response: 47% of *TH>hLRRK2* flies, $p<0.01$). The

reduced visual responses of *TH>Akt/w*$^{apricot}$ and *TH>Akt; hLRRK2* flies compared with *TH/w*$^{apricot}$ and *TH>hLRRK2* flies, respectively, could be due to the darker eye colour of these flies. Overexpressing *Akt* in the *TH>G2019S* background significantly increased the visual response of *TH>G2019S* flies (photoreceptor response: 162% increase, $p<0.001$; lamina response: 150% increase, $p<0.01$; medulla response: 184% increase, $p<0.01$).

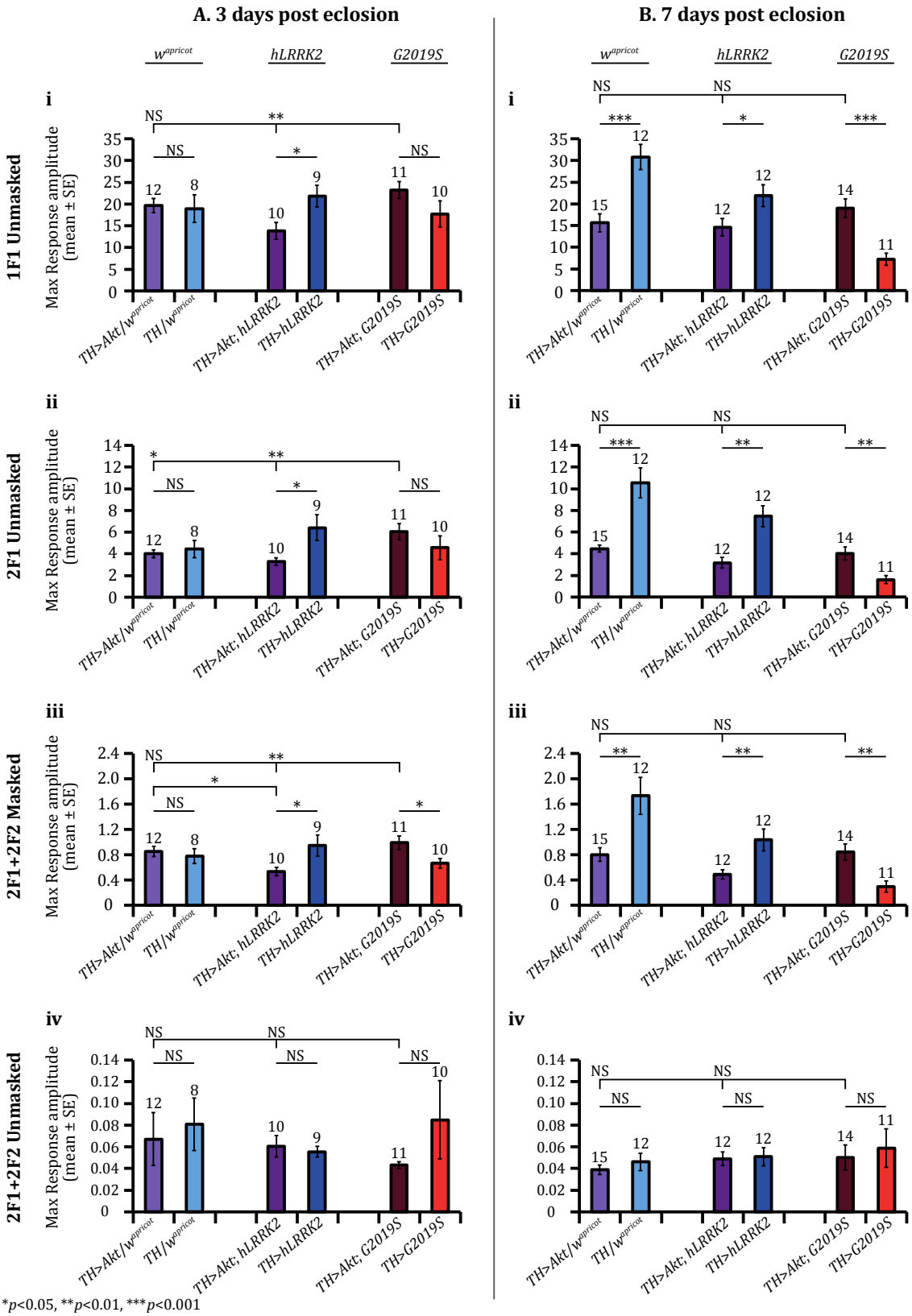


**Figure 4.18 Overexpression of *Akt* in the DA neurons increases the CRFs of flies with DA expression of *hLRRK2-G2019S,* but decreases the CRFs of controls**

Figure legend overleaf.

**Figure 4.18 Overexpression of *Akt* in the DA neurons increases the CRFs of flies with DA expression of *hLRRK2-G2019S,* but decreases the CRFs of controls**

Peak CRFs recorded from flies with DA expression of *Akt* in a non-transgenic background (*TH>Akt/w*$^{apricot}$; light purple), in combination with WT *hLRRK2* (*TH>Akt; hLRRK2*; dark purple), or in combination with *hLRRK2-G2019S* (*TH>Akt; G2019S*; dark red) at (A) 3 DPE and (B) 7 DPE. CRFs recorded from flies with DA expression of no transgene (light blue), *hLRRK2* only (dark blue), or *hLRRK2-G2019S* only (red) are also shown for comparison. Peak CRFs are shown for (i) 1F1, (ii) 2F1, (iv) 2F1+2F2, without a 30% mask and (iii) 2F1+2F2, with a 30% mask as the probe contrast is increased from 0 to 69%. (Ai-iii) At 3 DPE, co-expression of *Akt* with *hLRRK2-G2019S* significantly improved the masked 2F1+2F2 response only. Co-expression of *Akt* with *hLRRK2* significantly reduced all CRFs, whilst DA expression of *Akt* in a non-transgenic background did not affect the CRFs. (Bi-iii) At 7 DPE, co-expression of *Akt* with *hLRRK2-G2019S* significantly increased all CRFs. Co-expression of *Akt* with *hLRRK2* or *Akt* expression in a non-transgenic background significantly reduced all CRFs. There were no significant differences between the 7 DPE CRFs recorded from *TH>Akt/w*$^{apricot}$, *TH>Akt; hLRRK2* or *TH>Akt; G2019S* flies. (Aiv and Biv) At both 3 and 7 DPE, there were no significant differences in the unmasked 2F1+2F2 responses between genotypes, thus the baseline noise level was similar between experiments. Statistics between two genotypes are Student's t-test and statistics between multiple genotypes are ANOVA with post-hoc Bonferroni correction: ***$p$<0.001, **$p$<0.01, *$p$<0.05, NS, no significant difference, $p$>0.05. Data presented are mean ± SEM bars; n numbers are displayed above the bars.

### 4.3.5 Western blots provide inconclusive evidence for differences in total Akt or phosphorylated Akt$^{Ser473}$ levels between *hLRRK2-G2019S* untreated flies, those treated with UCA or UDCA, and controls

To determine if UCA and UDCA increase the phosphorylation of Akt at Ser$^{473}$ in the *LRRK2* fly model, western blotting was performed using fly head lysates. Lysates were extracted from *TH*/*w*$^{apricot}$ and *TH*>*hLRRK2* flies fed control food, *TH*>*G2019S* flies fed control food, UCA or UDCA, *TH*>*Akt* flies fed control food (positive control) and *TH*>*G2019S*/*Akt1* flies fed control food (negative control), all of which were 7 DPE and aged at 29˚C. For each genotype, 30 fly heads were collected and protein was extracted and processed as described in Chapter 2, section 2.5.1. A Bradford assay was used to determine the protein concentration of each sample and to ensure equal loading between samples. After adjustment, samples were loaded into a 10% SDS-PAGE gel and proteins were separated. Following protein transfer to a PDVF membrane, PDVF membranes were probed with either α-Akt, to detect total Akt levels, or α-Phospho-Akt (Ser473), to detect phosphorylated Akt$^{Ser473}$. PDVF membranes were also probed with α-Myosin, which was chosen as a suitable loading control.

Figure 4.19A shows the total Akt levels measured from each genotype. Two bands can be seen, one at ~60 kDa and a second at ~80 kDa, which represent the two isoforms of Akt found in *Drosophila.* The expression of the larger 80 kDa isoform was slightly lower in the negative control (lane 7) compared with the other samples, but the 60 kDa isoform was more or less equivalent between all samples. Unfortunately, the levels of the myosin loading control were lower in the three lanes that contain lysates from *TH*>*G2019S* flies (lanes 4-6). It is not clear if this was due to a loading error or due to levels of myosin being decreased in flies that express the *hLRRK2-G2019S* PD mutation. Figure 4.19B shows the levels of phosphorylated Akt$^{Ser473}$ from each genotype. Again, bands can be seen at ~60 kDa and ~80 kDa. As expected, there was less phosphorylated Akt$^{Ser473}$ in the negative control (lane 7), however the positive control failed to show increased levels (lane 1). Interestingly, levels of phosphorylated Akt$^{Ser473}$ were lower in *TH*>*G2019S* no drug lysates (lane 6)

compared with *TH>hLRRK2* and *TH*/w$^{apricot}$ no drug controls (lanes 2 and 3 respectively). Feeding *TH>G2019S* flies with UDCA or UCA (lanes 4 and 5 respectively) increased the amount of phosphorylated Akt$^{Ser473}$ to levels comparable to those observed in control genotypes. However, this evidence is inconclusive because the levels of the myosin loading control were slightly lower in lanes 4-7 than in lanes 1-3. Thus, it is not clear if the difference in phosphorylated Akt$^{Ser473}$ levels was due to the *hLRRK2-G2019S* mutation or if there was less protein loaded into these lanes.

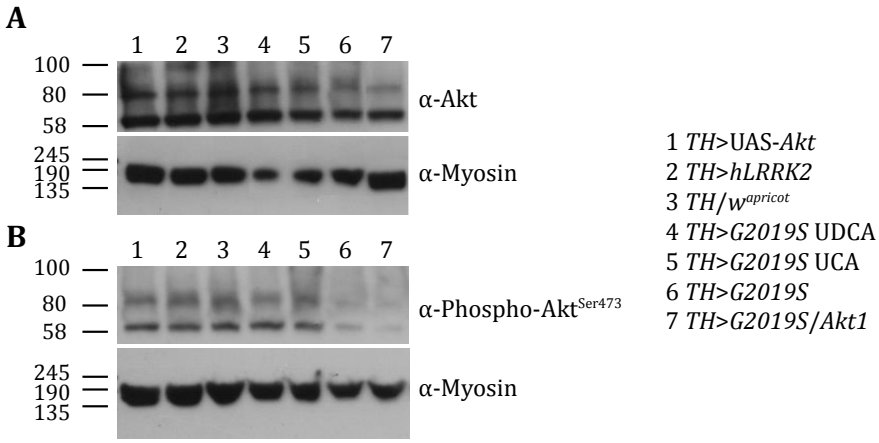


**Figure 4.19 Although total Akt levels are similar between genotypes, phospho-Akt$^{ser473}$ levels are lower in flies with DA expression of *hLRRK2-G2019S* compared with controls, but levels can be increased following treatment with UCA or UDCA**

Western blots showing (A) total Akt levels and (B) phospho-Akt$^{Ser473}$ levels in head lysates from flies with DA expression of UAS-*Akt* (1), WT *hLRRK2* (2), no transgene (3), *hLRRK2-G2019S* (4: with UDCA; 5: with UCA; 6: no drug), and *hLRRK2-G2019S* in combination with *Akt1* (7). For both A and B, α-Myosin was used as a loading control. (A) Probing with α-Akt revealed bands at ~60 kDa and ~80 kDa. The ~60 kDa isoform was similar across all genotypes. Expression of the ~80 kDa isoform was lower in *TH>G2019S/Akt1* lysates than in all other genotypes. Levels of myosin were lower in lysates from *TH>G2019S* flies, regardless of drug treatment, compared with controls. (B) Probing with α-phospho-Akt$^{Ser473}$ also revealed bands at ~60 kDa and ~80 kDa. Both isoforms were lower in lysates from *TH>G2019S/Akt1* flies. Both isoforms were also lower in lysates from untreated *TH>G2019S* flies but were increased following treatment with UDCA or UCA. Again, levels of myosin were lower in lysates from *TH>G2019S* flies, regardless of drug treatment, and also in *TH>G2019S/Akt1* flies compared with controls. Exposure time: 20 sec (α-Akt or α-phospho-Akt), 5 sec (α-Myosin).

### 4.3.6 Overexpression of *parkin* in the DA neurons increases the visual response of flies with DA expression of *hLRRK2-G2019S*

Mitochondrial dysfunction is a key feature of both *LRRK2*- and *parkin*-associated PD (Mortiboys et al., 2008, Mortiboys et al., 2010). Previous studies have reported a genetic interaction between LRRK2 and PINK1/parkin (Smith et al., 2005, Ng et al., 2009, Venderova et al., 2009). A study in *Drosophila* showed that co-expression of human *parkin* in *LRRK2-G2019S*-expressing flies provided a significant protection against *LRRK2-G2019S* mutant-induced DA neurodegeneration (Ng et al., 2009). We wanted to determine if overexpression of *parkin* in the *LRRK2-G2019S* fly model offered some protection and improved the weak CRFs recorded from these flies.

To determine if overexpressing *parkin* could rescue the visual response of *TH>G2019S* flies, UAS-*parkin* was crossed into the UAS-*G2019S* background and both genes were driven in the DA neurons using *TH*-GAL4 (these flies are referred to as *TH>parkin; G2019S* from hereon in). As controls, UAS-*parkin* was also crossed into the *TH>hLRRK2* (*TH>parkin; hLRRK2*) and *TH/w*$^{apricot}$ (*TH>parkin/w*$^{apricot}$) backgrounds. Females were transferred to instant fly food supplemented with 100% EtOH on the day of emergence and kept under the same conditions (29˚C, pulsating light incubator) as previous experiments to enable direct comparisons to be viable. CRFs were measured by SSVEPs at 3 and 7 DPE. The presence of the extra UAS-*parkin* transgene in the *TH/w*$^{apricot}$, *TH>hLRRK2* or *TH>G2019S* backgrounds caused a darker eye colour (Figure 4.20A-C), so when comparisons were made to flies that did not express the extra UAS-*parkin* transgene, the difference in eye colour was taken into consideration.

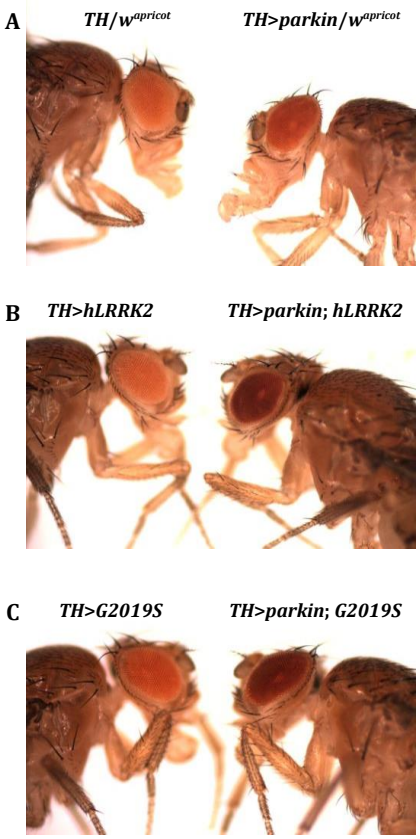


**Figure 4.20 Flies with DA expression of UAS-*parkin* and a second transgene have darker coloured eyes than flies with DA expression of one or no transgenes**

Example images of (A) flies expressing no transgene (left) compared to flies with DA expression of UAS-*parkin* (right), (B) flies expressing UAS-*hLRRK2* only (left) compared to flies with DA expression of UAS-*parkin* and UAS-*hLRRK2* (right), and (C) flies expressing UAS-*hLRRK2-G2019S* only (left) compared to flies with DA expression of UAS-*parkin* and UAS-*hLRRK2-G2019S* (right). Flies expressing two transgenes had darker coloured eyes than those expressing just one transgene or no transgene.

Figure 4.21Ai-iv shows the peak 3 DPE CRFs recorded from *TH>parkin/w*$^{apricot}$, *TH>parkin; hLRRK2* and *TH>parkin; G2019S* flies. To aid comparisons, 3 DPE CRFs previously recorded from *TH/w*$^{apricot}$, *TH>hLRRK2* and *TH>G2019S* flies are plotted on the same graphs. At 3 DPE, overexpression of *parkin* in the *TH>hLRRK2* or *TH>G2019S* backgrounds did not cause any significant changes to the visual response (Figure 4.21Ai-iv). When *parkin* was overexpressed in the *TH/w*$^{apricot}$ background, the photoreceptor responses were not affected but the lower-order neuronal responses were slightly increased compared with *TH/w*$^{apricot}$ flies (lamina response: 42% increase; medulla response: 31% increase; both $p<0.05$). A comparison between *TH>parkin/w*$^{apricot}$, *TH>parkin; hLRRK2* and *TH>parkin; G2019S* flies revealed that the lamina ($p<0.05$) and medulla ($p<0.01$) responses recorded from *TH>parkin/w*$^{apricot}$ flies were slightly higher than those recorded from *TH>parkin; hLRRK2* flies. The lamina responses were not significantly different between *TH>parkin/w*$^{apricot}$ and *TH>parkin; G2019S* flies, but the medulla responses recorded from *TH>parkin/w*$^{apricot}$ flies were slightly higher ($p<0.01$) than those recorded from *TH>parkin; G2019S* flies. The photoreceptor responses did not differ significantly between these three genotype.

Figure 4.21Bi-iv shows the peak 7 DPE CRFs recorded from *TH>parkin/w*$^{apricot}$, *TH>parkin; hLRRK2, TH>parkin; G2019S* flies and for comparison *TH/w*$^{apricot}$, *TH>hLRRK2* and *TH>G2019S* flies. At 7 DPE, overexpression of *parkin* in the *TH>G2019S* background significantly increased both the photoreceptor and lamina responses (both $p<0.05$; Figure 4.21Bi-iii). In contrast, overexpressing *parkin* in the *TH/w*$^{apricot}$ or *TH>hLRRK2* backgrounds caused significant reductions in all three components of the neuronal visual response (*TH>parkin/w*$^{apricot}$; photoreceptor response: 39% decrease, $p<0.01$; lamina response: 38% decrease, $p<0.05$; medulla response: 45% decrease, $p<0.05$; *TH>parkin; hLRRK2*; photoreceptor response: 40% decrease, $p<0.01$; lamina response: 62% decrease, $p<0.001$; medulla response: 58% decrease, $p<0.01$). These reductions could have been due to the darker eye colour of flies expressing UAS-*parkin*. A comparison between *TH>parkin/w*$^{apricot}$, *TH>parkin; hLRRK2* and *TH>parkin; G2019S* flies revealed that there were no significant differences between the CRFs recorded from *TH>parkin; hLRRK2* and *TH>parkin; G2019S* flies, but the lamina responses recorded from *TH>parkin; G2019S* flies were

slightly lower than those recorded from *TH>parkin/w*$^{apricot}$ flies ($p$<0.05). Overexpressing *parkin* in the *TH>hLRRK2* background had a more severe effect on the visual response than overexpressing *parkin* in the non-transgenic background; both the lamina ($p$<0.01) and medulla ($p$<0.05) responses recorded from *TH>parkin; hLRRK2* flies were significantly lower than those recorded from *TH>parkin/w*$^{apricot}$ flies. It is unsurprising that *TH>parkin/w*$^{apricot}$ flies gave better responses than *TH>parkin; hLRRK2* and *TH>parkin; G2019S* flies because they only express one transgene, whereas the other two genotypes both express two transgenes causing them to have darker eyes (see Figure 4.20).

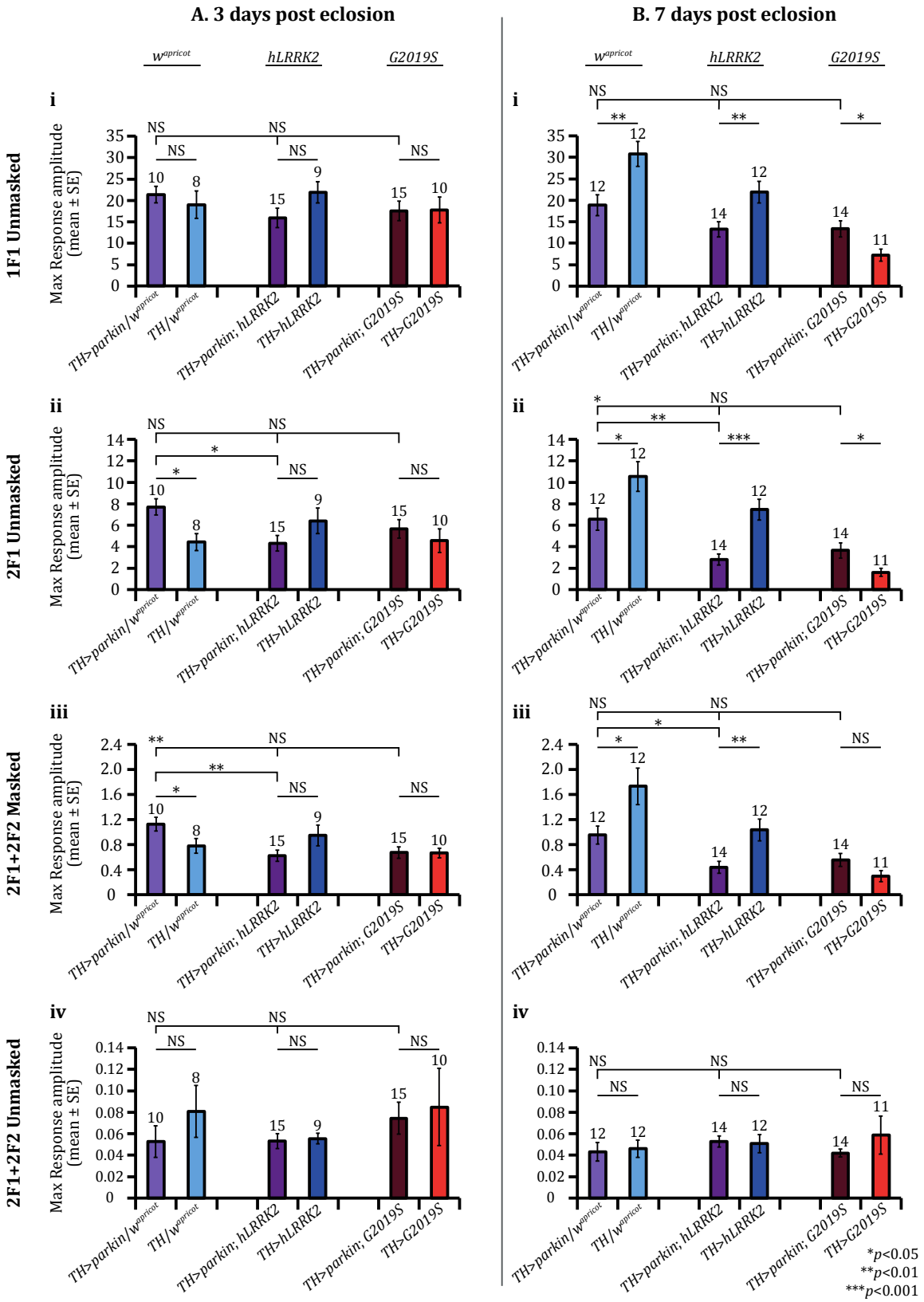


**Figure 4.21 Overexpression of *parkin* in the DA neurons increases the CRFs of flies with DA expression of *hLRRK2-G2019S,* but reduces the CRFs of controls**

Figure legend overleaf.

**Figure 4.21 Overexpression of *parkin* in the DA neurons increases the CRFs of flies with DA expression of *hLRRK2-G2019S,* but reduces the CRFs of controls**

Peak CRFs recorded from flies with DA expression of *parkin* in a non-transgenic background (*TH>parkin/w*$^{apricot}$; light purple), in combination with WT *hLRRK2* (*TH>parkin; hLRRK2*; dark purple), or in combination with *hLRRK2-G2019S* (*TH>parkin; G2019S*; dark red) at (A) 3 DPE and (B) 7 DPE. CRFs of flies with DA expression of no transgene (light blue), *hLRRK2* only (dark blue), or *hLRRK2-G2019S* only (red) are also shown for comparison. Peak CRFs are shown for (i) 1F1, (ii) 2F1, (iv) 2F1+2F2, without a 30% mask and (iii) 2F1+2F2, with a 30% mask as the probe contrast is increased from 0 to 69%. (Ai-iii) At 3 DPE, co-expression of *parkin* with either *hLRRK2* or *hLRRK2-G2019S* did not cause significant changes to any of the CRFs, whilst DA expression of *parkin* in a non-transgenic background significantly increased some components of the neuronal visual response. (Bi-iii) At 7 DPE, co-expression of *parkin* with *hLRRK2-G2019S* significantly increased CRFs from 1F1 and 2F1. However, co-expression of *parkin* with *hLRRK2* or expression of *parkin* in a non-transgenic background, significantly reduced all CRFs. (Aiv and Biv) At both 3 and 7 DPE, there are no significant differences in the unmasked 2F1+2F2 responses, thus the baseline noise level was similar between experiments. Statistics between two genotypes are Student's t-test and statistics between multiple genotypes are ANOVA with post-hoc Bonferroni correction: ***$p$<0.001, **$p$<0.01, *$p$<0.05, NS, no significant difference, $p$>0.05. Data presented are mean ± SEM bars; n numbers are displayed above the bars.

### 4.3.7 Treatment with the kinase inhibitor BMPPB-32 rescues the visual response of flies with DA expression of *hLRRK2-G2019S* at 7 DPE

As previously mentioned in Chapter 1, since mutations in the kinase domain of *LRRK2* were associated with PD, a major area of focus has been on developing *LRRK2* kinase inhibitors in the hope that these could be used as a treatment for *LRRK2*-associated PD. It is important to determine both the *in vivo* and *in vitro* effects of these inhibitors thus two of them, LRRK2-IN-1 and BMPPB-32, have been tested in the *LRRK2-G2019S* fly model. Whilst LRRK2-IN-1 has previously been identified as a *LRRK2* kinase inhibitor (Deng et al., 2011), BMPPB-32 was a novel LRRK2 inhibitor synthesised by our collaborators at the Neuroscience Drug Discovery department at Lundbeck (Afsari et al., 2014). Using the SSVEP assay it was shown that the contrast sensitivity

of young (1 DPE) *TH>G2019S* flies was dramatically increased compared with controls expressing WT *hLRRK2* or no transgene in their DA neurons (Afsari et al., 2014). The increased visual sensitivity is thought to originate in the photoreceptors and is then inherited by the second- and third-order lamina and medulla neurons. The initial hyperactivity of 1 DPE *TH>G2019S* flies could be rescued through feeding with either LRRK2-IN-1 or BMPPB-32, resulting in photoreceptor and neuronal responses that were comparable to control flies. The $dLRRK^{e03680}$ fly line (described in Chapter 3), which does not express *LRRK*, was used to test for off-target effects of the two kinase inhibitors. The SSVEP responses of $dLRRK^{e03680}$ flies were significantly increased when they were fed LRRK2-IN-1, suggesting that this compound is binding to other kinases. On the other hand, feeding BMPPB-32 to $dLRRK^{e03680}$ flies did not cause any significant changes to the SSVEP response, suggesting that this compound does not have any severe off-target effects (Afsari et al., 2014). During the initial study, BMPPB-32 was fed to flies throughout their entire lifespan (from larvae to adult fly). In the current study, we wanted to determine the *in vivo* effect of administrating this drug at the start of adult life only, which is when a neurophysiological phenotype is observed. This will hopefully mimic the situation of a PD patient more accurately, as they are likely to only start taking drugs later in life when symptoms become apparent.

Food containing BMPPB-32 was made through dissolving BMPPB-32 in 100% EtOH and then diluting into deionised water to achieve a final concentration of 2.5 µM. The drug solution was then mixed with instant fly food. Larvae were raised on drug-free food and female adult flies were transferred to food containing 2.5 µM BMPPB-32 on the day of eclosion. These flies were kept in the same conditions as previous drug experiments (29˚C, pulsating light incubator) so the BMPPB-32 treatment could be compared to untreated flies. CRFs were measured by SSVEP at 3 and 7 DPE.

Figure 4.22A-D shows the peak 3 DPE CRFs recorded from control $TH/w^{apricot}$ and *TH>hLRRK2* flies and mutant *TH>G2019S* flies that had been fed control food or food supplemented with BMPPB-32. For each genotype, the photoreceptor response was unchanged following treatment with BMPPB-32 (Figure 4.22A). Treatment with BMPPB-32 caused no significant changes in the neuronal responses of *TH>hLRRK2* or *TH>G2019S* flies (Figure 4.22B,C). In contrast, BMPPB-32 significantly reduced the

lamina ($p$<0.05) and medulla ($p$<0.01) responses of *TH/w*$^{apricot}$ flies. A comparison between BMPPB-32 treated *TH/w*$^{apricot}$ flies and BMPPB-32 treated *TH>hLRRK2* flies revealed that all three components of the neuronal visual response were significantly higher in *TH>hLRRK2* flies (photoreceptor response: 49% of *TH>hLRRK2* flies, $p$<0.01; lamina response: 25% of *TH>hLRRK2* flies, $p$<0.001; medulla response: 29% of *TH>hLRRK2* flies, $p$<0.001). BMPPB-32 treated *TH>hLRRK2* flies also showed significantly higher CRFs than BMPPB-32 treated *TH>G2019S* flies (photoreceptor response: 58% of *TH>hLRRK2* flies; lamina response: 54% of *TH>hLRRK2* flies; medulla response: 62% of *TH>hLRRK2* flies; all $p$<0.05). There were no significant differences recorded between BMPPB-32 treated *TH/w*$^{apricot}$ flies and BMPPB-32 treated *TH>G2019S* flies. A small difference in the unmasked 2F1+2F2 response was observed between *TH>hLRRK2* flies fed control food and those fed BMPPB-32 food (Figure 4.22D; $p$<0.05). This suggests that the baseline noise level was slightly different between these two conditions. This could have been caused by slight differences in the electrodes between experiments. No significant differences in the unmasked 2F1+2F2 responses were found between any of the other genotype/drug combinations (Figure 4.22D).

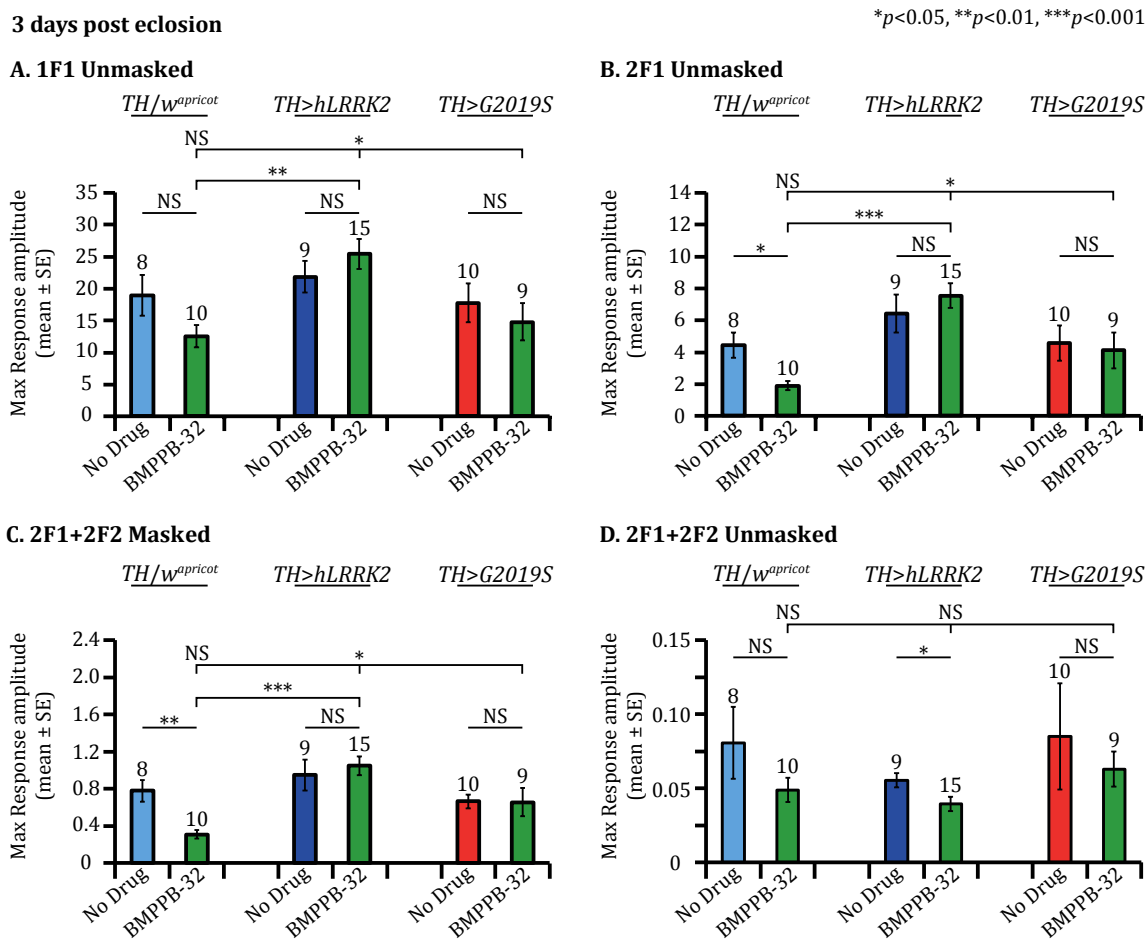


**Figure 4.22 At 3 DPE, treatment with BMPPB-32 does not alter the CRFS of flies with DA expression of *hLRRK2-G2019S* or *hLRRK2,* but slightly reduces the CRFs of flies expressing no transgene**

The 3 DPE peak CRFs recorded from flies expressing no transgene (light blue), WT *hLRRK2* (dark blue) or *hLRRK2-G2019S* (red) in the DA neurons, after being fed control food or food supplemented with BMPPB-32 (light green). Peak CRFs are shown for (A) 1F1, (B) 2F1, (D) 2F1+2F2, without a 30% mask and (C) 2F1+2F2, with a 30% mask as the probe contrast is increased from 0 to 69%. (A-C) Treatment with BMPPB-32 did not affect the CRFs recorded from *TH>G2019S* or *TH>hLRRK2* flies. However, the 2F1 and masked 2F1+2F2 responses of *TH/w*$^{apricot}$ flies were both reduced after treatment with BMPPB-32. CRFs of BMPPB-32 treated *TH>hLRRK2* flies were significantly higher than those recorded from *TH>G2019S* and *TH/w*$^{apricot}$ flies also treated with BMPPB-32. (D) The unmasked 2F1+2F2 response of *TH>hLRRK2* flies was significantly reduced following BMPPB-32 treatment. There were no significant differences in the unmasked 2F1+2F2 responses between genotypes following BMPPB-32 treatment, thus the baseline noise level was similar between experiments. Statistics within genotypes are Student's t-test and statistics between multiple genotypes are

ANOVA with post-hoc Bonferroni correction: ***$p$<0.001, **$p$<0.01, *$p$<0.05, NS, no significant difference, $p$>0.05. Data presented are mean ± SEM bars; n numbers are displayed above the bars.

Figure 4.23A-D shows the peak 7 DPE CRFs recorded from *TH/w*$^{apricot}$, *TH>hLRRK2* and *TH>G2019S* flies that had been fed control food or food supplemented with BMPPB-32. At 7 DPE, treatment with BMPPB-32 continued to reduce the photoreceptor and medulla responses recorded from *TH/w*$^{apricot}$ flies (Figure 4.23A,C; both $p$<0.05). The lamina responses were also reduced, but not significantly (Figure 4.23B). Treatment with BMPPB-32 did not change the photoreceptor or lamina responses recorded from *TH>hLRRK2* flies, but it caused a slight reduction in the medulla responses ($p$<0.05). As previously described in section 4.3.1, the visual responses of untreated *TH>G2019S* flies are dramatically reduced by 7 DPE. Feeding *TH>G2019S* flies food supplemented with BMPPB-32 significantly increased all three components of the neuronal visual response (photoreceptor response: 158% increase, $p$<0.001; lamina response: 258% increase, $p$<0.01; medulla response: 187% increase, $p$<0.01). A comparison between *TH>G2019S* flies fed BMPPB-32 with *TH/w*$^{apricot}$ and *TH>hLRRK2* flies also fed BMPPB-32, revealed that there were no significant differences in the CRFs recorded from these flies.

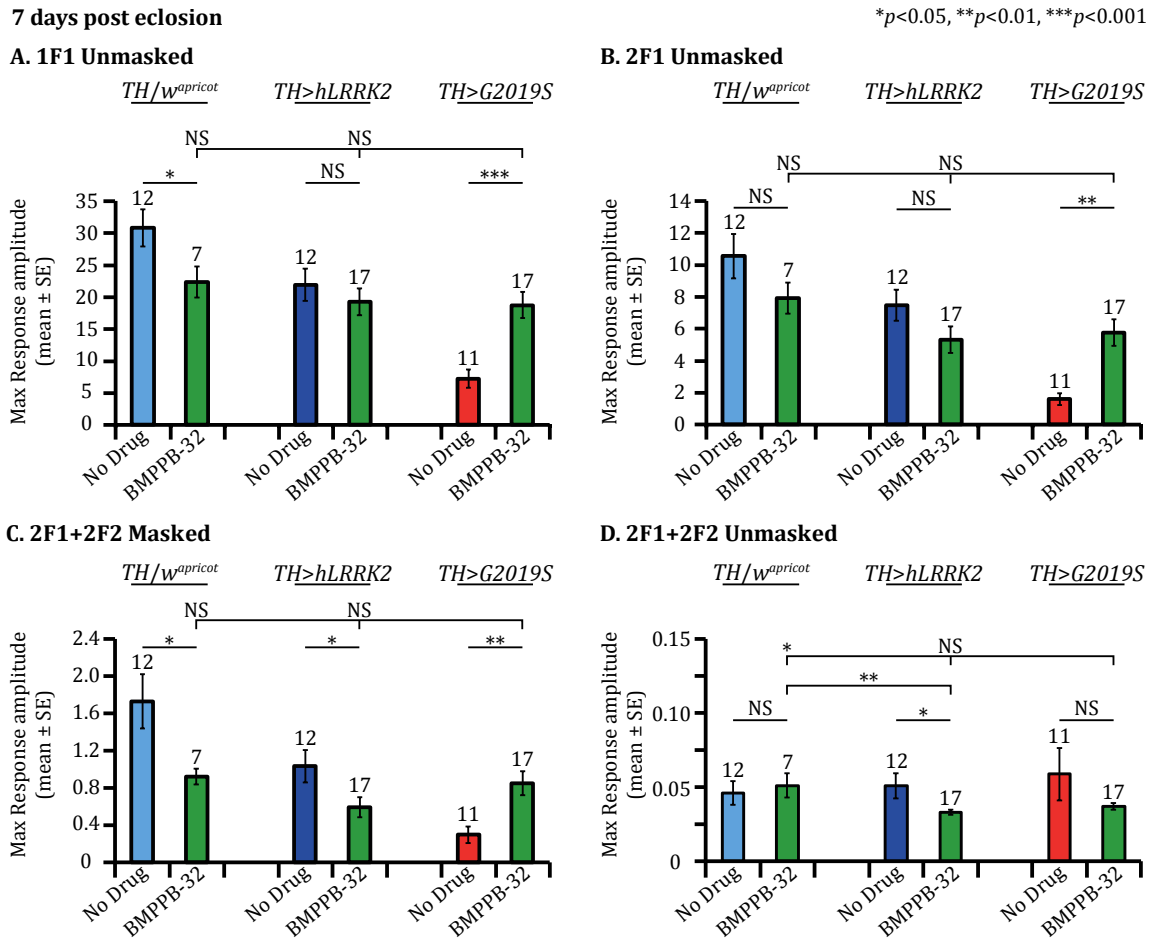


**Figure 4.23 At 7 DPE, treatment with BMPPB-32 increases the CRFs of flies with DA expression of *hLRRK2-G2019S,* but reduces the CRFs of controls**

The 7 DPE peak CRFs recorded from flies expressing no transgene (light blue), WT *hLRRK2* (dark blue) or *hLRRK2-G2019S* (red) in the DA neurons, after being fed control food or food supplemented with BMPPB-32 (light green). Peak CRFs are shown for (A) 1F1, (B) 2F1, (D) 2F1+2F2, without a 30% mask and (C) 2F1+2F2, with a 30% mask as the probe contrast is increased from 0 to 69%. (A-C) Treatment with BMPPB-32 significantly increased all CRFs recorded from *TH>G2019S* flies. However, treatment with BMPPB-32 significantly reduced some, but not all, components of the neuronal visual response recorded from *TH>hLRRK2* and *TH/w*$^{apricot}$ flies. The 1F1, 2F1 and masked 2F1+2F2 CRFs were not significantly different between genotypes following treatment with BMPPB-32. (D) The unmasked 2F1+2F2 responses of BMPPB-32 treated *TH/w*$^{apricot}$ flies were significantly higher than *TH>hLRRK2* and *TH>G2019S* treated flies. Statistics within genotypes are Student's t-test and statistics between multiple genotypes are ANOVA with post-hoc Bonferroni correction: ***$p$<0.001, **$p$<0.01, *$p$<0.05, NS, no significant difference, $p$>0.05. Data presented are mean ± SEM bars; n numbers are displayed above the bars.

## 4.4 Discussion

The ectopic expression of the dominant PD-associated *hLRRK2-G2019S* mutation in the DA neurons of flies has previously been shown to cause severe visual defects (Hindle et al., 2013, Afsari et al., 2014). In this chapter, the first key finding was that the chemically related mitochondrial rescue agents, UCA and UDCA, are able to dramatically improve the visual response of flies with DA expression of *hLRRK2-G2019S*. Secondly, parkin was shown to offer some protection against *hLRRK2-G2019S* induced visual dysfunction. Finally, the kinase inhibitor, BMPPB-32, which has previously been described to rescue the visual response of young (1 DPE) *hLRRK2-G2019S* flies, was shown here to also rescue the visual response of older (7 DPE) *hLRRK2-G2019S* flies after being administrated on the first day of eclosion. The results presented in this chapter build upon and reinforce the data from previous studies, whilst providing promising *in vivo* data for potential therapeutic compounds that should be considered for future PD-related drug trials.

### 4.4.1 *hLRRK2-G2019S*-induced visual dysfunction can be rescued through treatment with UCA or UDCA

In the present study, the SSVEP approach was adopted to test for abnormal physiology of the visual system of flies with DA expression of *hLRRK2-G2019S*. The flies were kept in a pulsating light incubator to accelerate the decline in visual function, which enabled SSVEPs to be recorded from flies at younger ages. At 3 DPE, the visual responses recorded from flies with DA expression of *hLRRK2-G2019S* were robust, but by 7 DPE they had substantially decreased and were significantly lower than those recorded from control flies. At 7 DPE, the photoreceptor responses recorded from flies expressing WT *hLRRK2* were also slightly lower than flies expressing no transgene, which may be attributable to the increased kinase activity caused by the expression of *hLRRK2* in addition to the flies own version of *LRRK*. Previously, Liu et al. (2008) found that overexpression of WT *hLRRK2* caused age-related retinal degeneration, locomotor impairment and DA neuron loss compared with WT flies, but expression of *hLRRK2-G2019S* caused even more severe phenotypes. This is in accordance with the SSVEP data recorded during this study, whereby visual dysfunction was evident is flies expressing WT *hLRRK2* but was much

more severe in those flies expressing the mutant *hLRRK2-G2019S*. By 14 DPE, the effect of increasing the energy demands on the visual system became apparent in control flies as well as flies expressing *hLRRK2-G2019S,* and the visual responses of all genotypes were substantially reduced. Afsari et al. (2014) previously identified that young (1 DPE) flies expressing *G2019S* in the DA neurons have increased contrast sensitivity compared with control flies, whilst Hindle et al. (2013) showed that old (28 DPE) flies expressing *G2019S* in the DA neurons have reduced flash ERG responses, which could be accelerated through increasing the energy demands of the visual system. The results presented in this chapter, along with those previously reported by Hindle et al. (2013) and Afsari et al. (2014), suggest that the period of hypersensitivity of 1 DPE flies starts an excitotoxic cascade due to the selective expression of *G2019S* in the DA neurons. This quickly leads to severe visual dysfunction by 7 DPE when flies are kept under conditions that increase DA neuronal energy demands, or a progressive loss of vision (between 10 and 28 DPE) when flies are kept in constant darkness, reviewed in West et al. (2015b). In old flies, the visual dysfunction caused by DA expression of *G2019S* is accompanied by apoptosis and autophagy (Hindle et al., 2013). Although evidence of apoptosis and autophagy were not investigated in the present study, it is likely that these degenerative events are accelerated with increased energy demands to the visual system and thus played a key part in the visual defects observed here.

The defective visual response of 7 DPE flies expressing *hLRRK2-G2019S* could be equally rescued through treatment with UCA or UDCA, however these compounds only rescued visual function to ~65-70% of control flies. It is possible that the 2.5 µM dose administered to the flies in the current study was too low to provide a complete rescue. A dose response curve generated for a kinase inhibitor, BMPPB-32, revealed 2.5 µM to be the most efficient concentration to improve the visual response of *TH>G2019S* flies (Afsari et al., 2014), thus we also chose to use 2.5 µM UDCA or UCA. However, excellent safety and tolerability of UDCA were reported in patients with motor neuron disease with doses of up to 50 mg/kg per day (Parry et al., 2010). Therefore, our fly model may be able to tolerate much higher doses, which could offer a complete rescue.

Hindle et al. (2013) found that the visual defects caused by *G2019S* are associated with mitochondrial deformity in the photoreceptors therefore similar mitochondrial dysfunction may contribute to the reduced SSVEPs recorded from 7 DPE *TH>G2019S* flies. Both UDCA and UCA are known to increase the activities of complexes I-IV of the mitochondrial respiratory chain in *LRRK2-G2019S*- and *parkin*-mutant fibroblasts (Mortiboys et al., 2013). Using the same mitochondrial activity assays as previously described, activities of complexes I-IV were also examined in the *hLRRK2-G2019S* fly model. Complex IV was of particular interest because specific impairment of this complex has previously been recorded in both M-*LRRK2-G2019S* and NM-*LRRK2-G2019S* carriers (Mortiboys et al., 2015). Unfortunately, we were unable to record any significant differences in the activities of complexes I, II or IV, between *hLRRK2-G2019S* flies and controls. In addition, we also found no significant effect of UCA or UDCA treatment on the activities of complexes I, II or IV in *hLRRK2-G2019S* or control flies. Due to the small number of repeats, especially for complexes I and IV, the error bars were very large, thus further repeats may help to reduce the size of the error bars and differences between genotypes/drug treatments may become apparent. However, at this stage we are unable to provide evidence of a specific impairment of complex IV in the fly model of *hLRRK2-G2019S.*

Interestingly TUDCA, the derivative of UDCA, has been shown to prevent photoreceptor cell death with decreases in oxidative stress and caspase activity in a rat model of photoreceptor detachment (Mantopoulos et al., 2011). It also provides cytoprotective effects against light-induced or oxidative stress-induced retinal damage in various mouse models (Boatright et al., 2006, Phillips et al., 2008, Oveson et al., 2011). Thus, it is possible that the neuroprotective effects of UDCA and UCA operate through a similar mechanism in our *Drosophila* model of *LRRK2-G2019S* PD. The defective visual response of *TH>G2019S* flies may occur through photoreceptor cell death and increased oxidative stress, which may be prevented with administration of UDCA or UCA.

### 4.4.2 Do UDCA and UCA mediate their beneficial effects through increasing the phosphorylation of Akt$^{Ser473}$?

Reducing the gene expression of Akt using the strong pan-neuronal driver *nsyb*-GAL4 to drive expression of *Akt*-RNAi caused visual defects by 7 DPE; both UDCA and UCA were able to significantly increase the responses from all three components of the neuronal visual response. The visual response was also slightly reduced when *Akt*-RNAi was expressed using the weaker pan-neuronal driver *elav*-GAL4; UCA didn't offer much of a beneficial effect on neuronal signalling, but UDCA increased all three components of the visual response. Driving expression of *Akt*-RNAi with *nsyb*-GAL4 caused a more severe loss of visual function than driving expression with *elav*-GAL4. Although *nsyb*-GAL4>*Akt*-RNAi flies have darker coloured eyes than *elav*-GAL4>*Akt*-RNAi flies, which could have played a part in the reduced visual response of these flies, we believe that *nsyb*-GAL4 was driving the expression of *Akt*-RNAi more strongly than *elav*-GAL4. CRFs recorded from 7 DPE *TH>Akt1/G2019S* transheterozygote flies were also reduced. Again, UDCA significantly improved the responses from the photoreceptors, lamina and medulla of these flies, but the beneficial effects of UCA were only observed in the photoreceptor response. Interestingly, the DA expression of one mutant copy of *Akt1* did not appear to worsen the visual response of flies also expressing *hLRRK2-G2019S.* A more severe phenotype may have been observed if two mutant copies of *Akt1* had been expressed, or if the expression of mutant *Akt1* had been ubiquitous rather than limited to the DA neurons. The neuronal visual response of flies with DA expression of *hLRRK2-G2019S* was improved with DA overexpression of WT *Akt*. However, overexpressing WT *Akt* in the DA neurons of control flies reduced their visual response. This could have been due to the darker coloured eyes of these flies. However Akt is involved in a number of different pathways so increasing the expression *in vivo* could lead to adverse effects in some or all of these pathways. It would be interesting to overexpress *Akt* either pan-neuronally or globally to produce survival curves for these vs WT flies, which may help us to determine if overexpression of *Akt* does cause adverse side effects.

It is possible that UCA and UDCA increased the phosphorylation of Akt in our *LRRK2-G2019S* fly model. UDCA and UCA both rescue mitochondrial dysfunction in *parkin*-mutant patient tissue through increasing the phosphorylation of Akt (Mortiboys et al., 2013), and TUDCA offers a partial neuroprotective effect on MPTP-induced DA cell death in a PD mouse model via activation of the Akt pro-survival pathway (Castro-Caldas et al., 2012). There is increasing evidence to suggest that alterations in Akt activation play a part in the pathogenesis of both familial and sporadic PD. Failure of Akt signalling has previously been described as the 'common core' that underlies neuronal degeneration and cell death in both familial and sporadic forms of PD (Greene et al., 2011). Immunostaining of *post-mortem* brains shows that Akt phosphorylation is reduced in DA SN neurons from sporadic PD patients (Malagelada et al., 2008, Timmons et al., 2009). Mutations in *LRRK2*, or deficiency of Parkin, PINK1 or DJ-1 all result in decreased Akt phosphorylation (Yang et al., 2005, Murata et al., 2011, Ohta et al., 2011). On the other hand, overexpression of *parkin* or *PINK1* has been shown to increase the levels of phosphorylated Akt (Murata et al., 2011, Yasuda et al., 2011). Akt activation is also reduced through increased expression of α-synuclein or through mutations in the *SNCA* gene (Chung et al., 2011). Whereas, in transgenic mice overexpressing human α-synuclein, virally-induced overexpression of β-synuclein enhanced Akt activity and reversed the neurodegeneration (Hashimoto et al., 2004b). In line with this, the protective effect of β-synuclein against rotenone in cultured neuroblastoma cells, was also mediated via increased Akt phosphorylation (Hashimoto et al., 2004a). As previously mentioned, a number of drugs used to treat PD through targeting the DA system have also been found to be neuroprotective via Akt activation (Sagi et al., 2007, Chen et al., 2008, Lim et al., 2008, Nair and Olanow, 2008, Yu et al., 2008). Taken together, these studies provide strong evidence to implicate Akt signalling in PD pathogenesis.

The results presented in this chapter, suggest that a reduction of Akt causes visual defects, whilst increasing Akt levels through overexpression of *Akt* or possibly via UDCA/UCA, improves the visual response of *hLRRK2-G2019S* mutant flies. However, these results do not directly show that UDCA and UCA increase the phosphorylation of $Akt^{Ser473}$, as previously reported in *parkin*-mutant fibroblasts (Mortiboys et al., 2013). To investigate this further, western blotting was used to detect total Akt levels

and phospho-Akt$^{Ser473}$ levels in flies that had been treated with no drug or those that had been treated with UDCA or UCA. Although total Akt levels were equivalent between all genotypes tested, phospho-Akt$^{Ser473}$ levels appeared to be reduced in flies with DA expression of *G2019S* compared with controls. Treating the *TH>G2019S* flies with either UDCA or UCA increased phospho-Akt$^{Ser473}$ levels. Although our data is inline with that previously reported by Mortiboys et al. (2013), at this stage it is inconclusive because in both blots the myosin loading control levels were variable between lysates. Interestingly, in both cases levels of myosin were lower in lysates from *TH>G2019S* flies compared with control flies. A QUICK (quantitative immunoprecipitation combined with knockdown) screen in NIH3T3 cells has previously revealed that LRRK2 interacts with myosins (Meixner et al., 2011). Furthermore, LRRK2 has been associated with other components of the cytoskeleton including tubulin, actin and moesin (Jaleel et al., 2007, Gandhi et al., 2008, Gillardon, 2009, Meixner et al., 2011). There is also increasing evidence to suggest that assembly of cytoskeletal components is a major characteristic of neurodegenerative disorders, including PD. Therefore, the *G2019S* mutation may affect the interaction of LRRK2 and myosins or other cytoskeletal components, which may in turn affect their expression. Although this is a possibility, loading errors between wells cannot be ruled out. It would be interesting to use a different cytoskeletal component as a loading control, such as tubulin or actin, to see if the levels of these proteins are also reduced in the presence of the *hLRRK2-G2019S* mutation. Unfortunately, we were unable to detect an increase in the level of total Akt or phospho-Akt$^{Ser473}$ in lysates from the positive control (*TH*>UAS-*Akt*) compared to the other genotypes. The major Akt phosphorylation sites in *Drosophila* are Ser505 and Thr342; these sites are homologous to the mammalian Ser473 and Thr308 activation sites, respectively (Scanga et al., 2000). Although the mammalian phospho-Akt$^{Ser473}$ antibody has previously been shown to detect *Drosophila* phosphorylated Akt$^{Ser505}$ perhaps it was unable to detect slight alterations in the levels of phosphorylated Akt$^{Ser505}$ in our fly model. A phospho-Akt$^{Ser505}$ antibody may have been more appropriate to use during this investigation. Further work is needed to determine whether UDCA and UCA increase the phosphorylation of Akt in our *LRRK2-G2019S* fly model.

### 4.4.3 The therapeutic potential of UDCA for treatment of PD

The results presented here, along with those reported by our collaborators, demonstrate a strong class effect for bile acids and their derivatives in providing a marked rescue effect on a biologically relevant pathomechanism for *LRRK2-G2019S*-linked PD, both *in vitro* and *in vivo* (Mortiboys et al., 2013, Mortiboys et al., 2015). As there is strong evidence of mitochondrial dysfunction in both sporadic and familial forms of PD, drugs that target the mitochondria offer a promising strategy for disease-modifying therapy in PD. The potential of UDCA is particularly exciting, because it is already an FDA-licensed drug that has been in clinical use for several decades to treat primary biliary cirrhosis (Poupon et al., 1994). Drug repositioning can be a time- and cost-saving strategy in comparison to *de novo* drug synthesis. Furthermore, cerebrospinal fluid (CSF) penetrance of UDCA has been established. One study reported that oral administration of UDCA is safe, tolerable and can penetrate into the CSF in a dose-dependent manner in patients with Amyotrophic lateral sclerosis (ALS) (Parry et al., 2010). A separate study used Yoo's solution, a well characterised increased water solubility version of UDCA, enabling it to penetrate the BBB (Min et al., 2012). When Yoo's solution was administered orally to ALS patients, CSF penetrance was also reported (Min et al., 2012). The efficacy and tolerability of TUDCA in ALS patients is already being tested in clinical trials (Clinical Trials registration: NCT00877604). Our data suggest that UDCA, or possibly the closely related UA, UCA and DUA, are promising candidates for future PD clinical trials.

### 4.4.4 Parkin may offer some protection against *hLRRK2-G2019S*-induced visual dysfunction

DA overexpression of *parkin* at 7 DPE offered partial protection against *hLRRK2-G2019S* induced visual dysfunction. In contrast, the visual responses of control flies were reduced with DA overexpression of *parkin*. A previous study found that pan-neuronal overexpression of *parkin* in WT flies significantly increased longevity without causing any obvious physiological trade-offs (Rana et al., 2013). Thus, it is possible that the reduced visual response of control flies in this chapter was due to the darker coloured eyes of these flies compared to those not expressing *parkin*, rather than *parkin* directly affecting visual function. However, further studies will be

required to examine the role of *parkin* within the fly visual system. It has previously been shown that expression of human *parkin* in *hLRRK2-G2019S* flies provides a significant protection against *LRRK2-G2019S* mutant-induced DA neurodegeneration (Ng et al., 2009). Therefore, our data are in agreement with the data from earlier studies, which showed an interaction between parkin and LRRK2 (Smith et al., 2005, Ng et al., 2009, Venderova et al., 2009).

Parkin belongs to a family of proteins that have conserved ubiquitin-like domains and RING finger motifs (Deshaies and Joazeiro, 2009, Dawson and Dawson, 2010). It functions as an ubiquitin E3 protein ligase (Imai et al., 2000, Shimura et al., 2000, Zhang, 2000). Mutations in *parkin* cause autosomal recessive PD and are the most common identifiable genetic cause for EOPD (Kitada et al., 1998, Lucking et al., 2000). Skin biopsies taken from *parkin*-mutant PD patients have shown that *parkin* mutations cause mitochondrial dysfunction, with specific impairment of complex I (Mortiboys et al., 2008). Mitochondrial pathology is also observed in the absence of parkin in a *Drosophila* model (Greene et al., 2003, Pesah et al., 2004); parkin knockout mice have features of mitochondrial dysfunction and oxidative damage (Palacino et al., 2004); and parkin-deficient patients show decreased lymphocyte mitochondrial complex I activity (Muftuoglu et al., 2004). Together, these studies implicate parkin in regulating mitochondrial function. Several other ubiquitin E3 ligases are known to have roles in the regulation of mitochondrial fusion and fission, thus parkin may also have a role in mitochondrial dynamics, related to its E3 ligase activity (Karbowski et al., 2007, Mortiboys et al., 2008). A number of studies have revealed a conserved function of parkin, in which it acts downstream of PINK1 to protect mitochondrial integrity and prevent oxidative stress-induced apoptosis (Clark et al., 2006, Park et al., 2006, Yang et al., 2006, Exner et al., 2007). Studies in *Drosophila* have also shown that *Drosophila parkin* and *PINK1* interact with components of the mitochondrial fission and fusion machinery (Deng et al., 2008, Yang et al., 2008, Park et al., 2009, Ziviani et al., 2010). PINK1 and parkin deficient *Drosophila* show enlarged and swollen mitochondria, suggesting that the PINK1/parkin pathway is also involved in regulating mitochondrial morphology (Poole et al., 2008). Although there is strong evidence to suggest that parkin plays a key role in regulating mitochondrial homeostasis/morphology, the precise mechanisms by which it does this remain

elusive. However, it is possible that parkin improves the visual response of our *hLRRK2-G2019S* mutant flies through helping to restore or prevent *LRRK2-G2019S* induced mitochondrial dysfunction.

It has already been shown that a class of bile acid mitochondrial rescue agents can completely rescue mitochondrial dysfunction in both *parkin*- and *LRRK2*-mutant fibroblasts (Mortiboys et al., 2013, Mortiboys et al., 2015). Furthermore, parkin is known to closely interact with PINK1, and mutations in PINK1 can also cause PD. Therefore, compounds targeting the mitochondria or that are able to increase the expression of *parkin* may be effective therapeutic compounds in multiple forms of familial PD.

### 4.4.5 *hLRRK2-G2019S* induced visual dysfunction can be rescued through treatment with BMPPB-32

In addition to testing the effect of mitochondrial rescue agents, a LRRK2-specific kinase inhibitor, BMPPB-32, was also tested for its neuroprotective effect on visual function. Using the SSVEP approach, it was found that BMPPB-32 significantly improved all three components of the neuronal visual response recorded from 7 DPE flies with DA expression of *hLRRK2-G2019S*. However, at 3 and 7 DPE, BMPPB-32 caused reductions in the visual function of control flies. This may have been caused by BMPPB-32 also targeting *dLRRK,* the fly orthologue of *hLRRK2*. It was previously shown in Chapter 3 that old *dLRRK*$^{-}$ LOF flies have severe visual defects, thus inhibiting the kinase function of *dLRRK* through BMPPB-32 may cause a similar, albeit less severe, phenotype.

Elevated kinase activity is a consistent feature of *LRRK2-G2019S* in biochemical assays and in animal models, reviewed in Greggio and Cookson (2009). Inhibition of LRRK2 kinase activity has been reported to protect against LRRK2-induced toxicity in both *in vitro* and *in vivo* studies (Lee et al., 2010a). Thus, it is unsurprising that a plethora of potential LRRK2 kinase inhibitors have been previously investigated (Covy and Giasson, 2009, Lee et al., 2010a, Deng et al., 2011, Liu et al., 2011b, Ramsden et al., 2011, Kavanagh et al., 2013). Unfortunately, only a handful of these kinase inhibitors are selective for LRRK2. For example, LRRK2-IN-1 has been found

to interact with only 12 other kinases in an analysis that included more than 470 kinases (Deng et al., 2011, Kavanagh et al., 2013). However, when this compound was given to *dLRRK*$^{-}$ null flies, in which the homologous *dLRRK* gene had been knocked-out, a severe change in the visual response was observed, suggesting that LRRK2-IN-1 binds to other kinases (Afsari et al., 2014). A second inhibitor, CZC25146 was found to have only 5 off-target enzymes when it was profiled against 185 kinases (Ramsden et al., 2011). The physiochemical and pharmacokinetic properties of LRRK2-IN-1 and CZC25146 have both been investigated in mice, but unfortunately neither were detected to cross the BBB to a substantial extent, limiting their use in both murine PD models and eventual translation to human clinical trials (Kavanagh et al., 2013). A previously reported inhibitor of anaplastic lymphoma kinase, namely TAE684, has also been shown to be a potent inhibitor of LRRK2 (Zhang et al., 2012). Although TAE684 demonstrated a favourable pharmacokinetic profile in mice, it was found to be considerably less selective than LRRK2-IN-1 and CZC25146 (Zhang et al., 2012). As previously mentioned in Chapter 1, recent clinical trials with a highly potent and selective LRRK2 kinase inhibitor produced by Genentech Inc. had to be stopped due to adverse side effects on kidney and lung function (Fuji et al., 2015). Thus, none of these currently available LRRK2 kinase inhibitors are viable for the treatment of PD.

Initial studies with BMPPB-32 have shown that it has no major off-target effects in the *hLRRK2-G2019S* fly model, and it has a clean kinase selectivity profile in mammalian cells (Afsari et al., 2014). Taken together, the data presented in this and previous studies suggest that BMPPB-32 could be a promising compound for disease-modifying therapy in LRRK2-related PD (Afsari et al., 2014, West et al., 2015b), either given independently or perhaps in combination with mitochondrial rescue agents such as UDCA. However, further studies will be required to determine the physiochemical and pharmacokinetic properties of BMPBB-32, as well as additional studies to assess any off-target effects.

## 4.5 Conclusions

In this chapter, we provide exciting *in vivo* evidence to show that a class of mitochondrial rescue agents can rescue visual dysfunction in the *hLRRK2-G2019S* fly model. Unfortunately, we were unable to provide sufficient evidence to suggest that

UDCA and UCA mediate their beneficial effects through increasing the phosphorylation of $Akt^{Ser473}$, but preliminary experiments indicate a role for Akt in the visual response and these can hopefully be built upon in the future. We believe that UDCA and/or UCA are promising candidates for future PD-related drug trials. We also provide evidence to suggest a neuroprotective effect of parkin in LRRK2-induced PD, but again further studies are required to confirm this. Finally, we show that a novel LRRK2-specific kinase inhibitor can rescue *hLRRK2-G2019S* induced visual dysfunction after being administrated to adult flies and further studies profiling its pharmacokinetics and pharmacodynamics should be considered.

# 5 A Possible Interaction Between *dLRRK* and the Eye Pigment Pathways

## 5.1 Introduction

In order to ensure data compatibility between genotypes, transgenic and control flies with matching eye colour should be utilised. In this chapter we considered transforming all fly lines so that they had uniform white eyes to improve the signal/noise ratio, as flies with white eyes produce larger ERG responses due to the absence of screening pigment (Stark, 1973). In doing this, we found some combinations of eye pigment genes and *dLRRK* that were lethal. This chapter explores the basis of the interaction between *dLRRK* and eye pigment genes, starting with an overview of fly eye pigmentation.

### 5.1.1 *Drosophila* eye pigment pathways

The *Drosophila* eye contains pigment cells that provide a layer of optical insulation from the exterior of the eye to the basal lamina (Summers et al., 1982). This insulating layer ensures that light entering through the lens remains isolated to one ommatidium thus preventing lateral transfer of light rays, which enhances contrast sensitivity and visual acuity (Tomlinson, 2012). The pigments that perform this function are known as screening pigments and the colour of a fly's eye is determined by the nature of the screening pigments that they contain (Summers et al., 1982). In *Drosophila* there are two key classes of screening pigment, the brown ommochromes and the red drosopterins (Summers et al., 1982). Although the biosynthetic pathways of the ommochromes and drosopterins are distinct and do not share enzymes, there is evidence to suggest developmental and biochemical interdependence between the two, such that variations in the level of one of the pigments affects the level of the other (Ryall and Howells, 1974, Reaume et al., 1991). As WT flies produce both ommochromes and drosopterins they have a dull red eye colour.

There are two types of pigment cell in the fly visual system, the primary and secondary pigment cells (Summers et al., 1982). The primary pigment cells surround the dioptric apparatus, whilst the secondary pigment cells surround the retinula cells

and the primary pigment cells. Ommochromes are present in both primary and secondary pigment cells and are usually found within distinct membrane-bound organelles of 0.2–1.0 μM in width, known as the pigment granules (Summers et al., 1982). Shoup (1966) referred to these ommochrome-containing granules as Type I granules. The drosopterins are thought to only occur in the secondary pigment cells but are also found in membrane-bound pigment granules, referred to as Type II granules by Shoup (1966).

#### 5.1.1.1 The kynurenine pathway

The ommochromes include the brown eye pigments xanthommatin and it's reduced form dihydroxanthommatin, thus eyes expressing only these pigments are brown in colour. Xanthommatin is biosynthetically derived from tryptophan via a series of oxidation reactions involving the intermediates formylkynurenine, kynurenine and 3-hydroxykynurenine (3-HK; Figure 5.1A). In *Drosophila,* the four eye colour genes, *white* (*w*), *scarlet* (*st*), *vermilion* (*v*) and *cinnabar* (*cn*) are crucial for the production of xanthommatin because null mutations at these loci abolish the production of brown pigment entirely (Searles and Voelker, 1986, Warren et al., 1996, Mackenzie et al., 1999). The *v* gene encodes tryptophan oxygenase, the first enzyme in the kynurenine pathway, which converts tryptophan to formylkynurenine (Searles and Voelker, 1986). The *cn* gene encodes the third enzyme in the pathway, kynurenine-3-hydroxylase, which is responsible for converting kynurenine to 3-HK (Warren et al., 1996). Flies that are null mutants of *v* or *cn* are unable to synthesise xanthommatin, thus they have eyes that are a much brighter red than WT flies. Both *st* and *w* encode products that are involved in the uptake and storage of xanthommatin precursors (Howells and Ryall, 1975, Sullivan and Sullivan, 1975). Both of these genes have been cloned and shown to belong to the ATP-binding cassette (ABC) super-family of membrane transporters (Mount, 1987, Higgins, 1992, Ewart and Howells, 1998). Mackenzie et al. (2000) provided evidence that the gene products of *w* and *st* are localised at the membrane of the pigment granules, suggesting that the white/scarlet complex is involved in the transportation of 3-HK from the cytoplasm into the pigment granules. Once in the pigment granule, phenoxazinone synthetase converts 3-HK to xanthommatin (Phillips et al., 1970, Summers et al., 1982). The role of the

kynurenine pathway is conserved from flies to humans, with the pathways both playing a central role in the formation of UV filters in the lens (Roberts, 2001).

### 5.1.1.2 The pteridine pathway

The drosopterin (or pteridine) pathway produces the drosopterins, which include the red-orange pigments neodrosopterin, drosopterin, isodrosopterin, aurodrosopterin, and fraction e, the yellow pigments sepiapterin and deoxysepiapterin, and UV pigments (Summers et al., 1982, Kim et al., 2013). Eyes expressing only drosopterins are bright red in colour. The drosopterins are composed of a pteridine moiety and a pyrimidodiazepine (PDA; 6-acetyle-2-amino-3,7,8,9-tetrahydro-4*H*-pyrimido[4,5-*b*][1,4]diazepin-4-one) moiety in a pentacyclic ring system (Yim et al., 1993, Kim et al., 2013). They were first isolated in 1940 and the five red-orange pigments have since been separated by cellulose thin layer chromatography (Ferre et al., 1986). Drosopterin and isodrosopterin are considered as the major pigments, whilst aurodrosopterin and neodrosopterin are the minor pigments, such that aurodrosopertin constitutes <10% of total drosopterins found in WT flies (Yim et al., 1993). There is still little known about neodrosopterin and fraction e.

In contrast to the well-characterised biosynthetic pathway of the ommochromes, the biosynthetic pathway of drosopterins has not yet been fully established. The drosopterins are biosynthetically derived from GTP via a series of enzymatic and non-enzymatic reactions (Kim et al., 2013) (Figure 5.1B). The initial and rate-limiting step of the biosynthesis of drosopterins involves the conversion of GTP to 7,8-dihydroneopterin triphosphate ($H_2$-NTP) with the release of formic acid by GTP cyclohydrolase I (GTPCH I) (Mackay and O'Donnell, 1983). *Drosophila* GTPCH I, which is encoded by the *punch* gene, shares approximately 80% similarity with the human GTPCH I protein (McLean et al., 1993). $H_2$-NTP is converted into 6-pyruvoyltetrahydropterin (6-PTP) by 6-PTP synthase, which is encoded by the *purple* gene (Krivi and Brown, 1979, Park et al., 1990). 6-PTP is then converted into PDA by PDA synthase, which is encoded by the *sepia* gene (Kim et al., 2006). Drosopterin and isodrosopterin are produced non-enzymatically with the one-to-one condensation of 7,8-dihydropterin with PDA under acidic conditions (Kim et al., 2013).

Aurodrosopterin is also produced non-enzymatically but with the one-to-one condensation of 7,8-dihydrolumazine with PDA, again under acidic conditions (Yim et al., 1993). The gene products of *w* and *brown* (*bw*) are thought to form an ABC transporter on the membrane of the Type II granules to transport drosopterin precursors into these pigment granules (Dreesen et al., 1988, Borycz et al., 2008).

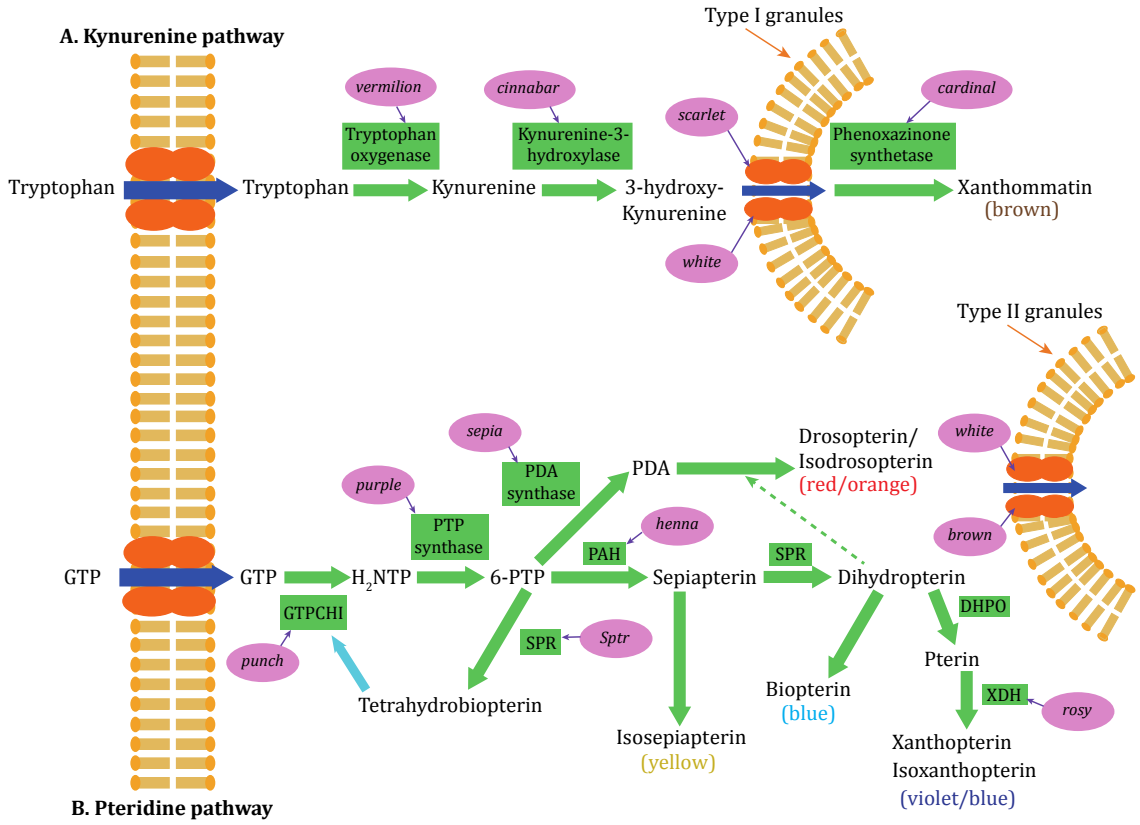


**Figure 5.1 Schematic of the eye pigment pathways in *Drosophila***

(A) The kynurenine pathway degrades tryptophan to the brown pigment xanthommatin. (B) The pteridine pathway utilises GTP to generate the red-orange drosopterins. The green boxes indicate the enzymes required for each step and the purple boxes indicate the gene that encodes the key enzyme, or transporter, in *Drosophila*. Abbreviations: GTP cyclohydrolase I (GTPCH I); dihydroneopterin triphosphate ($H_2$-NTP); 6-pyruvoyl-tetrahydropterin (PTP); pyrimidodiazepine (PDA); phenylalanine hydroxylase/ tetrahydropterin oxidase (PAH); Sepiapterin reductase (SPR); dihydropterin oxidase (DHPO); xanthine dehydrogenase (XDH). Adapted with permission from Croucher et al. (2013).

## 5.2 Aims

The aim of this chapter was to determine the nature of the interaction between the eye pigment pathways and *dLRRK*. This was achieved through using both genetic and physiological approaches in the complementary *dLRRK*$^{-}$ LOF and *hLRRK2-G2019S* GOF models. The specific aims of this chapter are outlined below.

1. Determine if *dLRRK* interacts with both the kynurenine and pteridine pathways through combining the *dLRRK*$^{-}$ LOF mutation with mutations in either the kynurenine or pteridine pathways.
2. Establish whether overexpression of genes in the kynurenine or pteridine pathways in the DA neurons or glial cells can rescue the visual dysfunction of *dLRRK*$^{-}$ LOF flies.
3. Assess the effect of expressing the GOF *hLRRK2-G2019S* mutation in the DA neurons of a white-eyed mutant background.

## 5.3 Results

### 5.3.1 Mutations in the kynurenine or pteridine pathways are synthetically lethal with LOF mutations in *dLRRK*

To generate flies with white eyes, mutations are required in genes from both the kynurenine and pteridine pathways. The *cn*$^{1}$*bw*$^{1}$ fly stock (Bloomington stock 264) has a null mutation in *cn*, the gene that encodes kynurenine-3-hydroxylase in the kynurenine pathway, and a null mutation in *bw*, the gene that is involved in transporting the pigment precursors into the pigment granules in the pteridine pathway. Flies that are homozygous for the *cn*$^{1}$*bw*$^{1}$ mutations are viable and have white eyes, whereas heterozygotes (*cn*$^{1}$*bw*$^{1}$/+) have red eyes, allowing easy identification of *cn*$^{1}$*bw*$^{1}$ homozygotes.

Here, *cn*$^{1}$*bw*$^{1}$ flies were crossed with *dLRRK*$^{e03680}$ flies with the aim of selecting flies that were homozygous for both the *cn*$^{1}$*bw*$^{1}$ mutation on the second chromosome and homozygous for the *dLRRK*$^{e03680}$ mutation on the third chromosome. Figure 5.2 shows a diagrammatic representation of the crossing scheme that was used and the possible progeny of this cross. The presence of the balancer chromosomes *CyO*, which gives

the fly curly wings, and TM6B, the humeral marker, are shown. The expected eye colour (either red or white) of each genotype is also indicated. Although *cn*$^{1}$*bw*$^{1}$ homozygotes are viable and *dLRRK*$^{e03680}$ homozygotes are also viable, no progeny were found in the current cross that were homozygous for both of these mutations in combination (*cn*$^{1}$*bw*$^{1}$/*cn*$^{1}$*bw*$^{1}$*; dLRRK*$^{-}$/*dLRRK*$^{-}$; indicated with a blue outline in Figure 5.2). In addition, no progeny were found that were *cn*$^{1}$*bw*$^{1}$ heterozygous and *dLRRK*$^{-}$ homozygous (*cn*$^{1}$*bw*$^{1}$*/CyO; dLRRK*$^{-}$/*dLRRK*$^{-}$). This cross was repeated three times to ensure that no errors had been made during the crossing scheme, but each time the result was the same. This was unexpected but it highlighted a possible interaction between *dLRRK* and genes in the eye pigment pathways.

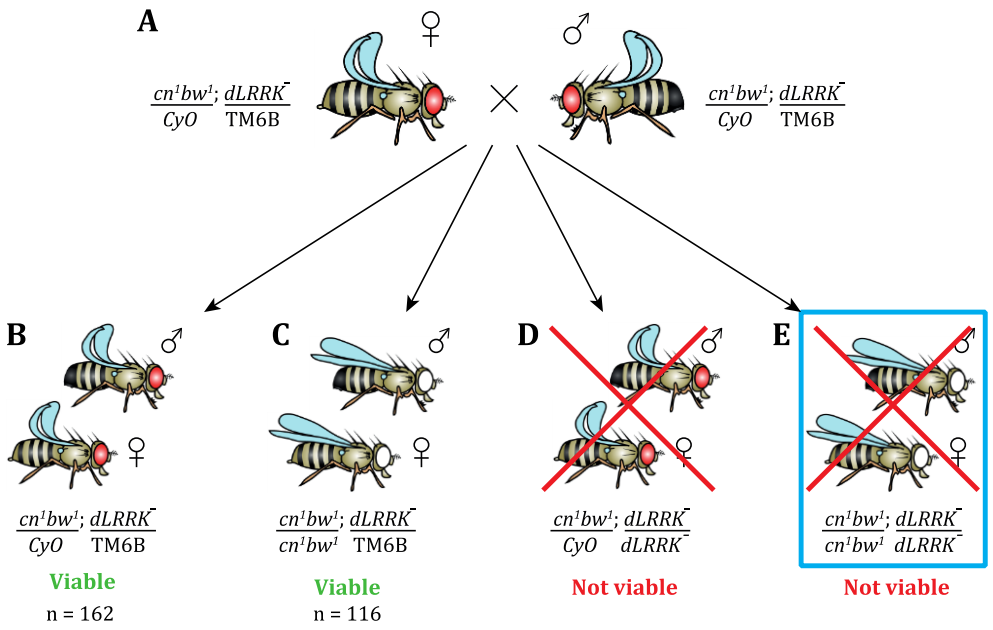


**Figure 5.2 Homozygous or heterozygous *cn¹bw¹* mutations are synthetically lethal with homozygous *dLRRK⁻* LOF mutations**

(A) An experimental cross with adult virgin female and male flies with the genotype *cn¹bw¹*/*CyO*; *dLRRK⁻*/TM6B was set up. (B-E) The possible progeny of this cross are shown. The expected eye colour of each genotype (red for the heterozygous *cn¹bw¹* mutation; white for the homozygous *cn¹bw¹* mutation) is indicated. The phenotypes produced by the presence of the *CyO* (curly wings) and TM6B (humeral marker) balancer chromosomes are also shown. The blue box around (E) indicates that this was the desired genotype from this cross. Flies that were heterozygous for the *dLRRK⁻* mutation were found whether in combination with the heterozygous *cn¹bw¹* mutation (B) or the homozygous *cn¹bw¹* mutation (C). Flies that were homozygous for the *dLRRK⁻* mutation were not found when in combination with the heterozygous *cn¹bw¹* mutation (D) or the homozygous *cn¹bw¹* mutation (E). n numbers of genotypes (B) and (C) are shown.

To determine if *dLRRK* interacts with genes from both of the pigment pathways, *dLRRK*$^{e03680}$ flies were crossed with flies with null mutations in either the kynurenine pathway (*cn*$^{3}$) or the pteridine pathway (*bw*$^{1}$). Homozygote *cn*$^{3}$ or *bw*$^{1}$ flies are viable and have red eyes. Interestingly, in all of these crosses no progeny were collected that were *dLRRK*$^{-}$ homozygous and homozygous for the mutation in the corresponding eye pigment gene (Figure 5.3; *cn*$^{3}$/*cn*$^{3}$; *dLRRK*$^{-}$/*dLRRK*$^{-}$ or *bw*$^{1}$/*bw*$^{1}$; *dLRRK*$^{-}$/*dLRRK*$^{-}$). Flies that were *dLRRK*$^{-}$ homozygous and heterozygous for the corresponding eye pigment gene were also not found (Figure 5.3; *cn*$^{3}$/*CyO*; *dLRRK*$^{-}$/*dLRRK*$^{-}$ or *bw*$^{1}$/*CyO*; *dLRRK*$^{-}$/*dLRRK*$^{-}$). Taken together, the results of these crosses suggest an interaction between *dLRRK* and components of both the kynurenine and pteridine pathways.

**Figure 5.3 Homozygous or heterozygous *cn*$^{3}$ or *bw*$^{1}$ mutations are synthetically lethal with homozygous *dLRRK*$^{-}$ LOF mutations**

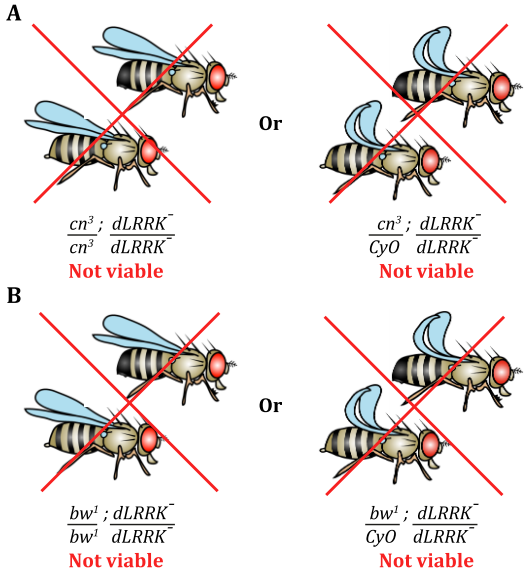


Progeny from experimental crosses that were homozygous or heterozygous for the mutations (A) *cn*$^{3}$ or (B) *bw*$^{1}$ were not viable in combination with the homozygous *dLRRK*$^{-}$ LOF mutation. Progeny that were heterozygous or homozygous for any of these mutations in combination with the heterozygous *dLRRK*$^{-}$ LOF mutation were viable. For each cross the total number of progeny collected was n≥212.

### 5.3.2 *cn¹bw¹* heterozygous flies are viable in a homozygous *dLRRK⁻* LOF background in the absence of the *CyO* balancer

Many balancer chromosomes carry other genetic elements such as dominant or recessive visible markers, which can be useful when identifying which progeny inherit the balancer during a crossing scheme, or to score for recombination events (Greenspan, 2004). For example, the *CyO* balancers carry *Cy* and the recessives *dumpy* (*dp$^{lv1}$*), *purple* (*pr¹*) and *cinnabar* (*cn²*) (Greenspan, 2004). In the previous crossing schemes (Figure 5.2 and Figure 5.3), the eye pigment mutations were balanced with *CyO*. Thus it is possible that flies thought to have been heterozygous for the *cn* mutation were actually homozygous due to the presence of the second *cn²* mutation carried on the *CyO* balancer. Therefore heterozygous *cn¹bw¹* mutant flies without the *CyO* balancer in the background were crossed into the *dLRRK⁻* LOF homozygous background (*cn¹bw¹*/+; *dLRRK⁻*/*dLRRK⁻*). These flies were viable, suggesting that either the *cn* mutation or another mutation on the *CyO* balancer was contributing to the lethality of the previous heterozygous stock. ERGs were recorded from these flies at 3 and 21 DPE. The 3 and 21 DPE ERG responses were also repeated for WT (*CS*/*w$^{1118}$*) and homozygous *dLRRK$^{e03680}$* (*dLRRK⁻*/*dLRRK⁻*) flies to ensure that all ERGs were recorded at a similar time for all genotypes utilised in this chapter.

Figure 5.4 shows representative ERG traces from WT, *dLRRK⁻*/*dLRRK⁻* and *cn¹bw¹*/+; *dLRRK⁻*/*dLRRK⁻* flies at 3 and 21 DPE. As previously observed in Chapter 3, all components of the WT ERG response were maintained at 21 DPE whereas the off-transient component of the *dLRRK⁻* LOF ERG was severely reduced by 21 DPE. As expected, the off-transient component of the *cn¹bw¹*/+; *dLRRK⁻*/*dLRRK⁻* ERG was also dramatically reduced from that recorded at 3 DPE. Both the on-transient and photoreceptor responses of the *cn¹bw¹*/+; *dLRRK⁻*/*dLRRK⁻* ERG were also reduced by 21 DPE, but as with the *dLRRK⁻*/*dLRRK⁻* flies, the loss of the off-transient was the most severe.

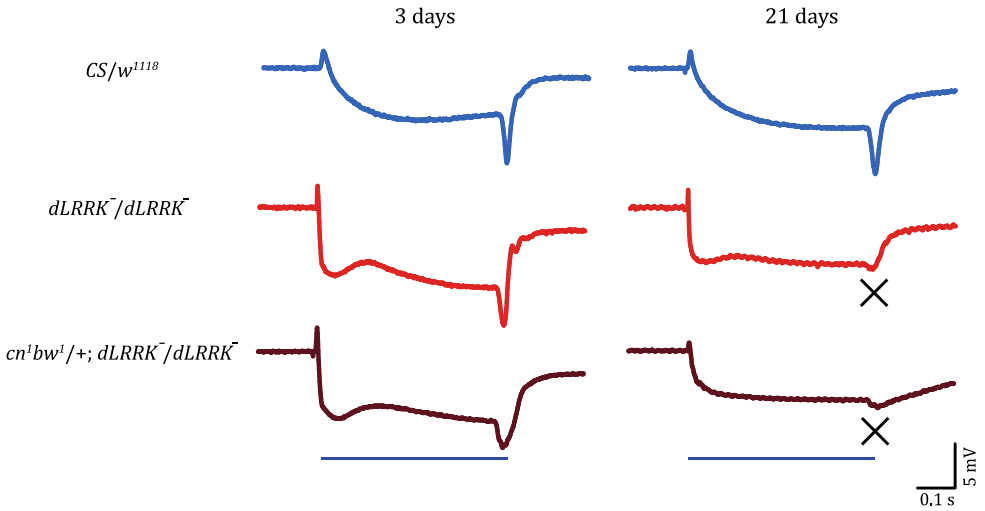


**Figure 5.4 *dLRRK*⁻ LOF flies with heterozygous *cn¹bw¹* mutations show the characteristic age-related, progressive loss of visual function**

Representative ERG traces from 3 (left) and 21 (right) DPE WT (*CS*/*w*$^{1118}$; blue), *dLRRK*⁻ LOF mutants (*dLRRK*⁻/*dLRRK*⁻; bright red), and flies heterozygous for the *cn¹bw¹* mutation in a *dLRRK*⁻ LOF background (*cn¹bw¹*/+; *dLRRK*⁻/*dLRRK*⁻; dark red). ERGs are recorded in response to 0.5 second blue light pulses. The blue line below the bottom ERG traces represents the duration of the light pulse. The on-transient, photoreceptor response, and off-transient were all maintained at 3 and 21 DPE in WT flies, whereas in both *dLRRK*⁻/*dLRRK*⁻ and *cn¹bw¹*/+; *dLRRK*⁻/*dLRRK*⁻ mutant flies all components of the ERG were reduced by 21 DPE. The loss of the off-transient component at 21 DPE was the most striking (indicated by the black crosses). Scale bars for time (seconds) and potential (mV) are shown. Each trace is the average of the fly's response to at least three flashes of light.

In order to determine if any of the ERG components were significantly reduced from 3 to 21 DPE, the individual ERG components were quantified separately for each genotype (Figure 5.5). As previously described, there were no significant differences between the 3 and 21 DPE ERG components recorded from WT flies, whereas all ERG components recorded from *dLRRK*⁻ LOF flies were significantly reduced by 21 DPE (all $p<0.001$). Similarly, all components of the *cn¹bw¹*/+; *dLRRK*⁻/*dLRRK*⁻ ERG response were significantly reduced by 21 DPE (peak-to-peak, on-transient and off-transient: $p<0.001$; photoreceptor response: $p<0.05$).

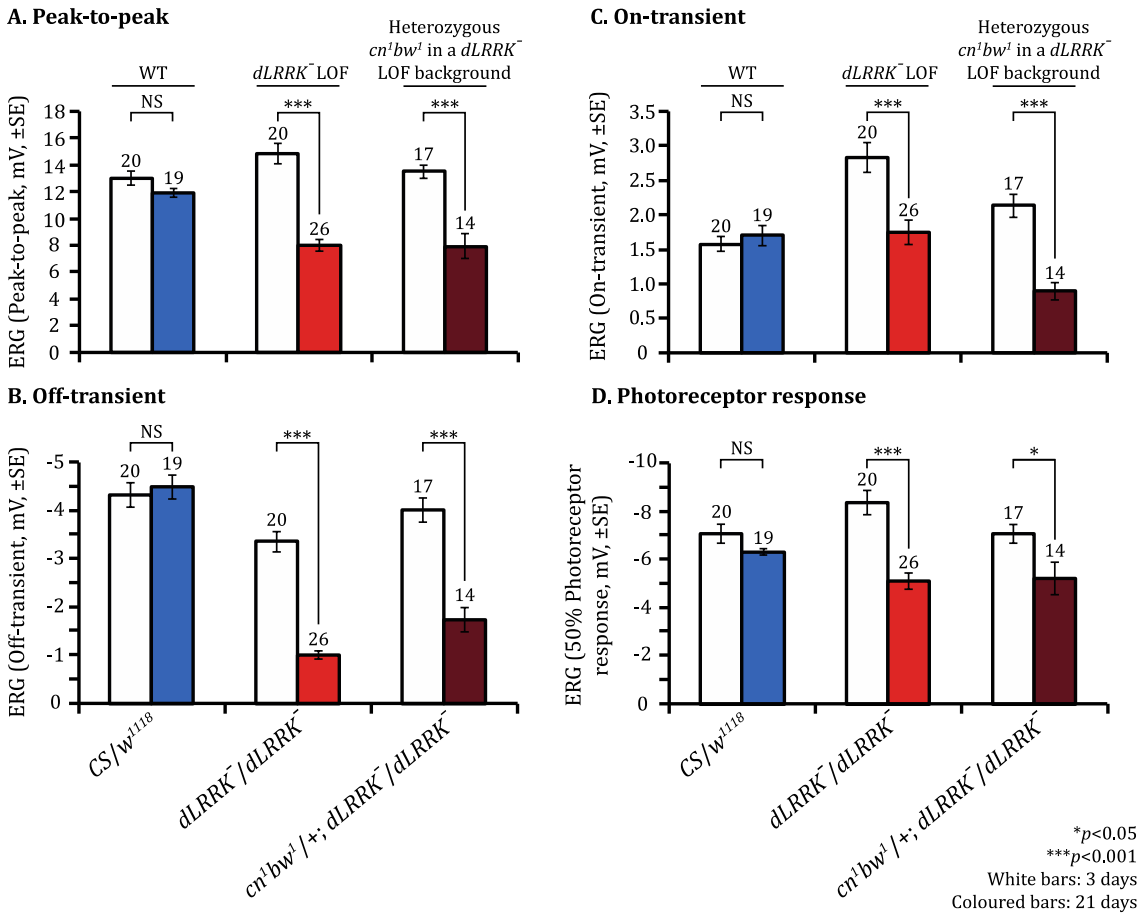


**Figure 5.5 Quantification of the individual ERG components showing the progressive loss of visual function in *dLRRK⁻* LOF flies with heterozygous *cn¹bw¹* mutations**

The ERG peak-to-peak response (A), on-transient (B), off-transient (C), and photoreceptor response (D) were quantified for WT (*CS/w¹¹¹⁸*), *dLRRK⁻* LOF mutants (*dLRRK⁻/dLRRK⁻*), and flies heterozygous for the *cn¹bw¹* mutation in a *dLRRK⁻* LOF background (*cn¹bw¹/+; dLRRK⁻/dLRRK⁻*) at 3 (white bars) and 21 (coloured bars) DPE. (A-D) All ERG components were significantly reduced from 3 to 21 DPE in the *dLRRK⁻* LOF mutants and *cn¹bw¹/+; dLRRK⁻/dLRRK⁻* flies. All ERG components were maintained at 21 DPE in WT flies. All statistics are Student's t-tests: ***$p<0.001$, *$p<0.05$, NS, no significant difference, $p>0.05$. Data presented are mean ± SEM bars; n numbers are displayed above the bars.

### 5.3.3 DA or glial expression of *brown* or *cinnabar* rescues the visual dysfunction of *dLRRK*¯ LOF flies

If *dLRRK* does operate within the same pathway as c*innabar* or *brown,* then it is possible that expression of these genes in a *dLRRK*¯ LOF background could rescue the loss of synaptic signalling that was previously observed in *dLRRK*¯/*dLRRK*¯ flies (see Chapter 3). To determine if these transgenes were able to improve the visual responses of *dLRRK*¯ LOF flies, the UAS/GAL4 system was utilised to express c*innabar* or *brown* in the DA neurons (*TH*-GAL4) or in the glial cells (*Repo*-GAL4) in a *dLRRK*¯ LOF background, and ERGs were recorded at 3 and 21 DPE.

A fly line expressing the *brown* transgene was a kind gift from Stephan Schneuwly. As we were unable to obtain a UAS-*cinnabar* fly stock at the time of this study, a fly line expressing the *cinnabar* transgene was generated (see Chapter 2, section 2.4.2). *cinnabar* cDNA was sub-cloned into the pUAST attB vector using standard sub-cloning techniques, before being microinjected into the phiC31 *vas-int; attp'-51C* fly line (Bloomington Stock 24482) at the University of Cambridge, Department of Genetics, Fly Facility. The UAS-*brown* and UAS-*cinnabar* transgenes were crossed separately into the *dLRRK*¯ LOF background and their expression was driven with *TH*-GAL4 or *Repo*-GAL4.

Figure 5.6 shows representative ERG traces from WT, *dLRRK*¯/*dLRRK*¯ and flies expressing *brown* or *cinnabar* in the DA neurons or the glial cells in a *dLRRK*¯ LOF background at 3 and 21 DPE. All components of the ERG trace were evident with DA or glial expression of *brown* or *cinnabar* at 3 and 21 DPE. However, the off-transient components of flies with glial expression of *brown* or *cinnabar,* or DA expression of *cinnabar,* were reduced at 21 DPE compared to those recorded at 3 DPE. This suggests that *brown* and *cinnabar* may partially rescue the visual function of *dLRRK*¯ LOF flies.

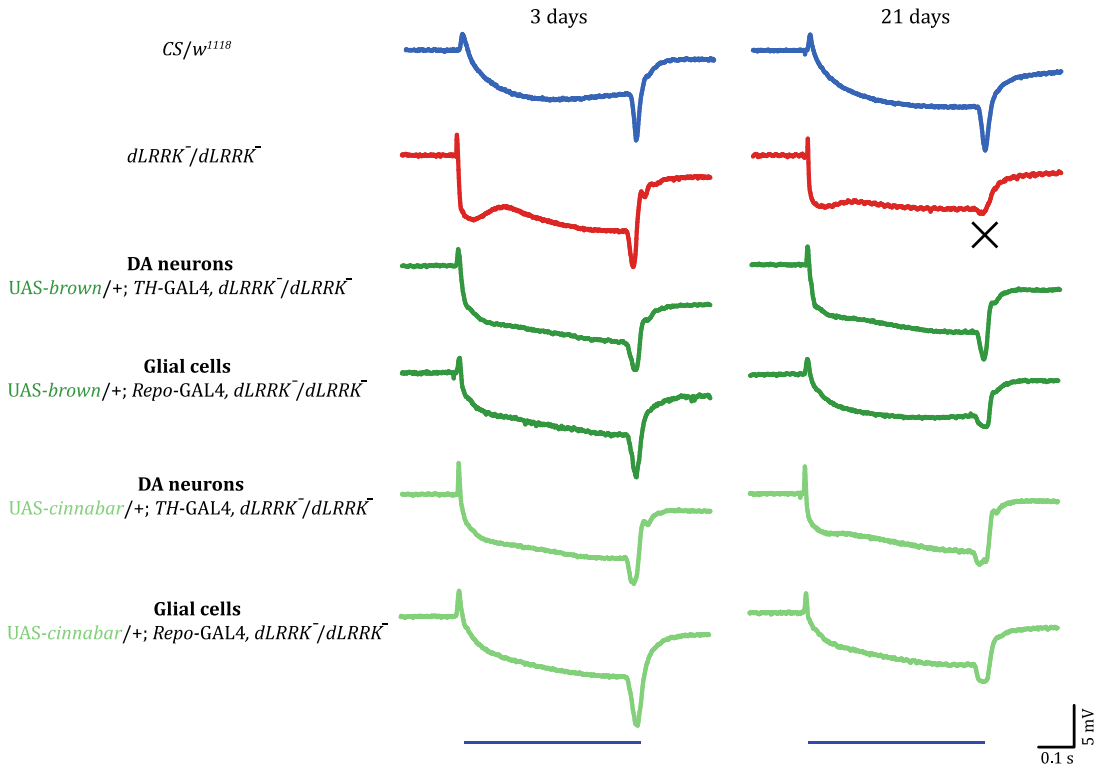


**Figure 5.6 DA or glial expression of *brown* or *cinnabar* in a *dLRRK*⁻ LOF background, completely or partially rescues the loss of visual function**

Representative ERG traces from 3 (left) and 21 (right) DPE WT flies (*CS*/*w*$^{1118}$; blue), *dLRRK*⁻ LOF mutants (*dLRRK*⁻/*dLRRK*⁻; bright red), and flies expressing *brown* or *cinnabar* specifically in the DA neurons (*TH*-GAL4) or glial cells (*Repo*-GAL4) in a *dLRRK*⁻ LOF background (shades of green). ERGs are recorded in response to 0.5 second blue light pulses. The blue lines drawn below the bottom ERG traces represent the duration of the light pulse. As previously described, all ERG components were maintained at 21 DPE in WT flies, but all ERG components were significantly reduced in *dLRRK*⁻ LOF mutants. All components of the ERG response were also maintained with DA or glial expression of *brown* or *cinnabar*, however the off-transient component was still reduced at 21 DPE in flies with glial expression of *brown* or *cinnabar* or DA expression of *cinnabar.* Scale bars for time (seconds) and potential (mV) are shown. Each trace is the average of the fly's response to at least three flashes of light.

In order to determine if any of the ERG components were significantly reduced from 3 to 21 DPE, the individual ERG components were quantified separately for each genotype (Figure 5.7A-D). DA expression of *brown* in a *dLRRK*$^{-}$ LOF background completely rescued the loss of synaptic signalling, as there were no significant differences between the 3 and 21 DPE ERG responses recorded from these flies. However, when *brown* was expressed in the glial cells, only the on-transient component was maintained at 21 DPE; all other components showed a significant reduction in size (peak-to-peak and off-transient: $p<0.001$; photoreceptor response: $p<0.05$). Neither the DA nor glial expression of *cinnabar* was able to completely rescue the loss of synaptic signalling, as the peak-to-peak (both $p<0.05$), on-transient (both $p<0.01$) and off-transient responses (DA expression of *cinnabar*: $p<0.01$; glial expression of *cinnabar*: $p<0.001$), were all significantly reduced by 21 DPE. However, the photoreceptor responses of flies with DA or glial expression of *cinnabar* was maintained at 21 DPE.

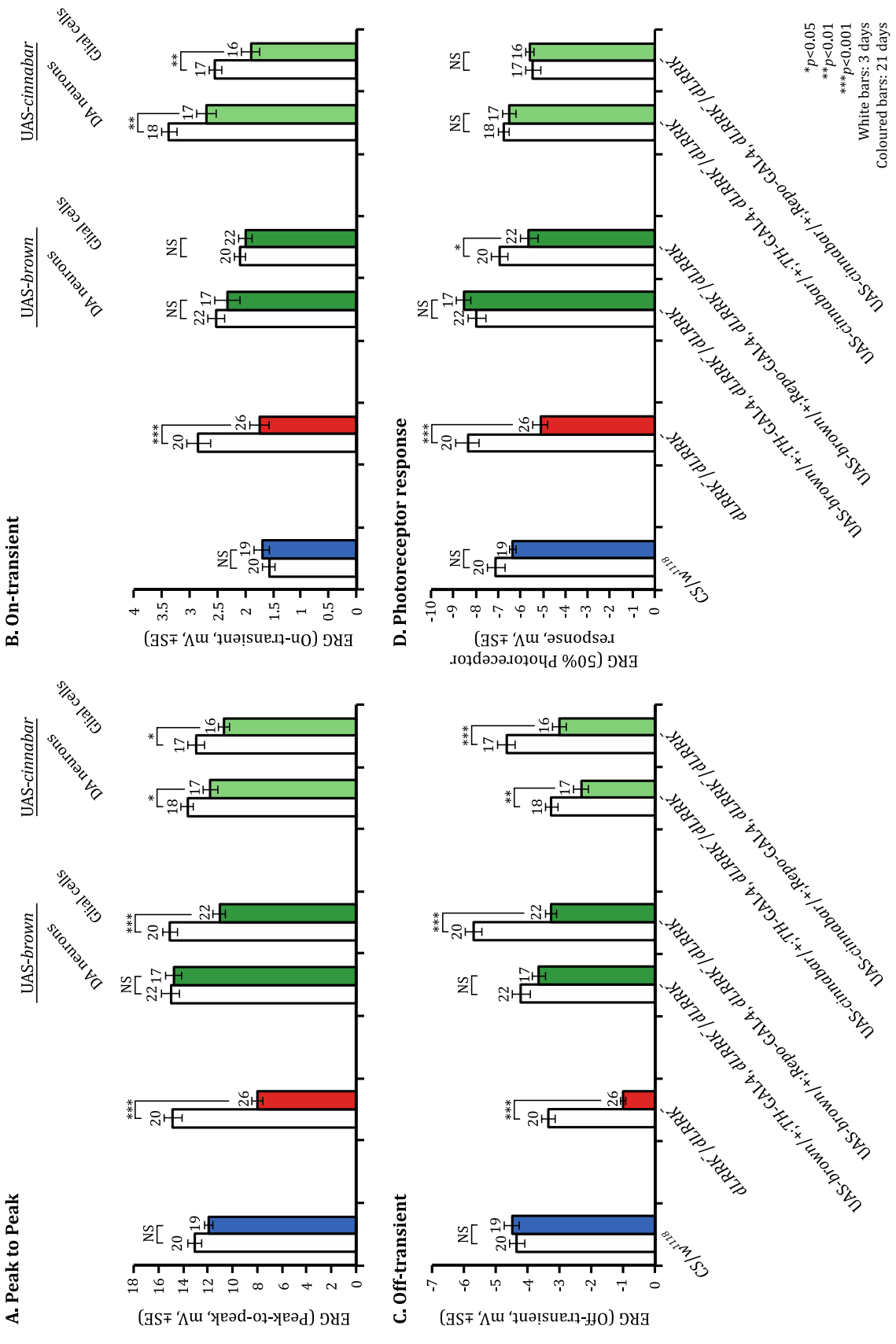


**Figure 5.7** Figure legend overleaf.

**Figure 5.7 Quantification of the individual ERG components showing the complete or partial rescue of visual function with DA or glial expression of *brown* or *cinnabar* in a *dLRRK*⁻ LOF background**

The ERG peak-to-peak response (A), on-transient (B), off-transient (C) and photoreceptor response (D) were quantified for WT flies (*CS*/*w*$^{1118}$), *dLRRK*⁻ LOF mutants (*dLRRK*⁻/*dLRRK*⁻), and flies expressing *brown* or *cinnabar* specifically in the DA neurons (*TH*-GAL4) or glial cells (*Repo*-GAL4) in a *dLRRK*⁻ LOF background, at 3 (white bars) and 21 (coloured bars) DPE. (A-D) Expressing *brown* in the DA neurons of *dLRRK*⁻ LOF flies, rescued the loss of all ERG components at 21 DPE. Some, but not all, of the ERG components were significantly reduced at 21 DPE with glial expression of *brown* (peak-to-peak, off-transient and photoreceptor response), or DA or glial expression of *cinnabar* (both peak-to-peak, on-transient and off-transient). All statistics are Student's t-tests: ***$p$<0.001, **$p$<0.01, *$p$<0.05, NS, no significant difference, $p$>0.05. Data presented are mean ± SEM bars; n numbers are displayed above the bars.

To compare the visual responses of flies expressing *brown* or *cinnabar* in the DA neurons or glial cells in a *dLRRK*⁻ LOF background to the visual responses of WT and *dLRRK*⁻ LOF flies, the average 21 DPE peak-to-peak and off-transient responses were plotted as a percentage of the 3 DPE responses for each genotype (Figure 5.8). Both the peak-to-peak and off-transient responses of *dLRRK*⁻ LOF flies were significantly lower than WT flies and all rescue genotypes (all $p$<0.001). Neither the peak-to-peak nor off-transient responses were significantly different between WT flies and flies with DA expression of *brown* in a *dLRRK*⁻ LOF background. In contrast, both the peak-to-peak and off-transient responses of flies with glial expression of *brown* were significantly reduced compared with WT flies ($p$<0.01 and $p$<0.001, respectively). In addition, the peak-to-peak and off-transient responses of flies with glial expression of *brown* were significantly lower than those recorded from flies with DA expression of *brown* (both $p$<0.001). The peak-to-peak responses of flies with DA or glial expression of *cinnabar* were not significantly different from WT flies, but the off-transient responses of these genotypes were both significantly reduced compared with WT flies (both $p$<0.001). There were no significant differences between flies with DA or glial expression of *cinnabar*. These data suggest that when *brown* expression is driven in the DA neurons, the loss of synaptic signalling caused by the loss of dLRRK function is rescued. Glial expression of *brown* or *cinnabar* or DA

expression of *cinnabar* appeared to offer a partial rescue of visual function. However, the visual response of flies with DA or glial expression of *cinnabar* or *brown* in a WT background have not yet been recorded, thus we do not know if expression of these transgenes affects the WT visual response at this stage.

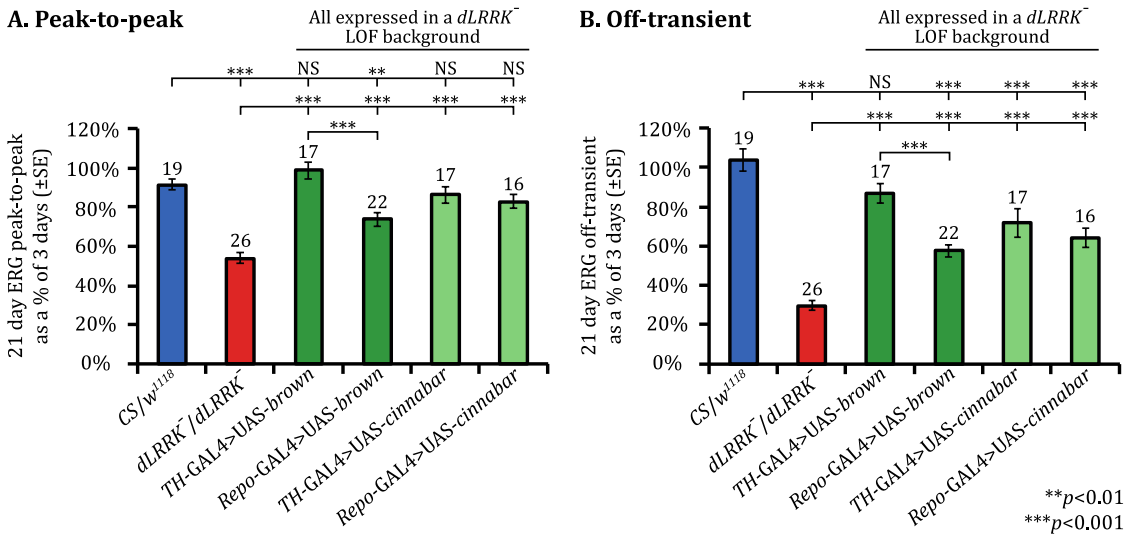


**Figure 5.8 The visual responses of flies with DA or glial expression of *brown* or *cinnabar* in a *dLRRK*⁻ LOF background are significantly better than those of *dLRRK*⁻ LOF flies**

The 21 DPE peak-to-peak (A) and off-transient (B) responses as a percentage of the 3 DPE responses for WT flies (*CS*/*w*$^{1118}$; blue), *dLRRK*⁻ LOF mutants (*dLRRK*⁻/*dLRRK*⁻; red), and flies expressing *brown* (dark green) or *cinnabar* (light green) specifically in the DA neurons (*TH*-GAL4) or glial cells (*Repo*-GAL4) in a *dLRRK*⁻ LOF background. (A-B) The 21 DPE peak-to-peak and off-transient responses of 21 DPE flies with DA expression of *brown* were not significantly different from WT flies, whereas both were significantly lower in 21 DPE flies with glial expression of *brown* compared with WT flies or compared with flies with DA expression of *brown.* Although the 21 DPE peak-to-peak responses of flies with DA or glial expression of *cinnabar* did not differ significantly from WT flies, the off-transient responses of both of these genotypes were significantly lower than WT flies. The peak-to-peak and off-transient responses of 21 DPE *dLRRK*⁻ LOF flies were significantly lower than all other genotypes. Comparisons to WT are ANOVA with post-hoc Dunnett's comparison; comparisons between other genotypes are all ANOVA with post-hoc Bonferroni correction: ***$p$<0.001, **$p$<0.01, NS, no significant difference, $p$>0.05. Data presented are mean ± SEM bars; n numbers are displayed above the bars.

### 5.3.4 Mutations in the eye pigment genes prevents the visual neurodegeneration caused by DA expression of *hLRRK2-G2019S*

To determine if flies with DA expression of the GOF *hLRRK2-G2019S* mutation were viable in a $cn^1bw^1$ homozygous mutant background, a cross was set up to generate flies with the genotype, $cn^1bw^1/cn^1bw^1$; *TH/G2019S.* Unlike flies with LOF of *dLRRK,* flies expressing the GOF *hLRRK2-G2019S* mutation were viable in the white-eyed background. To determine if these flies had similar defective visual responses to 7 DPE flies with DA expression of *hLRRK2-G2019S* in a WT red-eyed background (see Chapter 4), the SSVEP was examined. WT *hLRRK2* was also expressed in the DA neurons of $cn^1bw^1$ homozygous flies ($cn^1bw^1/cn^1bw^1$; *TH/hLRRK2*). Additional controls included a cross between TH/$w^{apricot}$ and $cn^1bw^1$ flies ($cn^1bw^1/cn^1bw^1$; *TH/*$w^{apricot}$), and $cn^1bw^1$ homozygous flies expressing no transgene or GAL4 ($cn^1bw^1/cn^1bw^1$). Due to homozygous mutations in both the kynurenine ($cn^1$) and pteridine ($bw^1$) pathways, all of these flies have white eyes. The SSVEP assay was utilised to record the visual response off all genotypes at 3 and 7 DPE. All flies were transferred to instant food supplemented with 100% EtOH on the day of eclosion and were kept in a 29°C pulsating light incubator; these are the same conditions previously used when recording the visual response of red-eyed *TH>G2019S* flies in Chapter 4.

At 3 DPE, robust CRFs were recorded from all genotypes (Figure 5.9A). CRFs recorded from the photoreceptors (1F1 masked), lamina (2F1 masked) and medulla (2F1+2F2 masked and unmasked) from flies with DA expression of *hLRRK2-G2019S* in the white-eyed $cn^1bw^1$ homozygous mutant background ($cn^1bw^1/cn^1bw^1$; *TH/G2019S* flies), were similar to those recorded from all other control genotypes (indicated by the black arrows in Figure 5.9). At 7 DPE, there was more variation in the CRFs recorded from the different genotypes (Figure 5.9B); surprisingly, the $cn^1bw^1/cn^1bw^1$; *TH/G2019S* mutant flies showed the largest CRF responses throughout the visual system, closely followed by flies with DA expression of WT *hLRRK2* ($cn^1bw^1/cn^1bw^1$; *TH/hLRRK2* flies).

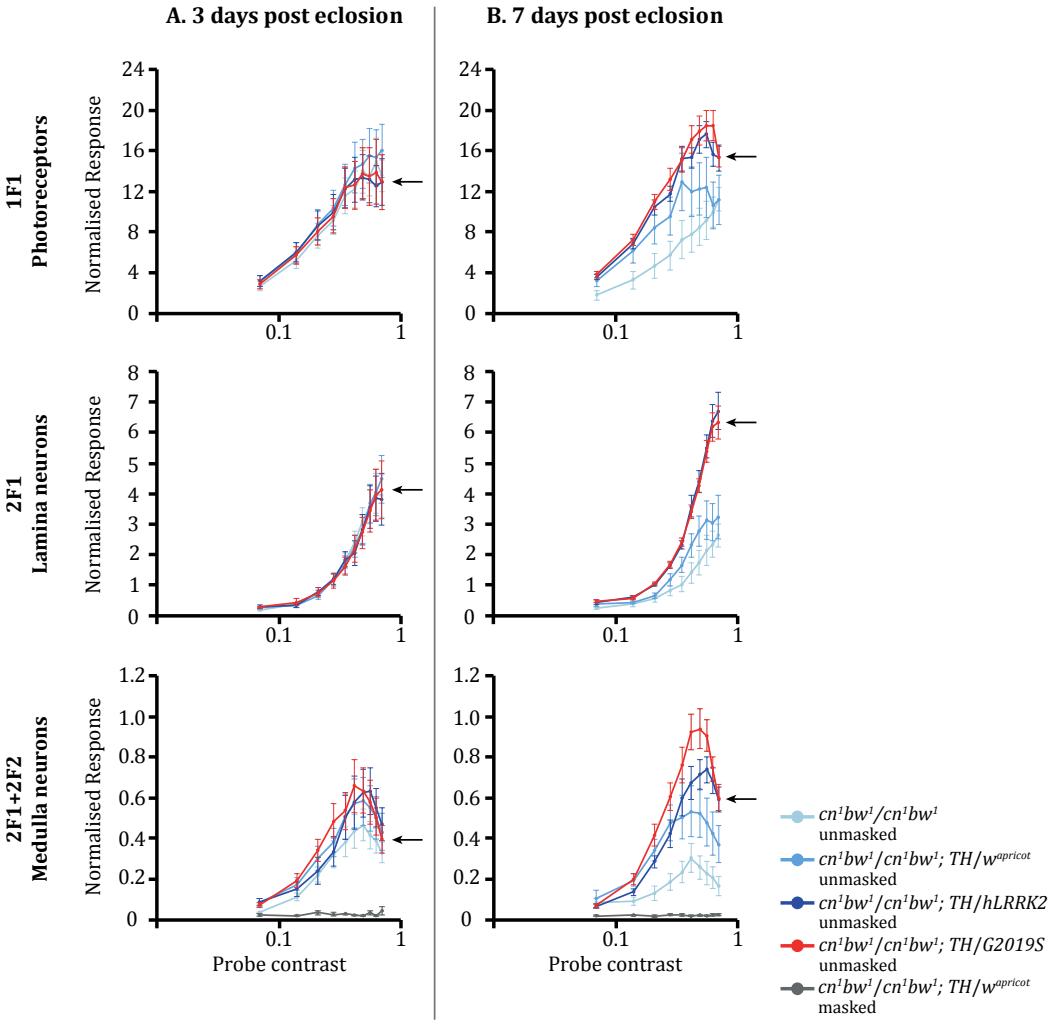


**Figure 5.9 Neural responses to swept contrast flicker are increased at 7 DPE in white-eyed flies with DA expression of *hLRRK2-G2019S* or WT *hLRRK2* compared with controls**

(A) 3 DPE CRFs and (B) 7 DPE CRFs recorded from white-eyed control flies (*cn¹bw¹/cn¹bw¹*: light blue), white-eyed flies expressing no transgene in the DA neurons (*cn¹bw¹/cn¹bw¹*; *TH/w^apricot*: darker blue), white-eyed flies expressing *hLRRK2* in the DA neurons (*cn¹bw¹/cn¹bw¹*; *TH/hLRRK2*: darkest blue), and white-eyed flies expressing *hLRRK2-G2019S* in the DA neurons (*cn¹bw¹/cn¹bw¹*; *TH/G2019S*: red) for 1F1 (first row), 2F1 (second row) and 2F1+2F2 (third row). (A) At 3 DPE, the CRFs were similar for all genotypes. (B) At 7 DPE, the 1F1, 2F1 and 2F1+2F2 masked responses were all higher in white-eyed flies with DA expression of *hLRRK2-G2019S* or *hLRRK2* compared with control white-eyed flies. The black arrows point to the responses from white-eyed flies with DA expression of *hLRRK2-G2019S*. Data are mean ± SEM bars. n≥9 for all genotypes.

To determine if the differences in the CRFs were significantly different between genotypes, the peak CRFs recorded from the photoreceptors, lamina and medulla neurons were plotted for each genotype. Figure 5.10 shows the peak CRFs recorded at 3 DPE. As expected from the CRF curves in Figure 5.9A, there were no significant differences between genotypes. The 2F1+2F2 unmasked response, which can be utilised as an indication of the baseline noise level, did not differ significantly between genotypes, suggesting that the baseline noise was similar between experiments.

Figure 5.11 shows the peak CRFs recorded at 7 DPE. As indicated by the CRF curves in Figure 5.9B, there was more variation in the CRF responses between genotypes. Throughout the visual system, the CRF responses recorded from $cn^1bw^1/cn^1bw^1$; *TH/G2019S* flies were significantly higher than those recorded from flies expressing no transgene (1F1: $p<0.05$; 2F1: $p<0.001$; 2F1+2F2 masked: $p<0.01$). The lamina and medulla responses recorded from $cn^1bw^1/cn^1bw^1$; *TH/G2019S* flies were also significantly higher than those recorded from flies expressing *TH*-GAL4 but no transgene ($p<0.001$ and $p<0.01$, respectively), but the photoreceptor responses of these two genotypes did not differ significantly. There were no significant differences in the CRFs recorded from $cn^1bw^1/cn^1bw^1$; *TH/G2019S* and $cn^1bw^1/cn^1bw^1$; *TH/hLRRK2* flies. The lamina responses of $cn^1bw^1/cn^1bw^1$; *TH/hLRRK2* flies were significantly higher than those recorded from $cn^1bw^1/cn^1bw^1$ and $cn^1bw^1/cn^1bw^1$; $TH/w^{apricot}$ flies (both $p<0.001$), whereas the medulla and photoreceptor responses of these flies were only significantly higher than those recorded from the $cn^1bw^1/cn^1bw^1$ flies ($p<0.05$ and $p<0.01$, respectively).

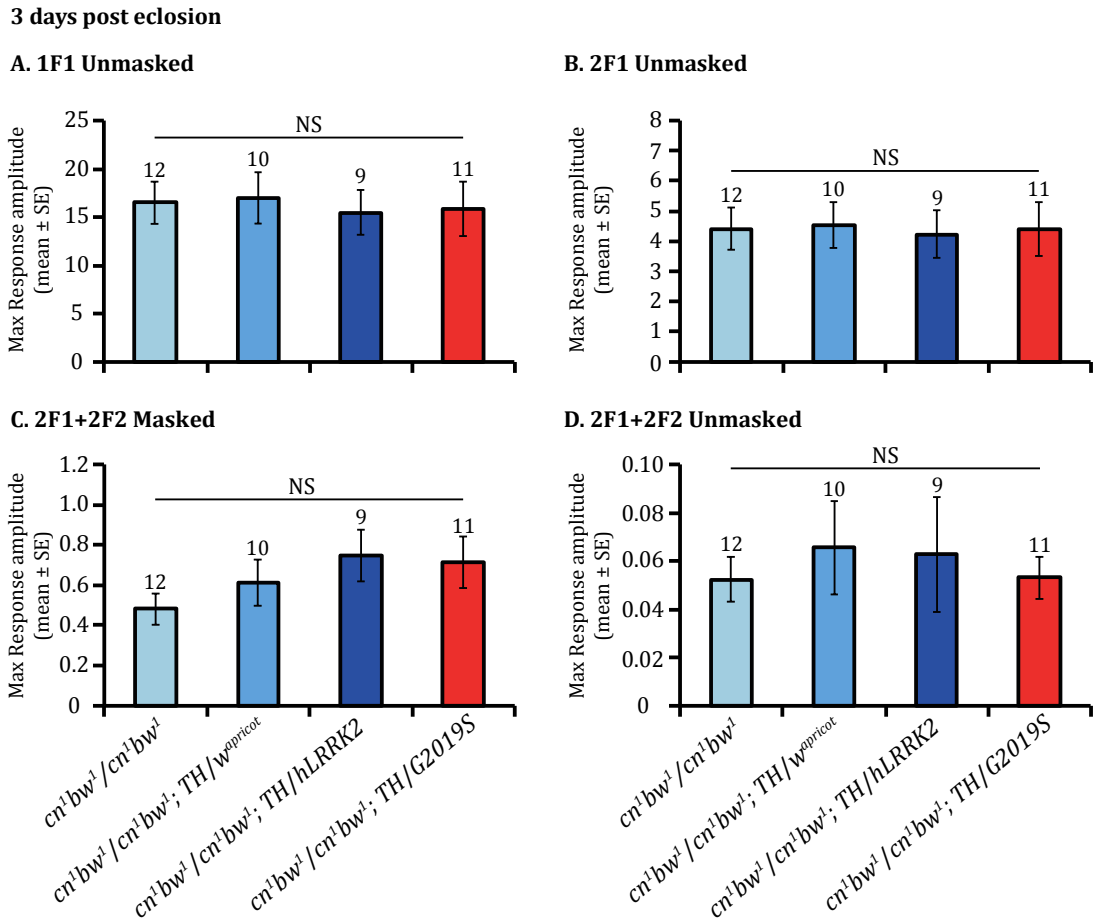


**Figure 5.10 At 3 DPE, peak CRFs do not differ between white-eyed flies with DA expression of *hLRRK2-G2019S* or white-eyed controls**

The 3 DPE peak CRFs recorded from white-eyed control flies (*cn¹bw¹/cn¹bw¹*: light blue), white-eyed flies expressing no transgene in the DA neurons (*cn¹bw¹/cn¹bw¹*: *TH/w^apricot*; darker blue), white-eyed flies expressing *hLRRK2* in the DA neurons (*cn¹bw¹/cn¹bw¹*; *TH/hLRRK2*: darkest blue), and white-eyed flies expressing *hLRRK2-G2019S* in the DA neurons (*cn¹bw¹/cn¹bw¹*; *TH/G2019S*: red) for (A) 1F1 photoreceptors, (B) 2F1 lamina, (D) 2F1+2F2 medulla, without a 30% mask and (C) 2F1+2F2, with a 30% mask as the probe contrast is increased from 0 to 69%. (A-C) There were no significant differences in the CRFs between genotypes. (D) There were no significant differences in the 2F1+2F2 unmasked responses between genotypes, thus the baseline noise level was similar between experiments. All statistics are ANOVA with post-hoc Bonferroni correction: NS, no significant difference, $p>0.05$. Data presented are mean ± SEM bars; n numbers are displayed above the bars.

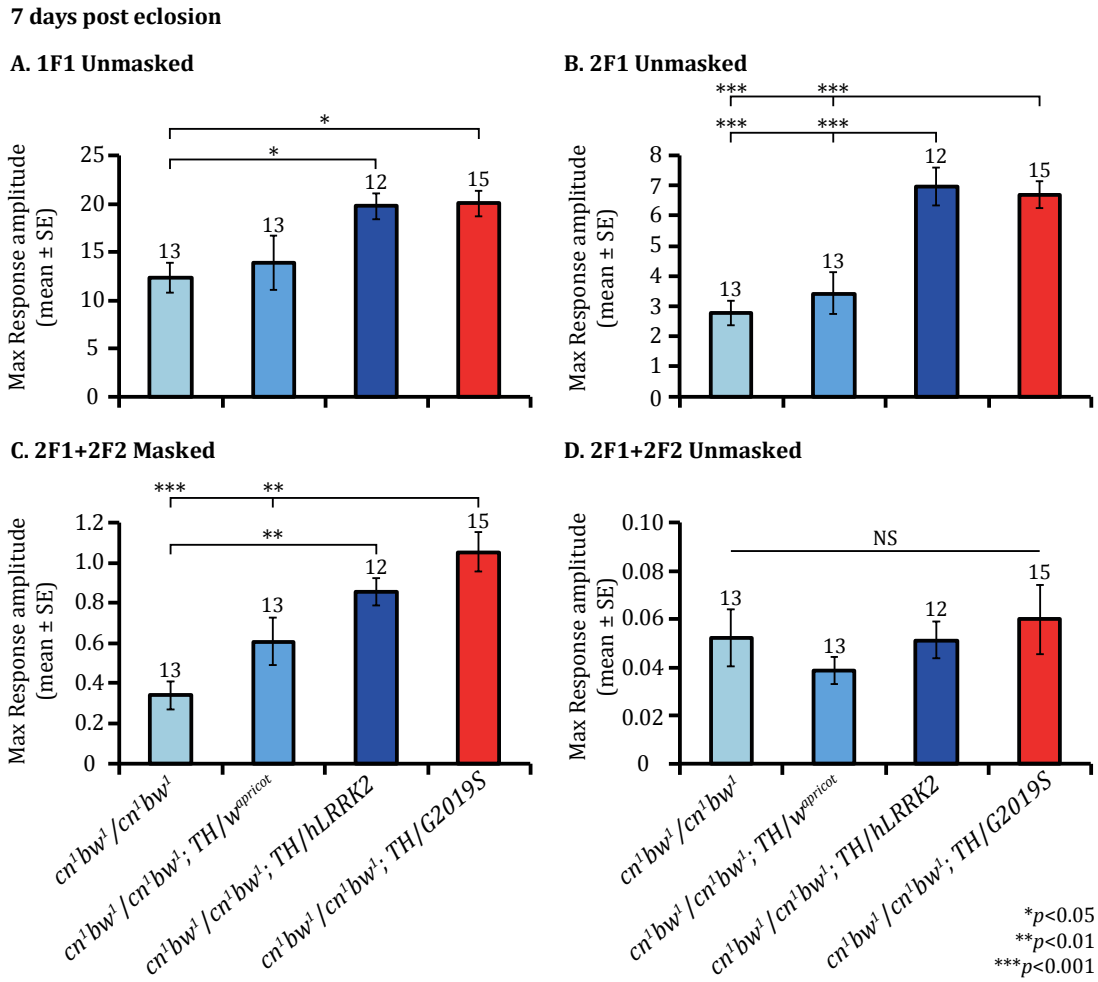


**Figure 5.11 At 7 DPE, peak CRFs are generally higher in white-eyed flies with DA expression of *hLRRK2-G2019S* or WT *hLRRK2* compared with white-eyed controls**

The 7 DPE peak CRFs recorded from white-eyed control flies ($cn^1bw^1/cn^1bw^1$: light blue), white-eyed flies expressing no transgene in the DA neurons ($cn^1bw^1/cn^1bw^1$: $TH/w^{apricot}$; darker blue), white-eyed flies expressing *hLRRK2* in the DA neurons ($cn^1bw^1/cn^1bw^1$; *TH/hLRRK2*: darkest blue), and white-eyed flies expressing *hLRRK2-G2019S* in the DA neurons ($cn^1bw^1/cn^1bw^1$; *TH/G2019S*: red) for (A) 1F1 photoreceptors, (B) 2F1 lamina, (D) 2F1+2F2 medulla, without a 30% mask and (C) 2F1+2F2, with a 30% mask as the probe contrast is increased from 0 to 69%. (A-C) The peak 1F1, 2F1 and 2F1+2F2 masked CRFs recorded from white-eyed flies with DA expression of *hLRRK2-G2019S* were significantly higher than those recorded from white-eyed controls, and both the 2F1 and 2F1+2F2 masked CRFs were also significantly higher than those recorded from white-eyed flies expressing no transgene in the DA neurons. The peak 1F1, 2F1 and 2F1+2F2 CRFs recorded from white-eyed flies with DA expression of WT *hLRRK2,* were also all significantly higher than those recorded from white-eyed controls. Only the peak 2F1 responses recorded from white-eyed *TH>hLRRK2* flies were significantly higher than the 2F1 responses recorded from white-eyed

flies expressing no transgene in the DA neurons. There were no significant differences between white-eyed flies with DA expression of *hLRRK2-G2019S* or *hLRRK2.* There were no significant differences between white-eyed control flies and white-eyed flies expressing no transgene in the DA neurons. (D) There were no significant differences in the 2F1+2F2 unmasked responses between genotypes, thus the baseline noise level was similar between experiments. All statistics are ANOVA with post-hoc Bonferroni correction: NS, no significant difference, $p>0.05$. Data presented are mean ± SEM bars; n numbers are displayed above the bars.

These results were unexpected because flies expressing *hLRRK2-G2019S* in the DA neurons in a red-eyed background showed severely reduced visual responses compared with controls at 7 DPE (see Chapter 4, Figure 4.6), whereas expressing *hLRRK2-G2019S* in the DA neurons in a white-eyed background led to significantly higher CRF responses at 7 DPE compared with controls (Figure 5.12). The 7 DPE peak photoreceptor responses of 7 DPE white-eyed flies with DA expression of *hLRRK2-G2019S* were significantly higher than red-eyed flies with DA expression of *hLRRK2-G2019S* ($p<0.001$; Student's t-test). There were no significant differences between the 7 DPE peak photoreceptor responses of red- or white-eyed flies with DA expression of *hLRRK2* ($p>0.05$; Student's t-test). The 7 DPE peak photoreceptor responses of white-eyed flies expressing no transgene in the DA neurons were significantly lower than red-eyed flies expressing no transgene in the DA neurons ($p<0.001$; Student's t-test).

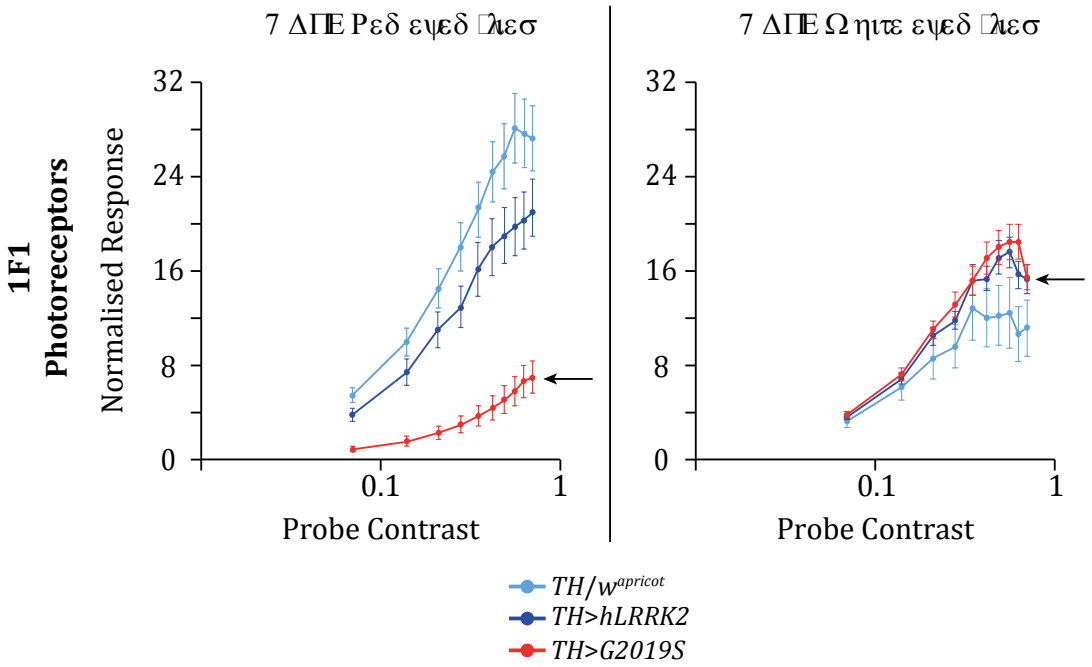


**Figure 5.12 At 7 DPE, the neurodegeneration seen with DA expression of *hLRRK2-G2019S* is prevented through mutations in eye colour genes**

7 DPE CRFs recorded from flies with DA expression of *hLRRK2-G2019S* (*TH>G2019S*; red line), *hLRRK2* (*TH>hLRRK2*; dark blue line), or no transgene (*TH/w*$^{apricot}$; light blue line), in a WT red-eyed background (left) or in a white-eyed mutant background (right). Red-eyed flies expressing *hLRRK2-G2019S* showed reduced visual responses compared with flies expressing *hLRRK2* or no transgene, indicating that red-eyed *TH>G2019S* flies have a severe loss of visual function. White-eyed flies expressing *hLRRK-G2019S* did not show a loss of visual function, rather their responses were very similar to flies expressing *hLRRK2* and were better than flies expressing no transgene. Data are mean ± SEM bars. n≥8 for each genotype.

## 5.4 Discussion

In this chapter, the first key observation was that mutations in the kynurenine gene, *cn,* or in the pteridine gene, *bw*, were synthetically lethal with LOF mutations in *dLRRK*. The second key observation was that DA or glial specific overexpression of *bw* or *cn* in a *dLRRK*$^{-}$ LOF background, completely or partially rescued the loss of visual function caused by LOF mutations in *dLRRK*. The final key observation was that mutations in the eye pigment genes, *cn* and *bw,* prevented the loss of visual neurodegeneration induced by DA expression of *hLRRK2-G2019S*. Taken together, our data identify novel, potent genetic interactions between LRRK2 and eye pigment mutations.

### 5.4.1 The kynurenine and pteridine pathways have links with PD

Like mammalian melanosomes, the *Drosophila* eye pigment granules are lysosome-related organelles (Dell'Angelica et al., 2000). This specialised group of organelles also includes platelet-dense granules, lytic granules of cytotoxic T lymphocytes, MHC class II compartments of antigen-presenting cells, and neutrophil primary granules (Dell'Angelica et al., 2000). Melanosomes are found in mammalian eyes, skin and in the human *substantia nigra* (Wasmeier et al., 2008, Wu and Hammer, 2014). If LRRK2 plays a key role in regulating lysosomal-related organelles, then disruption of the formation of the melanosomes in the *substantia nigra* may explain why the DA neurons are so sensitive to *LRRK2-G2019S* expression in humans. Furthermore, it may also explain why mice, which have no melanosomes in the *substantia nigra* (Marsden, 1961), have shown relatively limited success as a model of PD.

As previously described in section 5.1.1, the two pathways in flies that generate the eye pigments are the kynurenine pathway and the pteridine pathway. Imbalances in absolute and relative levels of neuroactive metabolites of the kynurenine pathway have been strongly associated with the pathogenesis of several neurodegenerative diseases including Huntington's disease (Jauch et al., 1995, Guidetti et al., 2004, Guidetti et al., 2006, Campesan et al., 2011, Green et al., 2012), Alzheimer's disease (Bonda et al., 2010, Gulaj et al., 2010, Schwarz et al., 2013), and importantly for this study, PD (Ogawa et al., 1992). Pharmacological and genetic manipulations in flies,

mice and worms have also indicated that an elevated kynurenic acid/3-HK ratio is neuroprotective in a range of neurodegenerative models, including PD (Campesan et al., 2011, van der Goot et al., 2012, Breda et al., 2016). Mutations in the pteridine pathway have also been linked to PD, including GTPCH I (Mencacci et al., 2014), the fly orthologue of *punch*, and Sepiapterin reductase (Tobin et al., 2007, Lohmann et al., 2012), the fly orthologue of *Sptr*. Interestingly, both GTPCH I and Sepiaterin reductase are required for the synthesis of tetrahydrobiopterin ($BH_4$). $BH_4$ helps to regulate dopamine synthesis, as it is an essential cofactor for TH. The activity of TH depends on the availability of its cofactor $BH_4$, however excess $BH_4$ is toxic to DA neurons, suggesting that mutations that lead to the breakdown of the feedback between GTPCH I, $BH_4$ and TH, may be particularly toxic to the SNPc. Recent evidence from the Elliott lab has shown that a mutation in *punch* ($pu^{R1}$) is also synthetically lethal in combination with LOF mutations in *dLRRK* (Cording and Elliott, unpublished).

### 5.4.2 The granule pathway and *dLRRK/LRRK2*

Unfortunately, it is still unknown how changes in metabolites of the kynurenine or pteridine pathways are linked to cell death. Taking data from previous studies along with the data that is presented in this chapter, we propose a key role for dLRRK/LRRK2 in the regulation of lysosome-related organelles. Our reasoning for this is outlined below.

There are two key routes by which lysosomes receive proteins; firstly, internalised proteins that are destined for degradation go through the early and late endocytic compartments before they reach the lysosomes; secondly, a number of resident lysosomal proteins can be delivered via the biosynthetic route from the Golgi without first appearing on the cell surface (Lloyd et al., 1998). It is known that the mammalian melanosomes receive proteins through both of these pathways and there is genetic evidence to suggest that the biogenesis of the *Drosophila* pigment granules involves molecular components that are required for protein delivery to lysosomes. Thus, mutations that affect vesicular transport to lysosomes can alter the eye colour in flies (Lloyd et al., 1998). The first evidence of a role for the vesicular trafficking pathway in the biogenesis of lysosome-related organelles was the discovery that the

*Drosophila* eye-colour gene *garnet* encodes the δ-subunit of the adaptor protein-3 (AP-3) complex (Ooi et al., 1997, Simpson et al., 1997), which is implicated in the Golgi-to-lysosome pathway in both yeast (Cowles et al., 1997) and mammalian cells (reviewed in Odorizzi et al. (1998)). Furthermore, *garnet* mutant flies have abnormal pigment granules. Subsequently, a number of other eye-colour genes have been identified to function in the delivery of proteins to lysosomes and pigment granules, rather than in the biosynthesis of pigments. Collectively these genes are known as the granule group (Lloyd et al., 1998). The granule group genes *ruby, carmine,* and *orange* were found to encode the remaining β3, μ3, and ς3 subunits of the AP-3 complex, respectively (Mullins et al., 1999, Mullins et al., 2000). In addition, three of the other granule group genes encode the *Drosophila* homologs of the yeast vacuolar protein sorting (VPS) gene products; the product of *light* is an orthologue of yeast Vps41p (Warner et al., 1998), which interacts with the AP-3 δ-subunit (Rehling et al., 1999); and the products of *deep orange* and *carnation* are orthologues of yeast Vps18p and Vps33p, respectively (Shestopal et al., 1997, Sevrioukov et al., 1999). In yeast, mutations in any of these subunits results in the accumulation of pre-vacuolar MVBs and impaired transport to the vacuole from both the biosynthetic and endocytic pathways (Rieder and Emr, 1997). Similarly, in flies it has been shown that mutations in *deep orange* result in the accumulation of MVBs and defective trafficking of an internalised ligand to lysosomes (Sevrioukov et al., 1999).

The key question raised in this chapter is how changes in the eye pigment metabolites are linked to cell death? One answer could be provided by the observation of Shoup (1966) that unfilled vesicles breakdown by autophagy. Shoup (1966) observed that failure to traffic ABCG transporters (notably white and scarlet proteins) from the Trans-Golgi-Network (TGN) to newly forming vesicles along the granule pathway, led to the production of autophagosomes and subsequent autophagy. Autophagy is a key theme in *LRRK2-G2019S* PD. Recently, electron micrographs have shown that flies with DA expression of *hLRRK2-G2019S* have fewer pigment granules, with many engulfed by autophagosomes (Cording and Elliott, unpublished), which extends the observations made by Shoup (1966). Furthermore, feeding these flies with LRRK2 kinase inhibitors ameliorates the loss of pigmentation (Cording and Elliott, unpublished). Interestingly, the granule pathway has already been linked to PD

through *Rab7L1* and *VPS35,* a core component of the retromer complex (MacLeod et al., 2013). The fly orthologue of *Rab7L1* is *lightoid*, and flies with mutations in *lightoid* have no pigment granules (Ma et al., 2004).

Taking these observations together, we hypothesise that the synthetic lethality reported in the present study arises from the intersection of the pigment synthesis pathways with a role for *dLRRK/LRRK2* in the traffic of cargo to the granules (Figure 5.13). It has recently been shown that *cardinal*/*dLRRK*$^{-}$ LOF double mutants are not lethal, implying that the lethal interaction between the kynurenine pathway and dLRRK must arise before *cardinal* (Cording and Elliott, unpublished). As cardinal is the last enzyme in the kynurenine pathway and acts inside the pigment granule, we believe that the intersection of the kynurenine pathway and *dLRRK* must be on the pigment granule membrane, somewhere between *cinnabar* and *cardinal.* It has previously been shown that a mutation in the *cardinal* gene (*cd*$^{1}$) increases levels of 3-HK without increasing levels of neurodegeneration in the eye, thus suggesting that the *cd*$^{1}$ mutation is neuroprotective (Campesan et al., 2011). The hypothesis that we propose, could explain this surprising observation.

### 5.4.3 PD and melanoma

Melanoma has consistently been associated with PD, especially *LRRK2*-linked PD (Saunders-Pullman et al., 2010, Pan et al., 2011, Inzelberg et al., 2012, Huang et al., 2015, Inzelberg et al., 2016). Although there are well-documented links between PD and melanoma, the mechanisms of this association remain to be elucidated. A number of studies have suggested that levodopa may increase the risk of melanoma (Skibba et al., 1972, Przybilla et al., 1985, Sandyk, 1992), however subsequent studies have shed doubts about any link between levodopa and melanoma (Sober and Wick, 1978, Pfutzner and Przybilla, 1997). Furthermore, it has been found that melanoma occurs at higher than expected rates in PD patients even before onset of PD and thus before the initiation of levodopa therapy, which strongly argues against an association between levodopa and melanoma (Zanetti et al., 2006, Olsen et al., 2007, Vermeij et al., 2009, Pan et al., 2011). It has since been suggested that the positive association between PD and melanoma may be explained by pigmentation changes in melanin and/or melanin synthesis enzymes (Pan et al., 2011, Herrero Hernandez, 2009).

Interestingly, two of the genes that are involved in the synthesis of melanin, namely tyrosinase and tyrosine hydroxylase, also have links to both PD and melanoma, suggesting that the link between these two diseases resides in genes that regulate pigmentation (Herrero Hernandez, 2009). Furthermore, the risk of PD has been shown to increase with decreasing darkness of hair colour, which again suggests a potential role of pigmentation in PD (Gao et al., 2009).

If LRRK2 does have a role in regulating lysosomal-related organelles, such as the melanosomes, then the hypothesis that is proposed here could explain why there is an increased risk of developing melanoma in *LRRK2*-linked PD. Thus melanocytes might be an interesting mammalian cell line in which to study PD.

### 5.4.4 Determining the interaction between *dLRRK/LRRK2* mutations and the eye pigment and granule pathways

The data presented in this chapter suggest an interaction between dLRRK/hLRRK2 and the eye pigment or granule pathways, however these data are very preliminary and further investigations will be required to fully characterise these interactions. Experiments that could be carried out to further define the interactions between *dLRRK*$^{-}$ LOF or *hLRRK2-G2019S* mutations and mutations in the kynurenine and pteridine pathways are outlined below.

Firstly, to define the interaction between mutations in the kynurenine pathway and *dLRRK* LOF, the UAS/GAL4 system could be utilised to express UAS-*cinnabar* both globally or specifically in the eye, as *cinnabar* also synthesises 3-HK in larval Malpighian tubules (Tearle, 1991), to test for a rescue. In addition 3-HK, which is the missing metabolite in *cn*$^{3}$; *dLRRK*$^{-}$ double mutants, could be fed to larvae to try and rescue lethality. Initial experiments have indicated that 1 mg/ml of 3-HK is enough to rescue both *cinnabar* and *vermilion* LOF mutants (Cording and Elliott, unpublished). Caspase antibodies and UAS-atg-GFP constructs (Hindle et al., 2013) can be utilised to observe the autophagic response of *cn*$^{3}$; *dLRRK*$^{-}$ double mutants by confocal microscopy, or through examining electron micrographs of the retina for autophagosomes.

Secondly, to define the interaction between mutations in the pteridine pathway and *dLRRK* LOF, a range of *punch* mutants could be examined in combination with *dLRRK*$^{-}$ LOF for lethality. With regards to PD, *punch* is the most interesting gene in the pteridine pathway, thus would be a valid starting point to determine the interaction between the pteridine pathway and *dLRRK.* UAS lines, which carry mutated forms of *punch*, could be used to achieve isoform-specific rescues. These lines can be crossed with lines in which *TH* expression is increased or decreased by RNAi, and ERGs recorded whilst dopamine levels are monitored via HPLC. The pharmacological effects of $BH_4$, the cofactor of *punch*, and other related compounds could be tested in the *pu*; *dLRRK*$^{-}$ double mutants. As with the kynurenine pathway, confocal and electron microscopy could also be used to examine the retina for evidence of autophagy. Together, these experiments would help to determine if *pu*; *dLRRK*$^{-}$ double mutant lethality is caused by excess $BH_4$ or TH, or through changes in autophagy.

It will also be important to demonstrate interactions between *dLRRK*$^{-}$ LOF mutations and the granule pathway to strengthen our hypothesis. Genes that are involved in the pigment granule or melanosome pathways encode proteins that have diverse functions. Some of these proteins are members of the AP-3 or BLOC sorting complexes (Lloyd et al., 1998, Cheli et al., 2010), others are GEFs or GTPases (Ma et al., 2004, Harris et al., 2011). As previously mentioned, the GTPase encoded by *lightoid* (*ltd*) is the homolog of the mammalian gene *Rab7L*, which is a risk factor in PD. RAB7L1 interacts with LRRK2, thus lightoid may physically interact with dLRRK or hLRRK2-G2019S in our fly model (MacLeod et al., 2013, Beilina et al., 2014). In a similar manner to the previous kynurenine and pteridine pathway mutations, a LOF strategy could be used to examine the interaction between *ltd* and *dLRRK*$^{-}$ LOF mutations. Other granule pathway mutants could also be examined in combination with *dLRRK*$^{-}$ LOF mutations including the *ltd*-GEF, *claret*, and mutations in *garnet* and *ruby* to determine if the interaction occurs in the AP-3 or BLOC pathway (Ma et al., 2004).

Here, it was shown that eye pigment mutations in *cn*$^{1}$*bw*$^{1}$ prevent the loss of vision seen in old, red-eyed flies with DA expression of *hLRRK2-G2019S*. It has since been shown that the *cn*$^{1}$ mutation on its own is also protective for *G2019S*-induced loss of

vision (Cording and Elliott, unpublished). Interestingly, *cn* mutations have also been shown to be neuroprotective in an α-synuclein model of PD (Breda et al., 2016). Using the UAS/GAL4 system, the effect of co-expressing UAS-*cinnabar* in *TH>G2019S* flies could be examined; we would predict that this would lead to a more severe phenotype. In addition, an interaction between *cn* and other LRRK2 mutants, including the kinase-dead version (*D1994A*), the GTPase dead version (*Y1699C*) and the neuroprotective (*R1398H*) mutant, could be examined. It would also be interesting to express the *hLRRK2-G2019S* mutation in the *brown* background, to determine if the *brown* mutations are as effective as *cinnabar*, or if the rescue of the *hLRRK2-G2019S* induced visual response if entirely due to the action of *cinnabar.* The *hLRRK2-G2019S* mutation could also be expressed in other eye pigment mutant backgrounds, for example *punch* as this shows a strong interaction with *hLRRK2-G2019S.* To compliment these genetic experiments, available inhibitors of eye pigment genes, including inhibitors of *cinnabar*: 680C91 (Breda et al., 2016), *punch*: DAHP (Funderburk et al., 2006), and a more potent inhibitor of $BH_4$ synthesis: SPRi1 (Latremoliere et al., 2015), could be used to test for rescue of visual dysfunction in old *TH>G2019S* flies.

### 5.4.5 Conclusions

In this chapter, two converging pathways that intersect to provide a critical opportunity to understand the action of LRRK2 have been identified. The data presented in this chapter, together with the future experiments that we propose will be able to demonstrate which eye pigment mutants interact with *dLRRK*. From this, we will be able to determine exactly how *dLRRK* interacts with eye pigment metabolites, granule synthesis pathways or autophagy. Thus key sites for intervention in *hLRRK2-G2019S* and pharmacological studies can be identified. We hope that our findings will reveal a new role for eye pigment mutations in LRRK2 pathology and will bring to light new targets in these pathways that could provide a new class of drug treatment to ameliorate visual deficits in PD.

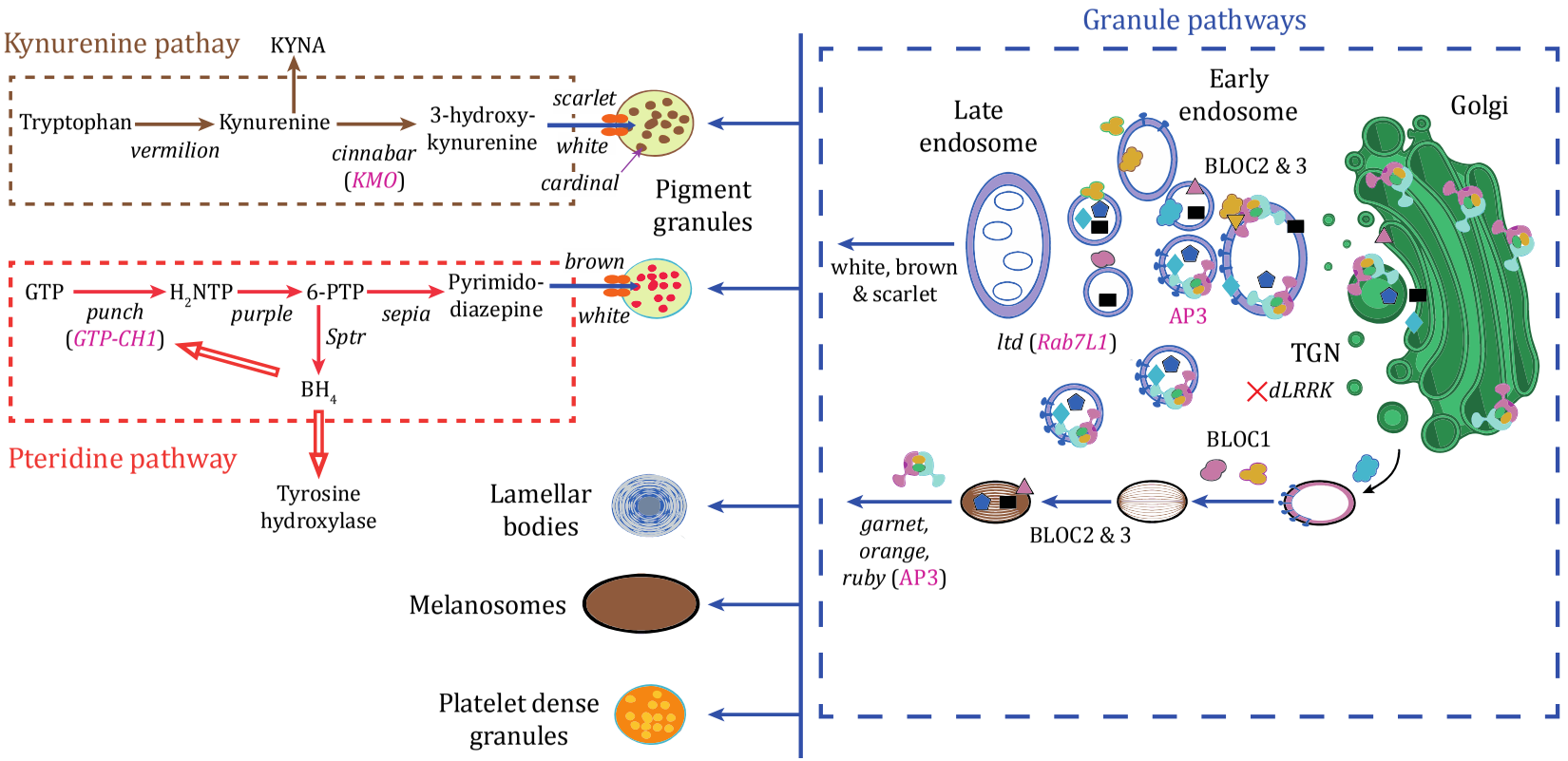


**Figure 5.13 The production of the pigment granules depends on the interaction of pigment synthesis pathways and the granule pathways**

The synthetic lethality of *cn/dLRRK*⁻ LOF, *bw/dLRRK*⁻ LOF, and *pu/dLRRK*⁻ LOF suggests that *dLRRK* must act in the granule pathway, possibly near to the TGN (the LOF of dLRRK in the present study is indicated by the red cross next to *dLRRK*). This is supported by the *hLRRK2-G2019S/Rab7L1* interaction in PD; the fly homolog of *Rab7L1* is *ltd* (*lightoid*) located within the granule pathway.

# 6 Discussion and Future Research

## 6.1 Introduction

The main aim of this investigation was to advance our understanding of LRRK2 *in vivo* through using complementary loss-of-function and gain-of-function approaches in *Drosophila*. In order to achieve this, the following primary questions were investigated:

1. Does the loss of dLRRK function lead to age-related visual defects in adult flies?
2. Can two chemically related compounds, UCA and UDCA, rescue the visual response of flies expressing the GOF *hLRRK2-G2019S* mutation in the DA neurons?
3. What is the nature of the interaction between eye colour genes and *dLRRK*?

This final chapter looks to determine which of these questions have been answered through providing a succinct overview of the key data generated in this thesis, and looks to pose further research questions that have arisen as a result of this study.

## 6.2 LRRK2, prion-like proteins and exosomes

Here, it was shown that old *dLRRK*¯ LOF mutant flies and flies with DA expression of the *hLRRK2-G2019S* mutation have abnormal ERGs. Although a loss of photoreceptor function has previously been described as the cause of the abnormal ERG of *hLRRK2-G2019S* flies (Hindle et al., 2013), a specific early loss of the ERG off-transient component in the *dLRRK*¯ LOF model indicated that the defect was in the adaptation of lower-order visual neurons rather than in the photoreceptors. The visual response of *dLRRK*¯ LOF flies could be rescued with expression of *dLRRK* specifically in the lamina, but also in the DA neurons, photoreceptors or glial cells, suggesting that LRRKs action can extend to cells that lack autonomous expression of LRRK and that transcellular signalling is key to LRRKs *in vivo* role. Hindle et al. (2013) previously identified a role for LRRK2 in transcellular signalling. She expressed *hLRRK2-G2019S* in the DA neurons of flies and found that it caused a progressive loss of photoreceptor

function. Through using fly head sections, it was shown that the DA expression of *hLRRK2-G2019S* led to extensive neurodegeneration throughout the visual system, including regions that are not directly innervated by DA neurons. Expressing the normal human form of *hLRRK2* did not affect photoreceptor function or cause neurodegeneration in the visual system. Thus, expression of *hLRRK2-G2019S* in one kind of neuron (DA neurons) caused a LOF and degeneration of another type (photoreceptors). Similarly, here it was shown that expression of *dLRRK* in one kind of tissue (photoreceptors, DA neurons, glial cells) could rescue the LOF of another type (lamina neurons).

The key question posed by these data is how does LRRKs action spread from cell-to-cell? The possibilities in the literature include alterations in the release of dopamine or another neurotransmitter, changes in secretion of growth factors, or diffusion of free radicals. However, due to LRRKs close association with the endocytic pathway, we are drawn to the possibility that LRRK is either secreted by exosomes or it affects the release of some other component. The neuronal and functional degeneration seen in the *hLRRK2-G2019S* PD fly model may spread through the *G2019S* mutation causing the release of mis-folded, prion-like proteins in exosomes. Exosomes are a class of small extra-cellular vesicles that are derived from MVBs within the endomembrane system. They have already been shown to mediate the progression of prion diseases, and similar mechanisms are thought to occur in other neurodegenerative disorders (Fevrier et al., 2004, Vella et al., 2007, Coleman et al., 2012). Interestingly, the concept of prion-like propagation has previously been described for α-synuclein (Mougenot et al., 2012, Masuda-Suzukake et al., 2013, Kovacs et al., 2014, Bernis et al., 2015, Chu and Kordower, 2015). This came after two studies showed that intra-striatal transplants of fetal ventral mesencephalic progenitors in PD patients developed α-synuclein-positive LB-like inclusions, a decade after transplantation (Kordower et al., 2008, Li et al., 2008). Although the mechanisms by which the α-synuclein amyloidogenic proteins transmit from a diseased neuron to its connective neuron are unknown, there is evidence for cell-to-cell spreading of pathogenic α-synuclein through exosomes (Emmanouilidou et al., 2010). Furthermore, prion-like tau proteins have also shown a spreading pathology, which has been linked to travel through exosomes and the endocytosis and

exocytosis pathways (Aguzzi and Rajendran, 2009, Frost and Diamond, 2010, Goedert et al., 2010). Thus, it is possible that the spread of mis-folded proteins in exosomes and subsequent aggregation, deposition and propagation are common mechanisms of neurodegeneration and common events in neurodegenerative disorders.

Our findings provide a platform to further investigate if there is a relationship between the spreading neurodegeneration seen in the *hLRRK2-G2019S* fly model of PD and exosomal release of hLRRK2-G2019S. Interestingly, a recent clinical trial started, which aims to determine if there are biomarkers associated with PD susceptibility and/or progression in exosome-proteomes and to determine if LRRK2 expression and/or phosphorylation are significantly lowered in the exosomes of individuals treated with a potent LRRK2 kinase inhibitor (Clinical Trials registration: NCT01860118).

## 6.3 LRRK2 and rab GTPases

Not only has LRRK2 been placed in the right places within the cell to be exported in exosomes, it has been shown to interact with a number of vesicle types and Rab proteins, which have key roles in all forms of intracellular vesicular trafficking events. For example, LRRK2 has been shown to physically interact with Rab7L1, which is itself a genetic risk factor for PD (Dodson et al., 2012, MacLeod et al., 2013, Beilina et al., 2014). It has also been shown to associate with Rab5b to regulate synaptic endocytosis (Shin et al., 2008, Yun et al., 2015), and Rab10, Rab1b and Rab8a have all been suggested as bona-fide LRRK2 targets (Steger et al., 2016). Aside from *Rab7L1*, several other members of the Rab GTPase family have been associated with PD pathogenesis; mutations in *Rab39b* predispose to PD in humans (Wilson et al., 2014, Rivero-Rios et al., 2015), while overexpression of *Rab8a*, *Rab1*, and *Rab3a* attenuate α-synuclein induced cytotoxicity in animal and cellular models of PD (Cooper et al., 2006, Gitler et al., 2008). In Chapter 5, it was shown that LRRK interacts with members of the eye pigment pathway. In light of this, a role for LRRK in the traffic of cargo to the lysosomal-related pigment granules was proposed, and interestingly Rab7L1 has also been linked to the granule pathway (MacLeod et al., 2013). LRRK2 has been implicated in the regulation of a variety of intracellular vesicular trafficking

events, which seems to be in a manner dependent on various Rab proteins. Moving forwards, it will be important to determine which LRRK2/Rab interactions are important in PD. Members of the Rab family of proteins with links to LRRK2 and PD, which are involved in the granule pathway or other vesicular trafficking pathways, may provide novel therapeutic targets for preventing the disease progression.

## 6.4 LRRK2 and potential therapeutic interventions for PD

As previously discussed in Chapter 1, there are currently no cures for PD and the clinical therapies that are available are unable to prevent on-going neurodegeneration. With an ageing population, the number of PD cases is expected to substantially increase over the next 30 years. Therefore, there is a need to identify new potential therapeutic targets and in turn ascertain promising drug candidates that will not only alleviate PD symptoms but will also prevent further neurodegeneration.

In this thesis, I have worked with our collaborators in Sheffield to explore the potential of a class of mitochondrial rescue agents in the *hLRRK2-G2019S* PD fly model. Exciting *in vivo* evidence showed that both UDCA and UCA are able to prevent visual dysfunction in *hLRRK2-G2019S* flies (Mortiboys et al., 2015). UDCA and UCA have previously been shown to rescue mitochondrial function in both *LRRK2*- and *parkin*-mutant fibroblasts, thus their beneficial effects are not limited to just one form of familial PD (Mortiboys et al., 2013). Other PD fly models including *parkin*, *PINK1*, *DJ-1*, and *α-synuclein* could be used to explore the *in vivo* effects of these compounds in the other forms of familial PD. Confocal and electron microscopy work would also be important to determine if these compounds can prevent the neurodegeneration of the photoreceptors previously reported in the *hLRRK2-G2019S* fly model. Although an optimal dose of UDCA and UCA in the *hLRRK2-G2019S* fly model still needs to be determined to achieve a complete rescue of visual function, and the mode of action of these compounds still needs to be confirmed, both UDCA and UCA are promising candidates that should be considered in future PD-related drug trials, especially given that UDCA is already a licensed drug.

The well-documented elevated kinase activity of *LRRK2-G2019S,* has led to the investigation of a plethora of potential LRRK2 kinase inhibitors. However, as previously discussed in Chapter 4, there has been little success with the currently available LRRK2 kinase inhibitors. As inhibition of LRRK2 kinase activity has been reported to protect against LRRK2-induced toxicity (Lee et al., 2010a), this is still an important avenue to progress down. Not being selective for LRRK2 kinase activity and adverse off-target effects have been the downfall of many of the current LRRK2 kinase inhibitors (Ramsden et al., 2011, Zhang et al., 2012, Kavanagh et al., 2013, Afsari et al., 2014, Fuji et al., 2015). A novel compound, BMPPB-32, identified by our collaborators at Lundbeck has thus far shown a promising potential to overcome these downfalls, through showing no major off-target effects in the 1 day old *hLRRK2-G2019S* fly model and a clean LRRK2 kinase selectivity profile in mammalian cells (Afsari et al., 2014). In Chapter 4, I expanded on the previously published *hLRRK2-G2019S* fly studies through feeding BMPPB-32 to newly emerged flies and testing the visual response of adult flies, which more closely mimics the situation in PD patients who would not start taking these compounds until later in life when PD symptoms become apparent. It was shown that BMPPB-32 has a neuroprotective effect on visual function when given to adult flies with DA expression of *hLRRK2-G2019S* (West et al., 2015b). Given that a recent clinical trial with a highly potent and selective LRRK2 kinase inhibitor had to be stopped due to adverse side effects on kidney and lung function, it will be important to fully characterise the physiochemical and pharmacokinetic properties of any future LRRK2 kinase inhibitors and identify potential off-target effects before they enter into human clinical trials.

As well as examining the *in vivo* effects of promising drug candidates, potential therapeutic pathways, which may provide future therapeutic targets, have also been identified in this thesis. Firstly, as discussed in section 6.2, there is evidence to suggest that the exosomal, endocytosis or exocytosis pathways are key to LRRK2s spreading pathology. Thus, members of these pathways, in particular the Rab GTPases, should be further investigated and their links to PD fully characterised. Secondly, in Chapter 3 it was shown that DA or glial expression of the gain-of-kinase-function *hLRRK2-G2019S* or the kinase-dead *hLRRK2-D1994A* transgenes rescued the visual response of *dLRRK*¯ LOF flies to a similar extent. Thus, it was suggested that the

GTPase domain of LRRK2 might be more important than the kinase domain in maintaining the visual response and there is increasing evidence to suggest that decreased GTPase activity of LRRK2 also plays a key role in PD pathogenesis (Lewis et al., 2007, Li et al., 2007, West et al., 2007, Xiong et al., 2012a). The *LRRK2-R1441C/G* or *LRRK2-Y1699C* GTPase domain mutations could be expressed in the *dLRRK*¯ LOF fly model to determine if they can rescue the visual response, which would provide some indication as to whether the GTPase domain is more important than the kinase domain in the fly visual system. In terms of the therapeutic potential of the LRRK2 GTPase domain, there are already increasing efforts to study potential therapeutic strategies that target LRRK2 GTP binding and GTPase activity (Xiong et al., 2012a), and our data provides support for these investigations to continue. Thirdly, in Chapter 4 further evidence was provided to suggest that parkin provides a neuroprotective effect in LRRK2-induced PD. There is strong evidence to suggest that parkin, along with PINK1, plays a key role in regulating mitochondrial homeostasis and morphology (Clark et al., 2006, Park et al., 2006, Yang et al., 2006, Poole et al., 2008). It is already known that UDCA and UCA have the potential to be effective in both parkin- and LRRK2-linked PD, but other compounds that target the mitochondria or are able to increase the expression of *parkin*, may also prove to be effective therapeutic compounds for multiple forms of PD. The neuroprotective effects of parkin on LRRK2-induced PD need to be further investigated. Finally, in Chapter 5 synthetic lethality of mutations in the eye pigment pathways and LOF mutations in *dLRRK* were shown. It was also shown that mutations in the eye pigment genes prevent loss of visual neurodegeneration induced by DA expression of *hLRRK2-G2019S*. These data identify novel potent genetic interactions between LRRK2 and the eye pigment and/or granule pathways. Although the genetic interaction between LRRK2 and eye pigment mutations needs to be further characterised, this pathway may provide an exciting therapeutic potential to prevent neurodegeneration in LRRK2-linked PD.

## 6.5 Conclusion

Throughout this thesis, flash ERGs and SSVEPs have been utilised to record the visual response of flies with mutations in *dLRRK* or *hLRRK2*. Together, these approaches have provided us with a rapid assay of LRRKs function and have given us a

quantitative readout from both young and old flies, something that has been difficult to achieve in other PD models. Furthermore, they have proven to be a robust and stable platform for assessing the effectiveness and selectivity of drug development candidates. As previously described in Chapter 1, the neuronal networks of the fly visual system are complex and the main design principals are essentially identical to the human visual system. Importantly for PD, and providing a further similarity to humans, the fly visual system also contains DA neurons. Thus, through studying the role of LRRK within the visual system of flies, we may also begin to understand the role that LRRK plays within the human visual system. Currently, the same SSVEP approach used during this thesis is being used to record the visual response of humans in Tunisia, which is an area where the *hLRRK2-G2019S* mutation is common. This will enable us to confirm if the findings seen in our *hLRRK2-G2019S* fly model directly relate to LRRK2-linked PD in humans. Furthermore, Afsari et al. (2014) found that very young 1 day old flies expressing *hLRRK2-G2019S* have abnormal SSVEPs, thus if successful in humans, the SSVEP approach may be able to identify people who are at risk of PD before PD symptoms, and more importantly DA neuron loss, have started to occur. Although visual defects have been reported as a feature of PD, not all PD patients suffer with contrast sensitivity issues. This may be due to the underlying cause of their PD and the SSVEP approach could be used to identify which forms of PD are more closely associated with visual deficits. In accordance with this, an initial study in *Drosophila* has provided evidence that different forms of genetic PD affect DA visual signalling pathways in differing ways (West et al., 2015a). It has also been shown that there is an increased risk of melanoma in PD, especially LRRK2-linked PD (Pan et al., 2011, Huang et al., 2015, Inzelberg et al., 2016), and it is possible that this relates to the findings described in Chapter 5, that LRRK2 interacts with the eye pigment pathways. Thus, melanocytes could provide an interesting mammalian cell line in which to test, for example, for exported LRRK2, or to transfect with *G2019S*.

Given the extensive toolbox of *Drosophila*, both LOF and GOF approaches have been used to examine the function of LRRK. Although the GOF *hLRRK2-G2019S* mutation is the most common cause of familial PD, there are no reports of PD patients with a LOF of *hLRRK2*. In fact, in a recent study using zebrafish it was found that even a ~50%

knockdown of *LRRK2* was enough to cause severe neuronal loss, developmental and ocular abnormalities, and synuclein aggregation (Prabhudesai et al., 2016). Furthermore, LRRK2 knockout mice have shown impairment in synaptic transmission, with abnormal dendritic spine morphology (Parisiadou et al., 2014). In view of these deficits, it is not surprising that LRRK2 null humans have not been identified and studied. In contrast, dLRRK null flies are viable, fertile and do not have any obvious external developmental abnormalities. Therefore, these dLRRK null flies provide us with an important opportunity to explore the normal physiological function of LRRK, rather than investigating the consequences of producing too much LRRK, which may be the case in overexpression studies. Through using complementary GOF approaches with expression of the PD mutant *hLRRK2-G2019S* transgene, it can determined how LRRKs function is altered by this pathogenic mutation and the findings can be related back to the disease progression in humans. Although there are currently no animal models of PD that are able to fully recapitulate all of the key neuropathologic and clinical features of human PD, the fly model has proven to be a valuable model in which to study PD.

The findings presented in this thesis expand on currently published data of LRRK2 and have posed further research questions, which may bring us a step closer to understanding how mutations in this gene lead to PD.

## 6.6 Summary of key findings

The key results and conclusions of this study are summarised as follows:

1. Loss of dLRRK function in the visual system of *Drosophila* leads to a progressive, age-related loss of synaptic signalling from the photoreceptors to the underlying lamina neurons.
2. Tissue-specific expression of *dLRRK, hLRRK2* or *mLRRK1* in the DA neurons or expression of *dLRRK* in the non-dopaminergic lamina neurons, photoreceptors or glial cells completely or partially restores visual function in aged flies, suggesting that transcellular signalling, possibly through exosomes, is key to LRRK's *in vivo* role.

3. The mitochondrial rescue agents UDCA and UCA rescue the loss of photoreceptor function in flies with DA expression of *hLRRK2-G2019S.*
4. The kinase inhibitor BMPPB-32 rescues the loss of photoreceptor function when fed to adult flies with DA expression of *hLRRK2-G2019S.*
5. Mutations in the eye pigment pathways are synthetically lethal with LOF mutations in *dLRRK.*
6. Mutations in the eye pigment pathways prevent LRRK2-induced neurodegeneration in the visual system.
7. LRRK may be involved in the traffic of cargo to the pigment granules and novel therapies to treat PD could result from targeting members of the eye pigment pathways.

# 7 Appendix

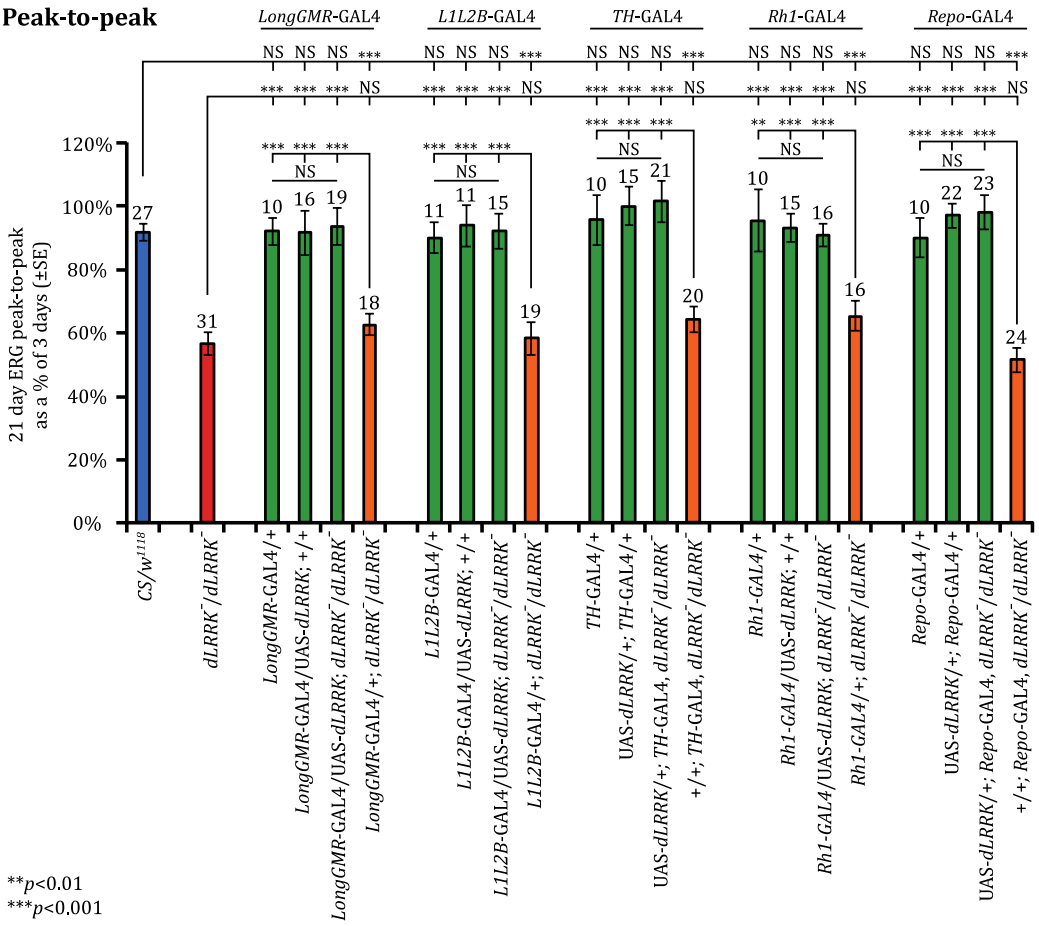


**Appendix 1 Peak-to-peak responses from WT flies, *dLRRK*⁻ LOF flies, and flies expressing either one or both components of the UAS/GAL4 system in a WT or *dLRRK*⁻ LOF background**

The 21 DPE peak-to-peak response of *dLRRK*⁻ LOF flies were substantially reduced compared with WT flies ($p$<0.001). Flies with the expression of one or both components of the UAS/GAL4 system in a WT background had similar peak-to-peak responses to WT flies (all $p$>0.05 compared to WT; all $p$<0.001 compared to *dLRRK*⁻/*dLRRK*⁻). Tissue-specific expression of *dLRRK* in the eyes (*LongGMR*), lamina neurons (*L1L2B*), DA neurons (*TH*), photoreceptors (*Rh1*) or glial cells (*Repo*) in a *dLRRK*⁻ LOF background rescued the peak-to-peak responses of *dLRRK*⁻ LOF flies (all $p$>0.05 compared to WT; all $p$<0.001 compared to *dLRRK*⁻/*dLRRK*⁻). Expression of only one component of the UAS/GAL4 system in a *dLRRK*⁻ LOF background did not rescue the peak-to-peak responses of *dLRRK*⁻ LOF flies (all $p$<0.001 compared to WT; all $p$>0.05 compared to *dLRRK*⁻/*dLRRK*⁻). All statistics are ANOVA with Bonferroni correction: ***$p$<0.001, **$p$<0.01, NS, no significant difference. Data presented are mean ± SEM; $n$ numbers are displayed above the bars.

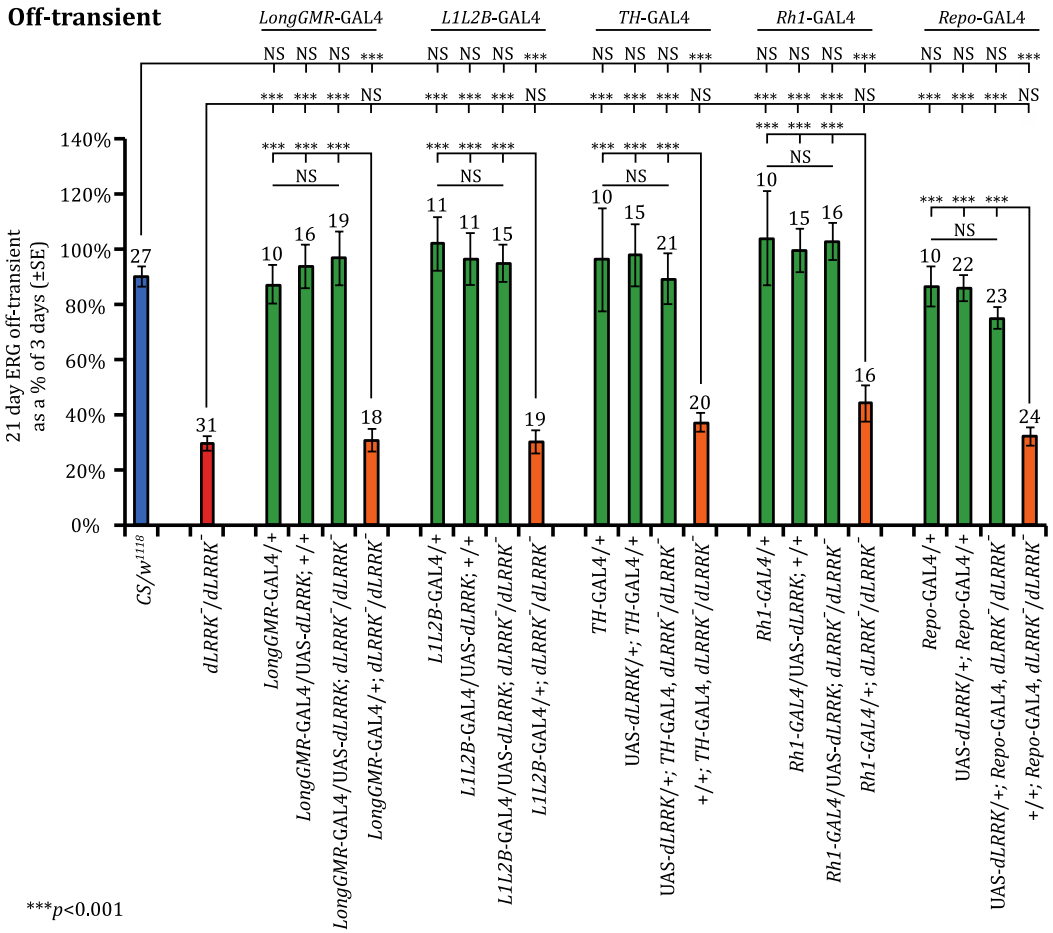


**Appendix 2 Off-transient responses from WT flies, *dLRRK*⁻ LOF flies, and flies expressing either one or both components of the UAS/GAL4 system in a WT or *dLRRK*⁻ LOF background**

The 21 DPE off-transient responses of *dLRRK*⁻ LOF flies were substantially reduced compared with WT flies ($p<0.001$). Flies with the expression of one or both components of the UAS/GAL4 system in a WT background had similar off-transient responses to WT flies (all $p>0.05$ compared to WT; all $p<0.001$ compared to *dLRRK*⁻/*dLRRK*⁻). Tissue-specific expression of *dLRRK* in the eyes (*LongGMR*), lamina neurons (*L1L2B*), DA neurons (*TH*), photoreceptors (*Rh1*) or glial cells (*Repo*) in a *dLRRK*⁻ LOF background rescued the off-transient responses of *dLRRK*⁻ LOF flies (all $p>0.05$ compared to WT; all $p<0.001$ compared to *dLRRK*⁻/*dLRRK*⁻). Expression of only one component of the UAS/GAL4 system in a *dLRRK*⁻ LOF background did not rescue the off-transient responses of *dLRRK*⁻ LOF flies (all $p<0.001$ compared to WT; all $p>0.05$ compared to *dLRRK*⁻/*dLRRK*⁻). All statistics are ANOVA with Bonferroni correction: ***$p<0.001$, NS, no significant difference. Data presented are mean ± SEM; *n* numbers are displayed above the bars.

# Abbreviations

| | |
|---|---|
| **°C** | Degrees Celsius |
| **µg** | Microgram |
| **µl** | Microlitre |
| **µm** | Micrometre |
| **µM** | Micromolar |
| **3D** | Three dimensional |
| **3-HK** | 3-hydroxykynurenine |
| **4E-BP** | 4E-binding protein |
| **6-OHDA** | 6-hydroxydopamine |
| **6-PTP** | 6-pyruvoyltetrahydropterin |
| **ABC** | ATP-binding cassette |
| **Acetyl CoA** | Acetyl coenzyme A |
| **Akt** | Protein kinase B |
| **ANOVA** | Analysis of variance |
| **AP-3** | Adaptor protein-3 |
| **ARM** | Armadillo repeats |
| **ATP** | Adenosine triphosphate |
| **BAC** | Bacterial artificial chromosome |
| **BBB** | Blood brain barrier |
| **$BH_4$** | Tetrahydrobiopterin |
| **BLOC** | Biogenesis of lysosome-related organelles complex |
| **bp** | Base pair |
| **BSA** | Bovine serum albumin |
| ***bw*** | *brown* |
| **$Ca^{2+}$** | Calcium |
| **$CaCl_2$** | Calcium chloride |
| **cAMP** | Cyclase adenosine monophosphate |
| **cDNA** | Complimentary deoxyribonucleic acid |
| **cGMP** | Cyclic guanosine monophosphate |
| **$Cl^-$** | Chloride |
| **cm** | Centimetre |
| ***cn*** | *cinnabar* |
| **CNS** | Central nervous system |
| **$CO_2$** | Carbon dioxide |
| **COR** | C-terminal of ROC |
| **CRF** | Contrast response function |
| **CS** | Canton-S |
| **DA** | Dopaminergic |
| **DAG** | Diacyl glycerol |
| **DCPIP** | Dichlorophenolindophenol |
| **$dH_2O$** | Distilled water |
| **dLRRK** | *Drosophila* Leucine-rich repeat kinase |
| **Dmef2** | *Drosophila* myocyte enhancer factor-2 |
| **DNA** | Deoxyribonucleic acid |
| **dNTP** | Deoxynucleotide triphosphate |
| **DPE** | Days post eclosion |

| | |
|---|---|
| **DTNB** | 5,5'-Dithiobis-(2-nitrobenzoic acid) |
| **DUA** | Dehydro (11,12) ursolic acid lactone |
| **ECL** | Enhanced chemiluminescence |
| ***E. coli*** | *Escherichia coli* |
| **EDTA** | Ethylenediaminetetraacetic acid |
| **EJP** | Excitatory junction potential |
| **elav** | Embryonic lethal, abnormal vision |
| **EOPD** | Early onset Parkinson's disease |
| **ERG** | Electroretinogram |
| **ETC** | Electron transport chain |
| **EtOH** | Ethanol |
| **$F_0$** | Parental generation |
| **$F_1$** | First generation |
| **$FADH_2$** | Flavin adenine dinucleotide |
| **$FeSO_4$** | Iron sulphate |
| **g** | Gram |
| ***g*** | Gravity |
| **GABA** | Gamma-aminobutyric acid |
| **GBA** | Glucocerebrosidase |
| **GCL** | Ganglion cell layer |
| **GDNF** | Glial cell-line-derived neurotrophic factor |
| **GFP** | Green fluorescent protein |
| **GOF** | Gain-of-function |
| **GTP** | Guanosine triphosphate |
| **GTPCH I** | Guanosine triphosphate cyclohydrolase I |
| **$H^+$** | Proton |
| **$H_2$-NTP** | 7,8-dihydroneopterin triphosphate |
| **$H_2O$** | Water |
| **HCl** | Hydrogen chloride |
| **HF** | High fidelity |
| **hLRRK1** | Human leucine-rich repeat kinase 1 |
| **hLRRK2** | Human leucine-rich repeat kinase 2 |
| **hrs** | Hours |
| **HRP** | Horseradish peroxidase |
| **Hz** | Hertz |
| **INL** | Inner nuclear layer |
| **$InsP_3$** | Inositol triphosphate |
| **IPL** | Inner plexiform layer |
| **kb** | Kilobase |
| **KCl** | Potassium chloride |
| **KCN** | Potassium cyanide |
| **kDa** | Kilodalton |
| **$KH_2PO_4$** | Monopotassium phosphate |
| **$KNaC_4H_4O_6 \cdot 4H_2O$** | Potassium sodium tartrate |
| **l** | Litre |
| **L1L2B** | Lamina monopolar cell 1 and 2 B |
| **LB** | Lewy bodies |
| **L-Broth** | Luria broth |
| **L-DOPA** | L-3,4-dihydroxyphenylalanine |

| | |
|---|---|
| **LED** | Light emitting diode |
| **LID** | Levodopa-induced dyskinesia |
| **LN** | Lewy neurites |
| **LOF** | Loss-of-function |
| **LongGMR** | Long glass multimer reporter |
| **LRR** | Leucine-rich repeat |
| ***ltd*** | *lightoid* |
| **mEPSCs** | Miniature excitatory postsynaptic currents |
| **mg** | Milligram |
| **$MgCl_2$** | Magnesium chloride |
| **min** | Minute |
| **ml** | Millilitre |
| **mLRRK1** | Mouse leucine-rich repeat kinase 1 |
| **mm** | Millimetre |
| **mM** | Millimolar |
| **MMP** | Mitochondrial membrane potential |
| **$MnCl_2$** | Manganese chloride |
| **$MPP^+$** | 1-methyl-4-phenylpyridinium |
| **MPTP** | 1-methyl-1,2,3,6-tetrahydropyridine |
| **mRNA** | Messenger ribonucleic acid |
| **ms** | Millisecond |
| **mt** | Mitochondria |
| **mV** | Millivolts |
| **MVBs** | Multivesicular bodies |
| **n/a** | Not applicable |
| **nA** | nanoampere |
| **NaCl** | Sodium chloride |
| **NADH** | Nicotinamide adenine dinucleotide |
| **NaOAc** | Sodium acetate |
| **NaOH** | Sodium hydroxide |
| **ng** | Nanogram |
| **nm** | Nanometre |
| **NM** | Non-manifesting |
| **NS** | Non-significant |
| **nsyb** | Neuronal synaptobrevin |
| **ONL** | Outer nuclear layer |
| **OPL** | Outer plexiform layer |
| **PCR** | Polymerase chain reaction |
| **PD** | Parkinson's disease |
| **PDA** | 6-acetyle-2-amino-3,7,8,9-tetrahydro-4*H*-pyrimido[4,5-*b*][1,4]diazepin-4-one |
| **PDK1** | Phosphoinositide-dependent kinase-1 |
| **pH** | Power of hydrogen |
| **PI3K** | Phosphatidylinositol 3-kinase |
| **PINK1** | Phosphatase and tensin homologue (PTEN)-induced putative kinase 1 |
| **PLC** | Phospholipase C |
| ***pu*** | *punch* |
| **PVDF** | Polyvinylidene fluoride |

| | |
|---|---|
| **R cells** | Photoreceptor cells |
| **Repo** | Reversed polarity |
| **RFP** | Red fluorescent protein |
| **RGC** | Retinal ganglion cell |
| **Rh1** | Rhodopsin-1 |
| **RNA** | Ribonucleic acid |
| **RNAi** | Ribonucleic acid interference |
| **ROC** | Ras of complex protein |
| **ROS** | Reactive oxygen species |
| **rpm** | Rotations per minute |
| **RT** | Room temperature |
| **sec** | Second |
| **SDS** | Sodium dodecyl sulfate |
| **SDS-PAGE** | Sodium dodecyl sulfate polyacrylamide gel electrophoresis |
| **SEM** | Standard error of the mean |
| **Ser** | Serine |
| **SN** | Substantia nigra |
| **SNpc** | Substantia nigra pars compacta |
| **SOC** | Super optimal broth with catabolite repression |
| **SSVEP** | Steady state visually evoked potential |
| **TBS** | Tris buffered saline |
| **TAE** | Tris acetate EDTA |
| **TE** | Tris-EDTA |
| **TH** | Tyrosine hydroxylase |
| **Thr** | Threonine |
| **$T_m$** | Melting temperature |
| **TRP** | Transient receptor potential |
| **TRPL** | Transient receptor potential like |
| **TUDCA** | Tauroursodeoxycholic acid |
| **UA** | Ursolic acid |
| **UAS** | Upstream activator sequence |
| **UCA** | Ursocholic acid |
| **UDCA** | Ursodeoxycholic acid |
| **V** | Volts |
| **vs** | Versus |
| **v/v** | Volume per volume |
| **WT** | Wild-type |
| **w/v** | Weight per volume |

# References


AASLY, J. O., VILARINO-GUELL, C., DACHSEL, J. C., WEBBER, P. J., WEST, A. B., HAUGARVOLL, K., JOHANSEN, K. K., TOFT, M., NUTT, J. G., PAYAMI, H., KACHERGUS, J. M., LINCOLN, S. J., FELIC, A., WIDER, C., SOTO-ORTOLAZA, A. I., COBB, S. A., WHITE, L. R., ROSS, O. A. & FARRER, M. J. 2010. Novel pathogenic LRRK2 p.Asn1437His substitution in familial Parkinson's disease. *Mov Disord,* 25**,** 2156-63.

ABCAM. 2016. *General western blot protocol* [Online]. Available: http://www.abcam.com/protocols/general-western-blot-protocol [Accessed 15 May 2016].

ADAMS, M. D., CELNIKER, S. E., HOLT, R. A., EVANS, C. A., GOCAYNE, J. D., AMANATIDES, P. G., SCHERER, S. E., LI, P. W., HOSKINS, R. A., GALLE, R. F., GEORGE, R. A., LEWIS, S. E., RICHARDS, S., ASHBURNER, M., HENDERSON, S. N., SUTTON, G. G., WORTMAN, J. R., YANDELL, M. D., ZHANG, Q., CHEN, L. X., BRANDON, R. C., ROGERS, Y. H., BLAZEJ, R. G., CHAMPE, M., PFEIFFER, B. D., WAN, K. H., DOYLE, C., BAXTER, E. G., HELT, G., NELSON, C. R., GABOR, G. L., ABRIL, J. F., AGBAYANI, A., AN, H. J., ANDREWS-PFANNKOCH, C., BALDWIN, D., BALLEW, R. M., BASU, A., BAXENDALE, J., BAYRAKTAROGLU, L., BEASLEY, E. M., BEESON, K. Y., BENOS, P. V., BERMAN, B. P., BHANDARI, D., BOLSHAKOV, S., BORKOVA, D., BOTCHAN, M. R., BOUCK, J., BROKSTEIN, P., BROTTIER, P., BURTIS, K. C., BUSAM, D. A., BUTLER, H., CADIEU, E., CENTER, A., CHANDRA, I., CHERRY, J. M., CAWLEY, S., DAHLKE, C., DAVENPORT, L. B., DAVIES, P., DE PABLOS, B., DELCHER, A., DENG, Z., MAYS, A. D., DEW, I., DIETZ, S. M., DODSON, K., DOUP, L. E., DOWNES, M., DUGAN-ROCHA, S., DUNKOV, B. C., DUNN, P., DURBIN, K. J., EVANGELISTA, C. C., FERRAZ, C., FERRIERA, S., FLEISCHMANN, W., FOSLER, C., GABRIELIAN, A. E., GARG, N. S., GELBART, W. M., GLASSER, K., GLODEK, A., GONG, F., GORRELL, J. H., GU, Z., GUAN, P., HARRIS, M., HARRIS, N. L., HARVEY, D., HEIMAN, T. J., HERNANDEZ, J. R., HOUCK, J., HOSTIN, D., HOUSTON, K. A., HOWLAND, T. J., WEI, M. H., IBEGWAM, C., et al. 2000. The genome sequence of Drosophila melanogaster. *Science,* 287**,** 2185-95.

ADAMS, M. D. & SEKELSKY, J. J. 2002. From sequence to phenotype: reverse genetics in Drosophila melanogaster. *Nat Rev Genet,* 3**,** 189-98.

AFSARI, F., CHRISTENSEN, K. V., SMITH, G. P., HENTZER, M., NIPPE, O. M., ELLIOTT, C. J. & WADE, A. R. 2014. Abnormal visual gain control in a Parkinson's disease model. *Hum Mol Genet,* 23**,** 4465-78.

AGUZZI, A. & RAJENDRAN, L. 2009. The transcellular spread of cytosolic amyloids, prions, and prionoids. *Neuron,* 64**,** 783-90.

AIRAKSINEN, M. S. & SAARMA, M. 2002. The GDNF family: signalling, biological functions and therapeutic value. *Nat Rev Neurosci,* 3**,** 383-94.

ALCALAY, R. N., MEJIA-SANTANA, H., TANG, M. X., RAKITIN, B., ROSADO, L., ROSS, B., VERBITSKY, M., KISSELEV, S., LOUIS, E. D., COMELLA, C. L., COLCHER, A., JENNINGS, D., NANCE, M. A., BRESSMAN, S., SCOTT, W. K., TANNER, C., MICKEL, S. F., ANDREWS, H. F., WATERS, C. H., FAHN, S., COTE, L. J., FRUCHT, S. J., FORD, B., REZAK, M., NOVAK, K., FRIEDMAN, J. H., PFEIFFER, R., MARSH, L., HINER, B., SIDEROWF, A., OTTMAN, R., CLARK, L. N., MARDER, K. S. & CACCAPPOLO, E. 2010. Self-report of cognitive impairment and mini-mental state

examination performance in PRKN, LRRK2, and GBA carriers with early onset Parkinson's disease. *J Clin Exp Neuropsychol,* 32**,** 775-9.

ALEGRE-ABARRATEGUI, J., CHRISTIAN, H., LUFINO, M. M., MUTIHAC, R., VENDA, L. L., ANSORGE, O. & WADE-MARTINS, R. 2009. LRRK2 regulates autophagic activity and localizes to specific membrane microdomains in a novel human genomic reporter cellular model. *Hum Mol Genet,* 18**,** 4022-34.

ALVAREZ-ERVITI, L., SEOW, Y., SCHAPIRA, A. H., GARDINER, C., SARGENT, I. L., WOOD, M. J. & COOPER, J. M. 2011. Lysosomal dysfunction increases exosome-mediated alpha-synuclein release and transmission. *Neurobiol Dis,* 42**,** 360-7.

ALVES DA COSTA, C., DUNYS, J., BRAU, F., WILK, S., CAPPAI, R. & CHECLER, F. 2006. 6-Hydroxydopamine but not 1-methyl-4-phenylpyridinium abolishes alpha-synuclein anti-apoptotic phenotype by inhibiting its proteasomal degradation and by promoting its aggregation. *J Biol Chem,* 281**,** 9824-31.

AMICK, M. M., CRONIN-GOLOMB, A. & GILMORE, G. C. 2003. Visual processing of rapidly presented stimuli is normalized in Parkinson's disease when proximal stimulus strength is enhanced. *Vision Res,* 43**,** 2827-35.

ANDRES-MATEOS, E., MEJIAS, R., SASAKI, M., LI, X., LIN, B. M., BISKUP, S., ZHANG, L., BANERJEE, R., THOMAS, B., YANG, L., LIU, G., BEAL, M. F., HUSO, D. L., DAWSON, T. M. & DAWSON, V. L. 2009. Unexpected lack of hypersensitivity in LRRK2 knock-out mice to MPTP (1-methyl-4-phenyl-1,2,3,6-tetrahydropyridine). *J Neurosci,* 29**,** 15846-50.

ARCHIBALD, N. K., CLARKE, M. P., MOSIMANN, U. P. & BURN, D. J. 2009. The retina in Parkinson's disease. *Brain,* 132**,** 1128-45.

ARMSTRONG, R. A. 2015. Oculo-Visual Dysfunction in Parkinson's Disease. *J Parkinsons Dis,* 5**,** 715-26.

ARRANZ, A. M., DELBROEK, L., VAN KOLEN, K., GUIMARAES, M. R., MANDEMAKERS, W., DANEELS, G., MATTA, S., CALAFATE, S., SHABAN, H., BAATSEN, P., DE BOCK, P. J., GEVAERT, K., BERGHE, P. V., VERSTREKEN, P., DE STROOPER, B. & MOECHARS, D. 2015. LRRK2 functions in synaptic vesicle endocytosis through a kinase-dependent mechanism. *J Cell Sci,* 128**,** 541-52.

ASADOLLAHI, A., MYSORE, S. P. & KNUDSEN, E. I. 2010. Stimulus-driven competition in a cholinergic midbrain nucleus. *Nat Neurosci,* 13**,** 889-95.

BANG, C. & THUM, T. 2012. Exosomes: new players in cell-cell communication. *Int J Biochem Cell Biol,* 44**,** 2060-4.

BEILINA, A., RUDENKO, I. N., KAGANOVICH, A., CIVIERO, L., CHAU, H., KALIA, S. K., KALIA, L. V., LOBBESTAEL, E., CHIA, R., NDUKWE, K., DING, J., NALLS, M. A., OLSZEWSKI, M., HAUSER, D. N., KUMARAN, R., LOZANO, A. M., BAEKELANDT, V., GREENE, L. E., TAYMANS, J. M., GREGGIO, E. & COOKSON, M. R. 2014. Unbiased screen for interactors of leucine-rich repeat kinase 2 supports a common pathway for sporadic and familial Parkinson disease. *Proc Natl Acad Sci U S A,* 111**,** 2626-31.

BELLACOSA, A., TESTA, J. R., STAAL, S. P. & TSICHLIS, P. N. 1991. A retroviral oncogene, akt, encoding a serine-threonine kinase containing an SH2-like region. *Science,* 254**,** 274-7.

BELLINGHAM, S. A., GUO, B. B., COLEMAN, B. M. & HILL, A. F. 2012. Exosomes: vehicles for the transfer of toxic proteins associated with neurodegenerative diseases? *Front Physiol,* 3**,** 124.

BERGER, Z., SMITH, K. A. & LAVOIE, M. J. 2010. Membrane localization of LRRK2 is associated with increased formation of the highly active LRRK2 dimer and changes in its phosphorylation. *Biochemistry,* 49**,** 5511-23.

BERNIS, M. E., BABILA, J. T., BREID, S., WÜSTEN, K. A., WÜLLNER, U. & TAMGÜNEY, G. 2015. Prion-like propagation of human brain-derived alpha-synuclein in transgenic mice expressing human wild-type alpha-synuclein. *Acta Neuropathol Commun,* 3.

BERWICK, D. C. & HARVEY, K. 2011. LRRK2 signaling pathways: the key to unlocking neurodegeneration? *Trends Cell Biol,* 21**,** 257-65.

BIER, E. 2005. Drosophila, the golden bug, emerges as a tool for human genetics. *Nat Rev Genet,* 6**,** 9-23.

BIER, E., VAESSIN, H., SHEPHERD, S., LEE, K., MCCALL, K., BARBEL, S., ACKERMAN, L., CARRETTO, R., UEMURA, T., GRELL, E. & ET AL. 1989. Searching for pattern and mutation in the Drosophila genome with a P-lacZ vector. *Genes Dev,* 3**,** 1273-87.

BIRCH-MACHIN, M. A., BRIGGS, H. L., SABORIDO, A. A., BINDOFF, L. A. & TURNBULL, D. M. 1994. An evaluation of the measurement of the activities of complexes I-IV in the respiratory chain of human skeletal muscle mitochondria. *Biochem Med Metab Biol,* 51**,** 35-42.

BISKUP, S., MOORE, D. J., CELSI, F., HIGASHI, S., WEST, A. B., ANDRABI, S. A., KURKINEN, K., YU, S. W., SAVITT, J. M., WALDVOGEL, H. J., FAULL, R. L., EMSON, P. C., TORP, R., OTTERSEN, O. P., DAWSON, T. M. & DAWSON, V. L. 2006. Localization of LRRK2 to membranous and vesicular structures in mammalian brain. *Ann Neurol,* 60**,** 557-69.

BLANDINI, F. & ARMENTERO, M. T. 2012. Animal models of Parkinson's disease. *Febs j,* 279**,** 1156-66.

BLANDINI, F., ARMENTERO, M. T. & MARTIGNONI, E. 2008. The 6-hydroxydopamine model: news from the past. *Parkinsonism Relat Disord,* 14 Suppl 2**,** S124-9.

BLOOMFIELD, S. A. & DACHEUX, R. F. 2001. Rod vision: pathways and processing in the mammalian retina. *Prog Retin Eye Res,* 20**,** 351-84.

BOATRIGHT, J. H., MORING, A. G., MCELROY, C., PHILLIPS, M. J., DO, V. T., CHANG, B., HAWES, N. L., BOYD, A. P., SIDNEY, S. S., STEWART, R. E., MINEAR, S. C., CHAUDHURY, R., CIAVATTA, V. T., RODRIGUES, C. M., STEER, C. J., NICKERSON, J. M. & PARDUE, M. T. 2006. Tool from ancient pharmacopoeia prevents vision loss. *Mol Vis,* 12**,** 1706-14.

BODIS-WOLLNER, I., MARX, M. S., MITRA, S., BOBAK, P., MYLIN, L. & YAHR, M. 1987. Visual dysfunction in Parkinson's disease. Loss in spatiotemporal contrast sensitivity. *Brain,* 110 ( Pt 6)**,** 1675-98.

BODIS-WOLLNER, I. & TZELEPI, A. 1998. The push-pull action of dopamine on spatial tuning of the monkey retina: the effects of dopaminergic deficiency and selective D1 and D2 receptor ligands on the pattern electroretinogram. *Vision Res,* 38**,** 1479-87.

BONDA, D. J., MAILANKOT, M., STONE, J. G., GARRETT, M. R., STANISZEWSKA, M., CASTELLANI, R. J., SIEDLAK, S. L., ZHU, X., LEE, H. G., PERRY, G., NAGARAJ, R. H. & SMITH, M. A. 2010. Indoleamine 2,3-dioxygenase and 3-hydroxykynurenine modifications are found in the neuropathology of Alzheimer's disease. *Redox Rep,* 15**,** 161-8.

BONIFATI, V., RIZZU, P., VAN BAREN, M. J., SCHAAP, O., BREEDVELD, G. J., KRIEGER, E., DEKKER, M. C., SQUITIERI, F., IBANEZ, P., JOOSSE, M., VAN DONGEN, J. W.,

VANACORE, N., VAN SWIETEN, J. C., BRICE, A., MECO, G., VAN DUIJN, C. M., OOSTRA, B. A. & HEUTINK, P. 2003. Mutations in the DJ-1 gene associated with autosomal recessive early-onset parkinsonism. *Science,* 299**,** 256-9.

BORST, A. 2009. Drosophila's view on insect vision. *Curr Biol,* 19**,** R36-47.

BORYCZ, J., BORYCZ, J. A., KUBÓW, A., LLOYD, V. & MEINERTZHAGEN, I. A. 2008. Drosophila ABC transporter mutants white, brown and scarlet have altered contents and distribution of biogenic amines in the brain. *Journal of Experimental Biology,* 211**,** 3454-3466.

BRAAK, H., DEL TREDICI, K., RUB, U., DE VOS, R. A., JANSEN STEUR, E. N. & BRAAK, E. 2003. Staging of brain pathology related to sporadic Parkinson's disease. *Neurobiol Aging,* 24**,** 197-211.

BRAAK, H., GHEBREMEDHIN, E., RUB, U., BRATZKE, H. & DEL TREDICI, K. 2004. Stages in the development of Parkinson's disease-related pathology. *Cell Tissue Res,* 318**,** 121-34.

BRAND, A. H. & PERRIMON, N. 1993. Targeted gene expression as a means of altering cell fates and generating dominant phenotypes. *Development,* 118**,** 401-15.

BRAS, J. M., GUERREIRO, R. J., RIBEIRO, M. H., JANUARIO, C., MORGADINHO, A., OLIVEIRA, C. R., CUNHA, L., HARDY, J. & SINGLETON, A. 2005. G2019S dardarin substitution is a common cause of Parkinson's disease in a Portuguese cohort. *Mov Disord,* 20**,** 1653-5.

BRAVO-SAN PEDRO, J. M., NISO-SANTANO, M., GOMEZ-SANCHEZ, R., PIZARRO-ESTRELLA, E., AIASTUI-PUJANA, A., GOROSTIDI, A., CLIMENT, V., LOPEZ DE MATURANA, R., SANCHEZ-PERNAUTE, R., LOPEZ DE MUNAIN, A., FUENTES, J. M. & GONZALEZ-POLO, R. A. 2013. The LRRK2 G2019S mutant exacerbates basal autophagy through activation of the MEK/ERK pathway. *Cell Mol Life Sci,* 70**,** 121-36.

BREDA, C., SATHYASAIKUMAR, K. V., SOGRATE IDRISSI, S., NOTARANGELO, F. M., ESTRANERO, J. G., MOORE, G. G., GREEN, E. W., KYRIACOU, C. P., SCHWARCZ, R. & GIORGINI, F. 2016. Tryptophan-2,3-dioxygenase (TDO) inhibition ameliorates neurodegeneration by modulation of kynurenine pathway metabolites. *Proc Natl Acad Sci U S A,* 113**,** 5435-40.

BULENS, C., MEERWALDT, J. D. & VAN DER WILDT, G. J. 1988. Effect of stimulus orientation on contrast sensitivity in Parkinson's disease. *Neurology,* 38**,** 76-81.

BURNS, R. S., LEWITT, P. A., EBERT, M. H., PAKKENBERG, H. & KOPIN, I. J. 1985. The clinical syndrome of striatal dopamine deficiency. Parkinsonism induced by 1-methyl-4-phenyl-1,2,3,6-tetrahydropyridine (MPTP). *N Engl J Med,* 312**,** 1418-21.

BUSSE, L., WADE, A. R. & CARANDINI, M. 2009. Representation of concurrent stimuli by population activity in visual cortex. *Neuron,* 64**,** 931-42.

CAJAL, S. R. S., D. 1915. Contribucion al conocimiento de los centros nerviosos de los insectos. *Trab. Lab. Inv. Biol.,* 13**,** 1-68.

CAMPESAN, S., GREEN, E. W., BREDA, C., SATHYASAIKUMAR, K. V., MUCHOWSKI, P. J., SCHWARCZ, R., KYRIACOU, C. P. & GIORGINI, F. 2011. The kynurenine pathway modulates neurodegeneration in a Drosophila model of Huntington's disease. *Curr Biol,* 21**,** 961-6.

CANDY, T. R., SKOCZENSKI, A. M. & NORCIA, A. M. 2001. Normalization models applied to orientation masking in the human infant. *J Neurosci,* 21**,** 4530-41.

CASTRO-CALDAS, M., CARVALHO, A. N., RODRIGUES, E., HENDERSON, C. J., WOLF, C. R., RODRIGUES, C. M. & GAMA, M. J. 2012. Tauroursodeoxycholic acid prevents MPTP-induced dopaminergic cell death in a mouse model of Parkinson's disease. *Mol Neurobiol,* 46**,** 475-86.

CAUCHI, R. J. & VAN DEN HEUVEL, M. 2006. The fly as a model for neurodegenerative diseases: is it worth the jump? *Neurodegener Dis,* 3**,** 338-56.

CERIANI, M. F., HOGENESCH, J. B., YANOVSKY, M., PANDA, S., STRAUME, M. & KAY, S. A. 2002. Genome-wide expression analysis in Drosophila reveals genes controlling circadian behavior. *J Neurosci,* 22**,** 9305-19.

CHA, G. H., KIM, S., PARK, J., LEE, E., KIM, M., LEE, S. B., KIM, J. M., CHUNG, J. & CHO, K. S. 2005. Parkin negatively regulates JNK pathway in the dopaminergic neurons of Drosophila. *Proc Natl Acad Sci U S A,* 102**,** 10345-50.

CHAN, D., CITRO, A., CORDY, J. M., SHEN, G. C. & WOLOZIN, B. 2011. Rac1 protein rescues neurite retraction caused by G2019S leucine-rich repeat kinase 2 (LRRK2). *J Biol Chem,* 286**,** 16140-9.

CHANG, H. Y., GRYGORUK, A., BROOKS, E. S., ACKERSON, L. C., MAIDMENT, N. T., BAINTON, R. J. & KRANTZ, D. E. 2006. Overexpression of the Drosophila vesicular monoamine transporter increases motor activity and courtship but decreases the behavioral response to cocaine. *Mol Psychiatry,* 11**,** 99-113.

CHARTIER-HARLIN, M. C., DACHSEL, J. C., VILARINO-GUELL, C., LINCOLN, S. J., LEPRETRE, F., HULIHAN, M. M., KACHERGUS, J., MILNERWOOD, A. J., TAPIA, L., SONG, M. S., LE RHUN, E., MUTEZ, E., LARVOR, L., DUFLOT, A., VANBESIEN-MAILLIOT, C., KREISLER, A., ROSS, O. A., NISHIOKA, K., SOTO-ORTOLAZA, A. I., COBB, S. A., MELROSE, H. L., BEHROUZ, B., KEELING, B. H., BACON, J. A., HENTATI, E., WILLIAMS, L., YANAGIYA, A., SONENBERG, N., LOCKHART, P. J., ZUBAIR, A. C., UITTI, R. J., AASLY, J. O., KRYGOWSKA-WAJS, A., OPALA, G., WSZOLEK, Z. K., FRIGERIO, R., MARAGANORE, D. M., GOSAL, D., LYNCH, T., HUTCHINSON, M., BENTIVOGLIO, A. R., VALENTE, E. M., NICHOLS, W. C., PANKRATZ, N., FOROUD, T., GIBSON, R. A., HENTATI, F., DICKSON, D. W., DESTEE, A. & FARRER, M. J. 2011. Translation initiator EIF4G1 mutations in familial Parkinson disease. *Am J Hum Genet,* 89**,** 398-406.

CHAUDHURI, A., BOWLING, K., FUNDERBURK, C., LAWAL, H., INAMDAR, A., WANG, Z. & O'DONNELL, J. M. 2007. Interaction of genetic and environmental factors in a Drosophila parkinsonism model. *J Neurosci,* 27**,** 2457-67.

CHELI, V. T., DANIELS, R. W., GODOY, R., HOYLE, D. J., KANDACHAR, V., STARCEVIC, M., MARTINEZ-AGOSTO, J. A., POOLE, S., DIANTONIO, A., LLOYD, V. K., CHANG, H. C., KRANTZ, D. E. & DELL'ANGELICA, E. C. 2010. Genetic modifiers of abnormal organelle biogenesis in a Drosophila model of BLOC-1 deficiency. *Hum Mol Genet,* 19**,** 861-78.

CHEN, D. M., CHRISTIANSON, J. S., SAPP, R. J. & STARK, W. S. 1992. Visual receptor cycle in normal and period mutant Drosophila: microspectrophotometry, electrophysiology, and ultrastructural morphometry. *Visual Neuroscience,* 9**,** 125-35.

CHEN, S., ZHANG, X., YANG, D., DU, Y., LI, L., LI, X., MING, M. & LE, W. 2008. D2/D3 receptor agonist ropinirole protects dopaminergic cell line against rotenone-induced apoptosis through inhibition of caspase- and JNK-dependent pathways. *FEBS Lett,* 582**,** 603-10.

CHIUEH, C. C., MARKEY, S. P., BURNS, R. S., JOHANNESSEN, J. N., JACOBOWITZ, D. M. & KOPIN, I. J. 1984. Neurochemical and behavioral effects of 1-methyl-4-

phenyl-1,2,3,6- tetrahydropyridine (MPTP) in rat, guinea pig, and monkey. *Psychopharmacol Bull,* 20**,** 548-53.
CHU, Y. & KORDOWER, J. H. 2015. The prion hypothesis of Parkinson's disease. *Curr Neurol Neurosci Rep,* 15**,** 28.
CHUN, H. S. & LOW, W. C. 2012. Ursodeoxycholic acid suppresses mitochondria-dependent programmed cell death induced by sodium nitroprusside in SH-SY5Y cells. *Toxicology,* 292**,** 105-12.
CHUNG, J. Y., LEE, S. J., LEE, S. H., JUNG, Y. S., HA, N. C., SEOL, W. & PARK, B. J. 2011. Direct interaction of alpha-synuclein and AKT regulates IGF-1 signaling: implication of Parkinson disease. *Neurosignals,* 19**,** 86-96.
CHYB, S., HEVERS, W., FORTE, M., WOLFGANG, W. J., SELINGER, Z. & HARDIE, R. C. 1999. Modulation of the light response by cAMP in Drosophila photoreceptors. *J Neurosci,* 19**,** 8799-807.
CLARK, I. E., DODSON, M. W., JIANG, C., CAO, J. H., HUH, J. R., SEOL, J. H., YOO, S. J., HAY, B. A. & GUO, M. 2006. Drosophila pink1 is required for mitochondrial function and interacts genetically with parkin. *Nature,* 441**,** 1162-6.
COLEMAN, B. M., HANSSEN, E., LAWSON, V. A. & HILL, A. F. 2012. Prion-infected cells regulate the release of exosomes with distinct ultrastructural features. *Faseb j,* 26**,** 4160-73.
COLIN, E., REGULIER, E., PERRIN, V., DURR, A., BRICE, A., AEBISCHER, P., DEGLON, N., HUMBERT, S. & SAUDOU, F. 2005. Akt is altered in an animal model of Huntington's disease and in patients. *Eur J Neurosci,* 21**,** 1478-88.
COOMBE, P. E. 1986. The large monopolar cells L1 and L2 are responsible for ERG transients inDrosophila. *Journal of Comparative Physiology A,* 159**,** 655-665.
COOPER, A. A., GITLER, A. D., CASHIKAR, A., HAYNES, C. M., HILL, K. J., BHULLAR, B., LIU, K., XU, K., STRATHEARN, K. E., LIU, F., CAO, S., CALDWELL, K. A., CALDWELL, G. A., MARSISCHKY, G., KOLODNER, R. D., LABAER, J., ROCHET, J. C., BONINI, N. M. & LINDQUIST, S. 2006. Alpha-synuclein blocks ER-Golgi traffic and Rab1 rescues neuron loss in Parkinson's models. *Science,* 313**,** 324-8.
CORREIA GUEDES, L., FERREIRA, J. J., ROSA, M. M., COELHO, M., BONIFATI, V. & SAMPAIO, C. 2010. Worldwide frequency of G2019S LRRK2 mutation in Parkinson's disease: a systematic review. *Parkinsonism Relat Disord,* 16**,** 237-42.
COTZIAS, G. C., PAPAVASILIOU, P. S. & GELLENE, R. 1969. Modification of Parkinsonism--chronic treatment with L-dopa. *N Engl J Med,* 280**,** 337-45.
COULOM, H. & BIRMAN, S. 2004. Chronic exposure to rotenone models sporadic Parkinson's disease in Drosophila melanogaster. *J Neurosci,* 24**,** 10993-8.
COVY, J. P. & GIASSON, B. I. 2009. Identification of compounds that inhibit the kinase activity of leucine-rich repeat kinase 2. *Biochem Biophys Res Commun,* 378**,** 473-7.
COWLES, C. R., ODORIZZI, G., PAYNE, G. S. & EMR, S. D. 1997. The AP-3 Adaptor Complex Is Essential for Cargo-Selective Transport to the Yeast Vacuole. *Cell,* 91**,** 109-118.
CROUCHER, P. J., BREWER, M. S., WINCHELL, C. J., OXFORD, G. S. & GILLESPIE, R. G. 2013. De novo characterization of the gene-rich transcriptomes of two color-polymorphic spiders, Theridion grallator and T. californicum (Araneae: Theridiidae), with special reference to pigment genes. *BMC Genomics,* 14**,** 862.
DACEY, D. M. 1990. The dopaminergic amacrine cell. *J Comp Neurol,* 301**,** 461-89.

DAGDA, R. K., CHERRA, S. J., 3RD, KULICH, S. M., TANDON, A., PARK, D. & CHU, C. T. 2009. Loss of PINK1 function promotes mitophagy through effects on oxidative stress and mitochondrial fission. *J Biol Chem,* 284**,** 13843-55.

DANIELS, V., VANCRAENENBROECK, R., LAW, B. M., GREGGIO, E., LOBBESTAEL, E., GAO, F., DE MAEYER, M., COOKSON, M. R., HARVEY, K., BAEKELANDT, V. & TAYMANS, J. M. 2011. Insight into the mode of action of the LRRK2 Y1699C pathogenic mutant. *J Neurochem,* 116**,** 304-15.

DAVIDSDOTTIR, S., CRONIN-GOLOMB, A. & LEE, A. 2005. Visual and spatial symptoms in Parkinson's disease. *Vision Res,* 45**,** 1285-96.

DAWSON, T. M. & DAWSON, V. L. 2010. The role of parkin in familial and sporadic Parkinson's disease. *Mov Disord,* 25 Suppl 1**,** S32-9.

DAWSON, T. M., KO, H. S. & DAWSON, V. L. 2010. Genetic animal models of Parkinson's disease. *Neuron,* 66**,** 646-61.

DELL'ANGELICA, E. C., MULLINS, C., CAPLAN, S. & BONIFACINO, J. S. 2000. Lysosome-related organelles. *Faseb j,* 14**,** 1265-78.

DENG, H., DODSON, M. W., HUANG, H. & GUO, M. 2008. The Parkinson's disease genes pink1 and parkin promote mitochondrial fission and/or inhibit fusion in Drosophila. *Proc Natl Acad Sci U S A,* 105**,** 14503-8.

DENG, X., DZAMKO, N., PRESCOTT, A., DAVIES, P., LIU, Q., YANG, Q., LEE, J. D., PATRICELLI, M. P., NOMANBHOY, T. K., ALESSI, D. R. & GRAY, N. S. 2011. Characterization of a selective inhibitor of the Parkinson's disease kinase LRRK2. *Nat Chem Biol,* 7**,** 203-5.

DESHAIES, R. J. & JOAZEIRO, C. A. 2009. RING domain E3 ubiquitin ligases. *Annu Rev Biochem,* 78**,** 399-434.

DESPLATS, P., LEE, H. J., BAE, E. J., PATRICK, C., ROCKENSTEIN, E., CREWS, L., SPENCER, B., MASLIAH, E. & LEE, S. J. 2009. Inclusion formation and neuronal cell death through neuron-to-neuron transmission of alpha-synuclein. *Proc Natl Acad Sci U S A,* 106**,** 13010-5.

DI FONZO, A., CHIEN, H. F., SOCAL, M., GIRAUDO, S., TASSORELLI, C., ILICETO, G., FABBRINI, G., MARCONI, R., FINCATI, E., ABBRUZZESE, G., MARINI, P., SQUITIERI, F., HORSTINK, M. W., MONTAGNA, P., LIBERA, A. D., STOCCHI, F., GOLDWURM, S., FERREIRA, J. J., MECO, G., MARTIGNONI, E., LOPIANO, L., JARDIM, L. B., OOSTRA, B. A., BARBOSA, E. R. & BONIFATI, V. 2007. ATP13A2 missense mutations in juvenile parkinsonism and young onset Parkinson disease. *Neurology,* 68**,** 1557-62.

DIEDERICH, N. J., GOETZ, C. G., RAMAN, R., PAPPERT, E. J., LEURGANS, S. & PIERY, V. 1998. Poor visual discrimination and visual hallucinations in Parkinson's disease. *Clin Neuropharmacol,* 21**,** 289-95.

DODSON, M. W., LEUNG, L. K., LONE, M., LIZZIO, M. A. & GUO, M. 2014. Novel ethyl methanesulfonate (EMS)-induced null alleles of the Drosophila homolog of LRRK2 reveal a crucial role in endolysosomal functions and autophagy in vivo. *Dis Model Mech,* 7**,** 1351-63.

DODSON, M. W., ZHANG, T., JIANG, C., CHEN, S. & GUO, M. 2012. Roles of the Drosophila LRRK2 homolog in Rab7-dependent lysosomal positioning. *Hum Mol Genet,* 21**,** 1350-63.

DOREY, S. E., NEVEU, M. M., BURTON, L. C., SLOPER, J. J. & HOLDER, G. E. 2003. The clinical features of albinism and their correlation with visual evoked potentials. *Br J Ophthalmol,* 87**,** 767-72.

DOWLING, J. E. & RIPPS, H. 1973. Effect of magnesium on horizontal cell activity in the skate retina. *Nature,* 242**,** 101-3.
DOYLE, S. E., GRACE, M. S., MCIVOR, W. & MENAKER, M. 2002a. Circadian rhythms of dopamine in mouse retina: the role of melatonin. *Vis Neurosci,* 19**,** 593-601.
DOYLE, S. E., MCIVOR, W. E. & MENAKER, M. 2002b. Circadian rhythmicity in dopamine content of mammalian retina: role of the photoreceptors. *J Neurochem,* 83**,** 211-9.
DREESEN, T. D., JOHNSON, D. H. & HENIKOFF, S. 1988. The brown protein of Drosophila melanogaster is similar to the white protein and to components of active transport complexes. *Mol Cell Biol,* 8**,** 5206-15.
DUAN, W. M., RODRIGUES, C. M., ZHAO, L. R., STEER, C. J. & LOW, W. C. 2002. Tauroursodeoxycholic acid improves the survival and function of nigral transplants in a rat model of Parkinson's disease. *Cell Transplant,* 11**,** 195-205.
DUTY, S. & JENNER, P. 2011. Animal models of Parkinson's disease: a source of novel treatments and clues to the cause of the disease. *Br J Pharmacol,* 164**,** 1357-91.
DZAMKO, N., INESTA-VAQUERA, F., ZHANG, J., XIE, C., CAI, H., ARTHUR, S., TAN, L., CHOI, H., GRAY, N., COHEN, P., PEDRIOLI, P., CLARK, K. & ALESSI, D. R. 2012. The IkappaB kinase family phosphorylates the Parkinson's disease kinase LRRK2 at Ser935 and Ser910 during Toll-like receptor signaling. *PLoS One,* 7**,** e39132.
EDWARDS, T. N. & MEINERTZHAGEN, I. A. 2010. The functional organisation of glia in the adult brain of Drosophila and other insects. *Prog Neurobiol,* 90**,** 471-97.
ELLIOTT, D. A. & BRAND, A. H. 2008. The GAL4 system : a versatile system for the expression of genes. *Methods Mol Biol,* 420**,** 79-95.
EMERY, P. 2007. Protein extraction from Drosophila heads. *Methods Mol Biol,* 362**,** 375-7.
EMMANOUILIDOU, E., MELACHROINOU, K., ROUMELIOTIS, T., GARBIS, S. D., NTZOUNI, M., MARGARITIS, L. H., STEFANIS, L. & VEKRELLIS, K. 2010. Cell-Produced $\alpha$-Synuclein Is Secreted in a Calcium-Dependent Manner by Exosomes and Impacts Neuronal Survival. *J Neurosci,* 30**,** 6838-51.
EWART, G. D. & HOWELLS, A. J. 1998. ABC transporters involved in transport of eye pigment precursors in Drosophila melanogaster. *Methods Enzymol,* 292**,** 213-24.
EXNER, N., LUTZ, A. K., HAASS, C. & WINKLHOFER, K. F. 2012. Mitochondrial dysfunction in Parkinson's disease: molecular mechanisms and pathophysiological consequences. *Embo j,* 31**,** 3038-62.
EXNER, N., TRESKE, B., PAQUET, D., HOLMSTROM, K., SCHIESLING, C., GISPERT, S., CARBALLO-CARBAJAL, I., BERG, D., HOEPKEN, H. H., GASSER, T., KRUGER, R., WINKLHOFER, K. F., VOGEL, F., REICHERT, A. S., AUBURGER, G., KAHLE, P. J., SCHMID, B. & HAASS, C. 2007. Loss-of-function of human PINK1 results in mitochondrial pathology and can be rescued by parkin. *J Neurosci,* 27**,** 12413-8.
FALLON, L., BELANGER, C. M., CORERA, A. T., KONTOGIANNEA, M., REGAN-KLAPISZ, E., MOREAU, F., VOORTMAN, J., HABER, M., ROULEAU, G., THORARINSDOTTIR, T., BRICE, A., VAN BERGEN EN HENEGOUWEN, P. M. & FON, E. A. 2006. A regulated interaction with the UIM protein Eps15 implicates parkin in EGF receptor trafficking and PI(3)K-Akt signalling. *Nat Cell Biol,* 8**,** 834-42.

FARRER, M. J. 2006. Genetics of Parkinson disease: paradigm shifts and future prospects. *Nat Rev Genet,* 7**,** 306-18.

FEANY, M. B. & BENDER, W. W. 2000. A Drosophila model of Parkinson's disease. *Nature,* 404**,** 394-8.

FERRE, J., SILVA, F. J., REAL, M. D. & MENSUA, J. L. 1986. Pigment patterns in mutants affecting the biosynthesis of pteridines and xanthommatin in Drosophila melanogaster. *Biochem Genet,* 24**,** 545-69.

FEVRIER, B., VILETTE, D., ARCHER, F., LOEW, D., FAIGLE, W., VIDAL, M., LAUDE, H. & RAPOSO, G. 2004. Cells release prions in association with exosomes. *Proc Natl Acad Sci U S A,* 101**,** 9683-8.

FISCHBACH, K. F. & DITTRICH, A. P. M. 1989. The optic lobe of Drosophila melanogaster. I. A Golgi analysis of wild-type structure. *Cell and Tissue Research,* 258**,** 441-475.

FOX, S. H., KATZENSCHLAGER, R., LIM, S. Y., RAVINA, B., SEPPI, K., COELHO, M., POEWE, W., RASCOL, O., GOETZ, C. G. & SAMPAIO, C. 2011. The Movement Disorder Society Evidence-Based Medicine Review Update: Treatments for the motor symptoms of Parkinson's disease. *Mov Disord,* 26 Suppl 3**,** S2-41.

FRANKE, A., MCGOVERN, D. P., BARRETT, J. C., WANG, K., RADFORD-SMITH, G. L., AHMAD, T., LEES, C. W., BALSCHUN, T., LEE, J., ROBERTS, R., ANDERSON, C. A., BIS, J. C., BUMPSTEAD, S., ELLINGHAUS, D., FESTEN, E. M., GEORGES, M., GREEN, T., HARITUNIANS, T., JOSTINS, L., LATIANO, A., MATHEW, C. G., MONTGOMERY, G. W., PRESCOTT, N. J., RAYCHAUDHURI, S., ROTTER, J. I., SCHUMM, P., SHARMA, Y., SIMMS, L. A., TAYLOR, K. D., WHITEMAN, D., WIJMENGA, C., BALDASSANO, R. N., BARCLAY, M., BAYLESS, T. M., BRAND, S., BUNING, C., COHEN, A., COLOMBEL, J. F., COTTONE, M., STRONATI, L., DENSON, T., DE VOS, M., D'INCA, R., DUBINSKY, M., EDWARDS, C., FLORIN, T., FRANCHIMONT, D., GEARRY, R., GLAS, J., VAN GOSSUM, A., GUTHERY, S. L., HALFVARSON, J., VERSPAGET, H. W., HUGOT, J. P., KARBAN, A., LAUKENS, D., LAWRANCE, I., LEMANN, M., LEVINE, A., LIBIOULLE, C., LOUIS, E., MOWAT, C., NEWMAN, W., PANES, J., PHILLIPS, A., PROCTOR, D. D., REGUEIRO, M., RUSSELL, R., RUTGEERTS, P., SANDERSON, J., SANS, M., SEIBOLD, F., STEINHART, A. H., STOKKERS, P. C., TORKVIST, L., KULLAK-UBLICK, G., WILSON, D., WALTERS, T., TARGAN, S. R., BRANT, S. R., RIOUX, J. D., D'AMATO, M., WEERSMA, R. K., KUGATHASAN, S., GRIFFITHS, A. M., MANSFIELD, J. C., VERMEIRE, S., DUERR, R. H., SILVERBERG, M. S., SATSANGI, J., SCHREIBER, S., CHO, J. H., ANNESE, V., HAKONARSON, H., DALY, M. J. & PARKES, M. 2010. Genome-wide meta-analysis increases to 71 the number of confirmed Crohn's disease susceptibility loci. *Nat Genet,* 42**,** 1118-25.

FRANKE, T. F., TARTOF, K. D. & TSICHLIS, P. N. 1994. The SH2-like Akt homology (AH) domain of c-akt is present in multiple copies in the genome of vertebrate and invertebrate eucaryotes. Cloning and characterization of the Drosophila melanogaster c-akt homolog Dakt1. *Oncogene,* 9**,** 141-8.

FRASER, K. B., MOEHLE, M. S., DAHER, J. P., WEBBER, P. J., WILLIAMS, J. Y., STEWART, C. A., YACOUBIAN, T. A., COWELL, R. M., DOKLAND, T., YE, T., CHEN, D., SIEGAL, G. P., GALEMMO, R. A., TSIKA, E., MOORE, D. J., STANDAERT, D. G., KOJIMA, K., MOBLEY, J. A. & WEST, A. B. 2013. LRRK2 secretion in exosomes is regulated by 14-3-3. *Hum Mol Genet,* 22**,** 4988-5000.

FREDERICK, J. M., RAYBORN, M. E., LATIES, A. M., LAM, D. M. & HOLLYFIELD, J. G. 1982. Dopaminergic neurons in the human retina. *J Comp Neurol,* 210**,** 65-79.

FRIGGI-GRELIN, F., COULOM, H., MELLER, M., GOMEZ, D., HIRSH, J. & BIRMAN, S. 2003. Targeted gene expression in Drosophila dopaminergic cells using regulatory sequences from tyrosine hydroxylase. *J Neurobiol,* 54**,** 618-27.

FROST, B. & DIAMOND, M. I. 2010. Prion-like mechanisms in neurodegenerative diseases. *Nat Rev Neurosci,* 11**,** 155-9.

FUJI, R. N., FLAGELLA, M., BACA, M., BAPTISTA, M. A., BRODBECK, J., CHAN, B. K., FISKE, B. K., HONIGBERG, L., JUBB, A. M., KATAVOLOS, P., LEE, D. W., LEWIN-KOH, S. C., LIN, T., LIU, X., LIU, S., LYSSIKATOS, J. P., O'MAHONY, J., REICHELT, M., ROOSE-GIRMA, M., SHENG, Z., SHERER, T., SMITH, A., SOLON, M., SWEENEY, Z. K., TARRANT, J., URKOWITZ, A., WARMING, S., YAYLAOGLU, M., ZHANG, S., ZHU, H., ESTRADA, A. A. & WATTS, R. J. 2015. Effect of selective LRRK2 kinase inhibition on nonhuman primate lung. *Sci Transl Med,* 7**,** 273ra15.

FUNAYAMA, M., HASEGAWA, K., KOWA, H., SAITO, M., TSUJI, S. & OBATA, F. 2002. A new locus for Parkinson's disease (PARK8) maps to chromosome 12p11.2-q13.1. *Ann Neurol,* 51**,** 296-301.

FUNAYAMA, M., HASEGAWA, K., OHTA, E., KAWASHIMA, N., KOMIYAMA, M., KOWA, H., TSUJI, S. & OBATA, F. 2005. An LRRK2 mutation as a cause for the parkinsonism in the original PARK8 family. *Ann Neurol,* 57**,** 918-21.

FUNDERBURK, C. D., BOWLING, K. M., XU, D., HUANG, Z. & O'DONNELL, J. M. 2006. A typical N-terminal extensions confer novel regulatory properties on GTP cyclohydrolase isoforms in Drosophila melanogaster. *J Biol Chem,* 281**,** 33302-12.

GABRIEL, R., DE SOUZA, S., ZIFF, E. B. & WITKOVSKY, P. 2002. Association of the AMPA receptor-related postsynaptic density proteins GRIP and ABP with subsets of glutamate-sensitive neurons in the rat retina. *J Comp Neurol,* 449**,** 129-40.

GANDHI, P. N., WANG, X., ZHU, X., CHEN, S. G. & WILSON-DELFOSSE, A. L. 2008. The Roc domain of leucine-rich repeat kinase 2 is sufficient for interaction with microtubules. *J Neurosci Res,* 86**,** 1711-20.

GAO, X., SIMON, K. C., HAN, J., SCHWARZSCHILD, M. A. & ASCHERIO, A. 2009. Genetic determinants of hair color and Parkinson's disease risk. *Ann Neurol,* 65**,** 76-82.

GARDET, A., BENITA, Y., LI, C., SANDS, B. E., BALLESTER, I., STEVENS, C., KORZENIK, J. R., RIOUX, J. D., DALY, M. J., XAVIER, R. J. & PODOLSKY, D. K. 2010. LRRK2 is involved in the IFN-gamma response and host response to pathogens. *J Immunol,* 185**,** 5577-85.

GAUTIER, C. A., KITADA, T. & SHEN, J. 2008. Loss of PINK1 causes mitochondrial functional defects and increased sensitivity to oxidative stress. *Proc Natl Acad Sci U S A,* 105**,** 11364-9.

GEGG, M. E., COOPER, J. M., SCHAPIRA, A. H. & TAANMAN, J. W. 2009. Silencing of PINK1 expression affects mitochondrial DNA and oxidative phosphorylation in dopaminergic cells. *PLoS One,* 4**,** e4756.

GEHRKE, S., IMAI, Y., SOKOL, N. & LU, B. 2010. Pathogenic LRRK2 negatively regulates microRNA-mediated translational repression. *Nature,* 466**,** 637-41.

GILL, S. S., PATEL, N. K., HOTTON, G. R., O'SULLIVAN, K., MCCARTER, R., BUNNAGE, M., BROOKS, D. J., SVENDSEN, C. N. & HEYWOOD, P. 2003. Direct brain infusion of glial cell line-derived neurotrophic factor in Parkinson disease. *Nat Med,* 9**,** 589-95.

GILLARDON, F. 2009. Leucine-rich repeat kinase 2 phosphorylates brain tubulin-beta isoforms and modulates microtubule stability--a point of convergence in parkinsonian neurodegeneration? *J Neurochem,* 110**,** 1514-22.

GILLARDON, F., KREMMER, E., FROEHLICH, T., UEFFING, M., HENGERER, B. & GLOECKNER, C. J. 2013. ATP-competitive LRRK2 inhibitors interfere with monoclonal antibody binding to the kinase domain of LRRK2 under native conditions. A method to directly monitor the active conformation of LRRK2? *J Neurosci Methods,* 214**,** 62-8.

GILLARDON, F., SCHMID, R. & DRAHEIM, H. 2012. Parkinson's disease-linked leucine-rich repeat kinase 2(R1441G) mutation increases proinflammatory cytokine release from activated primary microglial cells and resultant neurotoxicity. *Neuroscience,* 208**,** 41-8.

GILSBACH, B. K. & KORTHOLT, A. 2014. Structural biology of the LRRK2 GTPase and kinase domains: implications for regulation. *Front Mol Neurosci,* 7.

GISPERT, S., RICCIARDI, F., KURZ, A., AZIZOV, M., HOEPKEN, H. H., BECKER, D., VOOS, W., LEUNER, K., MULLER, W. E., KUDIN, A. P., KUNZ, W. S., ZIMMERMANN, A., ROEPER, J., WENZEL, D., JENDRACH, M., GARCIA-ARENCIBIA, M., FERNANDEZ-RUIZ, J., HUBER, L., ROHRER, H., BARRERA, M., REICHERT, A. S., RUB, U., CHEN, A., NUSSBAUM, R. L. & AUBURGER, G. 2009. Parkinson phenotype in aged PINK1-deficient mice is accompanied by progressive mitochondrial dysfunction in absence of neurodegeneration. *PLoS One,* 4**,** e5777.

GITLER, A. D., BEVIS, B. J., SHORTER, J., STRATHEARN, K. E., HAMAMICHI, S., SU, L. J., CALDWELL, K. A., CALDWELL, G. A., ROCHET, J. C., MCCAFFERY, J. M., BARLOWE, C. & LINDQUIST, S. 2008. The Parkinson's disease protein alpha-synuclein disrupts cellular Rab homeostasis. *Proc Natl Acad Sci U S A,* 105**,** 145-50.

GLINKA, Y., GASSEN, M. & YOUDIM, M. B. 1997. Mechanism of 6-hydroxydopamine neurotoxicity. *J Neural Transm Suppl,* 50**,** 55-66.

GLOECKNER, C. J., BOLDT, K., VON ZWEYDORF, F., HELM, S., WIESENT, L., SARIOGLU, H. & UEFFING, M. 2010. Phosphopeptide analysis reveals two discrete clusters of phosphorylation in the N-terminus and the Roc domain of the Parkinson-disease associated protein kinase LRRK2. *J Proteome Res,* 9**,** 1738-45.

GOEDERT, M., CLAVAGUERA, F. & TOLNAY, M. 2010. The propagation of prion-like protein inclusions in neurodegenerative diseases. *Trends Neurosci,* 33**,** 317-25.

GOETZ, C. G. 2011. The History of Parkinson's Disease: Early Clinical Descriptions and Neurological Therapies. *Cold Spring Harb Perspect Med,* 1.

GOKER-ALPAN, O., SCHIFFMANN, R., LAMARCA, M. E., NUSSBAUM, R. L., MCINERNEY-LEO, A. & SIDRANSKY, E. 2004. Parkinsonism among Gaucher disease carriers. *J Med Genet,* 41**,** 937-40.

GOLDWURM, S., ZINI, M., DI FONZO, A., DE GASPARI, D., SIRI, C., SIMONS, E. J., VAN DOESELAAR, M., TESEI, S., ANTONINI, A., CANESI, M., ZECCHINELLI, A., MARIANI, C., MEUCCI, N., SACILOTTO, G., CILIA, R., ISAIAS, I. U., BONETTI, A., SIRONI, F., RICCA, S., OOSTRA, B. A., BONIFATI, V. & PEZZOLI, G. 2006. LRRK2 G2019S mutation and Parkinson's disease: a clinical, neuropsychological and neuropsychiatric study in a large Italian sample. *Parkinsonism Relat Disord,* 12**,** 410-9.

GONZALES, P. A., PISITKUN, T., HOFFERT, J. D., TCHAPYJNIKOV, D., STAR, R. A., KLETA, R., WANG, N. S. & KNEPPER, M. A. 2009. Large-scale proteomics and phosphoproteomics of urinary exosomes. *J Am Soc Nephrol,* 20**,** 363-79.

GOROSTIDI, A., RUIZ-MARTINEZ, J., LOPEZ DE MUNAIN, A., ALZUALDE, A. & MARTI MASSO, J. F. 2009. LRRK2 G2019S and R1441G mutations associated with Parkinson's disease are common in the Basque Country, but relative prevalence is determined by ethnicity. *Neurogenetics,* 10**,** 157-9.

GOTTLOB, I., SCHNEIDER, E., HEIDER, W. & SKRANDIES, W. 1987. Alteration of visual evoked potentials and electroretinograms in Parkinson's disease. *Electroencephalogr Clin Neurophysiol,* 66**,** 349-57.

GREEN, E. W., CAMPESAN, S., BREDA, C., SATHYASAIKUMAR, K. V., MUCHOWSKI, P. J., SCHWARCZ, R., KYRIACOU, C. P. & GIORGINI, F. 2012. Drosophila eye color mutants as therapeutic tools for Huntington disease. *Fly (Austin),* 6**,** 117-20.

GREENAMYRE, J. T., CANNON, J. R., DROLET, R. & MASTROBERARDINO, P. G. 2010. Lessons from the rotenone model of Parkinson's disease. *Trends Pharmacol Sci,* 31**,** 141-2; author reply 142-3.

GREENE, J. C., WHITWORTH, A. J., KUO, I., ANDREWS, L. A., FEANY, M. B. & PALLANCK, L. J. 2003. Mitochondrial pathology and apoptotic muscle degeneration in Drosophila parkin mutants. *Proc Natl Acad Sci U S A,* 100**,** 4078-83.

GREENE, L. A., LEVY, O. & MALAGELADA, C. 2011. Akt as a victim, villain and potential hero in Parkinson's disease pathophysiology and treatment. *Cell Mol Neurobiol,* 31**,** 969-78.

GREENSPAN, R. J. 2004. *Fly Pushing, The theory and practice of Drosophila genetics,* Cold Spring Harbor, New York, Cold Spring Harbor Laboratory Press.

GREGGIO, E. & COOKSON, M. R. 2009. Leucine-rich repeat kinase 2 mutations and Parkinson's disease: three questions. *ASN Neuro,* 1.

GREGGIO, E., TAYMANS, J. M., ZHEN, E. Y., RYDER, J., VANCRAENENBROECK, R., BEILINA, A., SUN, P., DENG, J., JAFFE, H., BAEKELANDT, V., MERCHANT, K. & COOKSON, M. R. 2009. The Parkinson's disease kinase LRRK2 autophosphorylates its GTPase domain at multiple sites. *Biochem Biophys Res Commun,* 389**,** 449-54.

GRIFFIN, R. J., MOLONEY, A., KELLIHER, M., JOHNSTON, J. A., RAVID, R., DOCKERY, P., O'CONNOR, R. & O'NEILL, C. 2005. Activation of Akt/PKB, increased phosphorylation of Akt substrates and loss and altered distribution of Akt and PTEN are features of Alzheimer's disease pathology. *J Neurochem,* 93**,** 105-17.

GROSS, J. C., CHAUDHARY, V., BARTSCHERER, K. & BOUTROS, M. 2012. Active Wnt proteins are secreted on exosomes. *Nat Cell Biol,* 14**,** 1036-45.

GRUNEWALD, A., GEGG, M. E., TAANMAN, J. W., KING, R. H., KOCK, N., KLEIN, C. & SCHAPIRA, A. H. 2009. Differential effects of PINK1 nonsense and missense mutations on mitochondrial function and morphology. *Exp Neurol,* 219**,** 266-73.

GUIDETTI, P., BATES, G. P., GRAHAM, R. K., HAYDEN, M. R., LEAVITT, B. R., MACDONALD, M. E., SLOW, E. J., WHEELER, V. C., WOODMAN, B. & SCHWARCZ, R. 2006. Elevated brain 3-hydroxykynurenine and quinolinate levels in Huntington disease mice. *Neurobiology of Disease,* 23**,** 190-197.

GUIDETTI, P., LUTHI-CARTER, R. E., AUGOOD, S. J. & SCHWARCZ, R. 2004. Neostriatal and cortical quinolinate levels are increased in early grade Huntington's disease. *Neurobiology of Disease,* 17**,** 455-461.

GUILLERY, R. W. 1986. Neural abnormalities of albinos. *Trends in Neurosciences,* 9**,** 364-367.
GULAJ, E., PAWLAK, K., BIEN, B. & PAWLAK, D. 2010. Kynurenine and its metabolites in Alzheimer's disease patients. *Advances in Medical Sciences,* 55**,** 204-211.
GUSTINCICH, S., FEIGENSPAN, A., SIEGHART, W. & RAVIOLA, E. 1999. Composition of the GABA(A) receptors of retinal dopaminergic neurons. *J Neurosci,* 19**,** 7812-22.
HAAXMA, C. A., HORSTINK, M. W., ZIJLMANS, J. C., LEMMENS, W. A., BLOEM, B. R. & BORM, G. F. 2015. Risk of Disabling Response Fluctuations and Dyskinesias for Dopamine Agonists Versus Levodopa in Parkinson's Disease1. *J Parkinsons Dis,* 5**,** 847-53.
HAEGGENDAL, J. & MALMFORS, T. 1963. EVIDENCE OF DOPAMINE-CONTAINING NEURONS IN THE RETINA OF RABBITS. *Acta Physiol Scand,* 59**,** 295-6.
HAKIMI, M., SELVANANTHAM, T., SWINTON, E., PADMORE, R. F., TONG, Y., KABBACH, G., VENDEROVA, K., GIRARDIN, S. E., BULMAN, D. E., SCHERZER, C. R., LAVOIE, M. J., GRIS, D., PARK, D. S., ANGEL, J. B., SHEN, J., PHILPOTT, D. J. & SCHLOSSMACHER, M. G. 2011. Parkinson's disease-linked LRRK2 is expressed in circulating and tissue immune cells and upregulated following recognition of microbial structures. *J Neural Transm,* 118**,** 795-808.
HAMMOND, S. M., CAUDY, A. A. & HANNON, G. J. 2001. Post-transcriptional gene silencing by double-stranded RNA. *Nat Rev Genet,* 2**,** 110-9.
HAN, D. D., STEIN, D. & STEVENS, L. M. 2000. Investigating the function of follicular subpopulations during Drosophila oogenesis through hormone-dependent enhancer-targeted cell ablation. *Development,* 127**,** 573-83.
HARDIE, R. C. & JUUSOLA, M. 2015. Phototransduction in Drosophila. *Curr Opin Neurobiol,* 34**,** 37-45.
HARDIE, R. C. & RAGHU, P. 2001. Visual transduction in Drosophila. *Nature,* 413**,** 186-93.
HARNOIS, C. & DI PAOLO, T. 1990. Decreased dopamine in the retinas of patients with Parkinson's disease. *Invest Ophthalmol Vis Sci,* 31**,** 2473-5.
HARRIS, D. A., KIM, K., NAKAHARA, K., VASQUEZ-DOORMAN, C. & CARTHEW, R. W. 2011. Cargo sorting to lysosome-related organelles regulates siRNA-mediated gene silencing. *J Cell Biol,* 194**,** 77-87.
HARRIS, W. A., STARK, W. S. & WALKER, J. A. 1976. Genetic dissection of the photoreceptor system in the compound eye of Drosophila melanogaster. *J Physiol,* 256**,** 415-39.
HASHIMOTO, M., BAR-ON, P., HO, G., TAKENOUCHI, T., ROCKENSTEIN, E., CREWS, L. & MASLIAH, E. 2004a. Beta-synuclein regulates Akt activity in neuronal cells. A possible mechanism for neuroprotection in Parkinson's disease. *J Biol Chem,* 279**,** 23622-9.
HASHIMOTO, M., ROCKENSTEIN, E., MANTE, M., CREWS, L., BAR-ON, P., GAGE, F. H., MARR, R. & MASLIAH, E. 2004b. An antiaggregation gene therapy strategy for Lewy body disease utilizing beta-synuclein lentivirus in a transgenic model. *Gene Ther,* 11**,** 1713-23.
HAUG, B. A., TRENKWALDER, C., ARDEN, G. B., OERTEL, W. H. & PAULUS, W. 1994. Visual thresholds to low-contrast pattern displacement, color contrast, and luminance contrast stimuli in Parkinson's disease. *Mov Disord,* 9**,** 563-70.
HEALY, D. G., FALCHI, M., O'SULLIVAN, S. S., BONIFATI, V., DURR, A., BRESSMAN, S., BRICE, A., AASLY, J., ZABETIAN, C. P., GOLDWURM, S., FERREIRA, J. J., TOLOSA,

E., KAY, D. M., KLEIN, C., WILLIAMS, D. R., MARRAS, C., LANG, A. E., WSZOLEK, Z. K., BERCIANO, J., SCHAPIRA, A. H., LYNCH, T., BHATIA, K. P., GASSER, T., LEES, A. J. & WOOD, N. W. 2008. Phenotype, genotype, and worldwide genetic penetrance of LRRK2-associated Parkinson's disease: a case-control study. *Lancet Neurol,* 7**,** 583-90.

HEFTI, F. 1994. Neurotrophic factor therapy for nervous system degenerative diseases. *J Neurobiol,* 25**,** 1418-35.

HEISENBERG, M. 1971. Separation of receptor and lamina potentials in the electroretinogram of normal and mutant Drosophila. *J Exp Biol,* 55**,** 85-100.

HEO, H. Y., KIM, K. S. & SEOL, W. 2010. Coordinate Regulation of Neurite Outgrowth by LRRK2 and Its Interactor, Rab5. *Exp Neurobiol,* 19**,** 97-105.

HERRERO HERNANDEZ, E. 2009. Pigmentation genes link Parkinson's disease to melanoma, opening a window on both etiologies. *Med Hypotheses,* 72**,** 280-4.

HERZIG, M. C., KOLLY, C., PERSOHN, E., THEIL, D., SCHWEIZER, T., HAFNER, T., STEMMELEN, C., TROXLER, T. J., SCHMID, P., DANNER, S., SCHNELL, C. R., MUELLER, M., KINZEL, B., GREVOT, A., BOLOGNANI, F., STIRN, M., KUHN, R. R., KAUPMANN, K., VAN DER PUTTEN, P. H., ROVELLI, G. & SHIMSHEK, D. R. 2011. LRRK2 protein levels are determined by kinase function and are crucial for kidney and lung homeostasis in mice. *Hum Mol Genet,* 20**,** 4209-23.

HIGASHI, S., MOORE, D. J., YAMAMOTO, R., MINEGISHI, M., SATO, K., TOGO, T., KATSUSE, O., UCHIKADO, H., FURUKAWA, Y., HINO, H., KOSAKA, K., EMSON, P. C., WADA, K., DAWSON, V. L., DAWSON, T. M., ARAI, H. & ISEKI, E. 2009. Abnormal localization of leucine-rich repeat kinase 2 to the endosomal-lysosomal compartment in lewy body disease. *J Neuropathol Exp Neurol,* 68**,** 994-1005.

HIGGINS, C. F. 1992. ABC transporters: from microorganisms to man. *Annu Rev Cell Biol,* 8**,** 67-113.

HINDLE, S., AFSARI, F., STARK, M., MIDDLETON, C. A., EVANS, G. J., SWEENEY, S. T. & ELLIOTT, C. J. 2013. Dopaminergic expression of the Parkinsonian gene LRRK2-G2019S leads to non-autonomous visual neurodegeneration, accelerated by increased neural demands for energy. *Hum Mol Genet,* 22**,** 2129-40.

HINKLE, K. M., YUE, M., BEHROUZ, B., DACHSEL, J. C., LINCOLN, S. J., BOWLES, E. E., BEEVERS, J. E., DUGGER, B., WINNER, B., PROTS, I., KENT, C. B., NISHIOKA, K., LIN, W. L., DICKSON, D. W., JANUS, C. J., FARRER, M. J. & MELROSE, H. L. 2012. LRRK2 knockout mice have an intact dopaminergic system but display alterations in exploratory and motor co-ordination behaviors. *Mol Neurodegener,* 7**,** 25.

HIRSH, J., RIEMENSPERGER, T., COULOM, H., ICHE, M., COUPAR, J. & BIRMAN, S. 2010. Roles of dopamine in circadian rhythmicity and extreme light sensitivity of circadian entrainment. *Curr Biol,* 20**,** 209-14.

HIRTH, F. 2010. Drosophila melanogaster in the Study of Human Neurodegeneration. *CNS Neurol Disord Drug Targets,* 9**,** 504-23.

HOEPKEN, H. H., GISPERT, S., MORALES, B., WINGERTER, O., DEL TURCO, D., MULSCH, A., NUSSBAUM, R. L., MULLER, K., DROSE, S., BRANDT, U., DELLER, T., WIRTH, B., KUDIN, A. P., KUNZ, W. S. & AUBURGER, G. 2007. Mitochondrial dysfunction, peroxidation damage and changes in glutathione metabolism in PARK6. *Neurobiol Dis,* 25**,** 401-11.

HOON, M., OKAWA, H., DELLA SANTINA, L. & WONG, R. O. 2014. Functional architecture of the retina: development and disease. *Prog Retin Eye Res,* 42**,** 44-84.

HOTTA, Y. & BENZER, S. 1969. Abnormal electroretinograms in visual mutants of Drosophila. *Nature,* 222**,** 354-6.

HOWELLS, A. J. & RYALL, R. L. 1975. A biochemical study of the scarlet eye-color mutant of Drosophila melanogaster. *Biochem Genet,* 13**,** 273-82.

HSU, C., MOROHASHI, Y., YOSHIMURA, S., MANRIQUE-HOYOS, N., JUNG, S., LAUTERBACH, M. A., BAKHTI, M., GRONBORG, M., MOBIUS, W., RHEE, J., BARR, F. A. & SIMONS, M. 2010. Regulation of exosome secretion by Rab35 and its GTPase-activating proteins TBC1D10A-C. *J Cell Biol,* 189**,** 223-32.

HU, W., WANG, T., WANG, X. & HAN, J. 2015. Ih channels control feedback regulation from amacrine cells to photoreceptors. *PLoS Biol,* 13**,** e1002115.

HUANG, P., YANG, X. D., CHEN, S. D. & XIAO, Q. 2015. The association between Parkinson's disease and melanoma: a systematic review and meta-analysis. *Transl Neurodegener,* 4**,** 21.

HWANG, C. K., CHAURASIA, S. S., JACKSON, C. R., CHAN, G. C., STORM, D. R. & IUVONE, P. M. 2013. Circadian rhythm of contrast sensitivity is regulated by a dopamine-neuronal PAS-domain protein 2-adenylyl cyclase 1 signaling pathway in retinal ganglion cells. *J Neurosci,* 33**,** 14989-97.

IMAI, Y., GEHRKE, S., WANG, H. Q., TAKAHASHI, R., HASEGAWA, K., OOTA, E. & LU, B. 2008. Phosphorylation of 4E-BP by LRRK2 affects the maintenance of dopaminergic neurons in Drosophila. *Embo j,* 27**,** 2432-43.

IMAI, Y., SODA, M. & TAKAHASHI, R. 2000. Parkin suppresses unfolded protein stress-induced cell death through its E3 ubiquitin-protein ligase activity. *J Biol Chem,* 275**,** 35661-4.

INZELBERG, R., COHEN, O. S., AHARON-PERETZ, J., SCHLESINGER, I., GERSHONI-BARUCH, R., DJALDETTI, R., NITSAN, Z., EPHRATY, L., TUNKEL, O., KOZLOVA, E., INZELBERG, L., KAPLAN, N., FIXLER MEHR, T., MORY, A., DAGAN, E., SCHECHTMAN, E., FRIEDMAN, E. & HASSIN-BAER, S. 2012. The LRRK2 G2019S mutation is associated with Parkinson disease and concomitant non-skin cancers. *Neurology,* 78**,** 781-786.

INZELBERG, R., SAMUELS, Y., AZIZI, E., QUTOB, N., INZELBERG, L., DOMANY, E., SCHECHTMAN, E. & FRIEDMAN, E. 2016. Parkinson disease (PARK) genes are somatically mutated in cutaneous melanoma. *Neurology Genetics,* 2.

ITIER, J. M., IBANEZ, P., MENA, M. A., ABBAS, N., COHEN-SALMON, C., BOHME, G. A., LAVILLE, M., PRATT, J., CORTI, O., PRADIER, L., RET, G., JOUBERT, C., PERIQUET, M., ARAUJO, F., NEGRONI, J., CASAREJOS, M. J., CANALS, S., SOLANO, R., SERRANO, A., GALLEGO, E., SANCHEZ, M., DENEFLE, P., BENAVIDES, J., TREMP, G., ROONEY, T. A., BRICE, A. & GARCIA DE YEBENES, J. 2003. Parkin gene inactivation alters behaviour and dopamine neurotransmission in the mouse. *Hum Mol Genet,* 12**,** 2277-91.

IUVONE, P. M., GALLI, C. L., GARRISON-GUND, C. K. & NEFF, N. H. 1978. Light stimulates tyrosine hydroxylase activity and dopamine synthesis in retinal amacrine neurons. *Science,* 202**,** 901-2.

JACKSON, C. R., RUAN, G. X., ASEEM, F., ABEY, J., GAMBLE, K., STANWOOD, G., PALMITER, R. D., IUVONE, P. M. & MCMAHON, D. G. 2012. Retinal dopamine mediates multiple dimensions of light-adapted vision. *J Neurosci,* 32**,** 9359-68.

JACKSON-LEWIS, V., BLESA, J. & PRZEDBORSKI, S. 2012. Animal models of Parkinson's disease. *Parkinsonism Relat Disord,* 18 Suppl 1**,** S183-5.

JALEEL, M., NICHOLS, R. J., DEAK, M., CAMPBELL, D. G., GILLARDON, F., KNEBEL, A. & ALESSI, D. R. 2007. LRRK2 phosphorylates moesin at threonine-558: characterization of how Parkinson's disease mutants affect kinase activity. *Biochem J,* 405**,** 307-17.

JAMES, N. G., DIGMAN, M. A., GRATTON, E., BARYLKO, B., DING, X., ALBANESI, J. P., GOLDBERG, M. S. & JAMESON, D. M. 2012. Number and brightness analysis of LRRK2 oligomerization in live cells. *Biophys J,* 102**,** L41-3.

JANKOVIC, J. 2002. Levodopa strengths and weaknesses. *Neurology,* 58**,** S19-32.

JANKOVIC, J. 2008. Parkinson's disease: clinical features and diagnosis. *J Neurol Neurosurg Psychiatry,* 79**,** 368-76.

JAUCH, D., URBAŃSKA, E. M., GUIDETTI, P., BIRD, E. D., VONSATTEL, J. P. G., WHETSELL JR, W. O. & SCHWARCZ, R. 1995. Dysfunction of brain kynurenic acid metabolism in Huntington's disease: focus on kynurenine aminotransferases. *Journal of the Neurological Sciences,* 130**,** 39-47.

JEFFERY, G. 1997. The albino retina: an abnormality that provides insight into normal retinal development. *Trends Neurosci,* 20**,** 165-9.

KACHERGUS, J., MATA, I. F., HULIHAN, M., TAYLOR, J. P., LINCOLN, S., AASLY, J., GIBSON, J. M., ROSS, O. A., LYNCH, T., WILEY, J., PAYAMI, H., NUTT, J., MARAGANORE, D. M., CZYZEWSKI, K., STYCZYNSKA, M., WSZOLEK, Z. K., FARRER, M. J. & TOFT, M. 2005. Identification of a novel LRRK2 mutation linked to autosomal dominant parkinsonism: evidence of a common founder across European populations. *Am J Hum Genet,* 76**,** 672-80.

KALIA, L. V. & LANG, A. E. 2015. Parkinson's disease. *Lancet*.

KALMUS, H. 1943. The optomotor responses of some eye mutants of Drosophila. *J Genet,* 45**,** 206-213.

KAMIKAWAJI, S., ITO, G. & IWATSUBO, T. 2009. Identification of the autophosphorylation sites of LRRK2. *Biochemistry,* 48**,** 10963-75.

KARBOWSKI, M., NEUTZNER, A. & YOULE, R. J. 2007. The mitochondrial E3 ubiquitin ligase MARCH5 is required for Drp1 dependent mitochondrial division. *J Cell Biol,* 178**,** 71-84.

KARUNAKARAN, S., SAEED, U., MISHRA, M., VALLI, R. K., JOSHI, S. D., MEKA, D. P., SETH, P. & RAVINDRANATH, V. 2008. Selective activation of p38 mitogen-activated protein kinase in dopaminergic neurons of substantia nigra leads to nuclear translocation of p53 in 1-methyl-4-phenyl-1,2,3,6-tetrahydropyridine-treated mice. *J Neurosci,* 28**,** 12500-9.

KAVANAGH, M. E., DODDAREDDY, M. R. & KASSIOU, M. 2013. The development of CNS-active LRRK2 inhibitors using property-directed optimisation. *Bioorg Med Chem Lett,* 23**,** 3690-6.

KEENE, C. D., RODRIGUES, C. M., EICH, T., CHHABRA, M. S., STEER, C. J. & LOW, W. C. 2002. Tauroursodeoxycholic acid, a bile acid, is neuroprotective in a transgenic animal model of Huntington's disease. *Proc Natl Acad Sci U S A,* 99**,** 10671-6.

KIM, H., KIM, K. & YIM, J. 2013. Biosynthesis of drosopterins, the red eye pigments of Drosophila melanogaster. *IUBMB Life,* 65**,** 334-40.

KIM, J., SUH, H., KIM, S., KIM, K., AHN, C. & YIM, J. 2006. Identification and characteristics of the structural gene for the Drosophila eye colour mutant

sepia, encoding PDA synthase, a member of the omega class glutathione S-transferases. *Biochem J,* 398**,** 451-60.

KIM, R. H., PETERS, M., JANG, Y., SHI, W., PINTILIE, M., FLETCHER, G. C., DELUCA, C., LIEPA, J., ZHOU, L., SNOW, B., BINARI, R. C., MANOUKIAN, A. S., BRAY, M. R., LIU, F. F., TSAO, M. S. & MAK, T. W. 2005. DJ-1, a novel regulator of the tumor suppressor PTEN. *Cancer Cell,* 7**,** 263-73.

KITADA, T., ASAKAWA, S., HATTORI, N., MATSUMINE, H., YAMAMURA, Y., MINOSHIMA, S., YOKOCHI, M., MIZUNO, Y. & SHIMIZU, N. 1998. Mutations in the parkin gene cause autosomal recessive juvenile parkinsonism. *Nature,* 392**,** 605-8.

KLEIN, C. & WESTENBERGER, A. 2012. Genetics of Parkinson's Disease. *Cold Spring Harb Perspect Med,* 2.

KOLB, H., CUENCA, N. & DEKORVER, L. 1991. Postembedding immunocytochemistry for GABA and glycine reveals the synaptic relationships of the dopaminergic amacrine cell of the cat retina. *J Comp Neurol,* 310**,** 267-84.

KOLB, H., CUENCA, N., WANG, H. H. & DEKORVER, L. 1990. The synaptic organization of the dopaminergic amacrine cell in the cat retina. *J Neurocytol,* 19**,** 343-66.

KORDOWER, J. H., CHU, Y., HAUSER, R. A., FREEMAN, T. B. & OLANOW, C. W. 2008. Lewy body-like pathology in long-term embryonic nigral transplants in Parkinson's disease. *Nat Med,* 14**,** 504-6.

KORKUT, C., ATAMAN, B., RAMACHANDRAN, P., ASHLEY, J., BARRIA, R., GHERBESI, N. & BUDNIK, V. 2009. Trans-synaptic transmission of vesicular Wnt signals through Evi/Wntless. *Cell,* 139**,** 393-404.

KOVACS, G. G., BREYDO, L., GREEN, R., KIS, V., PUSKA, G., LORINCZ, P., PERJU-DUMBRAVA, L., GIERA, R., PIRKER, W., LUTZ, M., LACHMANN, I., BUDKA, H., UVERSKY, V. N., MOLNAR, K. & LASZLO, L. 2014. Intracellular processing of disease-associated alpha-synuclein in the human brain suggests prion-like cell-to-cell spread. *Neurobiol Dis,* 69**,** 76-92.

KRAMER, T., LO MONTE, F., GÖRING, S., OKALA AMOMBO, G. M. & SCHMIDT, B. 2012. Small Molecule Kinase Inhibitors for LRRK2 and Their Application to Parkinson's Disease Models. *ACS Chem Neurosci,* 3**,** 151-60.

KRIVI, G. G. & BROWN, G. M. 1979. Purification and properties of the enzymes from Drosophila melanogaster that catalyze the synthesis of sepiapterin from dihydroneopterin triphosphate. *Biochem Genet,* 17**,** 371-90.

KUMAR, N., VAN GERPEN, J. A., BOWER, J. H. & AHLSKOG, J. E. 2005. Levodopa-dyskinesia incidence by age of Parkinson's disease onset. *Mov Disord,* 20**,** 342-4.

KUNKEL, S. D., SUNEJA, M., EBERT, S. M., BONGERS, K. S., FOX, D. K., MALMBERG, S. E., ALIPOUR, F., SHIELDS, R. K. & ADAMS, C. M. 2011. mRNA expression signatures of human skeletal muscle atrophy identify a natural compound that increases muscle mass. *Cell Metab,* 13**,** 627-38.

LANGSTON, J. W., BALLARD, P., TETRUD, J. W. & IRWIN, I. 1983. Chronic Parkinsonism in humans due to a product of meperidine-analog synthesis. *Science,* 219**,** 979-80.

LANGSTON, R. G., RUDENKO, I. N. & COOKSON, M. R. 2016. The function of orthologues of the human Parkinson's disease gene LRRK2 across species: implications for disease modelling in preclinical research. *Biochem J,* 473**,** 221-32.

LATREMOLIERE, A., LATINI, A., ANDREWS, N., CRONIN, S. J., FUJITA, M., GORSKA, K., HOVIUS, R., ROMERO, C., CHUAIPHICHAI, S., PAINTER, M., MIRACCA, G., BABANIYI, O., REMOR, A. P., DUONG, K., RIVA, P., BARRETT, L. B., FERREIROS, N., NAYLOR, A., PENNINGER, J. M., TEGEDER, I., ZHONG, J., BLAGG, J., CHANNON, K. M., JOHNSSON, K., COSTIGAN, M. & WOOLF, C. J. 2015. Reduction of Neuropathic and Inflammatory Pain through Inhibition of the Tetrahydrobiopterin Pathway. *Neuron,* 86**,** 1393-406.

LAVARA-CULEBRAS, E. & PARICIO, N. 2007. Drosophila DJ-1 mutants are sensitive to oxidative stress and show reduced lifespan and motor deficits. *Gene,* 400**,** 158-65.

LEE, B. D., DAWSON, V. L. & DAWSON, T. M. 2012a. Leucine-rich repeat kinase 2 (LRRK2) as a potential therapeutic target in Parkinson's disease. *Trends Pharmacol Sci,* 33**,** 365-73.

LEE, B. D., SHIN, J. H., VANKAMPEN, J., PETRUCELLI, L., WEST, A. B., KO, H. S., LEE, Y. I., MAGUIRE-ZEISS, K. A., BOWERS, W. J., FEDEROFF, H. J., DAWSON, V. L. & DAWSON, T. M. 2010a. Inhibitors of leucine-rich repeat kinase-2 protect against models of Parkinson's disease. *Nat Med,* 16**,** 998-1000.

LEE, S., IMAI, Y., GEHRKE, S., LIU, S. & LU, B. 2012b. The synaptic function of LRRK2. *Biochem Soc Trans,* 40**,** 1047-51.

LEE, S., LIU, H. P., LIN, W. Y., GUO, H. & LU, B. 2010b. LRRK2 kinase regulates synaptic morphology through distinct substrates at the presynaptic and postsynaptic compartments of the Drosophila neuromuscular junction. *J Neurosci,* 30**,** 16959-69.

LEE, S. B., KIM, W., LEE, S. & CHUNG, J. 2007. Loss of LRRK2/PARK8 induces degeneration of dopaminergic neurons in Drosophila. *Biochem Biophys Res Commun,* 358**,** 534-9.

LEE, T. & LUO, L. 1999. Mosaic analysis with a repressible cell marker for studies of gene function in neuronal morphogenesis. *Neuron,* 22**,** 451-61.

LELAN, F., BOYER, C., THINARD, R., REMY, S., USAL, C., TESSON, L., ANEGON, I., NEVEU, I., DAMIER, P., NAVEILHAN, P. & LESCAUDRON, L. 2011. Effects of Human Alpha-Synuclein A53T-A30P Mutations on SVZ and Local Olfactory Bulb Cell Proliferation in a Transgenic Rat Model of Parkinson Disease. *Parkinsons Dis,* 2011**,** 987084.

LESAGE, S., LEUTENEGGER, A. L., IBANEZ, P., JANIN, S., LOHMANN, E., DURR, A. & BRICE, A. 2005. LRRK2 haplotype analyses in European and North African families with Parkinson disease: a common founder for the G2019S mutation dating from the 13th century. *Am J Hum Genet,* 77**,** 330-2.

LEWIS, P. A., GREGGIO, E., BEILINA, A., JAIN, S., BAKER, A. & COOKSON, M. R. 2007. The R1441C mutation of LRRK2 disrupts GTP hydrolysis. *Biochem Biophys Res Commun,* 357**,** 668-71.

LEWY, F. H. 1912. *Paralysis agitans. 1. Pathologische Anatomie.,* Berlin, Julius Springer.

LEWY, F. H. 1923. *Die Lehre vom Tonus und der Bewegung: zugleich systematische Untersuchungen zur Klinik, Physiologie, Pathologie und Pathogenese der Paralysis Agitans*, Julius Springer.

LI, J. Y., ENGLUND, E., HOLTON, J. L., SOULET, D., HAGELL, P., LEES, A. J., LASHLEY, T., QUINN, N. P., REHNCRONA, S., BJORKLUND, A., WIDNER, H., REVESZ, T., LINDVALL, O. & BRUNDIN, P. 2008. Lewy bodies in grafted neurons in subjects with Parkinson's disease suggest host-to-graft disease propagation. *Nat Med,* 14**,** 501-3.

LI, X., PATEL, J. C., WANG, J., AVSHALUMOV, M. V., NICHOLSON, C., BUXBAUM, J. D., ELDER, G. A., RICE, M. E. & YUE, Z. 2010. Enhanced striatal dopamine transmission and motor performance with LRRK2 overexpression in mice is eliminated by familial Parkinson's disease mutation G2019S. *J Neurosci,* 30**,** 1788-97.

LI, X., TAN, Y. C., POULOSE, S., OLANOW, C. W., HUANG, X. Y. & YUE, Z. 2007. Leucine-rich repeat kinase 2 (LRRK2)/PARK8 possesses GTPase activity that is altered in familial Parkinson's disease R1441C/G mutants. *J Neurochem,* 103**,** 238-47.

LI, Y., LIU, W., OO, T. F., WANG, L., TANG, Y., JACKSON-LEWIS, V., ZHOU, C., GEGHMAN, K., BOGDANOV, M., PRZEDBORSKI, S., BEAL, M. F., BURKE, R. E. & LI, C. 2009. Mutant LRRK2(R1441G) BAC transgenic mice recapitulate cardinal features of Parkinson's disease. *Nat Neurosci,* 12**,** 826-8.

LIEB, K., BRUCKER, S., BACH, M., ELS, T., LUCKING, C. H. & GREENLEE, M. W. 1999. Impairment in preattentive visual processing in patients with Parkinson's disease. *Brain,* 122 ( Pt 2)**,** 303-13.

LIM, J. H., KIM, K. M., KIM, S. W., HWANG, O. & CHOI, H. J. 2008. Bromocriptine activates NQO1 via Nrf2-PI3K/Akt signaling: novel cytoprotective mechanism against oxidative damage. *Pharmacol Res,* 57**,** 325-31.

LIN, C. H., LI, H., LEE, Y. N., CHENG, Y. J., WU, R. M. & CHIEN, C. T. 2015. Lrrk regulates the dynamic profile of dendritic Golgi outposts through the golgin Lava lamp. *J Cell Biol,* 210**,** 471-83.

LIN, C. H., TSAI, P. I., WU, R. M. & CHIEN, C. T. 2010. LRRK2 G2019S mutation induces dendrite degeneration through mislocalization and phosphorylation of tau by recruiting autoactivated GSK3ss. *J Neurosci,* 30**,** 13138-49.

LIN, X., PARISIADOU, L., GU, X. L., WANG, L., SHIM, H., SUN, L., XIE, C., LONG, C. X., YANG, W. J., DING, J., CHEN, Z. Z., GALLANT, P. E., TAO-CHENG, J. H., RUDOW, G., TRONCOSO, J. C., LIU, Z., LI, Z. & CAI, H. 2009. Leucine-rich repeat kinase 2 regulates the progression of neuropathology induced by Parkinson's-disease-related mutant alpha-synuclein. *Neuron,* 64**,** 807-27.

LIU, M., KANG, S., RAY, S., JACKSON, J., ZAITSEV, A. D., GERBER, S. A., CUNY, G. D. & GLICKSMAN, M. A. 2011a. Kinetic, mechanistic, and structural modeling studies of truncated wild-type leucine-rich repeat kinase 2 and the G2019S mutant. *Biochemistry,* 50**,** 9399-408.

LIU, S., SAWADA, T., LEE, S., YU, W., SILVERIO, G., ALAPATT, P., MILLAN, I., SHEN, A., SAXTON, W., KANAO, T., TAKAHASHI, R., HATTORI, N., IMAI, Y. & LU, B. 2012. Parkinson's disease-associated kinase PINK1 regulates Miro protein level and axonal transport of mitochondria. *PLoS Genet,* 8**,** e1002537.

LIU, Z., HAMAMICHI, S., LEE, B. D., YANG, D., RAY, A., CALDWELL, G. A., CALDWELL, K. A., DAWSON, T. M., SMITH, W. W. & DAWSON, V. L. 2011b. Inhibitors of LRRK2 kinase attenuate neurodegeneration and Parkinson-like phenotypes in Caenorhabditis elegans and Drosophila Parkinson's disease models. *Hum Mol Genet,* 20**,** 3933-42.

LIU, Z., WANG, X., YU, Y., LI, X., WANG, T., JIANG, H., REN, Q., JIAO, Y., SAWA, A., MORAN, T., ROSS, C. A., MONTELL, C. & SMITH, W. W. 2008. A Drosophila model for LRRK2-linked parkinsonism. *Proc Natl Acad Sci U S A,* 105**,** 2693-8.

LLOYD, V., RAMASWAMI, M. & KRAMER, H. 1998. Not just pretty eyes: Drosophila eye-colour mutations and lysosomal delivery. *Trends Cell Biol,* 8**,** 257-9.

LOHMANN, E., KOROGLU, C., HANAGASI, H. A., DURSUN, B., TASAN, E. & TOLUN, A. 2012. A homozygous frameshift mutation of sepiapterin reductase gene

causing parkinsonism with onset in childhood. *Parkinsonism Relat Disord,* 18**,** 191-3.

LORENZO-BETANCOR, O., SAMARANCH, L., EZQUERRA, M., TOLOSA, E., LORENZO, E., IRIGOYEN, J., GAIG, C., PASTOR, M. A., SOTO-ORTOLAZA, A. I., ROSS, O. A., RODRIGUEZ-OROZ, M. C., VALLDEORIOLA, F., MARTI, M. J., LUQUIN, M. R., PEREZ-TUR, J., BURGUERA, J. A., OBESO, J. A. & PASTOR, P. 2012. LRRK2 haplotype-sharing analysis in Parkinson's disease reveals a novel p.S1761R mutation. *Mov Disord,* 27**,** 146-51.

LOUIE, K., GRATTAN, L. E. & GLIMCHER, P. W. 2011. Reward value-based gain control: divisive normalization in parietal cortex. *J Neurosci,* 31**,** 10627-39.

LU, B. & VOGEL, H. 2009. Drosophila models of neurodegenerative diseases. *Annu Rev Pathol,* 4**,** 315-42.

LUCKING, C. B., DURR, A., BONIFATI, V., VAUGHAN, J., DE MICHELE, G., GASSER, T., HARHANGI, B. S., MECO, G., DENEFLE, P., WOOD, N. W., AGID, Y. & BRICE, A. 2000. Association between early-onset Parkinson's disease and mutations in the parkin gene. *N Engl J Med,* 342**,** 1560-7.

LUE, N. F., CHASMAN, D. I., BUCHMAN, A. R. & KORNBERG, R. D. 1987. Interaction of GAL4 and GAL80 gene regulatory proteins in vitro. *Mol Cell Biol,* 7**,** 3446-51.

LUTHMAN, J., FREDRIKSSON, A., LEWANDER, T., JONSSON, G. & ARCHER, T. 1989. Effects of d-amphetamine and methylphenidate on hyperactivity produced by neonatal 6-hydroxydopamine treatment. *Psychopharmacology (Berl),* 99**,** 550-7.

MA, J., PLESKEN, H., TREISMAN, J. E., EDELMAN-NOVEMSKY, I. & REN, M. 2004. Lightoid and Claret: a rab GTPase and its putative guanine nucleotide exchange factor in biogenesis of Drosophila eye pigment granules. *Proc Natl Acad Sci U S A,* 101**,** 11652-7.

MA, J. & PTASHNE, M. 1987. The carboxy-terminal 30 amino acids of GAL4 are recognized by GAL80. *Cell,* 50**,** 137-42.

MACKAY, W. J. & O'DONNELL, J. M. 1983. A genetic analysis of the pteridine biosynthetic enzyme, guanosine triphosphate cyclohydrolase, in Drosophila melanogaster. *Genetics,* 105**,** 35-53.

MACKENZIE, S. M., BROOKER, M. R., GILL, T. R., COX, G. B., HOWELLS, A. J. & EWART, G. D. 1999. Mutations in the white gene of Drosophila melanogaster affecting ABC transporters that determine eye colouration. *Biochim Biophys Acta,* 1419**,** 173-85.

MACKENZIE, S. M., HOWELLS, A. J., COX, G. B. & EWART, G. D. 2000. Sub-cellular localisation of the white/scarlet ABC transporter to pigment granule membranes within the compound eye of Drosophila melanogaster. *Genetica,* 108**,** 239-52.

MACLEOD, D., DOWMAN, J., HAMMOND, R., LEETE, T., INOUE, K. & ABELIOVICH, A. 2006. The familial Parkinsonism gene LRRK2 regulates neurite process morphology. *Neuron,* 52**,** 587-93.

MACLEOD, D. A., RHINN, H., KUWAHARA, T., ZOLIN, A., DI PAOLO, G., MCCABE, B. D., MARDER, K. S., HONIG, L. S., CLARK, L. N., SMALL, S. A. & ABELIOVICH, A. 2013. RAB7L1 interacts with LRRK2 to modify intraneuronal protein sorting and Parkinson's disease risk. *Neuron,* 77**,** 425-39.

MALAGELADA, C., JIN, Z. H. & GREENE, L. A. 2008. RTP801 is induced in Parkinson's disease and mediates neuron death by inhibiting Akt phosphorylation/activation. *J Neurosci,* 28**,** 14363-71.

MALMFORS, T. 1963. Evidence of adrenergic neurons with synaptic terminals in the retina of rats demonstrated with fluorescence and electron microscopy. *Acta Physiol Scand,* 58**,** 99-100.

MANTOPOULOS, D., MURAKAMI, Y., COMANDER, J., THANOS, A., ROH, M., MILLER, J. W. & VAVVAS, D. G. 2011. Tauroursodeoxycholic acid (TUDCA) protects photoreceptors from cell death after experimental retinal detachment. *PLoS One,* 6**,** e24245.

MARIN, I. 2006. The Parkinson disease gene LRRK2: evolutionary and structural insights. *Mol Biol Evol,* 23**,** 2423-33.

MARIN, I. 2008. Ancient origin of the Parkinson disease gene LRRK2. *J Mol Evol,* 67**,** 41-50.

MARKS, W. J., JR., OSTREM, J. L., VERHAGEN, L., STARR, P. A., LARSON, P. S., BAKAY, R. A., TAYLOR, R., CAHN-WEINER, D. A., STOESSL, A. J., OLANOW, C. W. & BARTUS, R. T. 2008. Safety and tolerability of intraputaminal delivery of CERE-120 (adeno-associated virus serotype 2-neurturin) to patients with idiopathic Parkinson's disease: an open-label, phase I trial. *Lancet Neurol,* 7**,** 400-8.

MARSDEN, C. D. 1961. Pigmentation in the nucleus substantiae nigrae of mammals. *J Anat,* 95**,** 256-61.

MARTIN, I., KIM, J. W., LEE, B. D., KANG, H. C., XU, J. C., JIA, H., STANKOWSKI, J., KIM, M. S., ZHONG, J., KUMAR, M., ANDRABI, S. A., XIONG, Y., DICKSON, D. W., WSZOLEK, Z. K., PANDEY, A., DAWSON, T. M. & DAWSON, V. L. 2014. Ribosomal protein s15 phosphorylation mediates LRRK2 neurodegeneration in Parkinson's disease. *Cell,* 157**,** 472-85.

MASUDA-SUZUKAKE, M., NONAKA, T., HOSOKAWA, M., OIKAWA, T., ARAI, T., AKIYAMA, H., MANN, D. M. A. & HASEGAWA, M. 2013. Prion-like spreading of pathological $\alpha$-synuclein in brain. *Brain,* 136**,** 1128-38.

MATA, I. F., COSENTINO, C., MARCA, V., TORRES, L., MAZZETTI, P., ORTEGA, O., RAGGIO, V., ALJANATI, R., BUZO, R., YEAROUT, D., DIEGUEZ, E. & ZABETIAN, C. P. 2009. LRRK2 mutations in patients with Parkinson's disease from Peru and Uruguay. *Parkinsonism Relat Disord,* 15**,** 370-3.

MATTA, S., VAN KOLEN, K., DA CUNHA, R., VAN DEN BOGAART, G., MANDEMAKERS, W., MISKIEWICZ, K., DE BOCK, P. J., MORAIS, V. A., VILAIN, S., HADDAD, D., DELBROEK, L., SWERTS, J., CHAVEZ-GUTIERREZ, L., ESPOSITO, G., DANEELS, G., KARRAN, E., HOLT, M., GEVAERT, K., MOECHARS, D. W., DE STROOPER, B. & VERSTREKEN, P. 2012. LRRK2 controls an EndoA phosphorylation cycle in synaptic endocytosis. *Neuron,* 75**,** 1008-21.

MCGUIRE, S. E., LE, P. T., OSBORN, A. J., MATSUMOTO, K. & DAVIS, R. L. 2003. Spatiotemporal rescue of memory dysfunction in Drosophila. *Science,* 302**,** 1765-8.

MCLEAN, J. R., KRISHNAKUMAR, S. & O'DONNELL, J. M. 1993. Multiple mRNAs from the Punch locus of Drosophila melanogaster encode isoforms of GTP cyclohydrolase I with distinct N-terminal domains. *J Biol Chem,* 268**,** 27191-7.

MEINERTZHAGEN, I. A. & O'NEIL, S. D. 1991. Synaptic organization of columnar elements in the lamina of the wild type in Drosophila melanogaster. *J Comp Neurol,* 305**,** 232-63.

MEIXNER, A., BOLDT, K., VAN TROYS, M., ASKENAZI, M., GLOECKNER, C. J., BAUER, M., MARTO, J. A., AMPE, C., KINKL, N. & UEFFING, M. 2011. A QUICK screen for Lrrk2 interaction partners--leucine-rich repeat kinase 2 is involved in actin cytoskeleton dynamics. *Mol Cell Proteomics,* 10**,** M110.001172.

MELAMED, E., FRUCHT, Y., LEMOR, M., UZZAN, A. & ROSENTHAL, Y. 1984. Dopamine turnover in rat retina: a 24-hour light-dependent rhythm. *Brain Res,* 305**,** 148-51.

MELROSE, H. L., DÄCHSEL, J. C., BEHROUZ, B., LINCOLN, S. J., YUE, M., HINKLE, K. M., KENT, C., KORVATSKA, E., TAYLOR, J. P., WITTEN, L., LIANG, Y., BEEVERS, J. E., BOULES, M., SERNA, V., GAUKHMAN, A., YU, X., CASTANEDES-CASEY, M., BRAITHWAITE, A. T., OGHOLIKHAN, S., YU, N., BASS, D., TYNDALL, G., SCHELLENBERG, G. D., DICKSON, D. W., JANUS, C. & FARRER, M. J. 2010. Impaired dopaminergic neurotransmission and microtubule-associated protein tau alterations in human LRRK2 transgenic mice. *Neurobiol Dis,* 40**,** 503-17.

MENCACCI, N. E., ISAIAS, I. U., REICH, M. M., GANOS, C., PLAGNOL, V., POLKE, J. M., BRAS, J., HERSHESON, J., STAMELOU, M., PITTMAN, A. M., NOYCE, A. J., MOK, K. Y., OPLADEN, T., KUNSTMANN, E., HODECKER, S., MUNCHAU, A., VOLKMANN, J., SAMNICK, S., SIDLE, K., NANJI, T., SWEENEY, M. G., HOULDEN, H., BATLA, A., ZECCHINELLI, A. L., PEZZOLI, G., MAROTTA, G., LEES, A., ALEGRIA, P., KRACK, P., CORMIER-DEQUAIRE, F., LESAGE, S., BRICE, A., HEUTINK, P., GASSER, T., LUBBE, S. J., MORRIS, H. R., TABA, P., KOKS, S., MAJOUNIE, E., RAPHAEL GIBBS, J., SINGLETON, A., HARDY, J., KLEBE, S., BHATIA, K. P. & WOOD, N. W. 2014. Parkinson's disease in GTP cyclohydrolase 1 mutation carriers. *Brain,* 137**,** 2480-92.

MENZIES, F. M., YENISETTI, S. C. & MIN, K. T. 2005. Roles of Drosophila DJ-1 in survival of dopaminergic neurons and oxidative stress. *Curr Biol,* 15**,** 1578-82.

MEULENER, M., WHITWORTH, A. J., ARMSTRONG-GOLD, C. E., RIZZU, P., HEUTINK, P., WES, P. D., PALLANCK, L. J. & BONINI, N. M. 2005. Drosophila DJ-1 mutants are selectively sensitive to environmental toxins associated with Parkinson's disease. *Curr Biol,* 15**,** 1572-7.

MIGHELI, R., DEL GIUDICE, M. G., SPISSU, Y., SANNA, G., XIONG, Y., DAWSON, T. M., DAWSON, V. L., GALIOTO, M., ROCCHITTA, G., BIOSA, A., SERRA, P. A., CARRI, M. T., CROSIO, C. & IACCARINO, C. 2013. LRRK2 affects vesicle trafficking, neurotransmitter extracellular level and membrane receptor localization. *PLoS One,* 8**,** e77198.

MIN, J. H., HONG, Y. H., SUNG, J. J., KIM, S. M., LEE, J. B. & LEE, K. W. 2012. Oral Solubilized Ursodeoxycholic Acid Therapy in Amyotrophic Lateral Sclerosis: A Randomized Cross-Over Trial. *J Korean Med Sci,* 27**,** 200-6.

MOEHLE, M. S., WEBBER, P. J., TSE, T., SUKAR, N., STANDAERT, D. G., DESILVA, T. M., COWELL, R. M. & WEST, A. B. 2012. LRRK2 inhibition attenuates microglial inflammatory responses. *J Neurosci,* 32**,** 1602-11.

MOLLEREAU, B., WERNET, M. F., BEAUFILS, P., KILLIAN, D., PICHAUD, F., KUHNLEIN, R. & DESPLAN, C. 2000. A green fluorescent protein enhancer trap screen in Drosophila photoreceptor cells. *Mech Dev,* 93**,** 151-60.

MORAIS, V. A., VERSTREKEN, P., ROETHIG, A., SMET, J., SNELLINX, A., VANBRABANT, M., HADDAD, D., FREZZA, C., MANDEMAKERS, W., VOGT-WEISENHORN, D., VAN COSTER, R., WURST, W., SCORRANO, L. & DE STROOPER, B. 2009. Parkinson's disease mutations in PINK1 result in decreased Complex I activity and deficient synaptic function. *EMBO Mol Med,* 1**,** 99-111.

MORGAN, T. H. 1910. SEX LIMITED INHERITANCE IN DROSOPHILA. *Science,* 32**,** 120-2.

MORTIBOYS, H., AASLY, J. & BANDMANN, O. 2013. Ursocholanic acid rescues mitochondrial function in common forms of familial Parkinson's disease. *Brain,* 136**,** 3038-50.

MORTIBOYS, H., FURMSTON, R., BRONSTAD, G., AASLY, J., ELLIOTT, C. & BANDMANN, O. 2015. UDCA exerts beneficial effect on mitochondrial dysfunction in LRRK2G2019S carriers and in vivo. *Neurology*.

MORTIBOYS, H., JOHANSEN, K. K., AASLY, J. O. & BANDMANN, O. 2010. Mitochondrial impairment in patients with Parkinson disease with the G2019S mutation in LRRK2. *Neurology,* 75**,** 2017-20.

MORTIBOYS, H., THOMAS, K. J., KOOPMAN, W. J., KLAFFKE, S., ABOU-SLEIMAN, P., OLPIN, S., WOOD, N. W., WILLEMS, P. H., SMEITINK, J. A., COOKSON, M. R. & BANDMANN, O. 2008. Mitochondrial function and morphology are impaired in parkin-mutant fibroblasts. *Ann Neurol,* 64**,** 555-65.

MOSES, K. & RUBIN, G. M. 1991. Glass encodes a site-specific DNA-binding protein that is regulated in response to positional signals in the developing Drosophila eye. *Genes Dev,* 5**,** 583-93.

MOUGENOT, A. L., NICOT, S., BENCSIK, A., MORIGNAT, E., VERCHERE, J., LAKHDAR, L., LEGASTELOIS, S. & BARON, T. 2012. Prion-like acceleration of a synucleinopathy in a transgenic mouse model. *Neurobiol Aging,* 33**,** 2225-8.

MOUNT, S. M. 1987. Sequence similarity. *Nature,* 325**,** 487.

MUFTUOGLU, M., ELIBOL, B., DALMIZRAK, O., ERCAN, A., KULAKSIZ, G., OGUS, H., DALKARA, T. & OZER, N. 2004. Mitochondrial complex I and IV activities in leukocytes from patients with parkin mutations. *Mov Disord,* 19**,** 544-8.

MULLINS, C., HARTNELL, L. M. & BONIFACINO, J. S. 2000. Distinct requirements for the AP-3 adaptor complex in pigment granule and synaptic vesicle biogenesis in Drosophila melanogaster. *Mol Gen Genet,* 263**,** 1003-14.

MULLINS, C., HARTNELL, L. M., WASSARMAN, D. A. & BONIFACINO, J. S. 1999. Defective expression of the mu3 subunit of the AP-3 adaptor complex in the Drosophila pigmentation mutant carmine. *Mol Gen Genet,* 262**,** 401-12.

MUNOZ-SORIANO, V. & PARICIO, N. 2011. Drosophila models of Parkinson's disease: discovering relevant pathways and novel therapeutic strategies. *Parkinsons Dis,* 2011**,** 520640.

MURATA, H., SAKAGUCHI, M., JIN, Y., SAKAGUCHI, Y., FUTAMI, J., YAMADA, H., KATAOKA, K. & HUH, N. H. 2011. A new cytosolic pathway from a Parkinson disease-associated kinase, BRPK/PINK1: activation of AKT via mTORC2. *J Biol Chem,* 286**,** 7182-9.

NAIR, V. D. & OLANOW, C. W. 2008. Differential modulation of Akt/glycogen synthase kinase-3beta pathway regulates apoptotic and cytoprotective signaling responses. *J Biol Chem,* 283**,** 15469-78.

NG, C. H., GUAN, M. S., KOH, C., OUYANG, X., YU, F., TAN, E. K., O'NEILL, S. P., ZHANG, X., CHUNG, J. & LIM, K. L. 2012. AMP kinase activation mitigates dopaminergic dysfunction and mitochondrial abnormalities in Drosophila models of Parkinson's disease. *J Neurosci,* 32**,** 14311-7.

NG, C. H., MOK, S. Z., KOH, C., OUYANG, X., FIVAZ, M. L., TAN, E. K., DAWSON, V. L., DAWSON, T. M., YU, F. & LIM, K. L. 2009. Parkin protects against LRRK2 G2019S mutant-induced dopaminergic neurodegeneration in Drosophila. *J Neurosci,* 29**,** 11257-62.

NGUYEN-LEGROS, J. 1988. Functional neuroarchitecture of the retina: hypothesis on the dysfunction of retinal dopaminergic circuitry in Parkinson's disease. *Surg Radiol Anat,* 10**,** 137-44.
NICKLAS, W. J., YOUNGSTER, S. K., KINDT, M. V. & HEIKKILA, R. E. 1987. MPTP, MPP+ and mitochondrial function. *Life Sci,* 40**,** 721-9.
NOWAK, J. Z. & ZURAWSKA, E. 1989. Dopamine in the rabbit retina and striatum: diurnal rhythm and effect of light stimulation. *J Neural Transm,* 75**,** 201-12.
NOYCE, A. J., BESTWICK, J. P., SILVEIRA-MORIYAMA, L., HAWKES, C. H., GIOVANNONI, G., LEES, A. J. & SCHRAG, A. 2012. Meta-analysis of early nonmotor features and risk factors for Parkinson disease. *Ann Neurol,* 72**,** 893-901.
NUTT, J. G., BURCHIEL, K. J., COMELLA, C. L., JANKOVIC, J., LANG, A. E., LAWS, E. R., JR., LOZANO, A. M., PENN, R. D., SIMPSON, R. K., JR., STACY, M. & WOOTEN, G. F. 2003. Randomized, double-blind trial of glial cell line-derived neurotrophic factor (GDNF) in PD. *Neurology,* 60**,** 69-73.
NUYTEMANS, K., RADEMAKERS, R., THEUNS, J., PALS, P., ENGELBORGHS, S., PICKUT, B., DE POOTER, T., PEETERS, K., MATTHEIJSSENS, M., VAN DEN BROECK, M., CRAS, P., DE DEYN, P. P. & VAN BROECKHOVEN, C. 2008. Founder mutation p.R1441C in the leucine-rich repeat kinase 2 gene in Belgian Parkinson's disease patients. *Eur J Hum Genet,* 16**,** 471-9.
O'KANE, C. J. & GEHRING, W. J. 1987. Detection in situ of genomic regulatory elements in Drosophila. *Proc Natl Acad Sci U S A,* 84**,** 9123-7.
ODORIZZI, G., COWLES, C. R. & EMR, S. D. 1998. The AP-3 complex: a coat of many colours. *Trends Cell Biol,* 8**,** 282-8.
OGAWA, T., MATSON, W. R., BEAL, M. F., MYERS, R. H., BIRD, E. D., MILBURY, P. & SASO, S. 1992. Kynurenine pathway abnormalities in Parkinson's disease. *Neurology,* 42**,** 1702-6.
OHTA, E., KAWAKAMI, F., KUBO, M. & OBATA, F. 2011. LRRK2 directly phosphorylates Akt1 as a possible physiological substrate: impairment of the kinase activity by Parkinson's disease-associated mutations. *FEBS Lett,* 585**,** 2165-70.
OLSEN, J. H., TANGERUD, K., WERMUTH, L., FREDERIKSEN, K. & FRIIS, S. 2007. Treatment with levodopa and risk for malignant melanoma. *Mov Disord,* 22**,** 1252-7.
OLSEN, S. R., BHANDAWAT, V. & WILSON, R. I. 2010. Divisive normalization in olfactory population codes. *Neuron,* 66**,** 287-99.
OOI, C. E., MOREIRA, J. E., DELL'ANGELICA, E. C., POY, G., WASSARMAN, D. A. & BONIFACINO, J. S. 1997. Altered expression of a novel adaptin leads to defective pigment granule biogenesis in the Drosophila eye color mutant garnet. *Embo j,* 16**,** 4508-18.
OSTROWSKI, M., CARMO, N. B., KRUMEICH, S., FANGET, I., RAPOSO, G., SAVINA, A., MOITA, C. F., SCHAUER, K., HUME, A. N., FREITAS, R. P., GOUD, B., BENAROCH, P., HACOHEN, N., FUKUDA, M., DESNOS, C., SEABRA, M. C., DARCHEN, F., AMIGORENA, S., MOITA, L. F. & THERY, C. 2010. Rab27a and Rab27b control different steps of the exosome secretion pathway. *Nat Cell Biol,* 12**,** 19-30; sup pp 1-13.
OVESON, B. C., IWASE, T., HACKETT, S. F., LEE, S. Y., USUI, S., SEDLAK, T. W., SNYDER, S. H., CAMPOCHIARO, P. A. & SUNG, J. U. 2011. Constituents of bile, bilirubin and TUDCA, protect against oxidative stress-induced retinal degeneration. *J Neurochem,* 116**,** 144-53.

OZELIUS, L. J., SENTHIL, G., SAUNDERS-PULLMAN, R., OHMANN, E., DELIGTISCH, A., TAGLIATI, M., HUNT, A. L., KLEIN, C., HENICK, B., HAILPERN, S. M., LIPTON, R. B., SOTO-VALENCIA, J., RISCH, N. & BRESSMAN, S. B. 2006. LRRK2 G2019S as a cause of Parkinson's disease in Ashkenazi Jews. *N Engl J Med,* 354**,** 424-5.

PAISAN-RUIZ, C. 2009. LRRK2 gene variation and its contribution to Parkinson disease. *Hum Mutat,* 30**,** 1153-60.

PAISAN-RUIZ, C., JAIN, S., EVANS, E. W., GILKS, W. P., SIMON, J., VAN DER BRUG, M., LOPEZ DE MUNAIN, A., APARICIO, S., GIL, A. M., KHAN, N., JOHNSON, J., MARTINEZ, J. R., NICHOLL, D., CARRERA, I. M., PENA, A. S., DE SILVA, R., LEES, A., MARTI-MASSO, J. F., PEREZ-TUR, J., WOOD, N. W. & SINGLETON, A. B. 2004. Cloning of the gene containing mutations that cause PARK8-linked Parkinson's disease. *Neuron,* 44**,** 595-600.

PAISAN-RUIZ, C., LEWIS, P. A. & SINGLETON, A. B. 2013. LRRK2: cause, risk, and mechanism. *J Parkinsons Dis,* 3**,** 85-103.

PALACINO, J. J., SAGI, D., GOLDBERG, M. S., KRAUSS, S., MOTZ, C., WACKER, M., KLOSE, J. & SHEN, J. 2004. Mitochondrial dysfunction and oxidative damage in parkin-deficient mice. *J Biol Chem,* 279**,** 18614-22.

PAN, T., LI, X. & JANKOVIC, J. 2011. The association between Parkinson's disease and melanoma. *Int J Cancer,* 128**,** 2251-60.

PANTAZIS, A., SEGARAN, A., LIU, C. H., NIKOLAEV, A., RISTER, J., THUM, A. S., ROEDER, T., SEMENOV, E., JUUSOLA, M. & HARDIE, R. C. 2008. Distinct roles for two histamine receptors (hclA and hclB) at the Drosophila photoreceptor synapse. *J Neurosci,* 28**,** 7250-9.

PARISIADOU, L. & CAI, H. 2010. LRRK2 function on actin and microtubule dynamics in Parkinson disease. *Commun Integr Biol,* 3**,** 396-400.

PARISIADOU, L., XIE, C., CHO, H. J., LIN, X., GU, X. L., LONG, C. X., LOBBESTAEL, E., BAEKELANDT, V., TAYMANS, J. M., SUN, L. & CAI, H. 2009. Phosphorylation of ezrin/radixin/moesin proteins by LRRK2 promotes the rearrangement of actin cytoskeleton in neuronal morphogenesis. *J Neurosci,* 29**,** 13971-80.

PARISIADOU, L., YU, J., SGOBIO, C., XIE, C., LIU, G., SUN, L., GU, X. L., LIN, X., CROWLEY, N. A., LOVINGER, D. M. & CAI, H. 2014. LRRK2 regulates synaptogenesis and dopamine receptor activation through modulation of PKA activity. *Nat Neurosci,* 17**,** 367-76.

PARK, J., KIM, S. Y., CHA, G. H., LEE, S. B., KIM, S. & CHUNG, J. 2005. Drosophila DJ-1 mutants show oxidative stress-sensitive locomotive dysfunction. *Gene,* 361**,** 133-9.

PARK, J., LEE, G. & CHUNG, J. 2009. The PINK1-Parkin pathway is involved in the regulation of mitochondrial remodeling process. *Biochem Biophys Res Commun,* 378**,** 518-23.

PARK, J., LEE, S. B., LEE, S., KIM, Y., SONG, S., KIM, S., BAE, E., KIM, J., SHONG, M., KIM, J. M. & CHUNG, J. 2006. Mitochondrial dysfunction in Drosophila PINK1 mutants is complemented by parkin. *Nature,* 441**,** 1157-61.

PARK, Y. S., KIM, J. H., JACOBSON, K. B. & YIM, J. J. 1990. Purification and characterization of 6-pyruvoyl-tetrahydropterin synthase from Drosophila melanogaster. *Biochim Biophys Acta,* 1038**,** 186-94.

PARKER, W. D., JR., PARKS, J. K. & SWERDLOW, R. H. 2008. Complex I deficiency in Parkinson's disease frontal cortex. *Brain Res,* 1189**,** 215-8.

PARKINSON, J. 2002. An essay on the shaking palsy. 1817. *J Neuropsychiatry Clin Neurosci,* 14**,** 223-36; discussion 222.

PARRY, G. J., RODRIGUES, C. M., ARANHA, M. M., HILBERT, S. J., DAVEY, C., KELKAR, P., LOW, W. C. & STEER, C. J. 2010. Safety, tolerability, and cerebrospinal fluid penetration of ursodeoxycholic Acid in patients with amyotrophic lateral sclerosis. *Clin Neuropharmacol,* 33**,** 17-21.

PASTINK, A., HEEMSKERK, E., NIVARD, M. J., VAN VLIET, C. J. & VOGEL, E. W. 1991. Mutational specificity of ethyl methanesulfonate in excision-repair-proficient and -deficient strains of Drosophila melanogaster. *Mol Gen Genet,* 229**,** 213-8.

PASTINK, A., SCHALET, A. P., VREEKEN, C., PARADI, E. & EEKEN, J. C. 1987. The nature of radiation-induced mutations at the white locus of Drosophila melanogaster. *Mutat Res,* 177**,** 101-15.

PAULK, A., MILLARD, S. S. & VAN SWINDEREN, B. 2013. Vision in Drosophila: seeing the world through a model's eyes. *Annu Rev Entomol,* 58**,** 313-32.

PEREZ, C., RUIZ, S., FERREIRO, M. J., MARCHESANO, M., AGUILERA, P., CAPUTI, A., ARANSAY, A. M., BARRIO, R. & CANTERA, R. 2014. Mutations in White Cause Neurodegeneration. *Neurofly 2014.* Crete, Greece.

PEREZ, F. A. & PALMITER, R. D. 2005. Parkin-deficient mice are not a robust model of parkinsonism. *Proc Natl Acad Sci U S A,* 102**,** 2174-9.

PESAH, Y., PHAM, T., BURGESS, H., MIDDLEBROOKS, B., VERSTREKEN, P., ZHOU, Y., HARDING, M., BELLEN, H. & MARDON, G. 2004. Drosophila parkin mutants have decreased mass and cell size and increased sensitivity to oxygen radical stress. *Development,* 131**,** 2183-94.

PFUTZNER, W. & PRZYBILLA, B. 1997. Malignant melanoma and levodopa: is there a relationship? Two new cases and a review of the literature. *J Am Acad Dermatol,* 37**,** 332-6.

PHILLIPS, D. P. 1990. Neural representation of sound amplitude in the auditory cortex: effects of noise masking. *Behav Brain Res,* 37**,** 197-214.

PHILLIPS, J. P., SIMMONS, J. R. & BOWMAN, J. T. 1970. Terminal synthesis of xanthommatin in Drosophila melanogaster. I. Roles of phenol oxidase and substrate availability. *Biochem Genet,* 4**,** 481-7.

PHILLIPS, M. J., WALKER, T. A., CHOI, H. Y., FAULKNER, A. E., KIM, M. K., SIDNEY, S. S., BOYD, A. P., NICKERSON, J. M., BOATRIGHT, J. H. & PARDUE, M. T. 2008. Tauroursodeoxycholic acid preservation of photoreceptor structure and function in the rd10 mouse through postnatal day 30. *Invest Ophthalmol Vis Sci,* 49**,** 2148-55.

PICCOLI, C., SARDANELLI, A., SCRIMA, R., RIPOLI, M., QUARATO, G., D'APRILE, A., BELLOMO, F., SCACCO, S., DE MICHELE, G., FILLA, A., IUSO, A., BOFFOLI, D., CAPITANIO, N. & PAPA, S. 2008. Mitochondrial respiratory dysfunction in familiar parkinsonism associated with PINK1 mutation. *Neurochem Res,* 33**,** 2565-74.

PICCOLI, G., CONDLIFFE, S. B., BAUER, M., GIESERT, F., BOLDT, K., DE ASTIS, S., MEIXNER, A., SARIOGLU, H., VOGT-WEISENHORN, D. M., WURST, W., GLOECKNER, C. J., MATTEOLI, M., SALA, C. & UEFFING, M. 2011. LRRK2 controls synaptic vesicle storage and mobilization within the recycling pool. *J Neurosci,* 31**,** 2225-37.

PICCOLI, G., ONOFRI, F., CIRNARU, M. D., KAISER, C. J., JAGTAP, P., KASTENMULLER, A., PISCHEDDA, F., MARTE, A., VON ZWEYDORF, F., VOGT, A., GIESERT, F., PAN, L., ANTONUCCI, F., KIEL, C., ZHANG, M., WEINKAUF, S., SATTLER, M., SALA, C., MATTEOLI, M., UEFFING, M. & GLOECKNER, C. J. 2014. Leucine-rich repeat

kinase 2 binds to neuronal vesicles through protein interactions mediated by its C-terminal WD40 domain. *Mol Cell Biol,* 34**,** 2147-61.

PIERI, V., DIEDERICH, N. J., RAMAN, R. & GOETZ, C. G. 2000. Decreased color discrimination and contrast sensitivity in Parkinson's disease. *J Neurol Sci,* 172**,** 7-11.

PINKHARDT, E. H. & KASSUBEK, J. 2011. Ocular motor abnormalities in Parkinsonian syndromes. *Parkinsonism Relat Disord,* 17**,** 223-30.

PLOWEY, E. D., CHERRA, S. J., 3RD, LIU, Y. J. & CHU, C. T. 2008. Role of autophagy in G2019S-LRRK2-associated neurite shortening in differentiated SH-SY5Y cells. *J Neurochem,* 105**,** 1048-56.

POGSON, J. H., IVATT, R. M., SANCHEZ-MARTINEZ, A., TUFI, R., WILSON, E., MORTIBOYS, H. & WHITWORTH, A. J. 2014. The complex I subunit NDUFA10 selectively rescues Drosophila pink1 mutants through a mechanism independent of mitophagy. *PLoS Genet,* 10**,** e1004815.

POLYMEROPOULOS, M. H., HIGGINS, J. J., GOLBE, L. I., JOHNSON, W. G., IDE, S. E., DI IORIO, G., SANGES, G., STENROOS, E. S., PHO, L. T., SCHAFFER, A. A., LAZZARINI, A. M., NUSSBAUM, R. L. & DUVOISIN, R. C. 1996. Mapping of a gene for Parkinson's disease to chromosome 4q21-q23. *Science,* 274**,** 1197-9.

POLYMEROPOULOS, M. H., LAVEDAN, C., LEROY, E., IDE, S. E., DEHEJIA, A., DUTRA, A., PIKE, B., ROOT, H., RUBENSTEIN, J., BOYER, R., STENROOS, E. S., CHANDRASEKHARAPPA, S., ATHANASSIADOU, A., PAPAPETROPOULOS, T., JOHNSON, W. G., LAZZARINI, A. M., DUVOISIN, R. C., DI IORIO, G., GOLBE, L. I. & NUSSBAUM, R. L. 1997. Mutation in the alpha-synuclein gene identified in families with Parkinson's disease. *Science,* 276**,** 2045-7.

PONSEN, M. M., STOFFERS, D., BOOIJ, J., VAN ECK-SMIT, B. L., WOLTERS, E. & BERENDSE, H. W. 2004. Idiopathic hyposmia as a preclinical sign of Parkinson's disease. *Ann Neurol,* 56**,** 173-81.

POOLE, A. C., THOMAS, R. E., ANDREWS, L. A., MCBRIDE, H. M., WHITWORTH, A. J. & PALLANCK, L. J. 2008. The PINK1/Parkin pathway regulates mitochondrial morphology. *Proc Natl Acad Sci U S A,* 105**,** 1638-43.

POSTUMA, R. B., AARSLAND, D., BARONE, P., BURN, D. J., HAWKES, C. H., OERTEL, W. & ZIEMSSEN, T. 2012. Identifying prodromal Parkinson's disease: pre-motor disorders in Parkinson's disease. *Mov Disord,* 27**,** 617-26.

POUPON, R. E., POUPON, R. & BALKAU, B. 1994. Ursodiol for the long-term treatment of primary biliary cirrhosis. The UDCA-PBC Study Group. *N Engl J Med,* 330**,** 1342-7.

POZDEYEV, N. V. & LAVRIKOVA, E. V. 2000. Diurnal changes of tyrosine, dopamine, and dopamine metabolites content in the retina of rats maintained at different lighting conditions. *J Mol Neurosci,* 15**,** 1-9.

PRABHUDESAI, S., BENSABEUR, F. Z., ABDULLAH, R., BASAK, I., BAEZ, S., ALVES, G., HOLTZMAN, N. G., LARSEN, J. P. & MOLLER, S. G. 2016. LRRK2 knockdown in zebrafish causes developmental defects, neuronal loss, and synuclein aggregation. *J Neurosci Res,* 94**,** 717-35.

PRZYBILLA, B., SCHWAB, U., LANDTHALER, M. & BRAUN-FALCO, O. 1985. Development of two malignant melanomas during administration of levodopa. *Acta Derm Venereol,* 65**,** 556-7.

PYŻA, E. & CYMBOROWSKI, B. 2001. Circadian rhythms in behaviour and in the visual system of the blow fly, Calliphora vicina. *Journal of Insect Physiology,* 47**,** 897-904.

PYZA, E. & MEINERTZHAGEN, I. A. 1995. Monopolar cell axons in the first optic neuropil of the housefly, Musca domestica L., undergo daily fluctuations in diameter that have a circadian basis. *J Neurosci,* 15**,** 407-18.
PYZA, E. & MEINERTZHAGEN, I. A. 1999. Daily rhythmic changes of cell size and shape in the first optic neuropil in Drosophila melanogaster. *J Neurobiol,* 40**,** 77-88.
QIAGEN. 2010. *QIAprep Spin Miniprep Kit* [Online]. Available: https://www.qiagen.com/gb/ [Accessed 15 May 2016].
QIAGEN. 2015. *(EN) - QIAquick Gel Extraction Kit* [Online]. Available: https://www.qiagen.com/gb/ [Accessed 15 May 2016].
RAJENDRAN, L., HONSHO, M., ZAHN, T. R., KELLER, P., GEIGER, K. D., VERKADE, P. & SIMONS, K. 2006. Alzheimer's disease beta-amyloid peptides are released in association with exosomes. *Proc Natl Acad Sci U S A,* 103**,** 11172-7.
RAMASWAMY, S. & KORDOWER, J. H. 2009. Are growth factors the answer? *Parkinsonism Relat Disord,* 15 Suppl 3**,** S176-80.
RAMONET, D., DAHER, J. P., LIN, B. M., STAFA, K., KIM, J., BANERJEE, R., WESTERLUND, M., PLETNIKOVA, O., GLAUSER, L., YANG, L., LIU, Y., SWING, D. A., BEAL, M. F., TRONCOSO, J. C., MCCAFFERY, J. M., JENKINS, N. A., COPELAND, N. G., GALTER, D., THOMAS, B., LEE, M. K., DAWSON, T. M., DAWSON, V. L. & MOORE, D. J. 2011. Dopaminergic neuronal loss, reduced neurite complexity and autophagic abnormalities in transgenic mice expressing G2019S mutant LRRK2. *PLoS One,* 6**,** e18568.
RAMSDEN, N., PERRIN, J., REN, Z., LEE, B. D., ZINN, N., DAWSON, V. L., TAM, D., BOVA, M., LANG, M., DREWES, G., BANTSCHEFF, M., BARD, F., DAWSON, T. M. & HOPF, C. 2011. Chemoproteomics-based design of potent LRRK2-selective lead compounds that attenuate Parkinson's disease-related toxicity in human neurons. *ACS Chem Biol,* 6**,** 1021-8.
RANA, A., RERA, M. & WALKER, D. W. 2013. Parkin overexpression during aging reduces proteotoxicity, alters mitochondrial dynamics, and extends lifespan. *Proc Natl Acad Sci U S A,* 110**,** 8638-43.
RANGANAYAKULU, G., SCHULZ, R. A. & OLSON, E. N. 1996. Wingless signaling induces nautilus expression in the ventral mesoderm of the Drosophila embryo. *Dev Biol,* 176**,** 143-8.
RAY, S. & LIU, M. 2012. Current understanding of LRRK2 in Parkinson's disease: biochemical and structural features and inhibitor design. *Future Med Chem,* 4**,** 1701-13.
REAUME, A. G., KNECHT, D. A. & CHOVNICK, A. 1991. The rosy locus in Drosophila melanogaster: xanthine dehydrogenase and eye pigments. *Genetics,* 129**,** 1099-109.
REGAN, D. & MAXNER, C. 1987. Orientation-selective visual loss in patients with Parkinson's disease. *Brain,* 110 ( Pt 2)**,** 415-32.
REHLING, P., DARSOW, T., KATZMANN, D. J. & EMR, S. D. 1999. Formation of AP-3 transport intermediates requires Vps41 function. *Nat Cell Biol,* 1**,** 346-53.
REITER, L. T., POTOCKI, L., CHIEN, S., GRIBSKOV, M. & BIER, E. 2001. A systematic analysis of human disease-associated gene sequences in Drosophila melanogaster. *Genome Res,* 11**,** 1114-25.
RIEDER, S. E. & EMR, S. D. 1997. A novel RING finger protein complex essential for a late step in protein transport to the yeast vacuole. *Mol Biol Cell,* 8**,** 2307-27.
RIES, V., HENCHCLIFFE, C., KAREVA, T., RZHETSKAYA, M., BLAND, R., DURING, M. J., KHOLODILOV, N. & BURKE, R. E. 2006. Oncoprotein Akt/PKB induces trophic

effects in murine models of Parkinson's disease. *Proc Natl Acad Sci U S A,* 103**,** 18757-62.
RISTER, J., PAULS, D., SCHNELL, B., TING, C. Y., LEE, C. H., SINAKEVITCH, I., MORANTE, J., STRAUSFELD, N. J., ITO, K. & HEISENBERG, M. 2007. Dissection of the peripheral motion channel in the visual system of Drosophila melanogaster. *Neuron,* 56**,** 155-70.
RIVERO-RIOS, P., GOMEZ-SUAGA, P., FERNANDEZ, B., MADERO-PEREZ, J., SCHWAB, A. J., EBERT, A. D. & HILFIKER, S. 2015. Alterations in late endocytic trafficking related to the pathobiology of LRRK2-linked Parkinson's disease. *Biochem Soc Trans,* 43**,** 390-5.
ROBERTS, J. E. 2001. Ocular phototoxicity. *J Photochem Photobiol B,* 64**,** 136-43.
RODRIGUES, C. M., SOLA, S., NAN, Z., CASTRO, R. E., RIBEIRO, P. S., LOW, W. C. & STEER, C. J. 2003. Tauroursodeoxycholic acid reduces apoptosis and protects against neurological injury after acute hemorrhagic stroke in rats. *Proc Natl Acad Sci U S A,* 100**,** 6087-92.
ROOTE, J. & PROKOP, A. 2013. How to design a genetic mating scheme: a basic training package for Drosophila genetics. *G3 (Bethesda),* 3**,** 353-8.
RORTH, P., SZABO, K., BAILEY, A., LAVERTY, T., REHM, J., RUBIN, G. M., WEIGMANN, K., MILAN, M., BENES, V., ANSORGE, W. & COHEN, S. M. 1998. Systematic gain-of-function genetics in Drosophila. *Development,* 125**,** 1049-57.
ROSS, O. A., SPANAKI, C., GRIFFITH, A., LIN, C. H., KACHERGUS, J., HAUGARVOLL, K., LATSOUDIS, H., PLAITAKIS, A., FERREIRA, J. J., SAMPAIO, C., BONIFATI, V., WU, R. M., ZABETIAN, C. P. & FARRER, M. J. 2009. Haplotype analysis of Lrrk2 R1441H carriers with parkinsonism. *Parkinsonism Relat Disord,* 15**,** 466-7.
RUIZ-MARTINEZ, J., GOROSTIDI, A., GOYENECHEA, E., ALZUALDE, A., POZA, J. J., RODRIGUEZ, F., BERGARECHE, A., MORENO, F., LOPEZ DE MUNAIN, A. & MARTI MASSO, J. F. 2011. Olfactory deficits and cardiac 123I-MIBG in Parkinson's disease related to the LRRK2 R1441G and G2019S mutations. *Mov Disord,* 26**,** 2026-31.
RYALL, R. L. & HOWELLS, A. J. 1974. Ommochrome biosynthetic pathway of Drosophila melanogaster: Variations in levels of enzyme activities and intermediates during adult development. *Insect Biochemistry,* 4**,** 47-61.
RYDER, E. & RUSSELL, S. 2003. Transposable elements as tools for genomics and genetics in Drosophila. *Brief Funct Genomic Proteomic,* 2**,** 57-71.
SAGI, Y., MANDEL, S., AMIT, T. & YOUDIM, M. B. 2007. Activation of tyrosine kinase receptor signaling pathway by rasagiline facilitates neurorescue and restoration of nigrostriatal dopamine neurons in post-MPTP-induced parkinsonism. *Neurobiol Dis,* 25**,** 35-44.
SAKITT, B. 1972. Counting every quantum. *J Physiol,* 223**,** 131-50.
SALCEDO, E., HUBER, A., HENRICH, S., CHADWELL, L. V., CHOU, W. H., PAULSEN, R. & BRITT, S. G. 1999. Blue- and green-absorbing visual pigments of Drosophila: ectopic expression and physiological characterization of the R8 photoreceptor cell-specific Rh5 and Rh6 rhodopsins. *J Neurosci,* 19**,** 10716-26.
SAMAN, S., KIM, W., RAYA, M., VISNICK, Y., MIRO, S., SAMAN, S., JACKSON, B., MCKEE, A. C., ALVAREZ, V. E., LEE, N. C. & HALL, G. F. 2012. Exosome-associated tau is secreted in tauopathy models and is selectively phosphorylated in cerebrospinal fluid in early Alzheimer disease. *J Biol Chem,* 287**,** 3842-9.
SAMPATH, A. P. & RIEKE, F. 2004. Selective transmission of single photon responses by saturation at the rod-to-rod bipolar synapse. *Neuron,* 41**,** 431-43.

SANCHO, R. M., LAW, B. M. & HARVEY, K. 2009. Mutations in the LRRK2 Roc-COR tandem domain link Parkinson's disease to Wnt signalling pathways. *Hum Mol Genet,* 18**,** 3955-68.
SANDYK, R. 1992. Accelerated growth of malignant melanoma by levodopa in Parkinson's disease and role of the pineal gland. *Int J Neurosci,* 63**,** 137-40.
SANES, J. R. & ZIPURSKY, S. L. 2010. Design principles of insect and vertebrate visual systems. *Neuron,* 66**,** 15-36.
SANNA, G., DEL GIUDICE, M. G., CROSIO, C. & IACCARINO, C. 2012. LRRK2 and vesicle trafficking. *Biochem Soc Trans,* 40**,** 1117-22.
SAPORITO, M. S., THOMAS, B. A. & SCOTT, R. W. 2000. MPTP activates c-Jun NH(2)-terminal kinase (JNK) and its upstream regulatory kinase MKK4 in nigrostriatal neurons in vivo. *J Neurochem,* 75**,** 1200-8.
SAUNDERS-PULLMAN, R., BARRETT, M. J., STANLEY, K. M., LUCIANO, M. S., SHANKER, V., SEVERT, L., HUNT, A., RAYMOND, D., OZELIUS, L. J. & BRESSMAN, S. B. 2010. LRRK2 G2019S mutations are associated with an increased cancer risk in Parkinson disease. *Movement Disorders,* 25**,** 2536-2541.
SAUNDERS-PULLMAN, R., STANLEY, K., WANG, C., SAN LUCIANO, M., SHANKER, V., HUNT, A., SEVERT, L., RAYMOND, D., OZELIUS, L. J., LIPTON, R. B. & BRESSMAN, S. B. 2011. Olfactory dysfunction in LRRK2 G2019S mutation carriers. *Neurology,* 77**,** 319-24.
SCANGA, S. E., RUEL, L., BINARI, R. C., SNOW, B., STAMBOLIC, V., BOUCHARD, D., PETERS, M., CALVIERI, B., MAK, T. W., WOODGETT, J. R. & MANOUKIAN, A. S. 2000. The conserved PI3'K/PTEN/Akt signaling pathway regulates both cell size and survival in Drosophila. *Oncogene,* 19**,** 3971-7.
SCHAPIRA, A. H., COOPER, J. M., DEXTER, D., JENNER, P., CLARK, J. B. & MARSDEN, C. D. 1989. Mitochondrial complex I deficiency in Parkinson's disease. *Lancet,* 1**,** 1269.
SCHNEEWEIS, D. M. & SCHNAPF, J. L. 1999. The photovoltage of macaque cone photoreceptors: adaptation, noise, and kinetics. *J Neurosci,* 19**,** 1203-16.
SCHULTE, E. C., ELLWANGER, D. C., DIHANICH, S., MANZONI, C., STANGL, K., SCHORMAIR, B., GRAF, E., ECK, S., MOLLENHAUER, B., HAUBENBERGER, D., PIRKER, W., ZIMPRICH, A., BRUCKE, T., LICHTNER, P., PETERS, A., GIEGER, C., TRENKWALDER, C., MEWES, H. W., MEITINGER, T., LEWIS, P. A., KLUNEMANN, H. H. & WINKELMANN, J. 2014. Rare variants in LRRK1 and Parkinson's disease. *Neurogenetics,* 15**,** 49-57.
SCHWARZ, M. J., GUILLEMIN, G. J., TEIPEL, S. J., BUERGER, K. & HAMPEL, H. 2013. Increased 3-hydroxykynurenine serum concentrations differentiate Alzheimer's disease patients from controls. *Eur Arch Psychiatry Clin Neurosci,* 263**,** 345-52.
SEARLES, L. L. & VOELKER, R. A. 1986. Molecular characterization of the Drosophila vermilion locus and its suppressible alleles. *Proc Natl Acad Sci U S A,* 83**,** 404-8.
SEPE, V., RENGA, B., FESTA, C., D'AMORE, C., MASULLO, D., CIPRIANI, S., DI LEVA, F. S., MONTI, M. C., NOVELLINO, E., LIMONGELLI, V., ZAMPELLA, A. & FIORUCCI, S. 2014. Modification on ursodeoxycholic acid (UDCA) scaffold. discovery of bile acid derivatives as selective agonists of cell-surface G-protein coupled bile acid receptor 1 (GP-BAR1). *J Med Chem,* 57**,** 7687-701.

SEVRIOUKOV, E. A., HE, J. P., MOGHRABI, N., SUNIO, A. & KRAMER, H. 1999. A role for the deep orange and carnation eye color genes in lysosomal delivery in Drosophila. *Mol Cell,* 4**,** 479-86.

SHANKER, V., GROVES, M., HEIMAN, G., PALMESE, C., SAUNDERS-PULLMAN, R., OZELIUS, L., RAYMOND, D. & BRESSMAN, S. 2011. Mood and cognition in leucine-rich repeat kinase 2 G2019S Parkinson's disease. *Mov Disord,* 26**,** 1875-80.

SHESTOPAL, S. A., MAKUNIN, I. V., BELYAEVA, E. S., ASHBURNER, M. & ZHIMULEV, I. F. 1997. Molecular characterization of the deep orange (dor) gene of Drosophila melanogaster. *Mol Gen Genet,* 253**,** 642-8.

SHIBASAKI, H., TSUJI, S. & KUROIWA, Y. 1979. Oculomotor abnormalities in Parkinson's disease. *Arch Neurol,* 36**,** 360-4.

SHIMURA, H., HATTORI, N., KUBO, S., MIZUNO, Y., ASAKAWA, S., MINOSHIMA, S., SHIMIZU, N., IWAI, K., CHIBA, T., TANAKA, K. & SUZUKI, T. 2000. Familial Parkinson disease gene product, parkin, is a ubiquitin-protein ligase. *Nat Genet,* 25**,** 302-5.

SHIN, N., JEONG, H., KWON, J., HEO, H. Y., KWON, J. J., YUN, H. J., KIM, C. H., HAN, B. S., TONG, Y., SHEN, J., HATANO, T., HATTORI, N., KIM, K. S., CHANG, S. & SEOL, W. 2008. LRRK2 regulates synaptic vesicle endocytosis. *Exp Cell Res,* 314**,** 2055-65.

SHISHIDO, E., TAKEICHI, M. & NOSE, A. 1998. Drosophila synapse formation: regulation by transmembrane protein with Leu-rich repeats, CAPRICIOUS. *Science,* 280**,** 2118-21.

SHOUP, J. R. 1966. The development of pigment granules in the eyes of wild type and mutant Drosophila melanogaster. *J Cell Biol,* 29**,** 223-49.

SIERRA, M., SANCHEZ-JUAN, P., MARTINEZ-RODRIGUEZ, M. I., GONZALEZ-ARAMBURU, I., GARCIA-GOROSTIAGA, I., QUIRCE, M. R., PALACIO, E., CARRIL, J. M., BERCIANO, J., COMBARROS, O. & INFANTE, J. 2013. Olfaction and imaging biomarkers in premotor LRRK2 G2019S-associated Parkinson disease. *Neurology,* 80**,** 621-6.

SILVEIRA-MORIYAMA, L., MUNHOZ, R. P., DE, J. C. M., RASKIN, S., ROGAEVA, E., DE, C. A. P., BRESSAN, R. A., FELICIO, A. C., BARSOTTINI, O. G., ANDRADE, L. A., CHIEN, H. F., BONIFATI, V., BARBOSA, E. R., TEIVE, H. A. & LEES, A. J. 2010. Olfactory heterogeneity in LRRK2 related Parkinsonism. *Mov Disord,* 25**,** 2879-83.

SIMPSON, F., PEDEN, A. A., CHRISTOPOULOU, L. & ROBINSON, M. S. 1997. Characterization of the Adaptor-related Protein Complex, AP-3. *J Cell Biol,* 137**,** 835-45.

SKIBBA, J. L., PINCKLEY, J., GILBERT, E. F. & JOHNSON, R. O. 1972. Multiple primary melanoma following administration of levodopa. *Arch Pathol,* 93**,** 556-61.

SLEVIN, J. T., GASH, D. M., SMITH, C. D., GERHARDT, G. A., KRYSCIO, R., CHEBROLU, H., WALTON, A., WAGNER, R. & YOUNG, A. B. 2007. Unilateral intraputamenal glial cell line-derived neurotrophic factor in patients with Parkinson disease: response to 1 year of treatment and 1 year of withdrawal. *J Neurosurg,* 106**,** 614-20.

SMITH, W. W., PEI, Z., JIANG, H., MOORE, D. J., LIANG, Y., WEST, A. B., DAWSON, V. L., DAWSON, T. M. & ROSS, C. A. 2005. Leucine-rich repeat kinase 2 (LRRK2) interacts with parkin, and mutant LRRK2 induces neuronal degeneration. *Proc Natl Acad Sci U S A,* 102**,** 18676-81.

SOBER, A. J. & WICK, M. M. 1978. Levodopa therapy and malignant melanoma. *Jama,* 240**,** 554-5.
SPILLANTINI, M. G., CROWTHER, R. A., JAKES, R., HASEGAWA, M. & GOEDERT, M. 1998. alpha-Synuclein in filamentous inclusions of Lewy bodies from Parkinson's disease and dementia with lewy bodies. *Proc Natl Acad Sci U S A,* 95**,** 6469-73.
SPRADLING, A. C., STERN, D., BEATON, A., RHEM, E. J., LAVERTY, T., MOZDEN, N., MISRA, S. & RUBIN, G. M. 1999. The Berkeley Drosophila Genome Project gene disruption project: Single P-element insertions mutating 25% of vital Drosophila genes. *Genetics,* 153**,** 135-77.
ST JOHNSTON, D. 2002. The art and design of genetic screens: Drosophila melanogaster. *Nat Rev Genet,* 3**,** 176-88.
STARK, W. S. 1973. The effect of eye colour pigments on the action spectrum of Drosophila. *J Insect Physiol,* 19**,** 999-1006.
STEGER, M., TONELLI, F., ITO, G., DAVIES, P., TROST, M., VETTER, M., WACHTER, S., LORENTZEN, E., DUDDY, G., WILSON, S., BAPTISTA, M. A. S., FISKE, B. K., FELL, M. J., MORROW, J. A., REITH, A. D., ALESSI, D. R. & MANN, M. 2016. Phosphoproteomics reveals that Parkinson's disease kinase LRRK2 regulates a subset of Rab GTPases. *eLife,* 5.
STRATAGENE. 2004. *XL1-Blue Competent Cells* [Online]. Available: http://www.chem-agilent.com/pdf/strata/200249.pdf [Accessed 15 May 2016].
SULLIVAN, D. T. & SULLIVAN, M. C. 1975. Transport defects as the physiological basis for eye color mutants of Drosophila melanogaster. *Biochem Genet,* 13**,** 603-13.
SUMMERS, K. M., HOWELLS, A. J. & PYLIOTIS, N. A. 1982. Biology of Eye Pigmentation in Insects. *In:* M.J. BERRIDGE, J. E. T. & WIGGLESWORTH, V. B. (eds.) *Advances in Insect Physiology.* Academic Press.
SURYANARAYANAN, A. & SLAUGHTER, M. M. 2006. Synaptic transmission mediated by internal calcium stores in rod photoreceptors. *J Neurosci,* 26**,** 1759-66.
TAGLIATI, M., BODIS-WOLLNER, I., KOVANECZ, I. & STANZIONE, P. 1994. Spatial frequency tuning of the monkey pattern ERG depends on D2 receptor-linked action of dopamine. *Vision Res,* 34**,** 2051-7.
TATTON, W. G., KWAN, M. M., VERRIER, M. C., SENIUK, N. A. & THERIAULT, E. 1990. MPTP produces reversible disappearance of tyrosine hydroxylase-containing retinal amacrine cells. *Brain Res,* 527**,** 21-31.
TAYMANS, J. M. & COOKSON, M. R. 2010. Mechanisms in dominant parkinsonism: The toxic triangle of LRRK2, alpha-synuclein, and tau. *Bioessays,* 32**,** 227-35.
TEARLE, R. 1991. Tissue specific effects of ommochrome pathway mutations in Drosophila melanogaster. *Genet Res,* 57**,** 257-66.
THANVI, B., LO, N. & ROBINSON, T. 2007. Levodopa‐induced dyskinesia in Parkinson's disease: clinical features, pathogenesis, prevention and treatment. *Postgrad Med J,* 83**,** 384-8.
THEVENET, J., PESCINI GOBERT, R., HOOFT VAN HUIJSDUIJNEN, R., WIESSNER, C. & SAGOT, Y. J. 2011. Regulation of LRRK2 expression points to a functional role in human monocyte maturation. *PLoS One,* 6**,** e21519.
THOMAS, B. B., ARAMANT, R. B., SADDA, S. R. & SEILER, M. J. 2005. Light response differences in the superior colliculus of albino and pigmented rats. *Neurosci Lett,* 385**,** 143-7.

TIMMONS, S., COAKLEY, M. F., MOLONEY, A. M. & C, O. N. 2009. Akt signal transduction dysfunction in Parkinson's disease. *Neurosci Lett,* 467**,** 30-5.

TING, C. Y. & LEE, C. H. 2007. Visual circuit development in Drosophila. *Curr Opin Neurobiol,* 17**,** 65-72.

TOBIN, J. E., CUI, J., WILK, J. B., LATOURELLE, J. C., LARAMIE, J. M., MCKEE, A. C., GUTTMAN, M., KARAMOHAMED, S., DESTEFANO, A. L. & MYERS, R. H. 2007. Sepiapterin reductase expression is increased in Parkinson's disease brain tissue. *Brain Res,* 1139**,** 42-7.

TOMLINSON, A. 2012. The Origin of the Drosophila Subretinal Pigment Layer. *J Comp Neurol,* 520**,** 2676-82.

TONG, Y., GIAIME, E., YAMAGUCHI, H., ICHIMURA, T., LIU, Y., SI, H., CAI, H., BONVENTRE, J. V. & SHEN, J. 2012. Loss of leucine-rich repeat kinase 2 causes age-dependent bi-phasic alterations of the autophagy pathway. *Mol Neurodegener,* 7**,** 2.

TONG, Y., PISANI, A., MARTELLA, G., KAROUANI, M., YAMAGUCHI, H., POTHOS, E. N. & SHEN, J. 2009. R1441C mutation in LRRK2 impairs dopaminergic neurotransmission in mice. *Proc Natl Acad Sci U S A,* 106**,** 14622-7.

TONG, Y., YAMAGUCHI, H., GIAIME, E., BOYLE, S., KOPAN, R., KELLEHER, R. J., 3RD & SHEN, J. 2010. Loss of leucine-rich repeat kinase 2 causes impairment of protein degradation pathways, accumulation of alpha-synuclein, and apoptotic cell death in aged mice. *Proc Natl Acad Sci U S A,* 107**,** 9879-84.

TRICK, G. L., KASKIE, B. & STEINMAN, S. B. 1994. Visual impairment in Parkinson's disease: deficits in orientation and motion discrimination. *Optom Vis Sci,* 71**,** 242-5.

TSAI, J. J., WADE, A. R. & NORCIA, A. M. 2012. Dynamics of normalization underlying masking in human visual cortex. *J Neurosci,* 32**,** 2783-9.

TUTHILL, J. C., NERN, A., RUBIN, G. M. & REISER, M. B. 2014. Wide-field feedback neurons dynamically tune early visual processing. *Neuron,* 82**,** 887-95.

UNGERSTEDT, U. 1968. 6-Hydroxy-dopamine induced degeneration of central monoamine neurons. *Eur J Pharmacol,* 5**,** 107-10.

UNITEDNATIONS 2013. World Population Ageing 2013. *In:* DEPARTMENT OF ECONOMIC AND SOCIAL AFFAIRS, P. D. (ed.) *ST/ESA/SER.A/348.* New York: United Nations publication.

VALENTE, E. M., ABOU-SLEIMAN, P. M., CAPUTO, V., MUQIT, M. M., HARVEY, K., GISPERT, S., ALI, Z., DEL TURCO, D., BENTIVOGLIO, A. R., HEALY, D. G., ALBANESE, A., NUSSBAUM, R., GONZALEZ-MALDONADO, R., DELLER, T., SALVI, S., CORTELLI, P., GILKS, W. P., LATCHMAN, D. S., HARVEY, R. J., DALLAPICCOLA, B., AUBURGER, G. & WOOD, N. W. 2004. Hereditary early-onset Parkinson's disease caused by mutations in PINK1. *Science,* 304**,** 1158-60.

VAN DER GOOT, A. T., ZHU, W., VÁZQUEZ-MANRIQUE, R. P., SEINSTRA RÉ, I., DETTMER, K., MICHELS, H., FARINA, F., KRIJNEN, J., MELKI, R., BUIJSMAN, R. C., RUIZ SILVA, M., THIJSSEN, K. L., KEMA, I. P., NERI, C., OEFNER, P. J. & NOLLEN, E. A. A. 2012. Delaying aging and the aging-associated decline in protein homeostasis by inhibition of tryptophan degradation. *Proc Natl Acad Sci U S A,* 109**,** 14912-7.

VELLA, L. J., SHARPLES, R. A., LAWSON, V. A., MASTERS, C. L., CAPPAI, R. & HILL, A. F. 2007. Packaging of prions into exosomes is associated with a novel pathway of PrP processing. *J Pathol,* 211**,** 582-90.

VENDEROVA, K., KABBACH, G., ABDEL-MESSIH, E., ZHANG, Y., PARKS, R. J., IMAI, Y., GEHRKE, S., NGSEE, J., LAVOIE, M. J., SLACK, R. S., RAO, Y., ZHANG, Z., LU, B., HAQUE, M. E. & PARK, D. S. 2009. Leucine-Rich Repeat Kinase 2 interacts with Parkin, DJ-1 and PINK-1 in a Drosophila melanogaster model of Parkinson's disease. *Hum Mol Genet,* 18**,** 4390-404.

VERMEIJ, J. D., WINOGRODZKA, A., TRIP, J. & WEBER, W. E. 2009. Parkinson's disease, levodopa-use and the risk of melanoma. *Parkinsonism Relat Disord,* 15**,** 551-3.

VILARINO-GUELL, C., WIDER, C., ROSS, O. A., DACHSEL, J. C., KACHERGUS, J. M., LINCOLN, S. J., SOTO-ORTOLAZA, A. I., COBB, S. A., WILHOITE, G. J., BACON, J. A., BEHROUZ, B., MELROSE, H. L., HENTATI, E., PUSCHMANN, A., EVANS, D. M., CONIBEAR, E., WASSERMAN, W. W., AASLY, J. O., BURKHARD, P. R., DJALDETTI, R., GHIKA, J., HENTATI, F., KRYGOWSKA-WAJS, A., LYNCH, T., MELAMED, E., RAJPUT, A., RAJPUT, A. H., SOLIDA, A., WU, R. M., UITTI, R. J., WSZOLEK, Z. K., VINGERHOETS, F. & FARRER, M. J. 2011. VPS35 mutations in Parkinson disease. *Am J Hum Genet,* 89**,** 162-7.

VILINSKY, I. & JOHNSON, K. G. 2012. Electroretinograms in Drosophila: a robust and genetically accessible electrophysiological system for the undergraduate laboratory. *J Undergrad Neurosci Educ,* 11**,** A149-57.

WALKER, M. D., VOLTA, M., CATALDI, S., DINELLE, K., BECCANO-KELLY, D., MUNSIE, L., KORNELSEN, R., MAH, C., CHOU, P., CO, K., KHINDA, J., MROCZEK, M., BERGERON, S., YU, K., CAO, L. P., FUNK, N., OTT, T., GALTER, D., RIESS, O., BISKUP, S., MILNERWOOD, A. J., STOESSL, A. J., FARRER, M. J. & SOSSI, V. 2014. Behavioral deficits and striatal DA signaling in LRRK2 p.G2019S transgenic rats: a multimodal investigation including PET neuroimaging. *J Parkinsons Dis,* 4**,** 483-98.

WALLINGS, R., MANZONI, C. & BANDOPADHYAY, R. 2015. Cellular processes associated with LRRK2 function and dysfunction. *Febs j,* 282**,** 2806-26.

WANG, D., QIAN, L., XIONG, H., LIU, J., NECKAMEYER, W. S., OLDHAM, S., XIA, K., WANG, J., BODMER, R. & ZHANG, Z. 2006. Antioxidants protect PINK1-dependent dopaminergic neurons in Drosophila. *Proc Natl Acad Sci U S A,* 103**,** 13520-5.

WANG, D., TANG, B., ZHAO, G., PAN, Q., XIA, K., BODMER, R. & ZHANG, Z. 2008. Dispensable role of Drosophila ortholog of LRRK2 kinase activity in survival of dopaminergic neurons. *Mol Neurodegener,* 3**,** 3.

WANG, X., WINTER, D., ASHRAFI, G., SCHLEHE, J., WONG, Y. L., SELKOE, D., RICE, S., STEEN, J., LAVOIE, M. J. & SCHWARZ, T. L. 2011. PINK1 and Parkin target Miro for phosphorylation and degradation to arrest mitochondrial motility. *Cell,* 147**,** 893-906.

WANG, X., YAN, M. H., FUJIOKA, H., LIU, J., WILSON-DELFOSSE, A., CHEN, S. G., PERRY, G., CASADESUS, G. & ZHU, X. 2012. LRRK2 regulates mitochondrial dynamics and function through direct interaction with DLP1. *Hum Mol Genet,* 21**,** 1931-44.

WARNER, T. S., SINCLAIR, D. A., FITZPATRICK, K. A., SINGH, M., DEVLIN, R. H. & HONDA, B. M. 1998. The light gene of Drosophila melanogaster encodes a homologue of VPS41, a yeast gene involved in cellular-protein trafficking. *Genome,* 41**,** 236-43.

WARREN, W. D., PALMER, S. & HOWELLS, A. J. 1996. Molecular characterization of the cinnabar region of Drosophila melanogaster: identification of the cinnabar transcription unit. *Genetica,* 98**,** 249-62.

WASMEIER, C., HUME, A. N., BOLASCO, G. & SEABRA, M. C. 2008. Melanosomes at a glance. *Journal of Cell Science,* 121**,** 3995-3999.
WASSLE, H. & CHUN, M. H. 1988. Dopaminergic and indoleamine-accumulating amacrine cells express GABA-like immunoreactivity in the cat retina. *J Neurosci,* 8**,** 3383-94.
WEBVISION. 2012. *Gross Anatomy of the Eye* [Online]. Moran Eye Center. Available: http://webvision.med.utah.edu/book/part-i-foundations/gross-anatomy-of-the-ey [Accessed 15 May 2016].
WEIHOFEN, A., THOMAS, K. J., OSTASZEWSKI, B. L., COOKSON, M. R. & SELKOE, D. J. 2009. Pink1 forms a multiprotein complex with Miro and Milton, linking Pink1 function to mitochondrial trafficking. *Biochemistry,* 48**,** 2045-52.
WEST, A. B., MOORE, D. J., BISKUP, S., BUGAYENKO, A., SMITH, W. W., ROSS, C. A., DAWSON, V. L. & DAWSON, T. M. 2005. Parkinson's disease-associated mutations in leucine-rich repeat kinase 2 augment kinase activity. *Proc Natl Acad Sci U S A,* 102**,** 16842-7.
WEST, A. B., MOORE, D. J., CHOI, C., ANDRABI, S. A., LI, X., DIKEMAN, D., BISKUP, S., ZHANG, Z., LIM, K. L., DAWSON, V. L. & DAWSON, T. M. 2007. Parkinson's disease-associated mutations in LRRK2 link enhanced GTP-binding and kinase activities to neuronal toxicity. *Hum Mol Genet,* 16**,** 223-32.
WEST, R. J., ELLIOTT, C. J. & WADE, A. R. 2015a. Classification of Parkinson's Disease Genotypes in Drosophila Using Spatiotemporal Profiling of Vision. *Sci Rep,* 5**,** 16933.
WEST, R. J., FURMSTON, R., WILLIAMS, C. A. & ELLIOTT, C. J. 2015b. Neurophysiology of Drosophila models of Parkinson's disease. *Parkinsons Dis,* 2015**,** 381281.
WHITE, O. B., SAINT-CYR, J. A., TOMLINSON, R. D. & SHARPE, J. A. 1983. Ocular motor deficits in Parkinson's disease. II. Control of the saccadic and smooth pursuit systems. *Brain,* 106 (Pt 3)**,** 571-87.
WHITWORTH, A. J., THEODORE, D. A., GREENE, J. C., BENES, H., WES, P. D. & PALLANCK, L. J. 2005. Increased glutathione S-transferase activity rescues dopaminergic neuron loss in a Drosophila model of Parkinson's disease. *Proc Natl Acad Sci U S A,* 102**,** 8024-9.
WIDER, C., DICKSON, D. W. & WSZOLEK, Z. K. 2010. Leucine-rich repeat kinase 2 gene-associated disease: redefining genotype-phenotype correlation. *Neurodegener Dis,* 7**,** 175-9.
WILKINSON-BERKA, J. L. 2004. Diabetes and retinal vascular disorders: role of the renin-angiotensin system. *Expert Reviews in Molecular Medicine,* 6**,** 1-18.
WILSON, G. R., SIM, J. C., MCLEAN, C., GIANNANDREA, M., GALEA, C. A., RISELEY, J. R., STEPHENSON, S. E., FITZPATRICK, E., HAAS, S. A., POPE, K., HOGAN, K. J., GREGG, R. G., BROMHEAD, C. J., WARGOWSKI, D. S., LAWRENCE, C. H., JAMES, P. A., CHURCHYARD, A., GAO, Y., PHELAN, D. G., GILLIES, G., SALCE, N., STANFORD, L., MARSH, A. P., MIGNOGNA, M. L., HAYFLICK, S. J., LEVENTER, R. J., DELATYCKI, M. B., MELLICK, G. D., KALSCHEUER, V. M., D'ADAMO, P., BAHLO, M., AMOR, D. J. & LOCKHART, P. J. 2014. Mutations in RAB39B cause X-linked intellectual disability and early-onset Parkinson disease with alpha-synuclein pathology. *Am J Hum Genet,* 95**,** 729-35.
WINKLHOFER, K. F. & HAASS, C. 2010. Mitochondrial dysfunction in Parkinson's disease. *Biochim Biophys Acta,* 1802**,** 29-44.
WINNER, B., MELROSE, H. L., ZHAO, C., HINKLE, K. M., YUE, M., KENT, C., BRAITHWAITE, A. T., OGHOLIKHAN, S., AIGNER, R., WINKLER, J., FARRER, M.

J. & GAGE, F. H. 2011. Adult neurogenesis and neurite outgrowth are impaired in LRRK2 G2019S mice. *Neurobiol Dis,* 41**,** 706-16.

WINTERMEYER, P., KRUGER, R., KUHN, W., MULLER, T., WOITALLA, D., BERG, D., BECKER, G., LEROY, E., POLYMEROPOULOS, M., BERGER, K., PRZUNTEK, H., SCHOLS, L., EPPLEN, J. T. & RIESS, O. 2000. Mutation analysis and association studies of the UCHL1 gene in German Parkinson's disease patients. *Neuroreport,* 11**,** 2079-82.

WITKOVSKY, P. 2004. Dopamine and retinal function. *Doc Ophthalmol,* 108**,** 17-40.

WU, C. F. & WONG, F. 1977. Frequency characteristics in the visual system of Drosophila: genetic dissection of electroretinogram components. *J Gen Physiol,* 69**,** 705-24.

WU, X. & HAMMER, J. A. 2014. Melanosome transfer: It is best to give and receive. *Curr Opin Cell Biol,* 0**,** 1-7.

WULLE, I. & WAGNER, H. J. 1990. GABA and tyrosine hydroxylase immunocytochemistry reveal different patterns of colocalization in retinal neurons of various vertebrates. *J Comp Neurol,* 296**,** 173-8.

XIONG, W. C., OKANO, H., PATEL, N. H., BLENDY, J. A. & MONTELL, C. 1994. repo encodes a glial-specific homeo domain protein required in the Drosophila nervous system. *Genes Dev,* 8**,** 981-94.

XIONG, Y., COOMBES, C. E., KILARU, A., LI, X., GITLER, A. D., BOWERS, W. J., DAWSON, V. L., DAWSON, T. M. & MOORE, D. J. 2010. GTPase activity plays a key role in the pathobiology of LRRK2. *PLoS Genet,* 6**,** e1000902.

XIONG, Y., DAWSON, V. L. & DAWSON, T. M. 2012a. LRRK2 GTPase Dysfunction in the Pathogenesis of Parkinson's disease. *Biochem Soc Trans,* 40**,** 1074-9.

XIONG, Y., YUAN, C., CHEN, R., DAWSON, T. M. & DAWSON, V. L. 2012b. ArfGAP1 is a GTPase activating protein for LRRK2: reciprocal regulation of ArfGAP1 by LRRK2. *J Neurosci,* 32**,** 3877-86.

YANG, Y., GEHRKE, S., HAQUE, M. E., IMAI, Y., KOSEK, J., YANG, L., BEAL, M. F., NISHIMURA, I., WAKAMATSU, K., ITO, S., TAKAHASHI, R. & LU, B. 2005. Inactivation of Drosophila DJ-1 leads to impairments of oxidative stress response and phosphatidylinositol 3-kinase/Akt signaling. *Proc Natl Acad Sci U S A,* 102**,** 13670-5.

YANG, Y., GEHRKE, S., IMAI, Y., HUANG, Z., OUYANG, Y., WANG, J. W., YANG, L., BEAL, M. F., VOGEL, H. & LU, B. 2006. Mitochondrial pathology and muscle and dopaminergic neuron degeneration caused by inactivation of Drosophila Pink1 is rescued by Parkin. *Proc Natl Acad Sci U S A,* 103**,** 10793-8.

YANG, Y., OUYANG, Y., YANG, L., BEAL, M. F., MCQUIBBAN, A., VOGEL, H. & LU, B. 2008. Pink1 regulates mitochondrial dynamics through interaction with the fission/fusion machinery. *Proc Natl Acad Sci U S A,* 105**,** 7070-5.

YASUDA, T., HAYAKAWA, H., NIHIRA, T., REN, Y. R., NAKATA, Y., NAGAI, M., HATTORI, N., MIYAKE, K., TAKADA, M., SHIMADA, T., MIZUNO, Y. & MOCHIZUKI, H. 2011. Parkin-mediated protection of dopaminergic neurons in a chronic MPTP-minipump mouse model of Parkinson disease. *J Neuropathol Exp Neurol,* 70**,** 686-97.

YE, Y., XI, W., PENG, Y., WANG, Y. & GUO, A. 2004. Long-term but not short-term blockade of dopamine release in Drosophila impairs orientation during flight in a visual attention paradigm. *Eur J Neurosci,* 20**,** 1001-7.

YESCAS, P., LOPEZ, M., MONROY, N., BOLL, M. C., RODRIGUEZ-VIOLANTE, M., RODRIGUEZ, U., OCHOA, A. & ALONSO, M. E. 2010. Low frequency of common

LRRK2 mutations in Mexican patients with Parkinson's disease. *Neurosci Lett,* 485**,** 79-82.

YIM, J., KIM, S., WALCHER, G. & PFLEIDERER, W. 1993. Pteridines. Part C. Structure and nonenzymatic synthesis of aurodrosopterin. *Helvetica Chimica Acta,* 76**,** 1970-1979.

YIN, M. C., LIN, M. C., MONG, M. C. & LIN, C. Y. 2012. Bioavailability, distribution, and antioxidative effects of selected triterpenes in mice. *J Agric Food Chem,* 60**,** 7697-701.

YU, Y., WANG, J. R., SUN, P. H., GUO, Y., ZHANG, Z. J., JIN, G. Z. & ZHEN, X. 2008. Neuroprotective effects of atypical D1 receptor agonist SKF83959 are mediated via D1 receptor-dependent inhibition of glycogen synthase kinase-3 beta and a receptor-independent anti-oxidative action. *J Neurochem,* 104**,** 946-56.

YUN, H. J., KIM, H., GA, I., OH, H., HO, D. H., KIM, J., SEO, H., SON, I. & SEOL, W. 2015. An early endosome regulator, Rab5b, is an LRRK2 kinase substrate. *J Biochem,* 157**,** 485-95.

YUN, H. J., PARK, J., HO, D. H., KIM, H., KIM, C. H., OH, H., GA, I., SEO, H., CHANG, S., SON, I. & SEOL, W. 2013. LRRK2 phosphorylates Snapin and inhibits interaction of Snapin with SNAP-25. *Exp Mol Med,* 45**,** e36.

ZANETTI, R., LORIA, D. & ROSSO, S. 2006. Melanoma, Parkinson's disease and levodopa: causal or spurious link? A review of the literature. *Melanoma Res,* 16**,** 201-6.

ZHANG, D. Q., ZHOU, T. R. & MCMAHON, D. G. 2007. Functional heterogeneity of retinal dopaminergic neurons underlying their multiple roles in vision. *J Neurosci,* 27**,** 692-9.

ZHANG, F. R., HUANG, W., CHEN, S. M., SUN, L. D., LIU, H., LI, Y., CUI, Y., YAN, X. X., YANG, H. T., YANG, R. D., CHU, T. S., ZHANG, C., ZHANG, L., HAN, J. W., YU, G. Q., QUAN, C., YU, Y. X., ZHANG, Z., SHI, B. Q., ZHANG, L. H., CHENG, H., WANG, C. Y., LIN, Y., ZHENG, H. F., FU, X. A., ZUO, X. B., WANG, Q., LONG, H., SUN, Y. P., CHENG, Y. L., TIAN, H. Q., ZHOU, F. S., LIU, H. X., LU, W. S., HE, S. M., DU, W. L., SHEN, M., JIN, Q. Y., WANG, Y., LOW, H. Q., ERWIN, T., YANG, N. H., LI, J. Y., ZHAO, X., JIAO, Y. L., MAO, L. G., YIN, G., JIANG, Z. X., WANG, X. D., YU, J. P., HU, Z. H., GONG, C. H., LIU, Y. Q., LIU, R. Y., WANG, D. M., WEI, D., LIU, J. X., CAO, W. K., CAO, H. Z., LI, Y. P., YAN, W. G., WEI, S. Y., WANG, K. J., HIBBERD, M. L., YANG, S., ZHANG, X. J. & LIU, J. J. 2009. Genomewide association study of leprosy. *N Engl J Med,* 361**,** 2609-18.

ZHANG, J., DENG, X., CHOI, H. G., ALESSI, D. R. & GRAY, N. S. 2012. Characterization of TAE684 as a potent LRRK2 kinase inhibitor. *Bioorg Med Chem Lett,* 22**,** 1864-9.

ZHANG, Y. 2000. Parkin functions as an E2-dependent ubiquitin– protein ligase. 97**,** 13354-9.

ZHENG, L., DE POLAVIEJA, G. G., WOLFRAM, V., ASYALI, M. H., HARDIE, R. C. & JUUSOLA, M. 2006. Feedback network controls photoreceptor output at the layer of first visual synapses in Drosophila. *J Gen Physiol,* 127**,** 495-510.

ZIMMERMAN, J. E., NAIDOO, N., RAIZEN, D. M. & PACK, A. I. 2008. Conservation of sleep: insights from non-mammalian model systems. *Trends Neurosci,* 31**,** 371-6.

ZIMPRICH, A., BENET-PAGES, A., STRUHAL, W., GRAF, E., ECK, S. H., OFFMAN, M. N., HAUBENBERGER, D., SPIELBERGER, S., SCHULTE, E. C., LICHTNER, P., ROSSLE,

S. C., KLOPP, N., WOLF, E., SEPPI, K., PIRKER, W., PRESSLAUER, S., MOLLENHAUER, B., KATZENSCHLAGER, R., FOKI, T., HOTZY, C., REINTHALER, E., HARUTYUNYAN, A., KRALOVICS, R., PETERS, A., ZIMPRICH, F., BRUCKE, T., POEWE, W., AUFF, E., TRENKWALDER, C., ROST, B., RANSMAYR, G., WINKELMANN, J., MEITINGER, T. & STROM, T. M. 2011. A mutation in VPS35, encoding a subunit of the retromer complex, causes late-onset Parkinson disease. *Am J Hum Genet,* 89**,** 168-75.

ZIMPRICH, A., BISKUP, S., LEITNER, P., LICHTNER, P., FARRER, M., LINCOLN, S., KACHERGUS, J., HULIHAN, M., UITTI, R. J., CALNE, D. B., STOESSL, A. J., PFEIFFER, R. F., PATENGE, N., CARBAJAL, I. C., VIEREGGE, P., ASMUS, F., MULLER-MYHSOK, B., DICKSON, D. W., MEITINGER, T., STROM, T. M., WSZOLEK, Z. K. & GASSER, T. 2004. Mutations in LRRK2 cause autosomal-dominant parkinsonism with pleomorphic pathology. *Neuron,* 44**,** 601-7.

ZIVIANI, E., TAO, R. N. & WHITWORTH, A. J. 2010. Drosophila Parkin requires PINK1 for mitochondrial translocation and ubiquitinates Mitofusin. *Proc Natl Acad Sci U S A,* 107**,** 5018-23.